CLIMATE RISK AND BUSINESS
HYDROPOWER

Kafue Gorge Lower
Zambia
Appendices

IFC International Finance Corporation
World Bank Group

Acknowledgements

Authored by
Vladimir Stenek, International Finance Corporation
Donna Boysen, Carla Buriks, William Bohn, Mark Evans, Tetra Tech, Inc.

The authors wish to acknowledge the extensive technical support provided for the following sections:
Appendix 1: Mariza Costa-Cabral, Hydrology Futures, LLC.
Appendix 2: Murthy Bachu, Uttam Singh, Kishore Dhore; RMSI, Inc.
Appendix 3: Richard Hayes, Tetra Tech, Inc.
Appendix 4: Urban Ziegler, RETScreen

The authors would like to thank the management and staff of ZESCO for their support and cooperation in this study, especially Romas Kamanga, Mellon Chinjila and Benny Sindowe. We also thank Israel Phiri and Clement Sasa from the Office for Promoting Private Power Investment (OPPI).

The authors also wish to thank the following institutions, and colleagues working in these institutions, for their valuable contributions to the study:

Department of Water Affairs of Zambia; Zambezi River Authority; Centre For Energy, Environment and Engineering Zambia (CEEEZ); Environmental Council of Zambia; Climate Change Facilitation Unit (Environment and Natural Resources Management Department, Zambia); Ministry of Agriculture of Zambia; Kafue District Health Department; Zambian Wildlife Authority; University of Zambia; World Bank and IFC (Zambia); International Union for Conservation of Nature (IUCN, Zambia); Imagen GSI Consulting; BRL Ingenierie / NIRAS; and UNDP (Zambia).

The data and information collected, elaborated, and generously provided by Zambia Meteorological Department, was essential for the elaboration of this study.

Reviewers
We thank Vahid Alavian, Jane Ebinger, Ian Noble (World Bank); Mellon Chinjila (ZESCO); and Nico Saporiti (IFC) for their critical comments and suggestions.

This work benefited from support provided by the Norwegian Trust Fund for Private Sector and Infrastructure (NTF-PSI).

About Climate Risk and Business
Starting in 2008, IFC initiated the Climate Risk and Adaptation Program, a series of pilot studies that analyzes climate risks and adaptation options for projects in various sectors and regions. The studies' focus are private sector projects but with a significant emphasis on the cooperation and synergies with the public sector, research institutions and the civil society. To help understand and respond to the risks of climate change, IFC is developing best practices in assessing private sector risk and adaptation strategies.

Published so far in the ***Climate Risk and Business*** series:
Hydropower (Run of the River), Khimti 1, Nepal
Agribusiness (Tropical Plantation and Refinery), GOPDC, Ghana
Manufacturing, Packages, Pakistan
Ports, Muelles el Bosque, Colombia
Financial Institutions and Climate Risk

For more information on the Program and to download the published studies, see www.ifc.org/climatechange.

CLIMATE RISK AND BUSINESS
HYDROPOWER

Kafue Gorge Lower
Zambia
Appendices

Appendix A1

Temperature and Precipitation Projections

The backbone of the IPCC (2007) Fourth Assessment Report are the results of the Coupled Model Intercomparison Project phase 3 (CMIP3) global climate model runs performed by dozens of research groups worldwide, assuming a suite of global greenhouse gas scenarios (Figure A1-1). CMIP3 is a project of the World Climate Research Programme (WCRP) (Meehl *et al.*, 2007). Although the global circulation model (GCM) runs included the CMIP3 include considerable uncertainty, they represent the most current knowledge about the global climate system and its response to greenhouse gas concentrations, and most current computational methods and capability performed. Their climate projections, once downscaled to finer resolution for a region of interest, represent appropriate study cases for climate change impact studies such as the present study.

Regional climate studies require downscaling of GCM results to regional scales, and downscaled CMIP3 results at 0.5° resolution (globally) for 16 GCMs and 3 SRES scenarios (A2, A1B and B1 – see later sections) have recently become available from Santa Clara University. This is the source of the statistically downscaled results that are used in this study.

The release of the SCU dataset for public use in 2009 has been of great benefit to this project, for three main reasons: First, for its breadth: it covers 150 years (1950-2099) of the CMIP3 runs for a wide selection of GCMs and for three contrasting SRES scenarios. Second, because the downscaling method used, as its baseline, a high-quality observational dataset for a 50-year period (1950-1999). Third, the SCU dataset includes the four main variables that are commonly required as input to hydrological models: precipitation, maximum daily temperature (T_{max}), minimum daily temperature (T_{min}), and wind speed. Once disaggregated to daily time resolution, the resulting daily time series can be used directly in hydrologic models.

1.1 Selection of Climate Projections

1.1.1 Selection of Time Horizons

The time horizons, listed in Table A1-1, were established for in the early project stages. These 30-year horizons are commonly used in climate change impact studies, given that a 30-year period is sufficiently long for dampening, by averaging, much of the year-to-year climatic variability, but is short enough to approximate its climate as approximately stationary (within the period). These horizons are particularly appropriate in light of the alignment between the end of the early period (see Table A1-1) and the approximate timing of the planned transition from public to private project investment.

Table A1-1: Time Horizons Used

Time Horizons	
1. Early Period	2010-2039
2. Mid-Century Period	2040-2069
3. End of Century Period	2070-2099

1.1.2 Selection of GHG Emission Scenarios

Greenhouse gas global emissions scenarios were developed by the IPCC and were published in the Special Report on Emission Scenarios (SRES; IPCC, 2003); see Figure A1-1. For the present project, the availability of downscaled AR4 datasets informed the selection of two SRES scenarios: A2, contrasted with B1.

Each SRES scenario is built on a storyline that relates emissions to driving forces. The two scenarios used in this project are described in the SRES as follows:

- SRES-A2: Based on a world that is regionally organized economically, in which technological change is fragmented, and population growth is high.
- SRES-B1: In contrast, describes a world with low population growth and rapid changes in economies toward service and information, with relatively rapid introduction of clean and resource efficient technologies.

A detailed description of these two scenarios is given in Nakicenovic *et al.* (2000).
Each of these two scenarios produces different atmospheric concentrations of GHGs throughout the period examined in this project. Scenario B1 is often used to represent the 21st century "best case" of the SRES emissions scenarios (Houghton *et al.*, 2001). Scenario A2 produces higher GHG emissions; although it is by no means a "worst case", however, CMIP3 data for more severe scenarios is limited. Therefore, A2 is the scenario with the highest GHG concentrations for which most modeling groups have completed simulations. A2 represent the higher emission case in this study. Scenario A2 is often the highest emissions scenario studied in many regional impact studies (e.g., Maurer *et al.*, 2009).

Figure A1-1: Atmospheric CO_2 concentrations resulting from different emissions scenarios through the 21st century (IPCC, 2001).

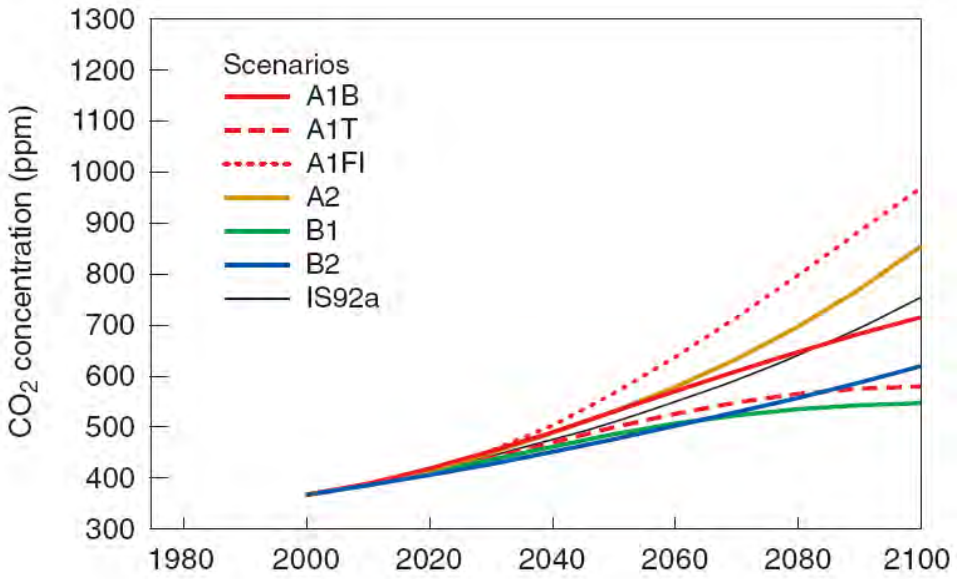

1.1.3 Selection of Global Climate Models

Statistically-downscaled GCM data from CMIP3 became available in 2009 from Edwin Maurer of Santa Clara University (SCU) and colleagues. This dataset is a high-quality and comprehensive dataset that includes 16 GCMs (listed in Table A1-2), downscaled to the spatial resolution of 0.5° in latitude and longitude, for SRES greenhouse gas emission scenarios A2, A1B and B2, through the year 2099.

There appears to be little advantage to including more than about five GCMs (Pierce *et* al, 2009; see Box 1, on page A1-6), and it appears that the choice of which five GCMs are used has relatively little impact on the results. For this project, six GCMs were selected on the basis of covering a geographically diverse list of modeling group countries; they are listed in Table A1-3.

Table A1-2: Global climate models included in Santa Clara University (SCU), California, U.S.A., statistically-downscaled dataset.

	Modeling Group	Model I.D.*	Primary Reference
1	Bjerknes Centre for Climate Research (Norway)	BCCR-BCM2.0	Furevik et al. (2003)
2	Canadian Centre for Climate Modeling & Analysis (Canada)	CGCM3.1 (T47)	Flato and Boer (2001)
3	Météo-France/Centre National des Recherches Météorologiques (France)	CNRM-CM3	Sala-Mélia *et al*. (2005)
4	CSIRO Atmospheric Research (Australia)	CSIRO-Mk3.0	Gordon *et al.* (2002)
5	U.S. Department of Commerce/NOAA/Geophysical Fluid Dynamics Laboratory (U.S.A.)	GFDL-CM2.0	Delworth *et al.* (2006)
6	U.S. Department of Commerce/NOAA/Geophysical Fluid Dynamics Laboratory (U.S.A.)	GFDL-CM2.1	Delworth *et al.* (2006)
7	NASA/Goddard Institute for Space Studies (U.S.A.)	GISS-ER	Russell *et al.* (2000)
8	Institute for Numerical Mathematics (Russia)	INM-CM3.0	Diansky and Volodin (2002)
9	Institut Pierre Simon Laplace (France)	IPSL-CM4	IPSL (2005)
10	Center for Climate System Research (U. Tokyo), National Institute for Environmental Studies, and Frontier Research Center for Global Change (JAMSTEC) (Japan)	MIROC3.2 (medres)	K-1 model developers (2004)
11	Meteorological Institute of U. Bonn, Meteorological Research Institute of KMA (Germany/Korea)	ECHO-G	Legutke and Voss (1999)
12	Max Planck Institute for Meteorology (Germany)	ECHAM5/MPI-OM	Jungclaus *et al.* (2006)
13	Meteorological Research Institute (Japan)	MRI-CGCM2.3.2	Yukimoto *et al*. (2001)
14	National Center for Atmospheric Research (U.S.A.)	PCM	Washington *et al.* (2000)
15	National Center for Atmospheric Research (U.S.A.)	CCSM3	Collins *et al.* (2006)
16	Hadley Centre for Climate Prediction and Research/Met Office (U.K.)	UKMO-HadCM3	Gordon *et al.* (2000)

* I.D. as used by the Intergovernmental Panel on Climate Change (IPCC).

Table A1-3: The six global climate models selected for this study.

	Modeling Group	Model I.D.*	Primary Reference
1	U.S. Department of Commerce/NOAA/Geophysical Fluid Dynamics Laboratory (U.S.A.)	GFDL-CM2.0	Delworth *et al.* (2006)
2	Institut Pierre Simon Laplace (France)	IPSL-CM4	IPSL (2005)
3	Max Planck Institute for Meteorology (Germany)	ECHAM5/MPI-OM	Jungclaus *et al.* (2006)
4	Hadley Centre for Climate Prediction and Research/Met Office (U.K.)	UKMO-HadCM3	Gordon *et al.* (2000)
5	Meteorological Research Institute (Japan)	MRI-CGCM2.3.2	Yukimoto *et al.* (2001)
6	NASA/Goddard Institute for Space Studies (U.S.A.)	GISS-ER	Russell *et al.* (2000)

* I.D. as used by the Intergovernmental Panel on Climate Change (IPCC).

BOX 1: GCM Selection (adapted with permission from a literature review on the topic of recently written by Edwin P. Maurer (*in preparation*)

GCMs are built upon the best current understanding of the atmospheric processes and atmosphere-land surface interactive processes that determine climate. They have been shown to accurately reproduce many observed climate features (e.g., Randall *et al.*, 2007), and improvements in GCM formulation over recent decades led to the capability of producing complex observed phenomena such as the El Niño/Southern Oscillation (ENSO), without any external adjustments (Meehl *et al.*, 2005; AchutaRao and Sperber, 2006; Reichler and Kim, 2008). GCMs are routinely relied upon in climate change impact studies such as the present study, to provide plausible, physically-based estimates (or "projections") of future climate in response to changes in atmospheric concentrations of greenhouse gases.

The selection of the specific GCMs for use in any given study may be performed under different considerations. In some studies, GCMs have been selected on the basis of their ability to reproduce specific regional climate features (e.g., Cayan *et al.*, 2008). Other studies have used differential weighting, with those GCMs scoring higher in some measure of skill over the region of interest being weighed more heavily; but the difference in outcomes compared to simply using an equal weighting was found to be small (Dettinger, 2005; Wilby and Harris, 2006). This was also noted by Wigley (2004), who showed a low signal-to-noise ratio for precipitation projections over California, meaning that the projected changes are small compared to the variability among model projections. It was once again concluded that including a sufficiently large ensemble of GCMs represented the most robust approach producing the greatest skill.

The above finding led some authors to weigh GCMs equally in their studies of hydrologic impacts of climate change (e.g., Lobell *et al.*, 2006; Christensen and Lettenmaier, 2007; and Maurer, 2007). Additionally, it has been shown that GCM performance skill concerning precipitation and other hydrologically-relevant variables is hard to assess objectively (Wigley, 2004; Brekke *et al.*, 2008) because the computed skill score varies widely with the (subjective) choice of skill metrics. For example, Brekke *et al.* (2008) showed that the UKMO-HadCM3 scored better than average for metrics related to water supply, but worse than average for metrics important for flood control.

Various recent studies (Christensen *et al.*, 2007; Reichler and Kim, 2008; Brekke *et al.*, 2008; Pierce *et al.*, 2009) have gone further, demonstrating that better predictive skill is obtained by using an ensemble of GCMs than by using any one individual GCM. The study by Brekke *et al.* (2008) focused on California and investigated whether accounting for the ability of a GCM to capture hydrologically important climate features of that specific region would result in different projections of future climate. It was found that to characterize the range of potential future climate it was most important to include results from many GCMs, and that selecting those GCMs with the highest score in a specific measure of skill made only small differences in impact projections.

In a separate study, Pierce *et al.* (2009) reached similar conclusions: "*Neither selecting the models based on the quality of their climate simulations in the region of interest nor forming an optimized ensemble average based on maximizing skill resulted in a superior result over the historical period.*" Pierce *et al.* (2009) also showed that adding many GCMs makes little difference for the range of future climate projections, once the number of GCMs reaches about five.

1.2 Climatic Datasets

This section describes the climatic datasets that entered this project from external sources; and the climatic datasets produced and delivered within this project to allow the study of projected climatic changes through statistical analysis and visual presentation, and to be used as climatic forcing of the hydrologic models.

1.2.1 Dataset Inputs

1.2.1.1 The SCU Dataset: Downscaled Monthly CMIP3 results (1950-2099)

The monthly CMIP3 results were downscaled to 0.5° resolution by statistical methods (Maurer *et al.*, 2009) and are available for public download at http://www.engr.scu.edu/~emaurer/global_data/.[1] The SCU dataset was created by downscaling the CMIP3 multi-GCM dataset using the bias-correction/spatial downscaling (BCSD) method (Wood et al., 2002, 2004) to a 0.5° grid, based on the 1950-1999 gridded observations of Adam and Lettenmaier (2003). The 0.5° grid cells are bound by meridian and parallel lines placed at full and half degrees (i.e., at values that are multiples of 0.5°); hence are centered at quarter degrees (0.25° and 0.75°) of latitude and longitude.

The BCSD method was originally developed for purposes of long-range streamflow forecasting (Wood *et al.*, 2002) and was later used for regional climate change impact studies (van Rheenen *et al.*, 2004; Maurer *et al.*, 2009; and many others). The BCSD method takes the time series of temperature and precipitation simulated by a GCM on its coarse grid and modifies the time series by replacing each simulated value with the *observed* value that has the same exceedance probability in 1950-1999. Thus, the cumulative density function (eCDF) of the simulated values is transformed, by quantile mapping, onto the eCDF of the observations. The same mapping is then applied to the 21st century GCM simulations. Thus, the bias corrected statistically downscaled GCM simulations will statistically match the observations for 1950-1999 (by construct); and will retain any trends (climate change signals) introduced by the higher future greenhouse gas concentrations, including trends in mean monthly values or in variability.

This SCU dataset reflects a monthly time scale (which is the time scale at which CMIP3 results are available). Disaggregation from monthly to daily time scale was performed for this project. The monthly datasets for the six selected GCMs (listed in Table A1-3) were downloaded from http://www.engr.scu.edu/~emaurer/global_data/, resulting in very large global data files. To select the data corresponding to *a)* Zambia and *b)* Kafue River basin, masks of these two regions, at 0.5° resolution, were drawn using a regional map from MapQuest™. There are 269 grid cells over Zambia, 70 of which are over Kafue River basin.

Given the large volume of data – 269 grid cells X 6 GCMs X 2 SRES scenarios X 2 regions (Zambia and Kafue River basin) X 2 variables (temperature and precipitation) X 4 time scales of

[1] This dataset is now also available (in complete functional form since January of 2010) from the Nature Conservancy's "Climate Wizard" web page: http://www.climatewizard.org

aggregation (baseline and projection periods) the data were condensed in different ways including computed statistics of GCM-projected temperature and precipitation; and image files for visualization of temperature and precipitation changes.

1.2.1.2 Observed Daily Gridded Dataset (1950-1999)

The observed daily gridded dataset of Maurer *et al.* (2009) is used in this project for its quality and to ensure internal consistency among the datasets used in the project – given that it is the observed dataset used as the baseline for the statistical downscaling that lead to the downscaled projections.[2]

The observed daily time series are for 1950-1999 and are gridded at 0.5° spatial resolution. The time series include precipitation, maximum daily temperature (T_{max}), minimum daily temperature (T_{min}), and wind speed. These are the four variables commonly used as input ("forcing") of distributed hydrologic models. The procedure used to create this dataset (which is part of a global dataset) is briefly described in Maurer *et al.* (2009), available at http://www.hydrol-earth-syst-sci.net/13/183/2009/hess-13-183-2009.html. The following description is based on Maurer *et al.* (2009) and references therein, in particular Willmott and Robeson (1995).

For precipitation, the daily observed dataset used by Maurer *et al.* (2009) was derived from the monthly dataset of Willmott and Matsuura (2001) (henceforth designated the "WM dataset"), by correction for gauge undercatch, and by disaggregation to daily time scale.[3] The correction for gauge undercatch principally affects snow, hence is generally small (<5%) in tropical areas (Adam and Lettenmaier, 2003; Maurer *et al.*, 2009).

The WM dataset is based on the Global Historical Climatology Network (GHCN version 2), described in Peterson and Vose (1997). Data from the GHCN network was interpolated onto a grid of 0.5° resolution. The interpolation was based on the novel method introduced by Willmott and Robeson (1995) designated "Climatologically Aided Interpolation" (CAI). The CAI method takes advantage of the higher density of more recent stations in order to interpolate the records of sparser, longer-record stations. The high-density global network used is the one compiled by Legates and Willmott (1990b), hereinafter referred to as the "LW stations network".

The CAI method exploits the spatial collinearity between the recent high-resolution station-based climatologies (LW stations network) and the monthly precipitation observations associated with the lower-resolution station network (GHCN). The term "climatologies" refers to the long-term monthly means of precipitation. Values for each month were interpolated separately. First, the stations' monthly climatologies of the LW stations network were interpolated into a grid following an extended inverse-distance method (see below). Second, the values of monthly mean precipitation for each station in the GHCN were interpolated using the scaling ratios established by the monthly climatologies of the LW stations network.

The extensions to the IDM method referred above were outlined Willmott and Robeson (1995):

[2] Available at http://www.engr.scu.edu/~emaurer/global_data/

[3] The WM dataset is available online at http://climate.geog.udel.edu/~climate/html_pages/download.html and is described in http://climate.geog.udel.edu/~climate/html_pages/archive.html.

a) the weights specified by inverse-distance are modified to account for uneven distribution (clustering) of stations, using the cosine-weighting function of Shepard (1968); and
b) "[p]rovision [is made] for extrapolating beyond the range of the nearby stations when spatial gradients warrant it" (Willmott and Robeson, 1995, p.223), such as, for example, when extrapolation extends into a region with a topographic gradient. Errors that arise from using the IDM method without these two extensions were documented by Wilmott and Legates (1991).

For minimum and maximum temperature (T_{min} and T_{max}), the monthly observed dataset used in the SCU dataset is that of New et al. (2000) updated by Mitchell et al. (2004).
For mean daily wind speed at 10 meter elevation, the NCEP/NCAR reanalysis dataset (Kalnay et al., 1996) was used, and regridded to 0.5° resolution by linear interpolation.

1.2.1.3 Zambia Meteorological Station Daily Data (1975-2005)

Daily time series of precipitation, T_{max}, T_{min} and wind speed were obtained from the Zambia Meteorological Department. Data for 12 stations located inside or very near the Kafue River basin were included. The 12 stations are: Chipata, Choma, Kabwe, Kafir, Kaoma, Kasempa, Lusaka (2 stations), Mumbwa, Ndola, Petauke, and Solwezi. For precipitation, the period of record is 1975-2005 for all stations except Mumbwa (1978-2005). For T_{max} and T_{min}, the period of record is nominally 1975-2005, however the data gaps are very many, particularly for recent years. For wind speed, the period of record is more limited and variable between stations. There is either no wind speed data or practically no data for Kasempa, Lusaka2, and Ndola.

The gridded observational dataset described in section 1.2.1.2, above, compares well against this stations dataset. See Figure A1-2 for example comparisons between the two datasets, obtained by picking the grid cell corresponding to the station location.

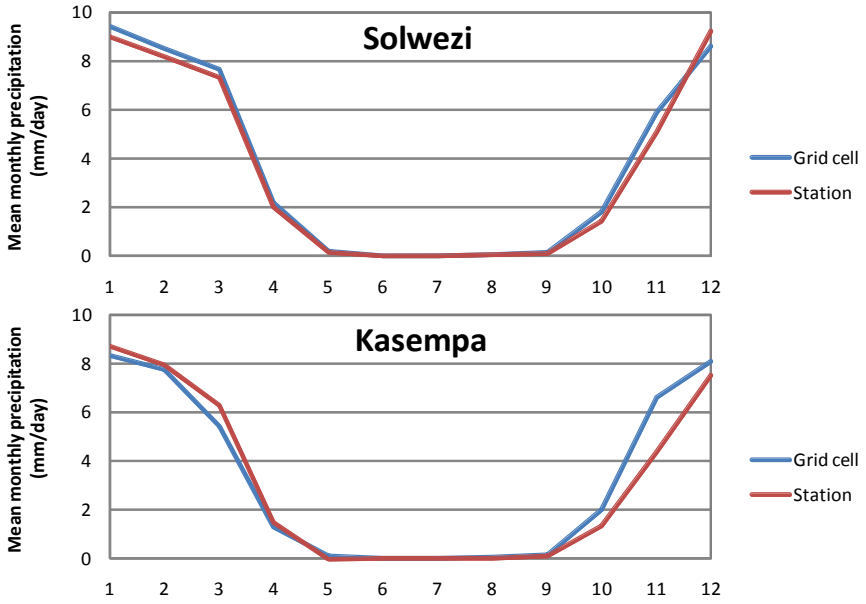

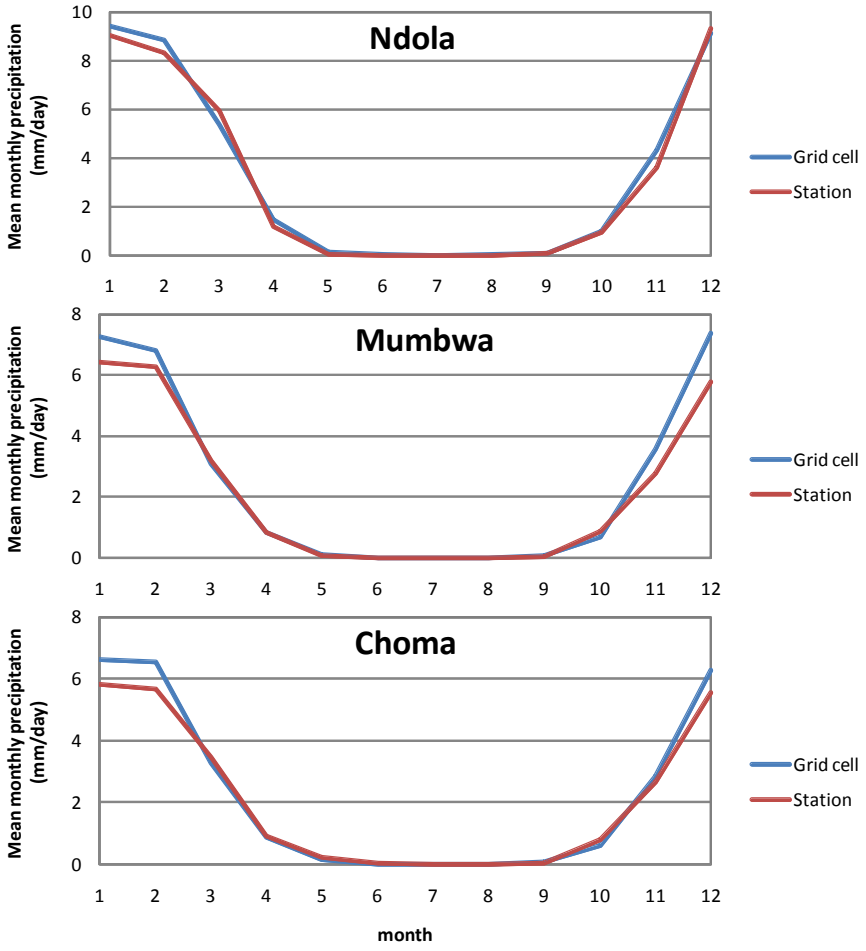

Figure A1-2: Comparison between monthly-mean station precipitation (records approx. 1975-2005) and the gridded observed dataset of Adam and Lettenmaier (2003) for the closest 0.5° grid cell, for selected stations (see Table A1-4 and Figure 2-4 for station location).

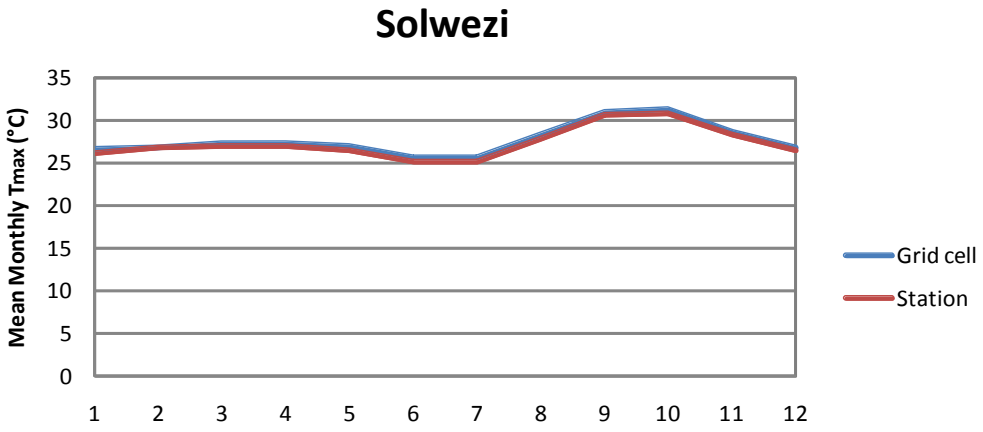

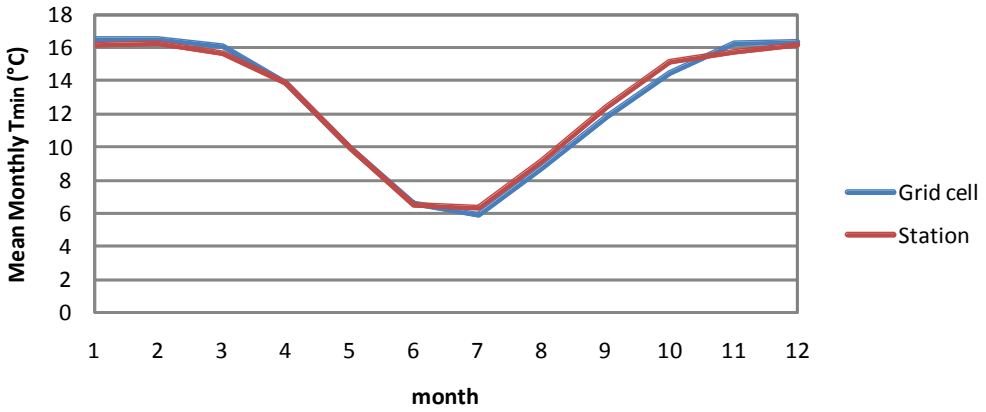

Figure A1-3: Comparison between the monthly-mean station T_{max} (top panel) and T_{min} (bottom panel) records for the Solwezi station and the closest grid cell of the gridded observed dataset of Adam and Lettenmaier (2003). See Table A1-4 and Figure A1-4 for station location.

1.2.2 Datasets Produced Within This Project

This section describes the climatic datasets produced to allow the study of projected climatic changes through statistical analysis and visual presentation, and to be used as climatic forcing of the hydrologic models.

1.2.2.1 Summary and Analysis of Monthly CMIP3 Dataset Results

Given the large volume of data – 269 grid cells X 6 GCMs X 2 SRES scenarios X 2 meteorological variables (temperature and precipitation) X several possible time scales of aggregation – the datasets entering this project cannot be appreciated directly without being summarized in various effective ways. Methods of summarizing the data within this project included:

- Data files containing computed statistics of temperature and precipitation GCM projections; and
- Image files for visualization of projected temperature and precipitation changes. Visuals include line plots of spatially-aggregated projected temperature and precipitation changes for Kafue River basin (and totals for Zambia); and color maps for Zambia, showing temporally aggregated values of temperature and precipitation.

Statistical values from the datasets were computed, including:

- Means (monthly, 4 seasonal, and annual means),
- 30-year running standard deviations, and
- 30-year linear trends.

For computing the 30-year running standard deviations, the linear trends found in the time series were first removed (de-trending), so as not to affect the computation.

Some of these visuals were presented as color maps for the following 21st century projected variables:

- Mean annual trend in temperature,
- Mean annual trend in precipitation,
- Trend in 30-year standard deviation of temperature and
- Trend in 30-year standard deviation of precipitation.

These plots were generated for each GCM and SRES scenario. Temperature values are reported in degrees Celcius. All trends are given in degrees Celcius per decade. All values of precipitation are given in mm/day. Trends are given in mm/day per decade.

1.2.2.2 Disaggregation of Downscaled CMIP3 Results to Daily Time Scale

To disaggregate the SCU dataset monthly time series (of all 4 variables – precipitation, T_{max}, T_{min} and wind speed) to daily time scale, random resampling of daily observations was used as outlined in Adam and Lettenmaier (2003). For this purpose, the daily observations dataset put together at Princeton University on the basis of NCEP/NCAR reanalysis (Sheffield *et al.*, 2006) was used for 1950-1995. To fill in the time gap for 1996-1999, the University of Washington stochastically generated climate data (Nijssen *et al.*, 2001) was used for those 4 years. See Table A1-4 and Figure A1-4 for the list of stations and their locations. The daily time series of temperature (=(T_{max} + T_{min})/2) and precipitation, when averaged to the monthly time scale, match (by construct) those from the monthly datasets (from which they were obtained via disaggregation).

Figure A1-4: Location (red dots) of the 39 meteorological stations in the dataset of Sheffield *et al.* (2006) and Nijssen *et al.* (2001), listed in Table A1-4. The red dot for Lusaka represents 3 closely located stations; and the red dots for Kabwe and Mfwe represent 2 closely located stations at each of those locations (see Table A1-4).

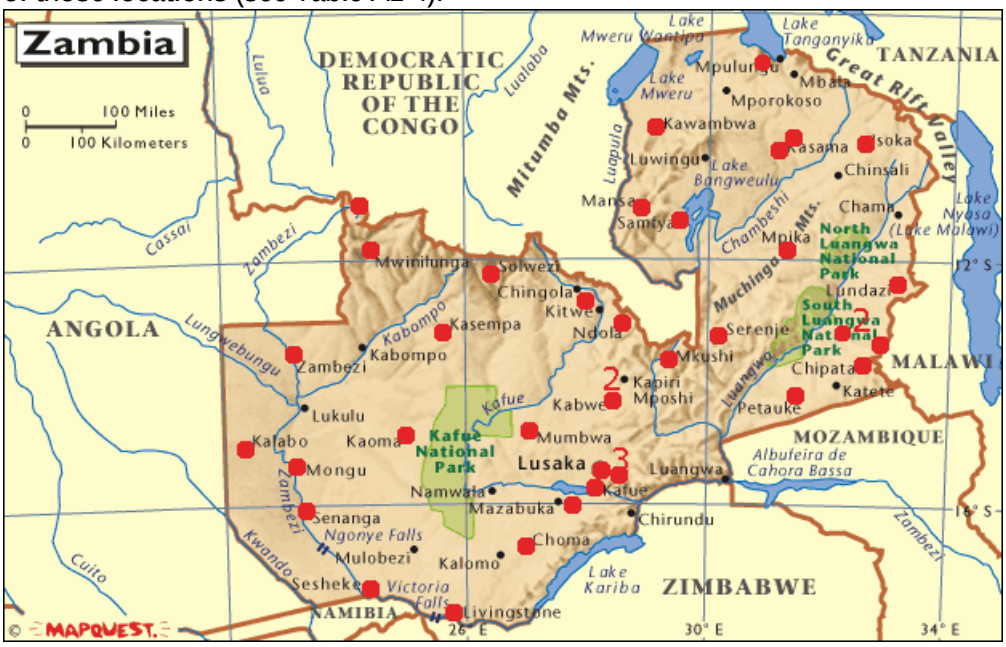

Table A1-4: List of 39 meteorological stations in the dataset of Sheffield *et al.* (2006) and Nijssen *et al.* (2001), shown in Figure A1-4.

Station #	Code	Name		Lat	Lon	Elev.(m)
675810	FLCP	CHIPATA	ZB	-1355	+03258	+1032
677530	FLCH	CHOMA	ZB	-1683	+02706	+1278
674810	FLIK	ISOKA	ZB	-1011	+03263	+1360
675430		KABOMPO	ZB	-1360	+02420	+1075
676630	FLKW	KABWE	ZB	-1445	+02846	+1207
676620		KABWE AGRIC	ZB	-1440	+02850	+1165
675630		KAFIRONDA	ZB	-1260	+02811	+1243
676590		KAFUE POLDER	ZB	-1576	+02791	+0978
676250		KALABO	ZB	-1485	+02270	+0000
676410	FLKO	KAOMA	ZB	-1480	+02480	+1213
674750	FLKS	KASAMA	ZB	-1021	+03113	+1384
675410	FLPA	KASEMPA	ZB	-1353	+02585	+1234
674030	FLKB	KAWAMBWA	ZB	-0980	+02908	+1324
677430	FLLI	LIVINGSTONE	ZB	-1781	+02581	+0986
675830	FLLD	LUNDAZI	ZB	-1228	+03320	+1143
676610	FLLC	LUSAKA CITY	ZB	-1541	+02833	+1280
676660	FLLC	LUSAKA CITY AIRPORT	ZB	-1541	+02846	+1280
676650	FLLS	LUSAKA INTERNATIONA	ZB	-1531	+02845	+1154
677510		MAGOYE	ZB	-1600	+02760	+1018
674610	FLMA	MANSA	ZB	-1110	+02885	+1384
674130	FLBA	MBALA	ZB	-0885	+03133	+1673
674420	FLMF	MFUWE	ZB	-1326	+03193	+0573
675990		MFUWE	ZB	-1326	+03193	+0570
674760		MISAMFU	ZB	-1010	+03125	+1536
675750		MKUSHI	ZB	-1363	+02943	+1237
676330	FLMG	MONGU	ZB	-1525	+02315	+1053
676670		MOUNT MAKULU	ZB	-1555	+02825	+1213
674770	FLMP	MPIKA	ZB	-1190	+03143	+1402
675800		MSEKERA	ZB	-1365	+03256	+1025
676550		MUMBWA	ZB	-1506	+02718	+1218
674410	FLMW	MWINILUNGA	ZB	-1175	+02443	+1363
675610	FLND	NDOLA	ZB	-1300	+02865	+1270
676730	FLPE	PETAUKE	ZB	-1425	+03128	+1036
674690		SAMFYA	ZB	-1135	+02953	+1171
677310	FLSN	SENANGA	ZB	-1610	+02326	+1027
675710	FLSE	SERENJE	ZB	-1323	+03021	+1384
677410	FLSS	SESHEKE	ZB	-1746	+02430	+0951
675510	FLSW	SOLWEZI	ZB	-1218	+02638	+1386
675310	FLZB	ZAMBEZI	ZB	-1353	+02311	+1078

1.3 Results: Climatic Projections for the 21st Century

Projected temperature rises, for which there is reasonable agreement among the six GCMs studied, are very large – about 3°C for emissions scenario B1 and 5°C for A2. Projected precipitation changes are small but are associated with large uncertainty, not unexpected given that the simulation of precipitation remains one of the principal challenges in global climate modeling.

1.3.1 Temperature

Figure A1-5 shows the projected mean annual temperature for the six GCMs studied, and their mean (black line), for Zambia and for Kafue river basin. The river basin's mean annual temperature is about 0.5°C cooler than the mean for Zambia. The spread among the six models in Figure A1-5 is reasonably small, all projecting large temperature rises over this century.

Projected temperature rise is similar for Zambia and the Kafue River Basin are about the same, the six-model average equaling about 3°C for emissions scenario B1, and 5°C for A2 (Figure A1-5). Model ECHAM5/MPI-OM projects the highest temperature increases (about 4°C and 6°C for scenarios B1 and A2, respectively).

The 30-year running means of the temperature projections in Figure A1-2 are shown in Figure A5-3. The plotting position corresponding to a given year (e.g., 2015), represents the mean in 2000-2029. Thus, the plotted lines do not extend to the first 15 years (1950-1964) or the last 14 years (2086-2099). Because most of the noise from year-to-year variability has been removed, the long-term trends are more clearly seen in Figure A1-6 than in Figure A1-2. The trends themselves (given in °C per year) are plotted in Figure A5-4, for the Kafue river basin. For scenario B1 (top panel of Figure A5-4), the average trend of all models remains fairly constant throughout the 21st century, with an average value of 0.023 °C/year. For scenario A2 (bottom panel of Figure A5-4), the model-average trend rises over the course of the 21st century, reaching values as high as 0.06 °C per year by century's end. The overall average trend for A2 is 0.036 °C/year (for 1965-2085).

Figure A1-8 shows the simulated seasonal temperature for the four seasons, for the A2 emission scenario, spatially averaged over the Kafue river basin. Projected temperature rise is greatest (about 6°C) for the spring season (September-November). It is least (about 4°C) for the summer season (December-February), which is the principal rainy season. Figure A1-9 shows projected temperature for each of the 12 months, for the end-of-century time horizon, for scenarios B1 and A2 over Kafue river basin.

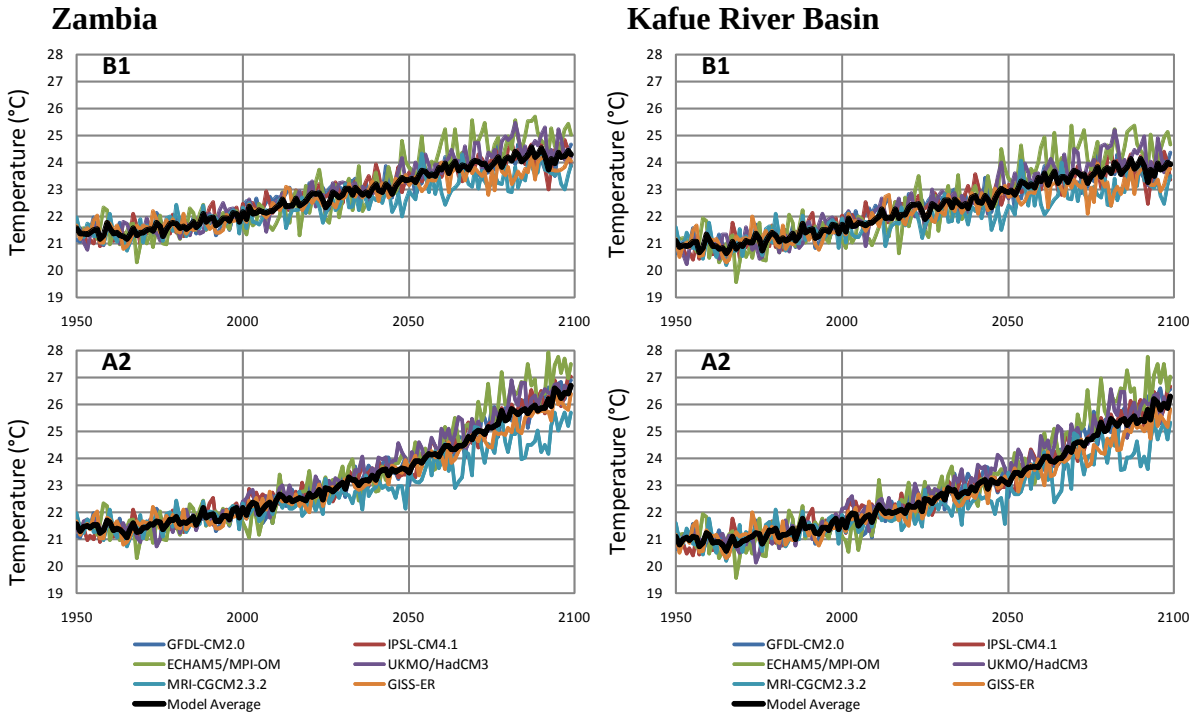

Figure A1-5: Simulated annual time series of temperature spatially averaged over Zambia (left panels) and the Kafue river basin (right panels), for the B1 (top) and A2 (bottom) emission scenarios.

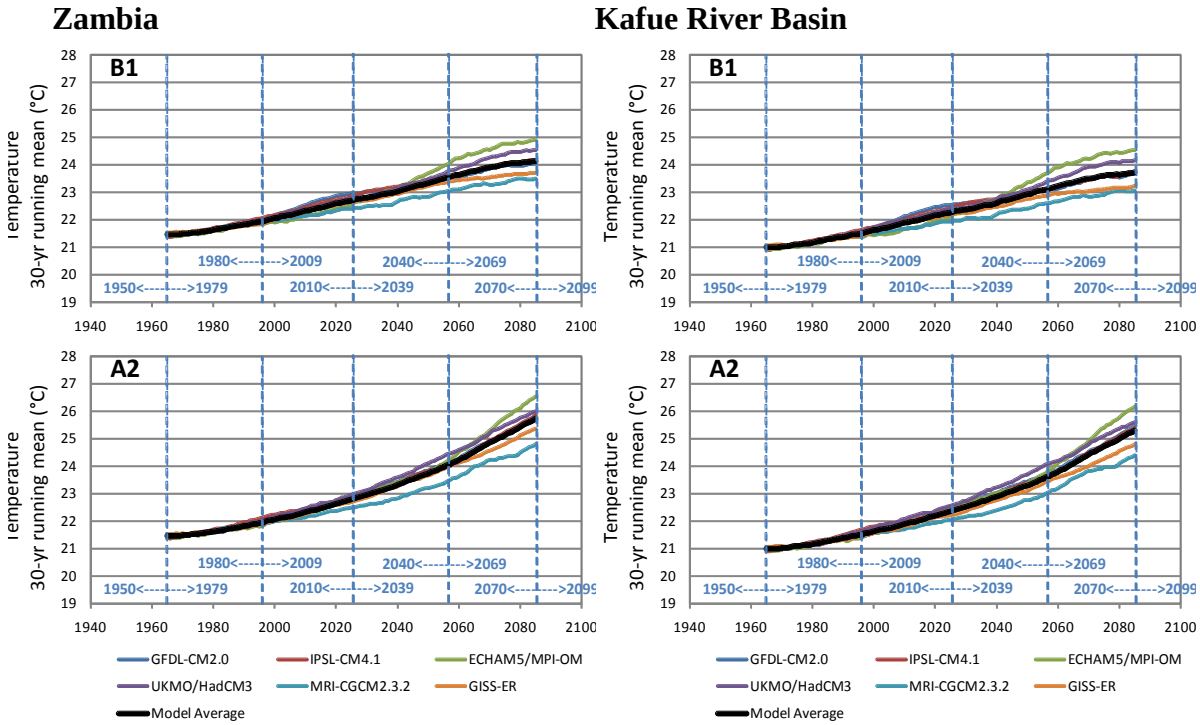

Figure A1-6: Thirty-year running means of the simulated annual time series of temperature spatially averaged over Zambia (left panels) and the Kafue river basin (right panels), for the B1 (top) and A2 (bottom) emission scenarios. In every case, model ECHAM5/MPI-OM projects the highest temperatu increases, and MRI-CGCM2.3.2 projects the lowest. Trends for Zambia and Kafue river basin are similar, the basin having about 0.5°C cooler temperatures than the Zambian average at any projecte time. See the subsequent figure for quantification of the trends seen here for Kafue river basin.

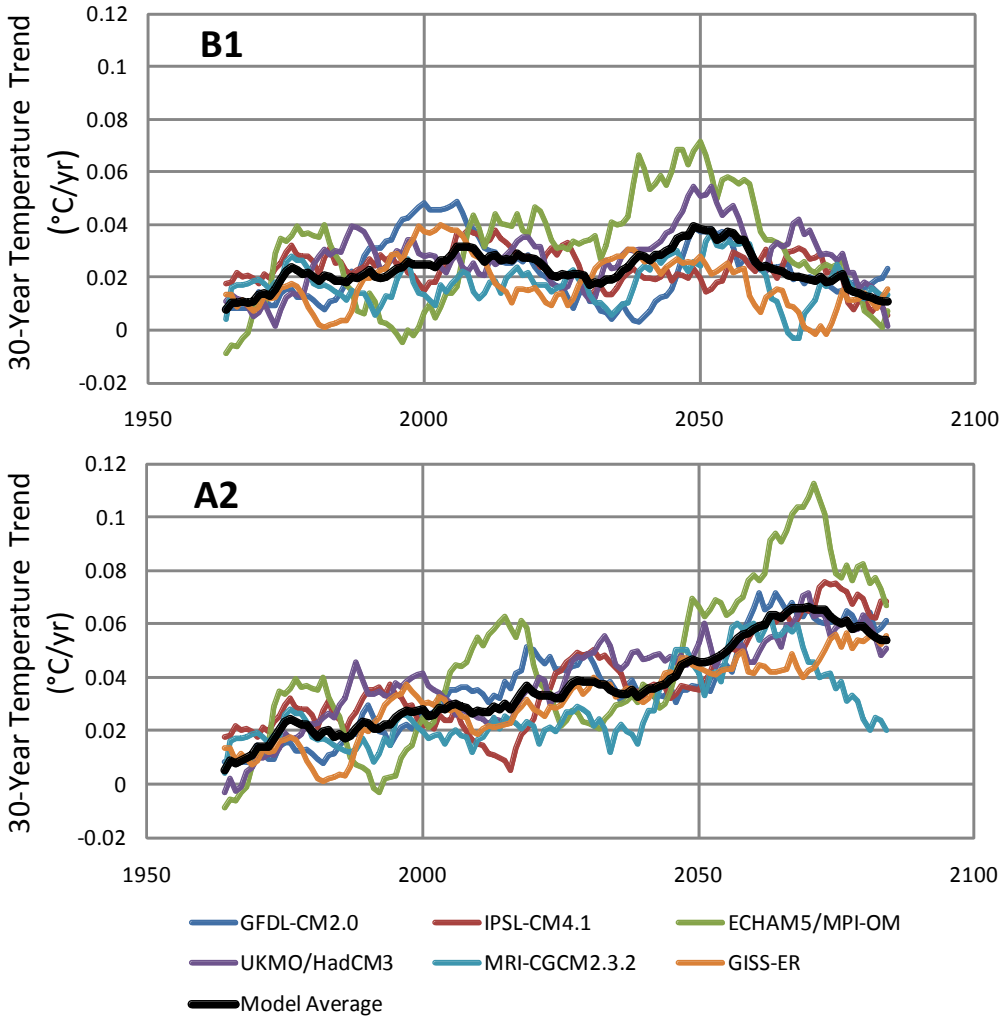

Figure A1-7: Thirty-year running trends, given in °C per year, in simulated temperature spatially averaged over the Kafue river basin. For scenario B1 (top panel), the average trend of all models remains fairly constant throughout the 21st century, with an average value of 0.023 °C/year. For scenario A2 (bottom panel), the model-average trend rises over the course of the 21st century, reaching values as high as 0.06 °C per year by century's end. The overall average trend for A2 is 0.036 °C/year.

A2

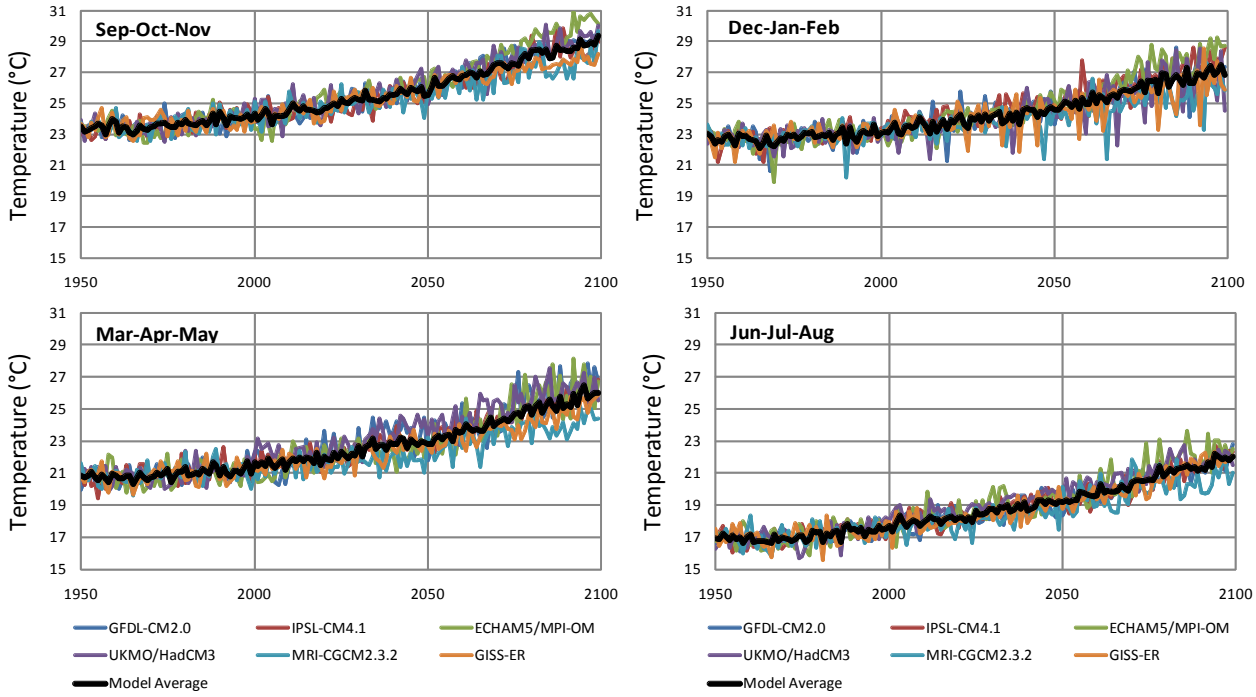

Figure A1-8: Simulated seasonal temperature (for the four seasons: SON, DJF, MAM and JJA), for the A2 emission scenario, spatially averaged over the Kafue river basin. Projected temperature rise is greatest (about 6°C) for the spring season (September-November). It is least (about 4C) for the summer season (December-February), which is the principal rain season.

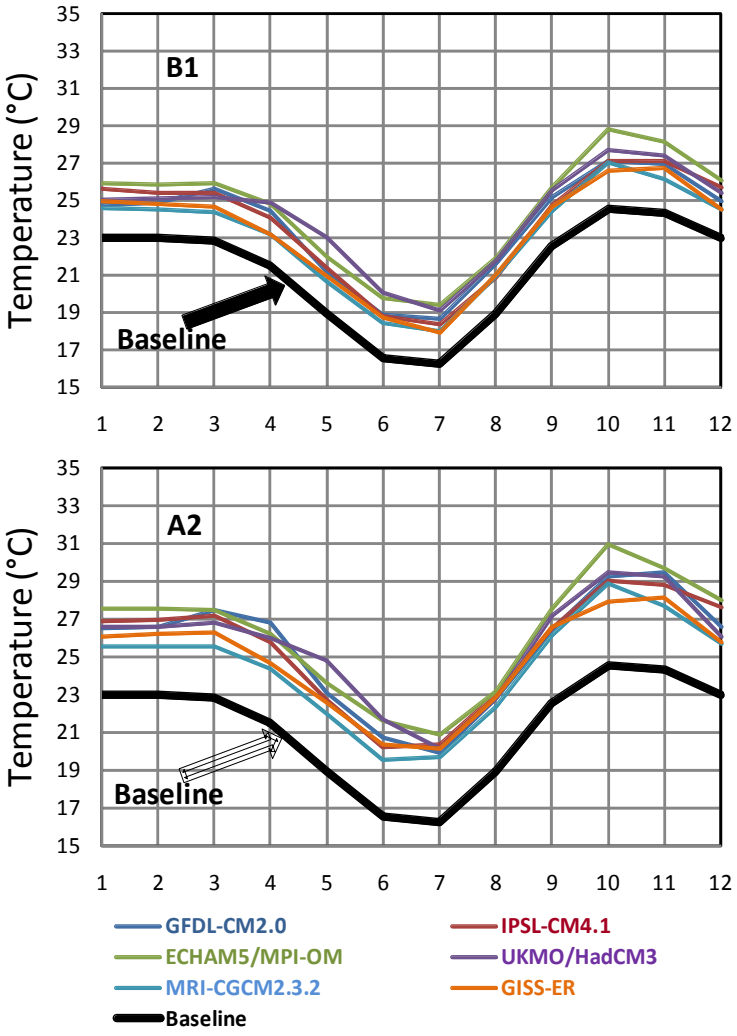

Figure A1-9: Simulated mean monthly temperature for the end of century time horizon (2070-2099) and baseline (1950-1999), spatially averaged over the Kafue river basin.

1.3.2 Precipitation

The mean annual precipitation projected through the 21st century by the six GCMs, and the model average (black line), are shown in Figure A1-10. None of the models projects significant changes in mean annual precipitation, for either emissions scenario B1 or A2. This is also clear from the plots of 30-year running means in Figure A1-11, and the plots for monthly projections in Figure A1-12. Projections specific to the wet season are shown in Figure A1-13, also showing little change.

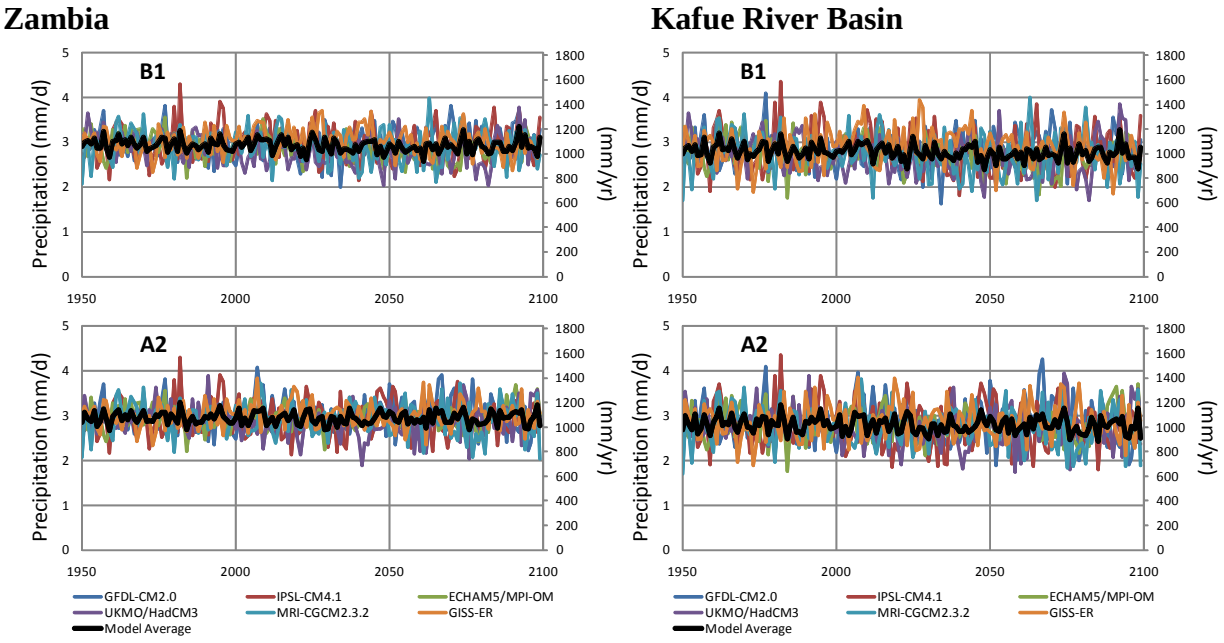

Figure A1-10: Simulated annual time series of precipitation spatially averaged over Zambia (left panels) and the Kafue river basin (right panels), for the B1 (top) and A2 (bottom) emission scenarios.

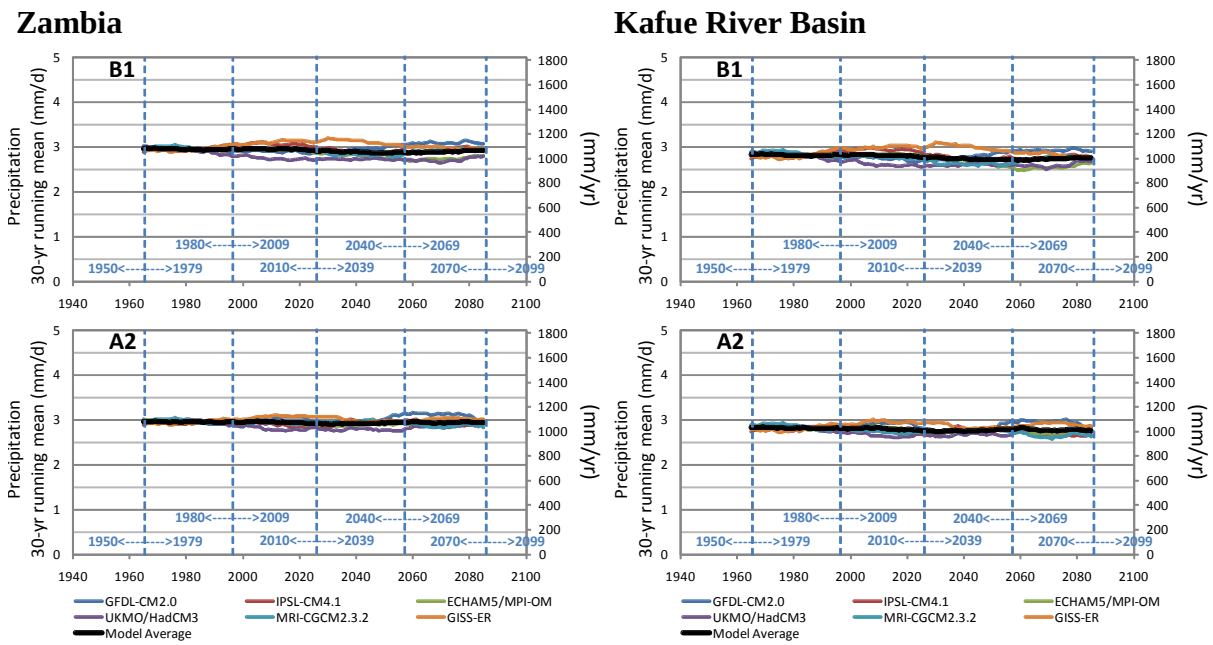

Figure A1-11: Thirty-year running means of the simulated annual time series of precipitation spatially averaged over Zambia (left panels) and the Kafue river basin (right panels), for the B1 (top) and A2 (bottom) emission scenarios.

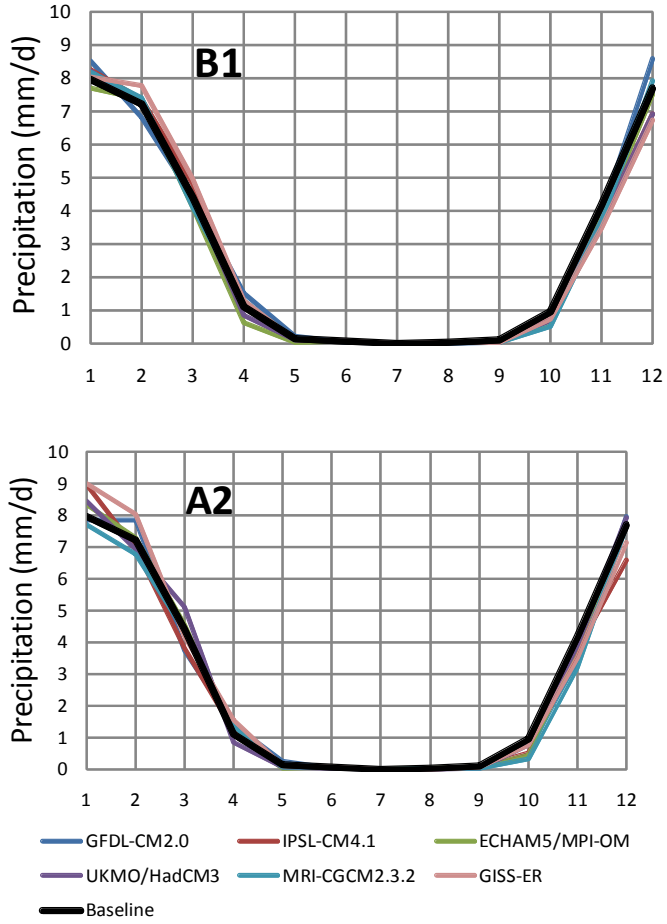

Figure A1-12: Simulated mean monthly precipitation for the end of century time horizon (2070-2099) and baseline (1950-1999), spatially averaged over the Kafue river basin. Projected changes are slight for all models.

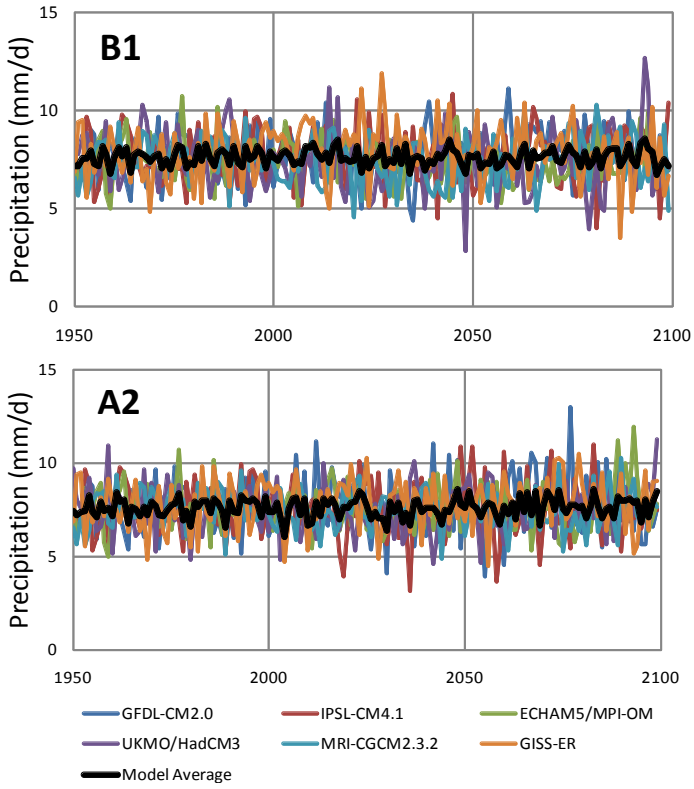

Figure A1-13: Simulated precipitation in the wet season (summer, i.e., December-February), spatially averaged over the Kafue river basin, for emissions scenarios B1 (top) and A2 (bottom).

1.3.3 Projected Spatial Patterns of Climatic Change and Variability

The spatial variability and pattern of temperature and precipitation changes are displayed in Figures A1-14, A1-15 and A1-16.

Figure A1-14 shows the spatial distribution over Zambia of the projected trend in mean annual temperature under the B1 and A2 emission scenarios, for 2070-2099 relative to the 1950-1999 baseline. Units are °C per decade. All six GCMs project temperature rises over all regions for both scenarios. The maximum local rise is, for B1, 0.45°C per decade (4.5°C over the 21st century) for Zambia, and 0.4°C (4.0°C over the 21st century) for the Kafue river basin; and for A2, 0.69°C per decade (6.9°C over the 21st century) for Zambia, and 0.5°C (5.0°C over the 21st century) for the Kafue river basin. Spatial patterns differ notably among models.

Figure A1-15 shows the spatial distribution of the projected trend in mean annual precipitation under the B1 and A2 emission scenarios, for 2070-2099 relative to the 1950-1999 baseline. Units are mm/day per decade. The GCMs project small precipitation rises as well as small declines, depending on spatial location and on the model. Maximum local changes are a 2% increase for B1, and 3% for A2.

B1

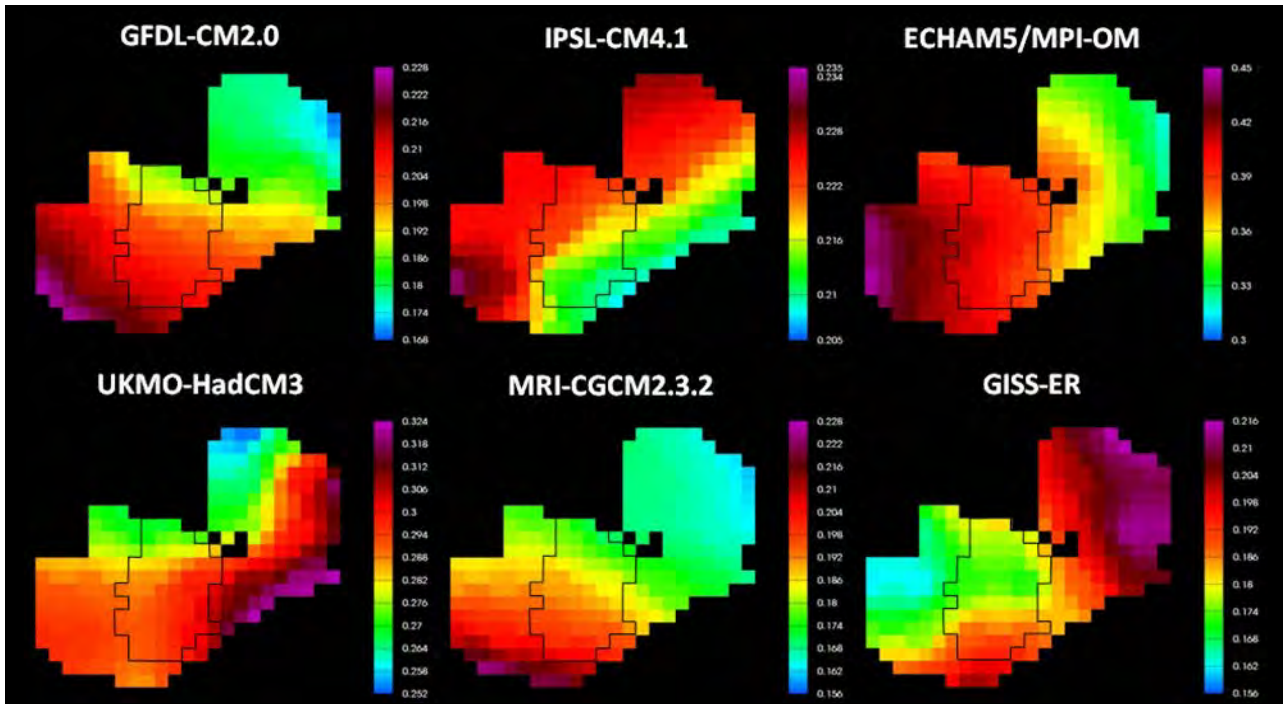

A2

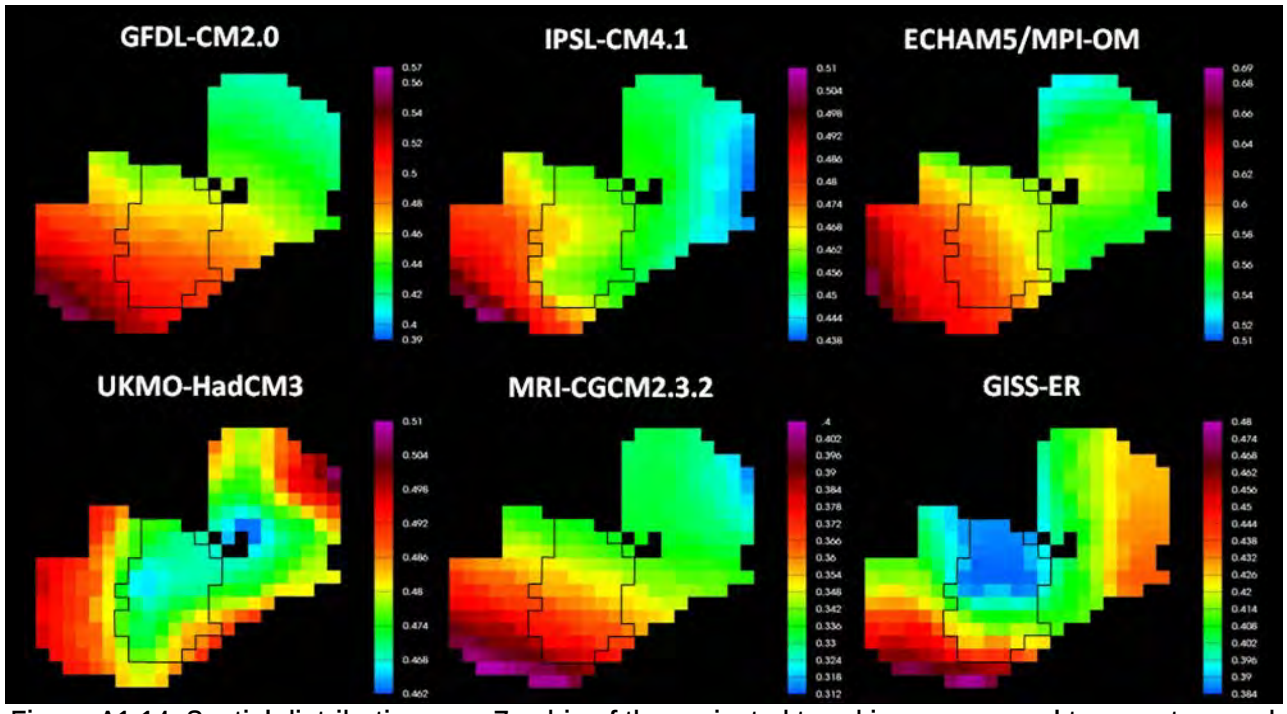

Figure A1-14: Spatial distribution over Zambia of the projected trend in mean annual temperature under the B1 (top) and A2 (bottom) emission scenarios, for 2070-2099 relative to the 1950-1999 baseline. Units are °C per decade. All six GCMs project temperature rises over all regions for both scenarios. The maximum local rise is, for B1, 0.45°C per decade (4.5°C over the 21st century) for Zambia, and 0.4°C (4.0°C over the 21st century) for the Kafue river basin; and for A2, 0.69°C per decade (6.9°C over the 21st century) for Zambia, and 0.5°C (5.0°C over the 21st century) for the Kafue river basin.

B1

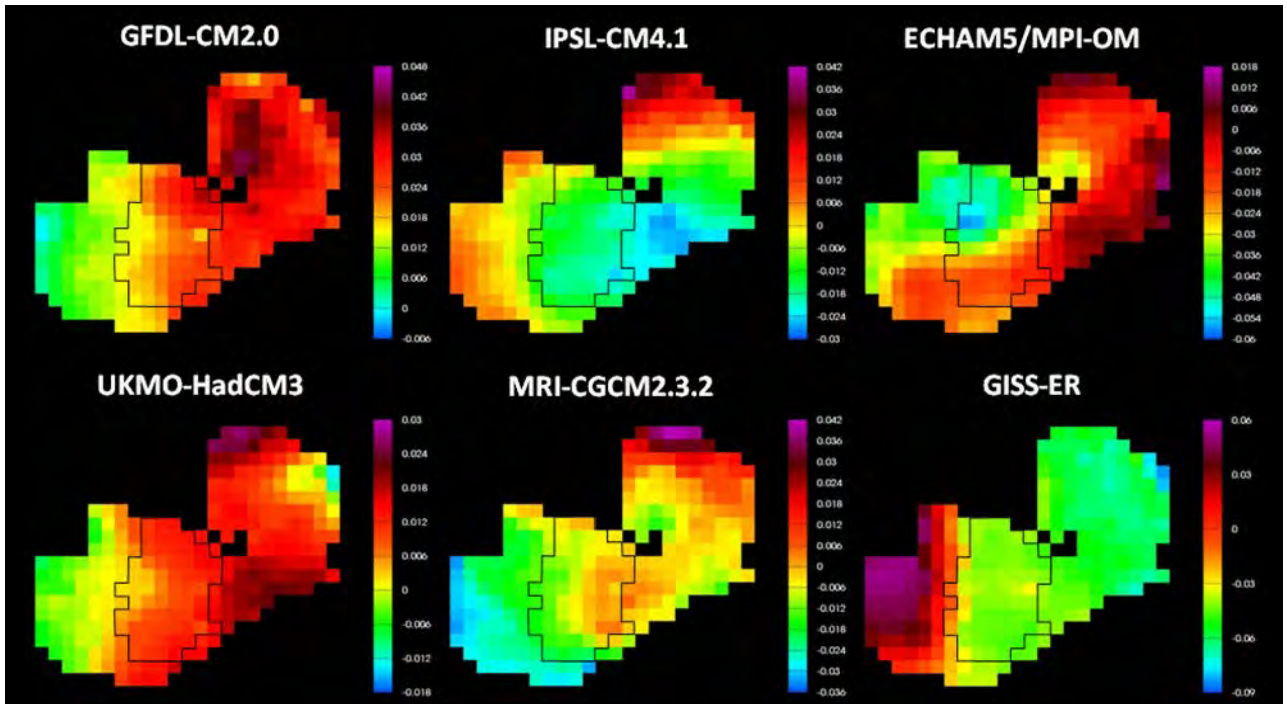

A2

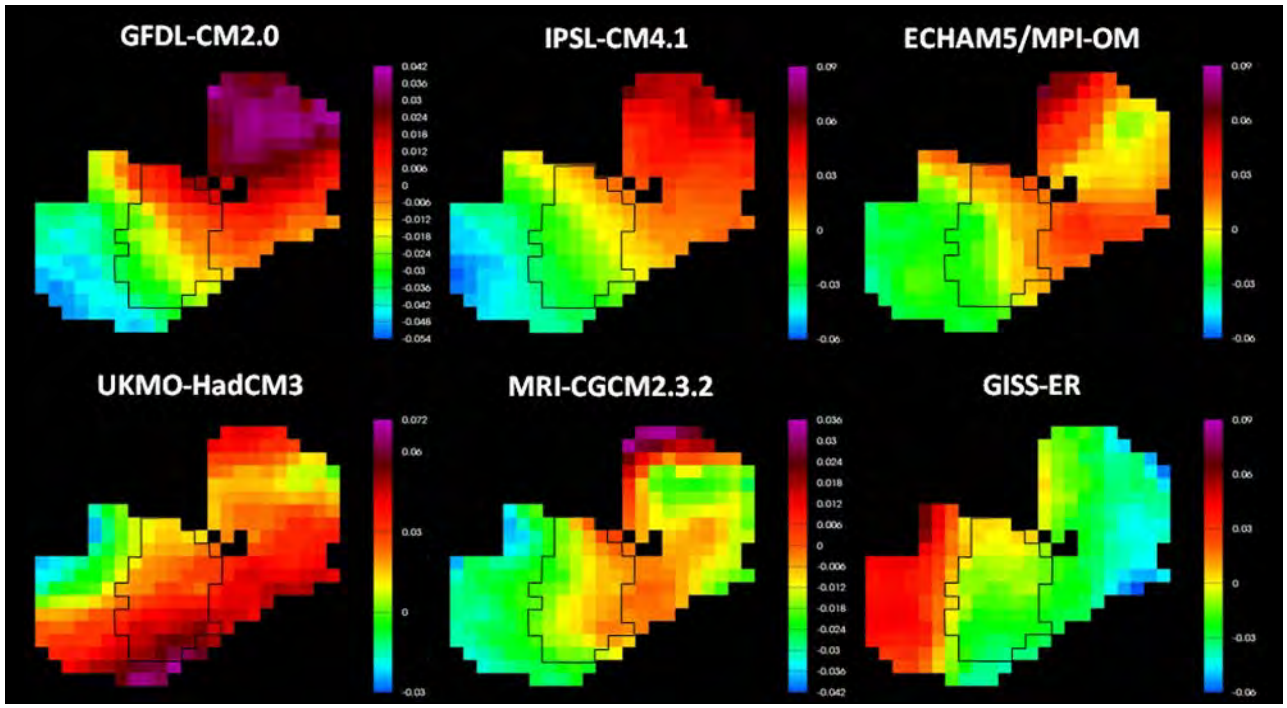

Figure A1-15: Spatial distribution over Zambia of the projected trend in mean annual precipitation under the B1 (top) and A2 (bottom) emission scenarios, for 2070-2099 relative to the 1950-1999 baseline. Units are mm/day per decade. The GCMs project small precipitation rises as well as small declines, depending on spatial location and on the model. Maximum local changes are a 2% increase for B1, and 3% for A2.

B1

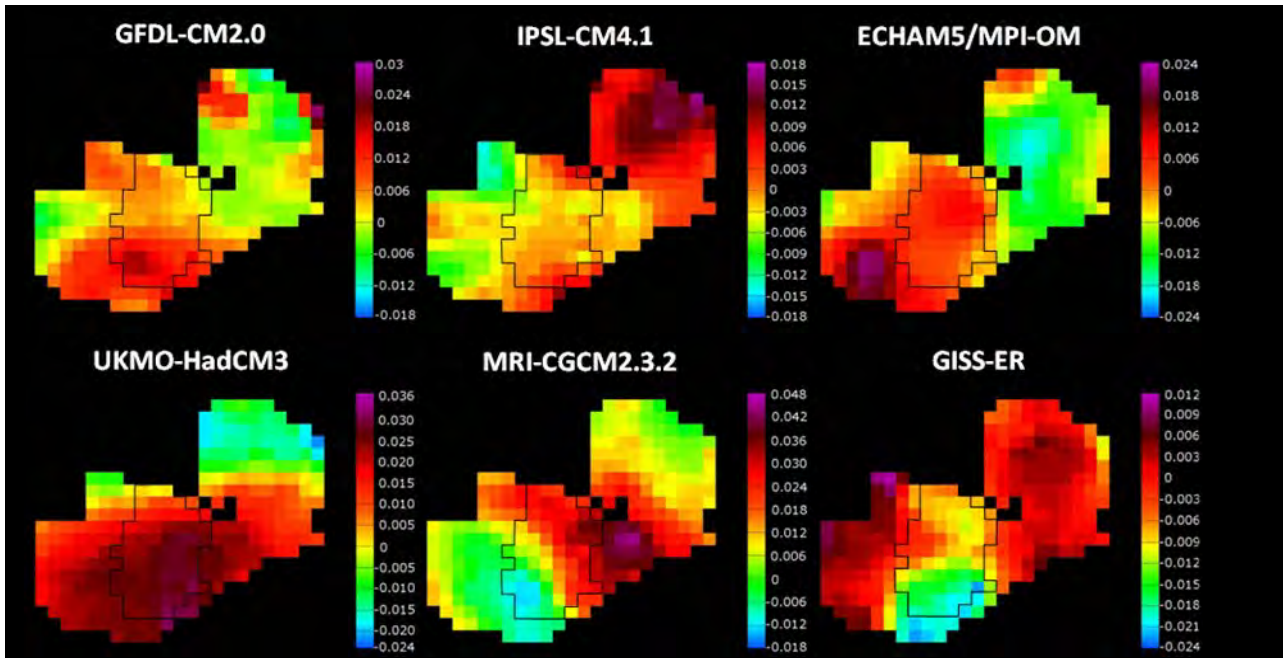

A2

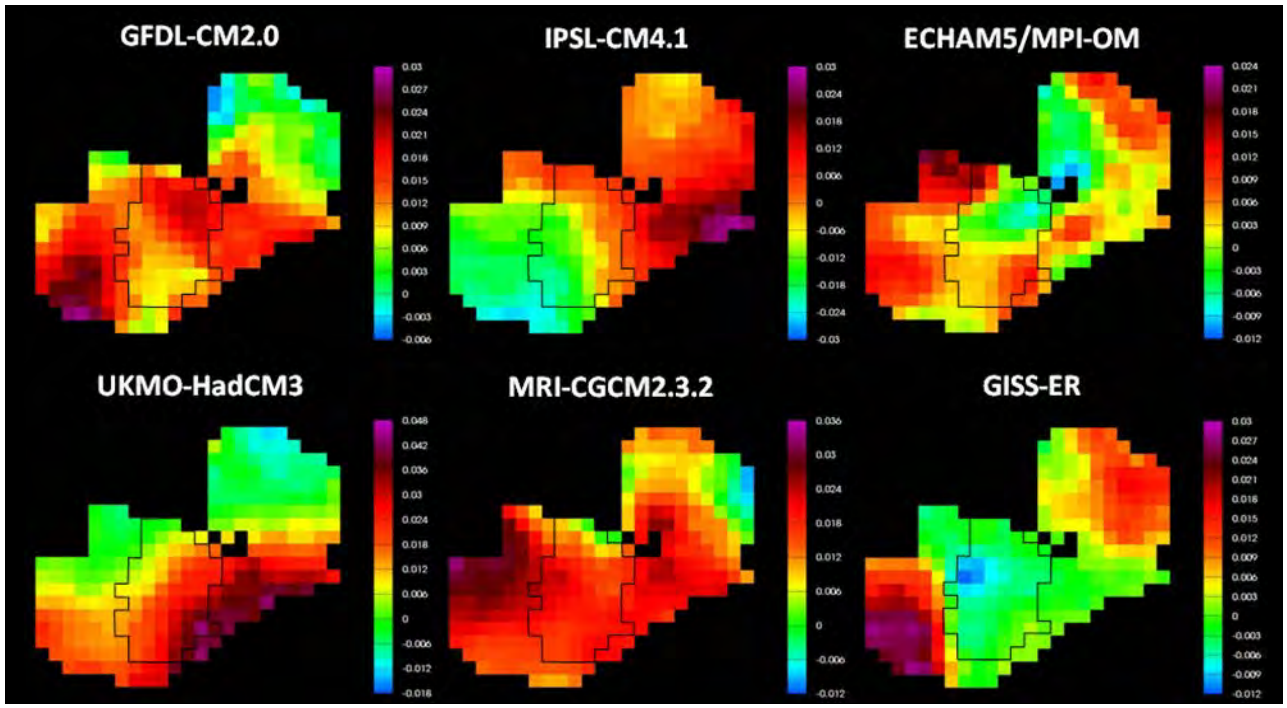

Figure A1-16: Spatial distribution over Zambia of the projected trend in the standard deviation of annual precipitation; a measure of year to year variability, under the B1 (top) and A2 (bottom) emission scenarios, for 2070-2099 relative to the 1950-1999 baseline. Units are mm/day per decade. Under either scenario, all GCMs project rises or declines in precipitation variability, depending on location. For scenario A2, projected changes range from -0.024 to 0.046 mm/d per decade.

1.4 Conclusions

The projected temperature rise – about 3°C for emissions scenario B1 and 5°C for A2 – is capable of greatly altering the geophysical, ecological, agricultural, economic, and human livelihood and health environment of Zambia. The highest temperature rises are projected for spring (September-November), reaching 6°C for the A2 scenario. Projected precipitation changes are small but are associated with large uncertainty, given that the simulation of precipitation remains one of the principal challenges in global climate modeling.

The geophysical impacts of climate change in Zambia and Kafue river basin, as derived from the downscaled CMIP3 model runs, are likely to be dominated by rises in evapo-transpiration and ecological and agricultural demand for water. The projected changes in evaporative demand can be expected to have substantial impacts on Zambian geophysical and ecological environment.

The temperature and precipitation changes projected for the 21st century, from the SCU downscaled CMIP3 results, are very large – about 3°C for greenhouse emissions scenario B1 and 5°C for A2. The highest temperature rises are projected for spring (September-November), reaching 6°C for the A2 scenario. For precipitation, no significant changes are projected. Representation of precipitation processes remains one of the principal challenges in global climate modeling, and these precipitation projections are associated with substantial uncertainty. A brief discussion on sources of uncertainty in GCM climate projections is included below.

1.5 Uncertainty

The uncertainties associated with GCM-based projections of climate change from CMIP3 have been categorized as 1) unknown future emissions of greenhouse gases; 2) uncertain response of the global climate system to increases in greenhouse gas concentrations; and 3) incomplete understanding of the regional manifestations that will result from global changes (IPCC, 2001). The first two are the largest sources of uncertainty and are of roughly equal magnitude on a global scale (Karl and Trenberth, 2003; Wigley and Raper, 2001). It is worth restating the following points about uncertainty.

Future Greenhouse Gas Emissions: up until year 2030, there is little uncertainty concerning GHG concentrations, and all SRES emissions scenarios agree closely on concentrations (as shown in Figure A1-1). This is because concentrations up until 2030 depend largely on emissions that have already taken place (see e.g. Trenberth, 2010). Significant divergence in concentrations after about 2030 among different emission scenarios starts about mid-century.

Climate response to rising GHG concentrations: due to complex interactions between the ocean, land, and atmosphere, the chaotic nature of the climate system, and the imperfect representation of the physics of the climate in climate models, our present ability to simulate climatic responses to greenhouse gas concentrations is limited. One of the most challenging processes is precipitation, whose representation remains poor in these models, for different reasons including the coarse scale and absent representation of surface features such as mountain ranges and coastlines. Global climate models do, however, represent our current understanding of the climate system at their coarse scale and are in that sense appropriate for obtaining plausible

projections of climatic responses. Because of differences in the representation of the physical processes, different global climate models can exhibit a wide range of sensitivity to changing GHG levels. To sample some of this uncertainty, we included six global climate models in this chapter. Even the entire realm of all CMIP3 model results does not represent certainty, because the true climatic response of the natural system may lie outside of this realm.

Regional climate response: to evaluate the regional response over Zambia and Kafue river basin to a given global change projection, statistical downscaling was used to translate the large-scale signal (from a global climate model) to the regional scale. This is an appropriate and accepted methodology, however it also introduces some uncertainty into the results.

1.6 References

Adam, J. C. and Lettenmaier, D. P. (2003): Adjustment of global gridded precipitation for systematic bias, *J. Geophys. Res.* 108: 1–14.

Christensen, J.H., B. Hewitson, A. Busuioc, A. Chen, X. Gao, I. Held, R. Jones, R.K. Kolli, W.-T. Kwon, R. Laprise, V. Magaña Rueda, L. Mearns, C.G. Menéndez, J. Räisänen, A. Rinke, A. Sarr and P. Whetton (2007): Regional climate projections. *In*: *Climate Change 2007: The Physical Science Basis. Contribution of Working Group I to the Fourth Assessment Report of the Intergovernmental Panel on Climate Change* S. Solomon, D. Qin, M. Manning, Z. Chen, M. Marquis, K. B. Averyt, M. Tignor and H.L. Miller. Cambridge University Press, Cambridge, United Kingdom and New York, NY, USA. Available at: http://www.ipcc.ch/

Houghton, J.T., Y. Ding, D.J. Griggs, M. Noguer, P.J. van der Linden, and D. Xiaosu (2001): *Climate Change 2001: The scientific basis. Contribution of Working Group I to the third assessment report of the Intergovernmental Panel on Climate Change.* Cambridge University Press, 881 pp.

IPCC, 2001: Climate Change 2001: the scientific basis. Contribution of Working Group I to the third assessment report of the Intergovernmental Panel on Climate Change. In: Houghton JT, Ding Y, Griggs DJ, Noguer M., van der Linden P.J., Dai X., Maskell K., Johnson C.A. (eds) Cambridge University Press, 881 pp.

Kalnay, E., M. Kanamitsu, R. Kistler, W. Collins, D. Deaven, L. Gandin, M. Iredell, S. Saha, G. White, J. Woollen, Y. Zhu, A. Leetmaa, and B. Reynolds (1996): The NCEP/NCAR 40-year reanalysis project. *Bulletin of the American Meteorological Society* 77: 437-472.

Karl, T. R., and K. E. Trenberth (2003), Modern global climate change, Science, 302, 1719–1723.

Legates, D.R. and C.J. Willmott (1990a): Mean seasonal and spatial variability of global surface air temperature. *Theoretical and Applied Climatology* 41: 11-21.

Legates, D.R. and C.J. Willmott (1990b): Mean seasonal and spatial variability in gauge-corrected, global precipitation. International Journal of Climatology 10: 111-127.

Maurer, E.P., J.C. Adam, and A.W. Wood (2009): Climate Model based consensus on the hydrologic impacts of climate change to the Rio Lempa basin of Central America, *Hydrology and Earth System Sciences* 13: 183-194. Available at: http://www.hydrol-earth-syst-sci.net/13/183/2009/hess-13-183-2009.html

Meehl, G. A., C. Covey, T. Delworth, M. Latif, B. McAvaney, J. F. B. Mitchell, R. J. Stouffer, and K. E. Taylor (2007): The WCRP CMIP3 multi-model dataset: A new era in climate change research, *Bulletin of the American Meteorological Society* 88: 1383-1394.

Mitchell, T.D., T.R. Carter, P.D. Jones, M. Hulme, and M.G. New (2004): A comprehensive set of high-resolution grids of monthly climate for Europe and the globe: the observed record (1901-2000) and 15 scenarios (2001-2100). Tyndall Center for Climate Change Research, University of East Anglia, Norwich, UK, 30 pp.

Nakicenovic, N., J. Alamo, G. Davis, B. De Vries, J. Fenhann, S. Gaffin, K. Gregory, A. Grübler, T. Yong Jung, T. Kram, E. Lebre La Rovere, L. Michaelis, S. Mori, T. Morita, W. Pepper, H. Pitcher, L. Price, K. Riahi, A. Roehrl, H.-H. Rogner, A. Sankovski, M. Schlesinger, P. Shukla, S. Smith, R. Swart, S. van Rooijen, N. Victor, and Z. Dadi (2000): Special report on emissions scenarios. Cambridge University Press, 570 pp.

New, M.G., M. Hulme, and P.D. Jones (2000): Representing twentieth-century space-time climate variability. Part II: development of 1961-1990 monthly grids of terrestrial surface climate. J. Climate 12: 829-856.

Nijssen, B., R. Schnur, and D.P. Lettenmaier (2001): Global retrospective estimation of soil moisture using the VIC land surface model, 1980-1993. *J. Climate* 14: 1790-1808.

Peterson, T.C., and R.S. Vose (1997): An overview of the Global Historical Climatology Network temperature data base. Bulletin of the American Meteorological Society 78: 2837-2849.

Raupach, M.R., G. Marland, P. Ciais, C. LeQuere, J.G. Canadell, and C.B. Field (2007): Global and regional drivers of accelerating CO2 emissions. *Proceedings of the National Academy of Sciences* 104: 10288-10293. doi:10.1073/pnas.0700609104.

Sheffield, J., G. Goteti, and E.F. Wood (2006): Development of a 50-yr high-resolution global dataset of meteorological forcings for land surface modeling. *J. Climate* 19: 3088-3111.

Shepard, D. (1968): A two-dimensional interpolation function for irregularly spaced data. In *Proceedings of the 1968 23rh ACM National Conference*, 517-523.

Trenberth, K. (2010): More knowledge, less certainty. *Nature reports climate change*, v.4, February 2010.

van Rheenen, N.T., A.W. Wood, R.N. Palmer, and D.P. Lettenmaier (2004): Potential implications of PCM climate change scenarios for Sacramento-San Joaquin River Basin hydrology and water resources. Climatic Change 62:257-281.

Wigley, T. M. L., and S. C. B. Raper (2001), Interpretation of high projections for global-mean warming, Science, 293, 451– 454.

Wood, A.W., E.P. Maurer, A. Kumar, and D.P. Lettenmaier (2002): Long-range experimental hydrologic forecasting for the eastern United States. *J. Geophysical Research – Atmospheres* 107: 4429. doi:10.1029/2001JD000659.

Wood, A. W., Leung, L. 5 R., Sridhar, V., and Lettenmaier, D. P. (2004): Hydrologic implications of dynamical and statistical approaches to downscaling climate model outputs, *Climatic Change* 62: 189–216.

Willmott, C.J., and D.R. Legates (1991): Rising estimates of terrestrial and global precipitation. *Climate Research* 1: 179-186.

Willmott, C.J. and K. Matsuura (2001): Terrestrial air temperature and precipitation: Monthly and annual time series (1950-1999). Center for Climate Research, University of Delaware, Newark, DE. Available at http://climate.geog.udel.edu/~climate/html_pages/archive.html.

Willmott, C.J., and S.M. Robeson (1995): Climatologically Aided Interpolation (CAI) of terrestrial air temperature. *International Journal of Climatology* 15: 221-229.

Willmott, C.J., C.M Rowe, and W.D. Philpot (1985): Small-scale climate maps: A sensitivity analysis of some common assumptions associated with grid-point interpolation and contouring. *American Cartographer* 12: 5-16.

Appendix A2

Hydrologic Modeling: HEC-HMS

This section describes the development and implementation of the study's hydrologic model. The U.S. Army Corps of Engineers (USACE) Hydrologic Engineering Center-Hydrologic-Modeling System (HEC-HMS) model was applied as the hydrologic modeling tool. This model is widely used for hydrologic modeling and is publically available from the USACE at no cost. The study used publically available tools, wherever possible, to allow further use by ZESCO as additional data become available or local conditions evolve. This section presents, (1) an introduction to the HEC-HMS model, (2) steps involved in model set up (general), (3) development of the project-specific model to represent the Kafue River Basin (project study area); (4) calibration and validation of the model using historic observed flow data; and (5) modeling of flows using the climate change projections (obtained from the climate modeling effort described in Section 3.1).

2.1 Introduction to HEC-HMS

This section introduces the model, including (1) model description, (2) model limitations and assumptions, and (3) general steps to establish the model for a particular basin.

2.1.1 Model Description

The HEC-HMS model is a generalized modeling system capable of representing many different watersheds. HEC-HMS is designed to simulate the precipitation-run-off processes of dendritic watershed systems. It is applicable across a wide range of geographic areas for addressing a wide range of project goals. Applications include large river basin water supply and flood hydrology, as well as supporting small urban or natural watershed run-off modeling (USACE, 2009).

To apply the model for a specific purpose and location, a model of the watershed is constructed by separating the hydrologic cycle into manageable pieces, by constructing boundaries around the watershed of interest, and establishing the appropriate geographic and other parameter data in the model. The model provides a completely integrated work environment, including a database, data entry utilities, computation engine, and results reporting tools, with a graphical user interface. Additional information on the model is available at: http://www.hec.usace.army.mil/software/hec-hms/.

2.1.2 Model Strengths, Limitations, and Assumptions

The HEC-HMS model has been widely applied for a range of hydrologic modeling purposes in the U.S. and internationally and uses standard hydrologic modeling approaches and equations that are widely accepted. Background documents reviewed for this study indicate that USACE modeling tools have been applied to the study area in the past (World Bank, 2009). The model can provide a water budget for most components of the hydrologic cycle. It is capable of modeling common types of hydraulic control structures, such as weirs, gates, pumps and

spillways. The model is also capable of exchanging data with the HEC Data Storage System (DSS), a database system designed to efficiently store and retrieve scientific data (USACE and South Florida Water Management District, 2002).

HEC-HMS is primarily a lumped modeling system in which, spatial variations in the physical processes are averaged over the watersheds or sub basins. Most of the models included in HEC-HMS are event based and deterministic (USACE, 2000). The model can also be applied for the continuous, long term simulation of rainfall-run-off.

The HEC-HMS model includes a number of assumptions (USACE, 1994), including: (1) precipitation excess and losses can be treated as basin-average (lumped) quantities; (2) the ordinates of a direct run-off hydrograph corresponding to precipitation excess of a given duration are directly proportional to the volume of excess (assumption of linearity); and (3) the direct run-off hydrograph resulting from a given increment of precipitation excess is independent of the time of occurrence of the excess (assumption of time invariance).

2.1.3 Major Steps for HEC-HMS Modeling

The core elements of the HEC-HMS model are the basin model, meteorological model, control specifications, and time series data manager. To develop the model for a particular use and location, seven steps are generally implemented. These are listed below, including the sub-section(s) of 2.2, 2.3, and 2.4 that discuss these steps for the KGL Kafue River Basin HEC-HMS model development:

- Basin Delineation (using HEC-GeoHMS) (Section 2.2.2)
- Creation of Basin Model (including all elements such as sub basins, channels, and reservoirs) (Section 2.2.3)
- Estimation of Physical Loss, Routing, and Transformation Parameters (for each sub basin element) (Section 2.3.2)
- Addition of Time Series Data (for various meteorological parameters) (Section 2.4.2)
- Setting Control Specifications (for running the model) (Section 2.5.2)
- Calibration and Validation (Sections 2.5 and 2.6)
- Interpretation of Flows at Critical Locations (Section 2.7)

The subsections below describe the application of these steps to develop the KGL Kafue River Basin HEC-HMS Model.

2.2 Model Development for Kafue River Basin

This section describes development of the HEC-HMS model for the KGL Kafue River Basin study area, including (1) basin delineation using HEC-GeoHMS, (2) creation of the basin model (including all elements such as sub basins, channels, and reservoirs), and (3) estimation of physical loss, routing, and transformation parameters (for each basin element). Before reviewing these steps, a brief description of the Kafue River Basin is provided.

2.2.1 Description of the Kafue River Basin

The Kafue River is one of the major tributaries of the Zambezi River. The area of Kafue River Basin measures about 156,000 square kilometers (km^2) and lies entirely within the borders of Zambia. The basin area occupies about 20% of Zambia's total land area. The Kafue River Basin originates in the Copper Belt Province (11° 33' 00" S, 27° 12' 56" E, at an elevation of 1,456 meters [m] above sea level). The basin is approximately 540 km long (North/South) and 320 km wide (East/West); the basin terminates at an elevation of 366 m above sea level at the confluence of the Kafue and the Zambezi Rivers (15° 56'36"S, 28° 55' 07"E). The total run length of the Kafue River is about 1500 km (Williams, 1977, Imagen Consulting Ltd, 2008). After originating at the Zambia-Congo divide, the Kafue River flows southwards or south-westwards close to the Lukanga Swamps and then into the Itezhi-Tezhi (IT) reservoir. The IT reservoir is a man-made reservoir that was constructed from 1973-1976 and provides water storage to support operation of the Kafue Gorge Upper (KGU) hydropower project (downstream of the reservoir). The KGU Dam and Hydropower Project were constructed in 1972. After the IT reservoir, the river turns eastwards and flows for approximately 350 km across the Kafue Flats and into the KGU reservoir. The Kafue Flats are a wide and flat area of the river, with natural water flow moving slowly across the flats at a shallow depth.

The Kafue River Basin plays a central role in Zambia's economy with most of the nation's mining, industrial, and agricultural activities and approximately 50% of Zambia's total population concentrated within the basin area (Mwelwa, 2004).

Figure A2-1: Location Map of Kafue River Basin

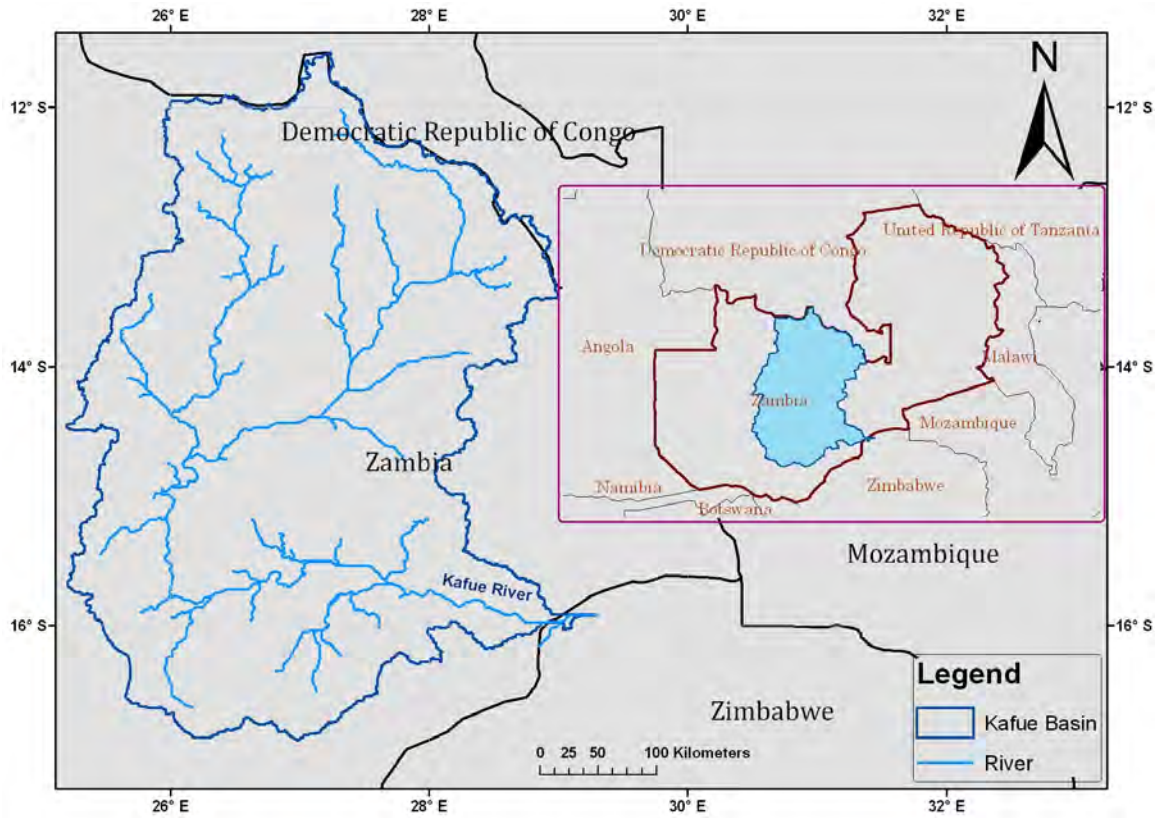

Figure A2-1 provides a location map for the Kafue River Basin; the figure shows the location of the basin within Zambia on the right hand and includes a representation of the major streams within the basin in the left portion of the figure.

Along the Kafue River, there are currently three areas with operating and/or planned hydropower projects: (1) IT dam (existing) and hydropower power plant (planned/existing in the short term); (2) KGU dam and hydropower plant (existing); and (3) the KGL dam and hydropower plant (planned). The planned KGL project is the focus of this risk assessment pilot project.

The KGL site lies about 65 km upstream of the confluence of the Kafue River with the Zambezi River, and about 20 km downstream from the existing KGU hydropower plant. Power unit capacities and operational parameters are presented in greater detail in the reservoir (energy) modeling section of this report (Section 2.2 and Appendix 3). For modeling purposes, all units (existing and planned) are modeled as operating power stations in this study.

Flow into the KGU reservoir is regulated by the IT dam, which creates the 6,008 million cubic meters (mcm) IT reservoir located on the Kafue River about 230 km upstream and west of the KGU hydropower project. Since the initiation of this climate risk assessment project for KGL, plans for a 120 megawatt (MW) turbine project at the IT dam have evolved rapidly. This new, planned capacity has been incorporated into the project assessment.

In addition to flows released from the IT dam, various local intervening inflows exist between the IT reservoir and the KGU hydropower project site. Flows released from the IT reservoir pass through the natural wetland area of the Kafue Flats. This area contains substantial environmental and ecological assets. Stakeholders including ZESCO, the World Wildlife Federation (WWF), and others are continuing to negotiate and plan for appropriate water release schemes from the IT reservoir to protect wildlife and fauna in the Kafue Flats area (Schelle and Pittock, 2005).

2.2.2 Basin Delineation Using HEC Geo-HMS

The project hydrologic model was established in a GIS framework using Environmental Systems Research Institute (ESRI) ArcGIS and HEC-GeoHMS 4.2 software. HEC-GeoHMS 4.2 is an extension application that supports identification of the river network and division of the catchment (basin area) into a number of sub areas. This procedure requires a digital elevation model (DEM). Figure A2-2 shows the Shuttle Radar Topography Mission (SRTM) 90 m resolution DEM produced by the U.S. National Aeronautics and Space Agency (NASA) (http://www2.jpl.nasa.gov/srtm/) and used for this project's basin and river network delineation. Using HEC Geo-HMS, the river network and sub basin are delineated using a step by step approach. The approach creates raster grids for catchment delineation. Activities to complete the model include addressing: filling sinks, flow direction, flow accumulation, catchment grid processing, and drainage line processing. Filling sinks is the process of numerical correction in the DEM, where large sinks (abnormal depressions) or voids are present.

Figure A2-2: Digital Elevation Data used for Delineation of Sub Basins

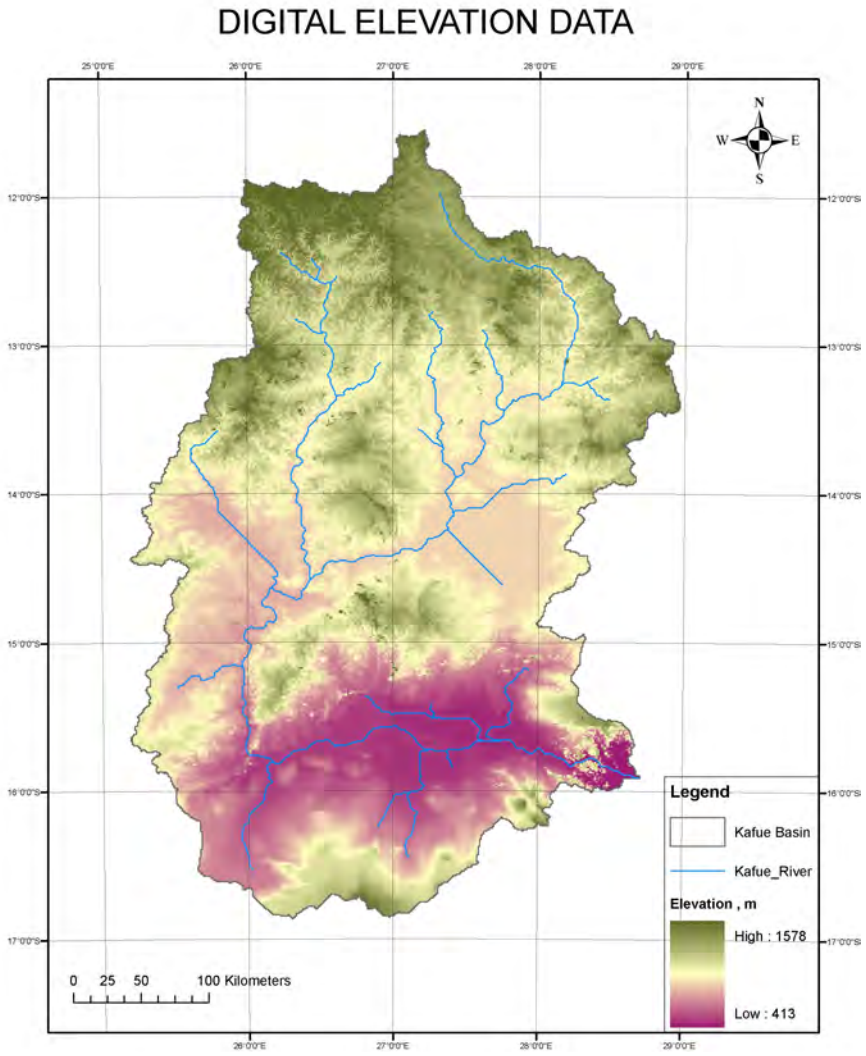

Physical representation of the basin incorporates various hydrologic elements (sub basins, river reaches, junctions, and reservoirs), which are connected in a dendritic network to simulate the rainfall-run-off process. Figure A2-3 shows the HEC-HMS schematic representation of the Kafue River Basin in the model. The Kafue River Basin hydrologic model includes 22 sub basins (also called sub catchments), 54 reaches, 28 junction elements, three dams (IT, KGU, and the proposed KGL), and the Kafue Flats (included as a pseudo reservoir). Stream flow gauging stations were incorporated to facilitate model calibration and validation, including from upstream to downstream: 4-669 Hook Bridge, 4-760 Namwala, and 4-977 Kasaka. After establishing the model's extent, it was compared to that provided in the literature (Imagen Consulting Ltd, 2008). The model's delineated area for the Kafue Basin is 154,500 km^2 compared to 156,000 km^2 reported in the literature. This correlates to a -1% difference which is acceptable, considering the resolution and accuracy of SRTM 90 m DEM.

Figure A2-3: HEC-HMS Schematic of the Kafue River Basin HEC-HMS Model

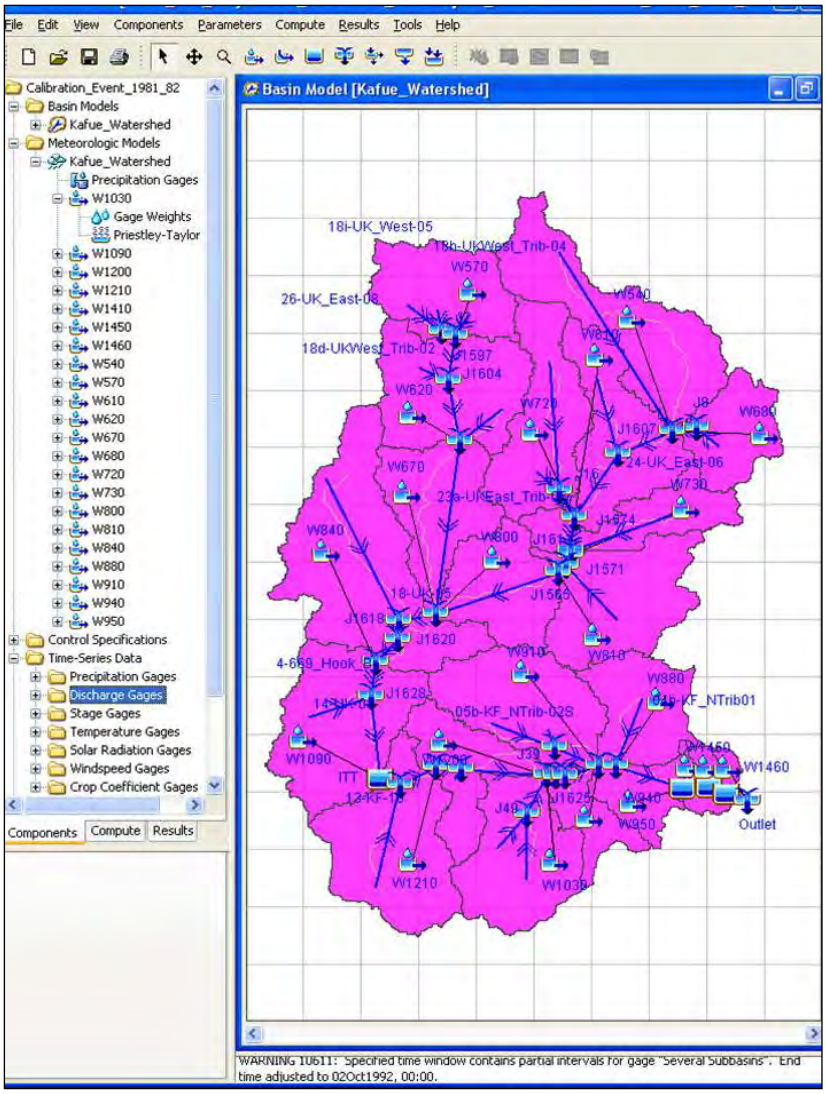

2.2.3 Hydrological Methods Applied For Basin and Meteorological Models

HEC-HMS allows the user to select from a number of methods to represent catchment characteristics. The methods used for this model include:

Basin Model:

- Rainfall Loss and Infiltration: Deficit and Constant Loss
- Rainfall-Runoff Transformation: U.S. Soil Conservation Service (SCS) Unit Hydrograph
- Stream Flow Routing: Muskingum Method
- Base Flow Method: Recession Method

Meteorological Model:

- Precipitation: Gauge Weights
- Evapotranspiration: Priestley-Taylor

These methods are summarized below and discussed further in Section 2.3.

Deficit and Constant Loss **-** The Deficit and Constant Loss Method uses a single soil layer to account for continuous changes in moisture content. This method is generally used in combination with a meteorological model that computes evapotranspiration. The potential evapotranspiration computed by the meteorological model is used in the hydrologic model to "dry out" the soil layer between precipitation events. Infiltration only occurs when the soil layer is saturated. The initial deficit is the initial soil condition for the method and indicates the amount of water that is required to saturate the soil layer to its maximum storage capacity. The maximum storage capacity is the amount of water the soil layer can hold, specified as a depth. The constant loss rate defines the infiltration rate when the soil layer is saturated. This constant loss applies only to unpaved areas of the sub-basin. In developed areas, the impervious surface cover is also accounted for because these areas do not allow water to infiltrate into the ground; the percentage of the sub basin which is considered an impervious area can be specified (USACE, 2009).

SCS Unit Hydrograph Transform Method **-** The transformation of excess precipitation into surface run-off is accomplished using the SCS Unit Hydrograph Transform Method. This method requires lag time as an input. The lag time was taken to be 60% of the time of concentration (USACE, 2005). The time of concentration represents the time required for a drop of water to travel from the most hydrologically remote point in the subcatchment to the outlet. The time of concentration (Tc) is calculated using the Kirpich formula (Kirpich, 1940), which requires the maximum length of flowpath and average slope of the watershed as inputs, as follows:

$$Tc\ (min) = 0.0078\ L^{0.77}\ S^{-0.385} \qquad (1)$$

Where L = flowpath length (m) and S = average slope (m/m).

Muskingum Method **-** The Muskingum Method (McCarthy, 1938) has been widely adopted for hydrologic flow routing and was used for stream flow routing through the streams. This method uses a simple conservation of mass approach to route flow through each stream. However, the method does not assume that the water surface is level. By assuming a linear, but non-level, water surface it is possible to account for increased storage during the rising side of a flood wave and decreased storage during the falling side. By adding a travel time for the stream and a weighting between the influence of inflow and outflow, it is possible to approximate attenuation. This method requires primarily two parameters, Muskingum K and X. The Muskingum K represents the travel time through the reach. For the KGL modeling effort, the Muskigum K was estimated from knowledge of the channel and flow properties. It was also used as a calibration parameter in the historic HEC-HMS runs for the study area. This approach is a general modeling practice that is applied when location specific data on a stream's geometry is not available.

The Muskingum X is the weighting between inflow and outflow influence; it can range from 0.0 to 0.5. In practical application, a value of 0.0 results in maximum attenuation and 0.5 results in no attenuation. Most stream reaches require an intermediate value estimated during the calibration process. This comprises a simplification of the continuity equation ($dS/dt = I-O$, where S is reach storage, t is time, I is reach inflow, and O is reach outflow); this equation assumes that inflow and outflow can be represented by simple linear functions and that:

$$S = K (x I - (1-x) O) \quad (2)$$

Where x is a dimensionless weighting factor and K is the travel time; X can vary between zero and 0.5, with typical values in the range 0.1 to 0.4.

The Recession (Base Flow) Method - The Recession (Base Flow) Method was implemented to estimate base flow. This method approximates the typical behavior observed in watersheds when channel flow recedes exponentially after an event. This method is intended primarily for event simulation. However, it also has the ability to automatically reset after each storm event and consequently may be used for continuous simulation. The initial base flow at the beginning of a simulation was specified.

Priestley-Taylor Method - The Priestley-Taylor Method implements the Priestley-Taylor equation to compute evapotranspiration. This method is capable of capturing diurnal variations in potential evapotranspiration through the use of a solar radiation gauge, so long as the simulation time step is less than 24 hours (USACE, 2009). To implement this method in the model, temperature, solar radiation, and crop coefficient gauges were incorporated as inputs through the model's time series data manager.

Gauge Weight Method - For the areal distribution of rainfall from rain gauge stations across a range of different sub basins, the Gauge Weight Method (also known as Thiessen Polygon Method) is used. Thiessen Polygons are straight-edged areas whose boundaries define the area that is closest to a specified point (in this case, a rain gauge) relative to all other points (other rain gauges). This polygon method subdivides a drainage basin into multiple polygons, each containing a rain gauge. First, the rain gauges are plotted on a base map. These rain gauge points are connected by drawing straight lines between them. The lines are bisected with perpendiculars which meet to form the polygons. The areas of the polygons are then calculated and expressed as fractions or weights of the total area of each sub basin. To calculate the rainfall in a basin, a weighted approach is used: (1) each fraction of the area is multiplied by the precipitation recorded by the rain gauge in that polygon, and (2) the weighted precipitations are then summed to represent the total precipitation for the sub basin (catchment area).

2.3 HEC-HMS Model Set Up

This subsection provides information on establishment of the HEC-HMS model for the KGL project, including: (1) biophysical data, and (2) model parameter estimation for hydrological parameters.

2.3.1 Biophysical Data

Soil type data and land use information are required to estimate the hydrologic response characteristics for each sub basin. Available data sets provided by project stakeholders and available through project background documents were reviewed. These data did not include soil data that could support the HEC-HMS model establishment. Therefore, soil data included in the United Nations Food Agriculture Organization (FAO) Harmonized World Soil Database was used. This soil data is provided as a set of land units, each with unique identification (ID)

number. This unique ID number is used to match the textural properties and other parameters of soils. Based on the soil textural class, a hydrological soil group was assigned to each land unit within the basin. Figure A2-4 provides the hydrological soil group map of the Kafue River Basin; the figure includes the following hydrological soil groups: (1) A - low run-off potential and high infiltration rates; (2) B - moderate infiltration rates; (3) C - low infiltration rates; and (4) D - high run-off potential and low infiltration rates. Soils in the basin are predominantly heavy clay and sandy clay loams.

Figure A2-4: Hydrological Soil Groups in the Kafue River Basin

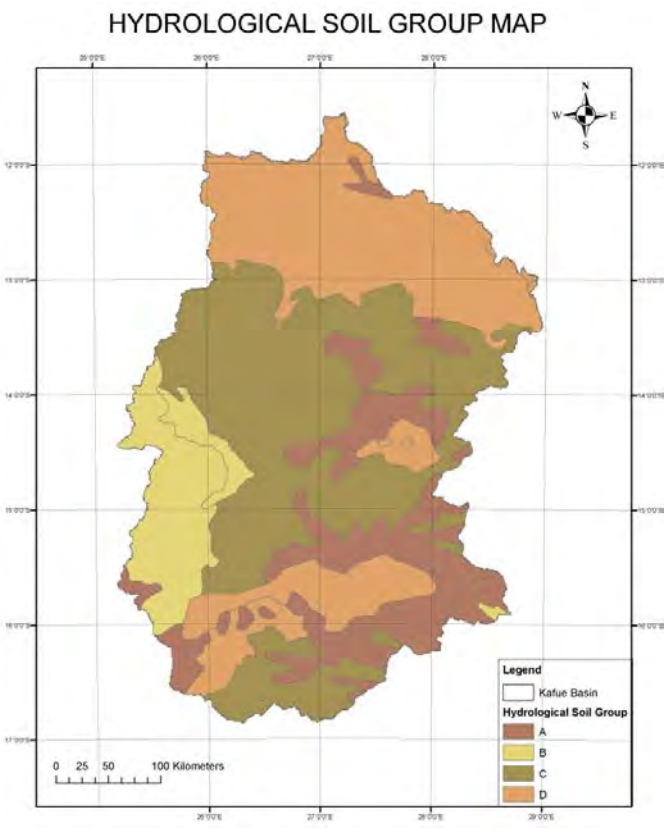

Figure A2-5 shows land use categories identified for the basin; land use is predominantly woodlands and cropland/pasture.

Figure A2-5: Land Use Classes in Kafue River Basin

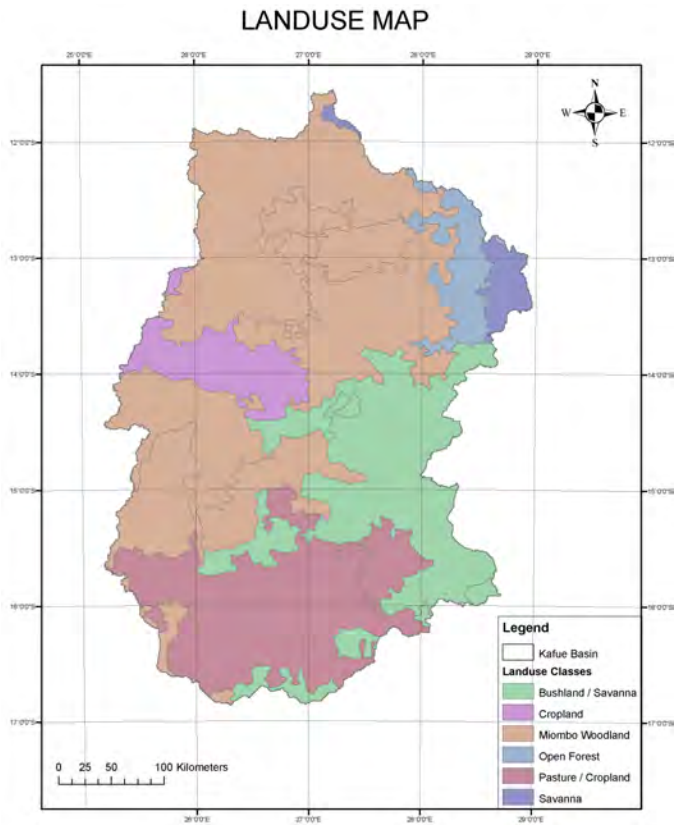

2.3.2 Model Parameter Estimation for Hydrological Methods

Based on soil textural classes, land use data, and GIS derived sub basins and streams, parameters for the hydrological methods were estimated. The length of the streams and areas of each sub basin were adopted from the HEC Geo-HMS delineation steps described previously.

For precipitation loss, initial deficit (mm), maximum storage (mm) and constant rate (mm/hr), and percent imperviousness were calculated from the soil and land use data. For the rainfall run-off transformation, a time of concentration was calculated using the Kirpich formula (Kirpich, 1940). The sub basin lag time was estimated using the calculated time of concentration.

For routing of flows in streams, the Muskingum parameters K and X, were calculated based on stream length and upstream and downstream elevations. Upstream and downstream elevations and stream lengths were based on the DEM data (see Section 2.2.2). For the base flows, initial discharge, recession coefficient, and ratio to peak were assumed initially based on the shape of flow hydrographs, hydro-geology, and professional judgments based on the nature of the area. These parameters were later refined and adjusted during the calibration of the model.

2.4 Meteorological Inputs

This section describes how meteorological inputs were established in the HEC-HMS model for the Kafue River Basin, including: (1) historical meteorological data, (2) spatial distribution of historical rainfall, and (3) estimation of solar radiation.

2.4.1 Historical Meteorological Data

As described in Section 3.1 of the report, two sets of historical meteorological data were applied for climate data projections. These included the following data sets (1) gridded data (reanalyzed) from 1950 to 1999 (provided with project outputs from Section 3.1), and (2) Lusaka Meteorological Data for the years 1975 to 2005. The Lusaka Meteorological Data were obtained during the site visit for this project in the fall of 2009. Since the Lusaka Meteorological Data is observed data provided by the Zambian Government and is available through a more current date (through 2005, as compared to the gridded data which is available only through 1999), Lusaka Meteorological Data was preferred for use in the hydrological modeling. Generally, gridded datasets (which are reanalyzed data) would be useful where no data from the national agency are available.

The historical meteorological data from the Lusaka Meteorological Department provided daily precipitation, temperature (maximum, minimum), and wind speed for the Kafue River Basin for 12 meteorological stations. The data sets were reviewed and missing data points were addressed using average values from the available data from the corresponding period. The data preparation process revealed that:

- For precipitation, the period of record is 1975-2005 for all meteorological stations except Mumbwa (1978-2005);

- For temperature (maximum and minimum), the period of record is 1975-2005; however, the data gaps are very large (that is a month to a year of missing data), particularly for recent years; and

- For wind speed, the period of record is more limited and variable between stations. There is practically no wind speed data for the Kasempa, Lusaka2, and Ndola stations.

Based on the location of the stations and a review of data completeness, seven of the 12 stations were selected for use in the hydrologic model across the common period of the 1975-2005. Figure A2-6 shows these stations which include: Choma, Kabwe, Kafiro, Kasempa, Lusaka, Ndola, and Solwezi. Mumbwa, which is shown on the figure, was not used because the 25% of the maximum temperature and 17% of the minimum temperature data are missing for the years 1975-2005.

Figure A2-6: Historical Rain Gauge Locations in the Kafue River Basin

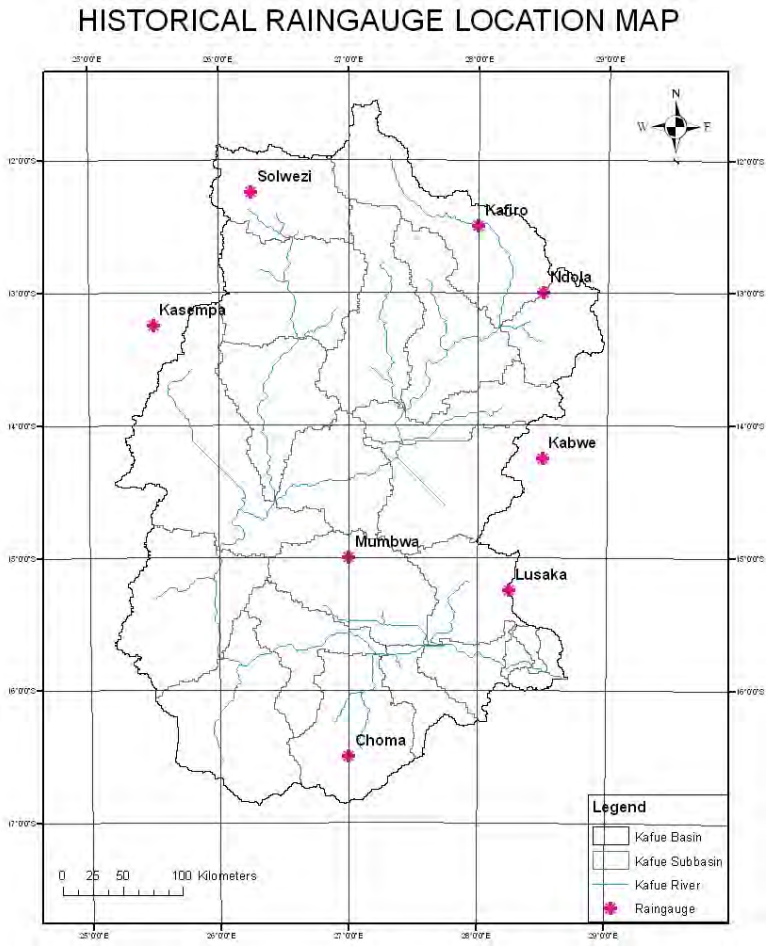

2.4.2 Spatial Distribution of Historical Precipitation

For the spatial distribution of precipitation across the basin and sub basins, the Thiessen Polygon Method was used. For the historical HEC-HMS simulations to calibrate and validate the model, data from seven selected meteorological station's rain gauges was used. These seven rain gauges lie inside or in the vicinity of the Kafue River Basin. Figure A2-7 shows the Thiessen Polygons for the historical rain gauges; each polygon contains one rain gauge station. In the HEC-HMS model, each sub basin is assigned with name of the grid point. The gauge weight from the respective grid point is assigned to the sub basin. The sum of the gauge weights in a sub basin is equal to 1. The daily level precipitation data for each grid point is given in the time series data, which is stored in the DSS file format.

Figure A2-7: Thiessen Polygons for Historic Rain Gauge Stations in the Kafue Basin

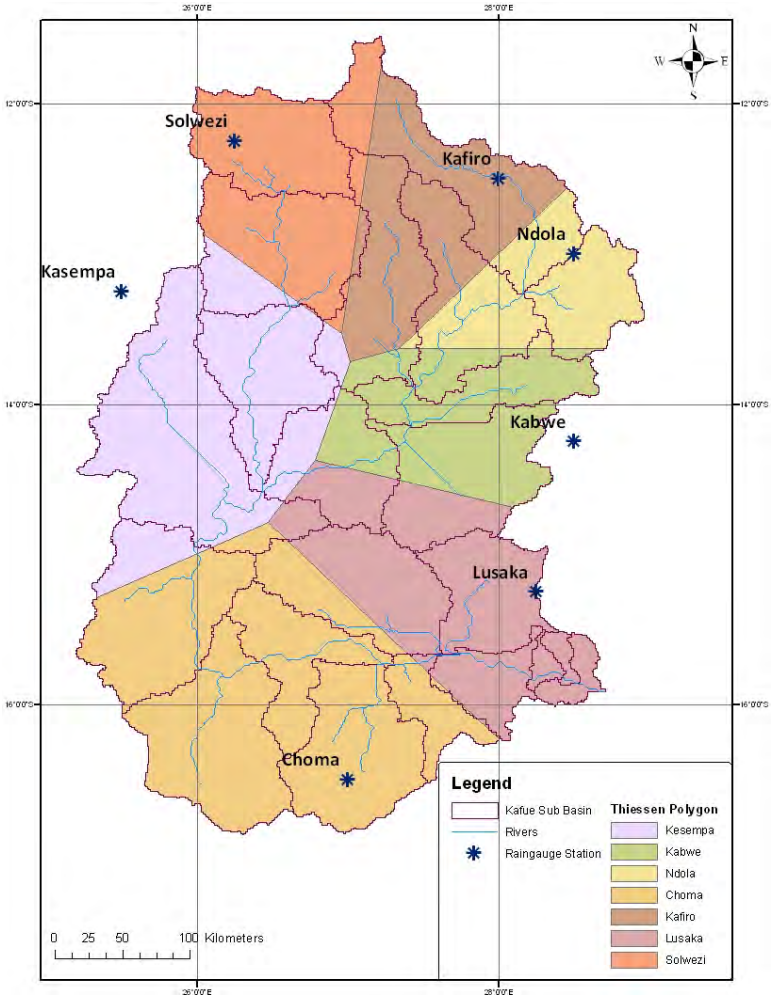

2.4.3 Estimation of Solar Radiation

The Hargreaves-Samani Method (Hargreaves and Samani, 1985) is an empirical method that can be used to compute daily potential evapotranspiration in cases where the availability of weather data is limited. Due to the unavailability of parameters such as relative humidity, wind speed, vapor pressure, net radiation, and pan evaporation for the study area, this method was selected for the KGL study. This method correlates solar radiation (Rs) with temperature and extra terrestrial radiation. Hargreaves and Samani (1982) calculated R_s as:

$$R_s = K_r (T_{max} - T_{min})^{0.5} R_a \qquad (3)$$

Where T_{max} and T_{min} are the mean daily maximum and minimum air temperature (^{0}C), respectively. R_a is the extraterrestrial radiation; and Kr is an empirical coefficient. This equation is based on the assumption that the difference between daily maximum and minimum temperatures provides a general indication of cloudiness (Allen, 1997). Kr is a significant variable in the equation above and is used to reflect different climatic conditions. Hargreaves (Hargreaves, 1994) suggested using Kr = 0.16 for interior regions and Kr = 0.19 for coastal regions. Each weather station with solar radiation values is called a solar radiation gauge and

those with temperature values are called temperature gauges. Both solar radiation and temperature gauges are used to compute evapotranspiration using the Priestly-Taylor Method. The solar radiation and temperature gauge nearest to the centroid of the sub basin are assigned to each sub basin. The solar radiation and temperature values for each grid point are given in the time series data, stored in the DSS file format.

2.5 HEC-HMS Model Calibration and Validation

This section describes calibration and validation of the KGL HEC-HMS model, including: (1) hydrological flow data availability, (2) HEC-HMS model calibration runs, and (3) HEC-HMS model validation runs.

2.5.1 Hydrological (Flow) Data Availability

Historical observed flow data are essential in calibration and validation processes for hydrological modeling. For the KGL study, historical flow data were available from ZESCO for nine flow gauge stations along the river. Table A2-1summarizes available flow data by time period for each station and two dams (IT dam and KGU dam).

Table A2-1: Observed (Historical) Flow Data

#	Station Name	Data Type	Time Period
1	4-350 Chilenga	Flow Observed	Oct-1969 - Aug-2009
2	4-450 Lubungu	Flow Observed	Jun-1951 - May-1996
3	4-560 Chifumpa	Flow Observed	Feb-1954 - Aug-2009
4	4-669 Hook's Bridge	Flow Observed	Oct-1973 - Mar-2008
5	4-760 Namwala Pontoon	Flow Observed	Dec-1951 - Sep-2006
6	4-890 Nyimba	Flow Observed	Jun-1975 - Jan-2008
7	4-941 Kaleya Dam	Flow Observed	Dec-1952 - Oct-2005
8	4-949 Kaleya Bridge	Flow Observed	May-1975 - Sep-2006
9	Itezhi-Itezhi Dam	Flow Reservoir Outflow	Sep-1978 - Sep-2006
10	4-977 Kasaka	Flow Observed	Oct-1963 - Jan-2007
11	KGU-Dam	Flow Power	Sep-1977 - Apr-2008
12	KGU-Dam	Flow Reservoir Outflow	Sep-1977 - Dec-2008

Source: Lusaka Meteorological Department, 2005.

Of the nine, non-dam gauge stations, historical flow data from three gauge stations (4-669 Hook's Bridge, 4-760 Namwala Pontoon, and 4-977 Kasaka), which are critically located in the study area, were selected to support model calibration and validation. Figure A2-8 shows these gauge stations. The location of the gauge stations within the Kafue River Basin study area is shown on the inset; an enlarged portion of the basin showing the gauges along the river is shown in the main body of the figure. The common period of data availability (that is, 1975-2005) for the historical meteorological data and stream flow data was adopted for calibration and validation of the hydrological model. Missing data were addressed with appropriate calculated values in the time series through linear interpolation between the days for which data is available using the "fill" function available in the HEC DSSView.

Figure A2-8: Locations of Flow Gauge Stations and Dams

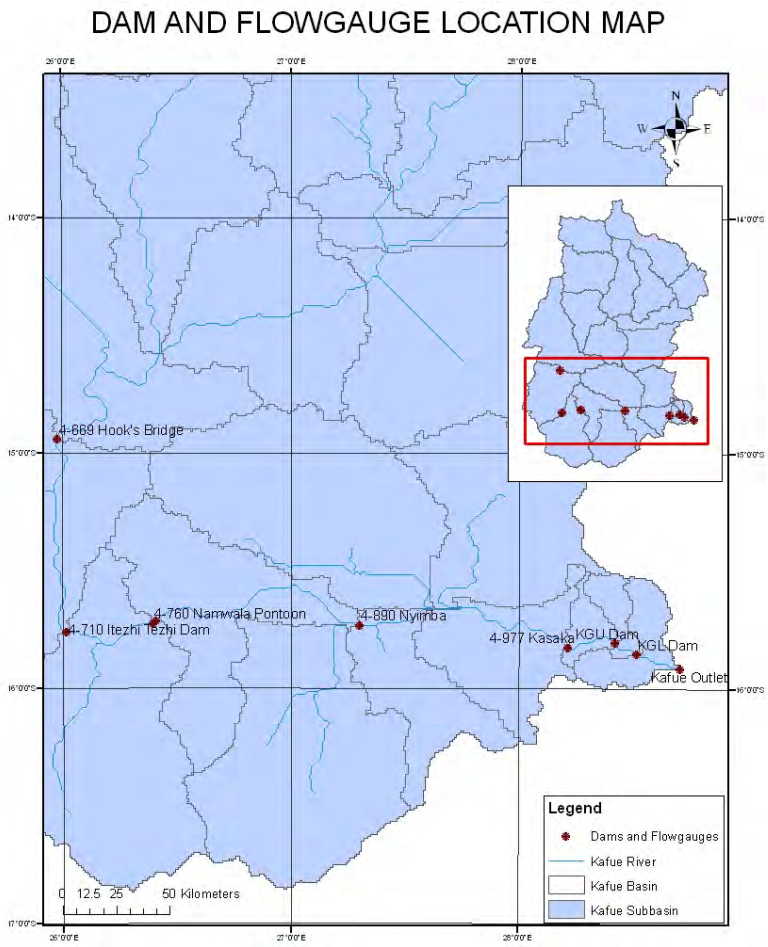

2.5.2 HEC-HMS Model Calibration

The HEC-HMS model calibration phase included running the model for a number of historical events for which both rainfall and stream flow records were available. To calibrate the model, historical and modeled flows were compared. Model parameters, such as those discussed in Section 2.4, were reviewed to obtain reasonable agreement between the observed and modeled flow hydrographs. In water availability studies, emphasis is placed on emulating the peak flow and the volume of water contained in the hydrograph. Ideally, a number of flood events can be fitted adequately with only small parameter variation. The calibration process is usually manual, using engineering judgment to iteratively adjust hydrologic parameters and evaluate the fit between the computed and observed hydrographs.

For this study, the model calibration and validation process was initiated at the most upstream flow gauge (4-669 Hook's Bridge), addressed the middle flow gauge (4-760 Namwala Pontoon), and considered the most downstream flow gauge (4-977 Kasaka). The 4-669 Hook's Bridge flow gauge location is upstream of the IT Dam, draining the upper and middle catchment area of the Kafue River Basin. The 4-760 Namwala Pontoon is downstream of the IT Dam, in an area that marks the beginning of Kafue Flats. The 4-977 Kasaka flow gauge is upstream of KGU

Dam, near the end of Kafue Flats. Therefore, flows at this gauge station are affected by the hydrology and hydraulics of Kafue Flats. Figure A2-9 shows the work flow chart for calibration and validation of the model.

Figure A2-9: Flow Chart for Calibration and Validation of Model

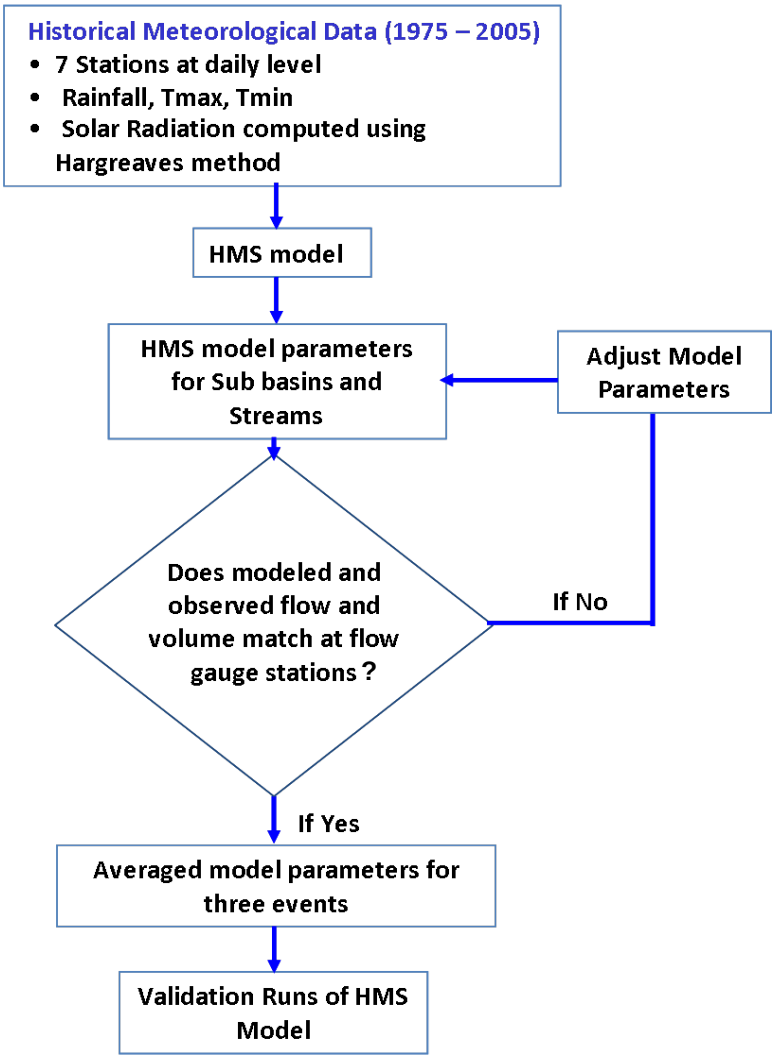

To calibrate the model, three events were modeled for the 4-669 Hook's Bridge flow gauge, including: 1981-82, 1988-89, and 1992-93. The "event" considered for each of these time periods is from October 1 to September 30 of the following year. During the calibration process, various sub basin parameters such as lag time, initial deficit, maximum storage, and constant rate were manually adjusted to improve the match between observed and modeled flows. For streams, parameters such as K and X were manually adjusted to match observed and modeled flows. Figures A2-10 to A2-12 show the observed and modeled run-off flows at 4-669 Hook's Bridge for the three calibration events. Tables A2-2 and A2-3 summarize the peak flows and flow volumes for these calibration events, respectively.

Figure A2-10: Comparison of Observed and Modeled Flows at 4-669 Hook's Bridge for the 1981-82 Event

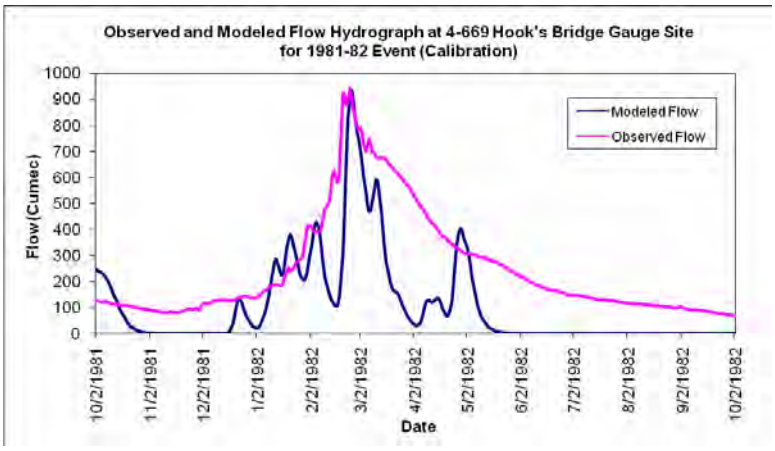

Figure A2-11: Comparison of Observed and Modeled Flows at 4-669 Hook's Bridge for the 1988-89 Event

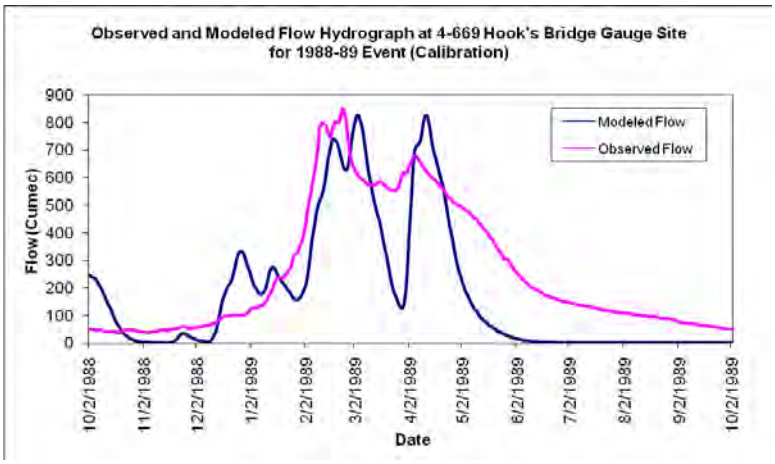

Figure A2-12: Comparison of Observed and Modeled Flows at 4-669 Hook's Bridge for the 1992-93 Event

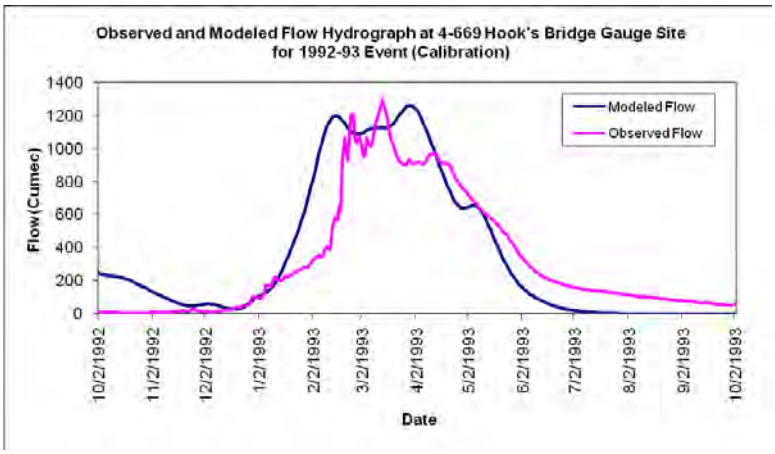

Table A2-2: Observed and Modeled Peak Flows at 4-669 Hook's Bridge for Calibration Events

Event	Modeled Flow (cms)	Observed Flow (cms)
1981-82	933.1	941.7
1988-89	826.4	849.7
1992-93	1.258.4	1.296.7

Notes: cms = cubic meters per second.

Table A2-3: Observed and Modeled Flow Volumes at 4-669 Hook's Bridge for Calibration Events

Event	Modeled Volume (1000 m^3)	Observed Volume (1000 m^3)
1981-82	3,402.081	7,820,179
1988-89	5,535,936	8,179,096
1992-93	11,270,967	10,261,149

Notes: m^3 = cubic meters.

From the calibration plots and summary tables, it was determined that the model is reasonably calibrated at this gauge site for the peak flows, as well as flow volume.

Figures A2-13 to A2-15, show the comparison between observed and modeled flow at the 4-760 Namwala Pontoon gauge station for three calibration events (1981-82, 1988-89, and 1992-93). Tables A2-4 and A2-5 show the summary of peak flows and flow volume for calibration events in given in Table A2-4 and Table A2-5, respectively.

Figure A2-13: Comparison of Observed and Modeled Flows at 4-760 Namwala Pontoon flow gauge station for the 1981-82 Event

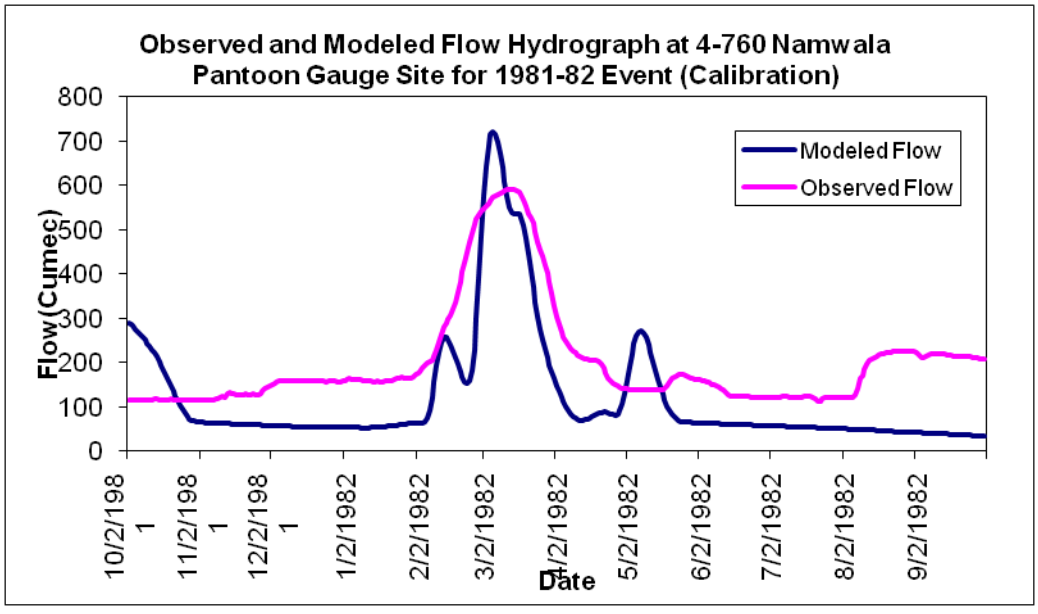

Figure A2-14: Comparison of Observed and Modeled Flows at 4-760 Namwala Pontoon Gauge Station for the 1988-89 Event

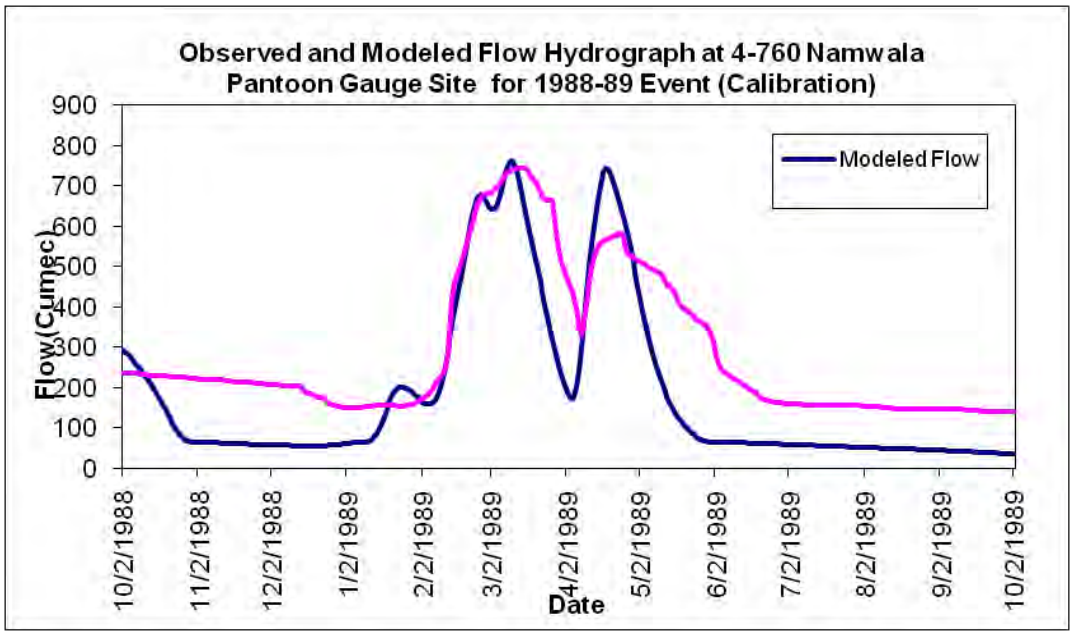

Figure A2-15: Comparison of Observed and Modeled Flows at 4-760 Namwala Pontoon Gauge Station for the 1992-93 Event

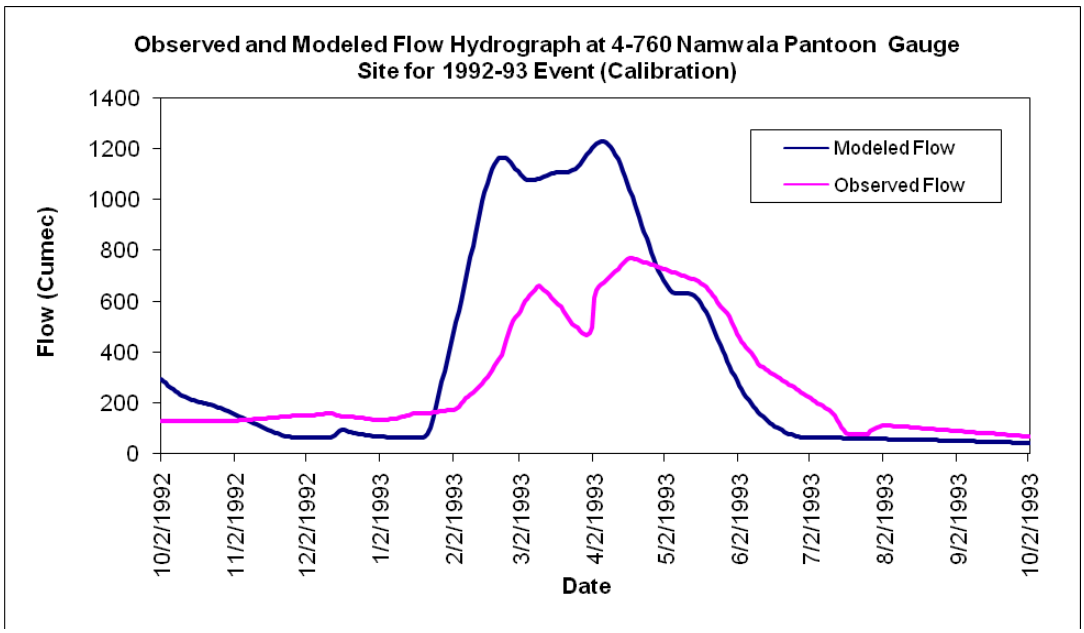

Table A2-4: Observed and Modeled Peak Flows at 4-760 Namwala Pontoon Gauge Station for Calibration Events

Event	Modeled Flow (cms)	Observed Flow (cms)
1981-82	722	592
1988-89	764	743
1992-93	1,228	769

Notes: cms = cubic meters per second.

Table A2-5: Observed and Modeled Flow Volumes at 4-760 Namwala Pontoon Gauge Station for Calibration Events

Event	Modeled Volume (1000 m^3)	Observed Volume (1000 m^3)
1981-82	3,833,476	636,823
1988-89	5,872,837	9,090,949
1992-93	11,472,159	9,037,468

Notes: m^3 = cubic meters.

For the 4-760 Namwala Pontoon, two of the three events show that the peak flow and hydrograph are reflected well in the calibration runs. The third event has an observed volume that aligns with the modeled flow, but the shapes of the two hydrographs do not align well. This may be caused by the sparse distribution of meteorological stations in the basins (see uncertainty discussion in Section 2.9 of the report).

The 4-977 Kasaka flow gauge station, which is located downstream of Kafue Flats, shows the typical nature of the hydrology of the flats. The model calibration at this flow gauge station was initiated with one event (1981-82).

Figure A2-16 provides the calibration graph and Tables A2-6 and A2-7 show the peak flow and flow volume for the modeled and observed flows. The calibration shows that there is considerable difference in the observed and modeled hydrograph; however the two peak flows almost match. As stated earlier, the primary goal for flow modeling is to align the peak flows and total volume, rather than the hydrograph shape. The Kafue Flats are an immense shallow flood plain, which floods to a depth of less than a meter in the rainy season (deeper in some lagoons and permanently swampy areas), and dries to a clayey black soil in the dry season. The impact of these physical conditions on the model performance has also been reported by other studies. (http://www.co.pierce.wa.us/xml/services/home/environ/water/ps/basinplans/keypen/KI-AppendixH.pdf). With these limitations, the calibrated model was accepted for the further use.

Figure A2-16: Comparison of Observed and Modeled Flows at 4-977 Kasaka Gauge Station for the 1981-82 Event

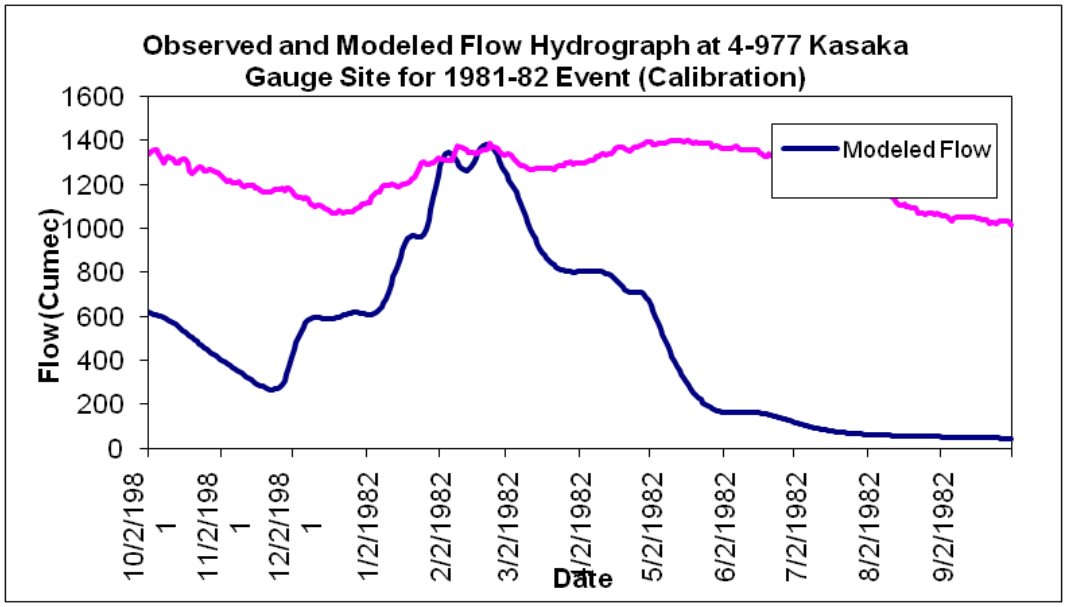

Table A2-6: Observed and Modeled Peak Flows at 4-977 Kasaka Station for Calibration Event

Event	Modeled Flow (cms)	Observed Flow (cms)
1981-82	1,382.5	1,400.0

Notes: cms = cubic meters per second.

Table A2-7: Observed and Modeled Flow Volumes at 4-977 Kasaka Station for Calibration Event

Event	Modeled Volume (1000 m^3)	Observed Volume (1000 m^3)
1981-82	15,642,954	29,217,270

Notes: m^3 = cubic meters.

2.5.3 HEC-HMS Model Validation

The validation process is intended to help ensure that the model parameters reflect the physical nature of the basin, as well as possible given the observed data, background information, and project resources and goals. The validation process uses events that were not included in the calibration process to evaluate the reliability of the model for other historical events.

For the validation of the HEC-HMS model for Kafue River Basin at 4-669 Hook's Bridge and the 4-760 Namwala Pontoon, the average values from the three calibration events for each model parameters were given as inputs for sub basins and streams above the respective flow gauge stations. For areas influenced by the 4-977 Kasaka flow gauge station, the model parameters from the 1981-82 event were used.

For 4-669 Hook's Bridge, the model was validated for the 2000 -2001 event. The comparison between observed and modeled run-off is shown in Figure A2-17. For the 4-760 Namwala

Pontoon gauge station, the model was validated for the 1976-77 event. The comparison between observed and modeled run-off is shown in Figure A2-18. For the 4-977 Kasaka gauge station, the model was validated for the 1992-93 event. The comparison between observed and modeled run-off is shown in Figure A2-19. The peak flows and flow volume of modeled and observed flows during the validation are summarized in the Tables A2-8 and A2-9.

Figure A2-17: Comparison of Observed and Modeled Flows at 4-669 Hook's Bridge for the 2000-01 Event

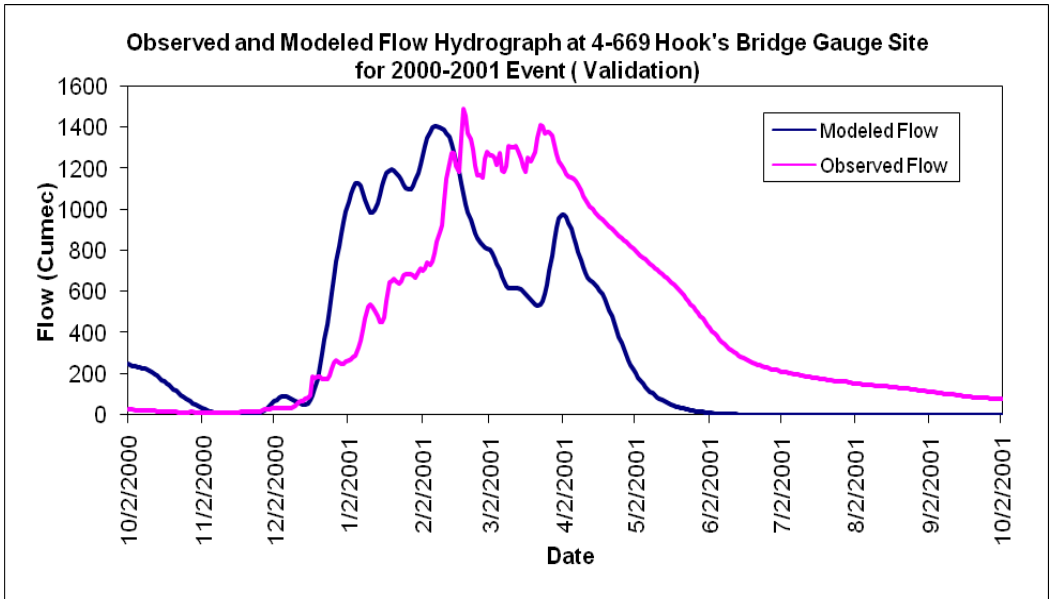

Figure A2-18: Comparison of Observed and Modeled Flows at 4-760 Namwala Pontoon for the 1976-77 Event

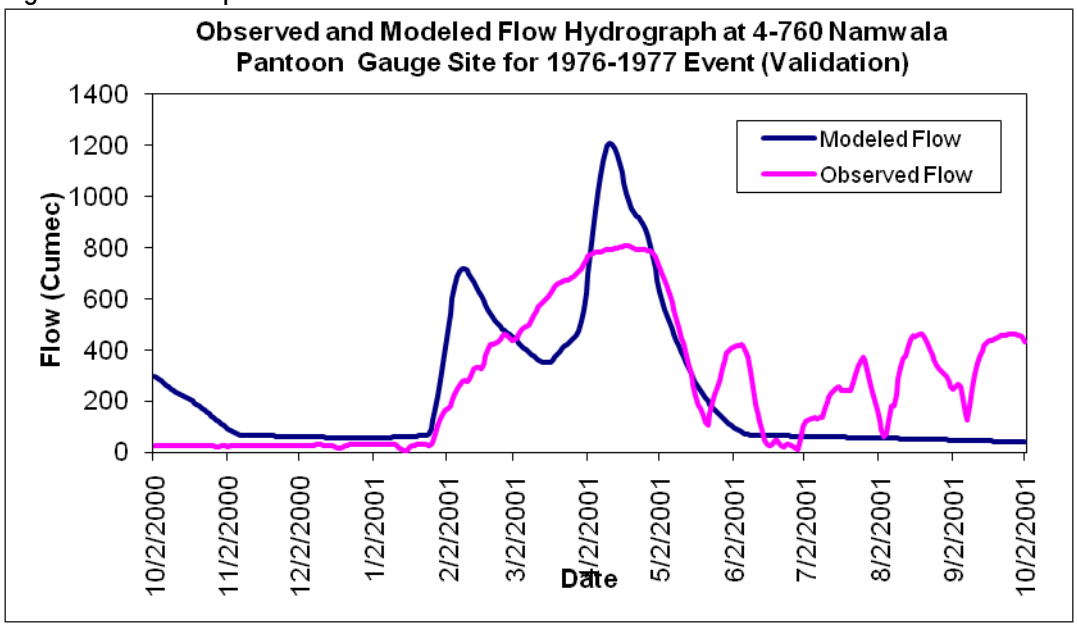

Figure A2-19: Comparison of Observed and Modeled Flows at 4-977 Kasaka for the 1992-93 Event

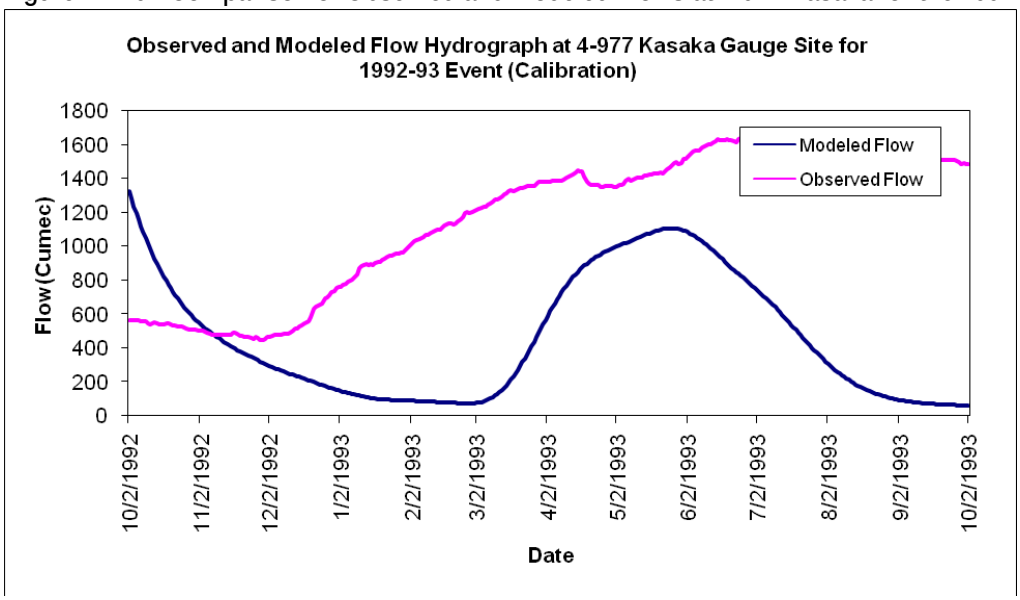

Table A2-8: Observed and Modeled Peak Flows for Three Gauge Stations for the Validation Event

Location	Event	Modeled Flow (cms)	Observed Flow (cms)
4-669 Hook's Bridge	2000-01	1407.1	1491.6
4-760 Namwala Pontoon	1976-77	1208.0	807.0
4-977 Kasaka	1992-93	1328.0	1658.0

Notes: cms = cubic meters per second.

Table A2-9: Observed and Modeled Flow Volumes for Three Gauge Stations for the Validation Event

Location	Event	Modeled Volume (1000 m^3)	Observed Volume (1000 m^3)
4-669 Hook's Bridge	2000-01	10,565,298	14,031,102
4-760 Namwala Pontoon	1976-77	7,539,646	8,575,581
4-977 Kasaka	1992-93	14,661,385	37,068,386

Notes: m^3 = cubic meters.

Figures A2-17 and A2-18 and Tables A2-8 and A2-9 show that the observed peak flow and flow volume are reflected well in the model for two of the three flow gauge stations, though the modeled peak flow for the 4-669 Hook's Bridge gauge station occurs earlier than the observed peak flow. With the above findings from the validation results, the model can be used further in considering the temperature and precipitation changes associated with GCM and emissions scenarios, even with the limited number and sparse distribution of meteorological stations over the basin. Uncertainty associated with the modeling effort, which arises from a number of pilot study steps, is discussed in appropriate sections of the main report.

2.6 GCM Climate Change Flow Modeling

This section provides an overview of hydrologic runs in the HEC-HMS model for the Kafue River Basin using three of the six GCMs, with two emissions scenarios across the selected time horizons.

2.6.1 Meteorological Data Availability for GCMs

As previously discussed, climate change projections were provided as an output of GCM project efforts for six GCMs. Before initiating HEC-HMS modeling of the climate change projections, three of the six GCMs were selected for hydrologic modeling. The climate data from the three GCMs were used to study the impact of climate change on basin flows. The three GCMs selected were ECHAM5, MRI, and IPSL, each with two emissions scenarios (A2 and B1). The three GCMs were selected based on representing a high, average, and low change scenario across the six GCMs.

The data outputs from GCM efforts described in Section 3.1 and Appendix 1 include: precipitation and temperature (minimum and maximum) at a daily time step with a spatial resolution of 0.5º (about 50 km). The locations of the GCM data grid points are shown in Figure A2-20. The climate data is available for the period 1950-2099 and was divided into two time horizons including a baseline period (1961-1990) and a future climate projection period (2010-2099). The projected climate period is further sub-divided into three, 30-year time horizons, including: (1) early 21st century (2010-2039), (2) mid 21st century (2040-2069), and (3) late 21st century (2070-2099). These gridded data sets were used to model flow for the baseline and three future time horizons for the three GCMs and two emissions scenarios (A2 and B1).

Figure A2-20: GCM Grid Point Locations (0.5º Resolution)

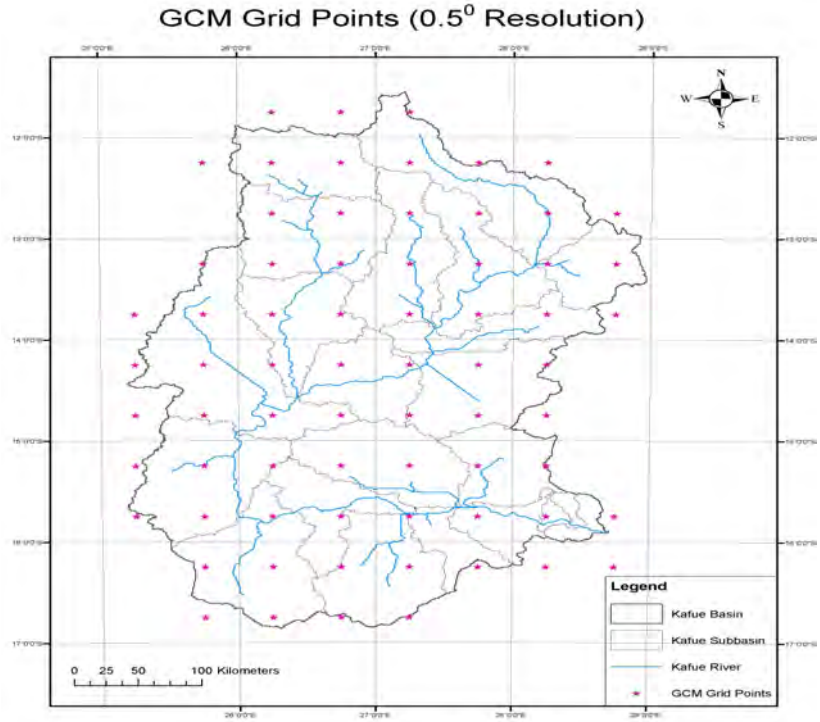

Figure A2-21: Thiessen Polygons for GCM Grid Points

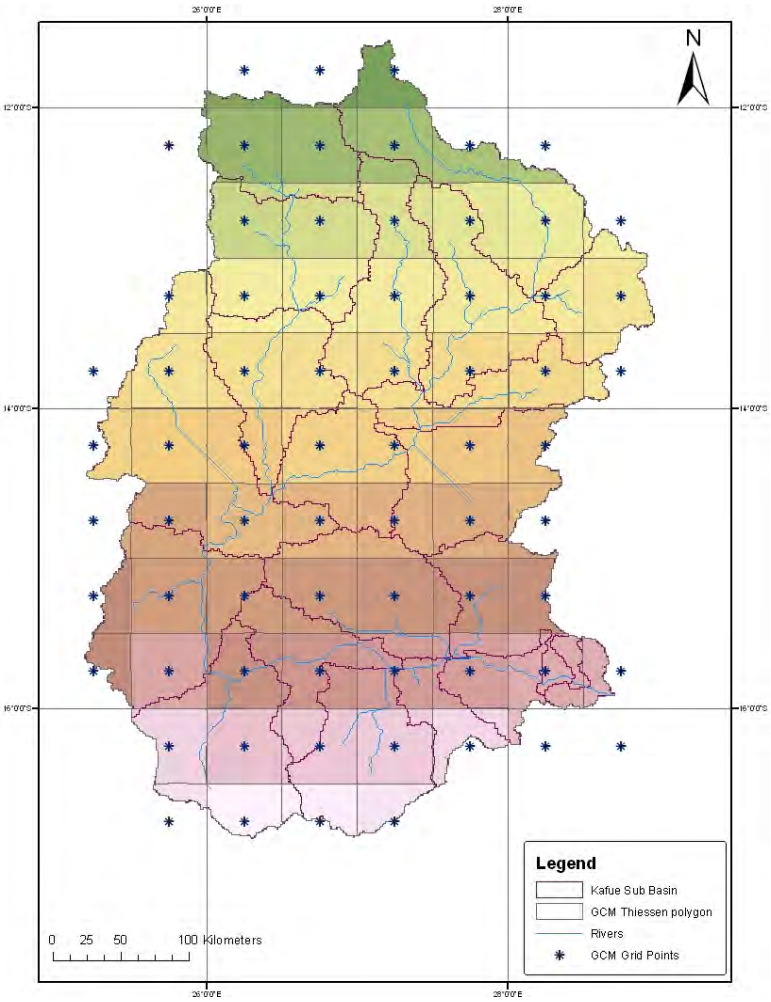

2.6.2 Spatial Distribution of Rainfall

Gauge-weighted GCM precipitation data (using the grid point outputs from climate change projections) were used as inputs for the model. The data were provided as inputs to the meteorological model of HEC-HMS. For the spatial distribution of precipitation data from GCM grid points over the Kafue River sub basins, Thiessen Polygons were developed for the data set and gauge precipitation weightings were determined. The Thiessen Polygons generated for the GCM grid points are shown in Figure A2-21. Each sub basin is assigned with the appropriate name of the grid point. The gauge weight from each respective grid point is then assigned to the appropriate sub basin. The sum of the grid point gauge weightings in a sub basin is equal to 1. The daily level precipitation data for each grid point is given in the time series data, which is stored in the DSS file format.

2.6.3 Estimation of Solar Radiation

Similarly to the historical data runs, hydrological runs for the GCM data also applied the Hargreaves-Samani method to estimate solar radiation. The solar radiation was computed for all grid points using the (1) location (latitude and longitude), and the (2) minimum and maximum temperature for each grid point. Each grid point with solar radiation values is called a solar

radiation gauge and each grid point with temperature values is called a temperature gauge. Both, the solar radiation and temperature gauges are used to compute evapotranspiration using the Priestly-Taylor Method. The solar radiation and temperature gauge nearest to the centroid of the sub basin were assigned to each sub basin. The solar radiation and temperature values for each grid point are given in the time series data and stored in the DSS file format.

2.6.4 HEC-HMS Model Runs using GCM Data

A new meteorological model was developed for each GCM, emissions scenario, and time horizon. The various hydrological model parameters for sub basins and streams for the basin model were adopted from the validation runs. Model set up was implemented for each set of meteorological data for three GCMs, two emissions scenarios, and four time horizons (baseline, early-, mid- and late-century). This provided 24 HEC-HMS model set-ups, each with different meteorological inputs (Table A2-10). Each of the 24 model set-ups was run for 30 years at a daily level time step. The water flows at various flow gauge locations were then estimated and compared. Changes in flow, with respect to the baseline, are discussed in Section 2.7.

Table A2-10: Summary of GCM (Climate Change) Hydrologic Modeling Runs

GCMs	ECHAM5, MRI, IPSL
SRES Emissions Scenarios	A2 and B1
Time Horizons	Baseline, Early, Mid, and Late Century

2.7 Discussion of Results

This section discusses flow results and changes for the GCM and emissions scenarios across the four time horizons modeled.

2.7.1 Flow Comparison under Different Scenarios at a Key Location

Daily flows were generated for each basin element (sub basins, streams, flows gauges, and reservoirs) of the model for the 24 modeling scenarios. To compare flows across various time horizons, GCMs, and emissions scenarios, average monthly flows were generated from the daily flow data (for each 30 year-period of simulated flow). The 4-760 Namwala Pontoon flow gauge station was chosen to evaluate flow changes because of its critical location in the Kafue River Basin. This gauge is downstream of the IT reservoir and upstream of the Kafue Flats. Figures A2-22 to A2-27 show the average monthly flow variation at this station for the ECHAM5 A2/BI, MRI A2/B1, and IPSL A2/B1 GCM and emissions scenarios and the four time horizons evaluated.

Figure A2-22: Flow Comparison for ECHAM5 A2 Scenario at 4-760 Namwala Pontoon

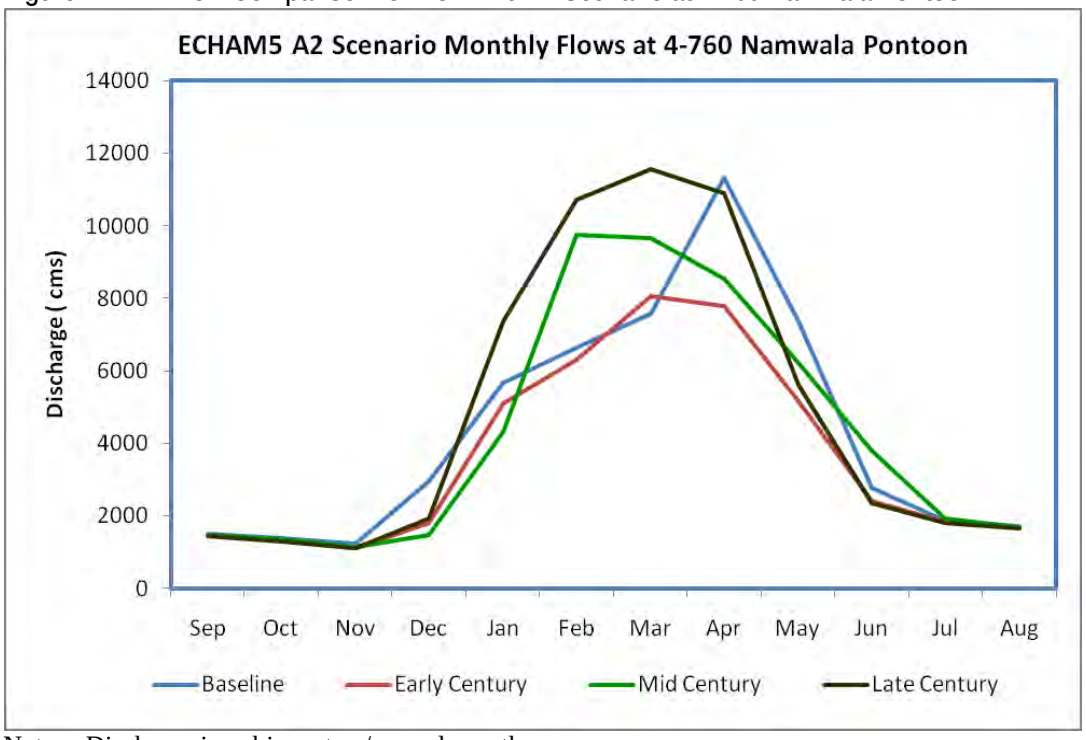

Notes: Discharge in cubic meters/second-months.

Figure A2-23: Flow Comparison for ECHAM5 B1 Scenario at 4-760 Namwala Pontoon

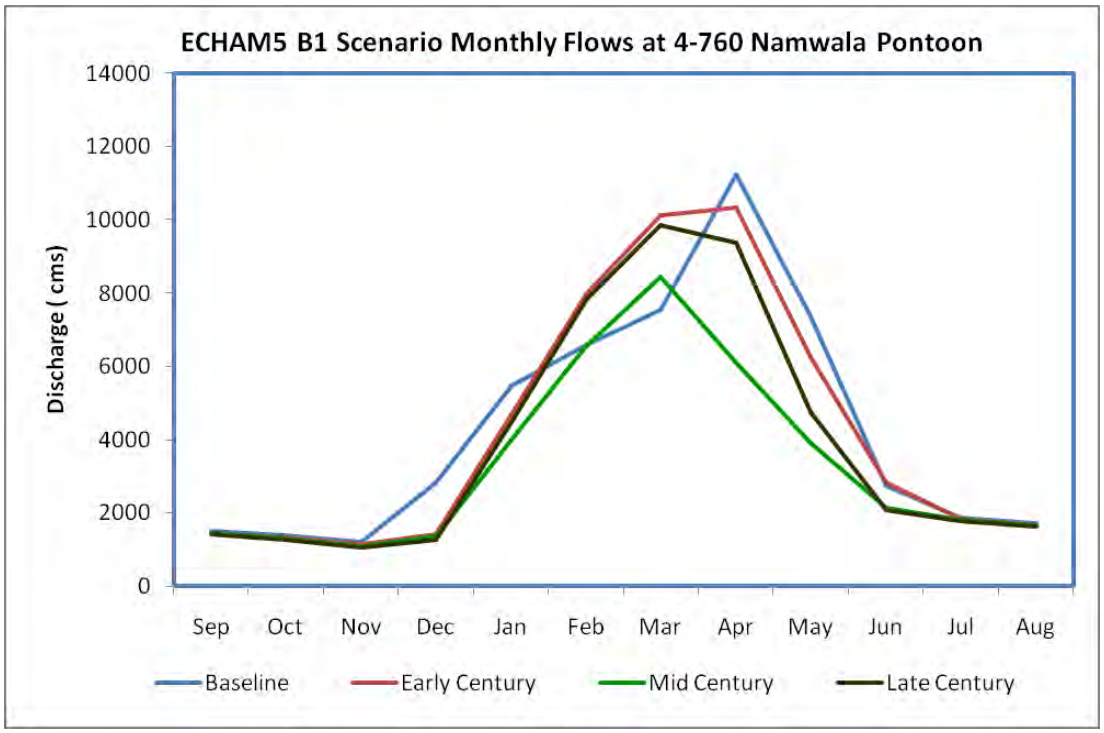

Notes: Discharge in cubic meters/second-months.

For all three future time horizons, the flow was compared temporally to the baseline flow. For the ECHAM5 A2 scenario (Figure A2-22), during the early and mid century periods, maximum average monthly flows are lower than in the baseline period, while there is considerable increase in flow in the late century maximum average monthly flows compared to the baseline.

For the ECHAM5 B1 scenario (Figure A2-23), a reduction in the maximum average monthly flow is observed across all three time horizons, compared to the baseline period. Also, the maximum average monthly flows occur earlier during the mid and late century, compared to baseline period.

Figure A2-24: Flow Comparison for IPSL A2 Scenario at 4-760 Namwala Pontoon

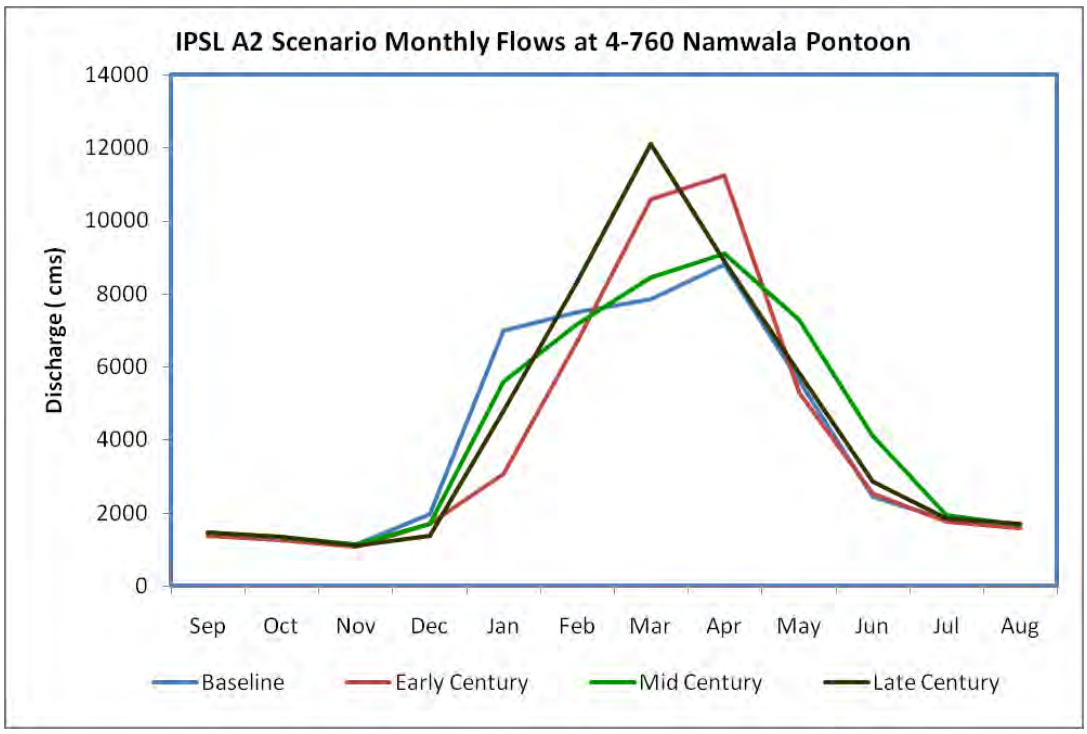

Notes: Discharge in cubic meters/second-months.

Figure A2-25: Flow Comparison for IPSL B1 Scenario at 4-760 Namwala Pontoon

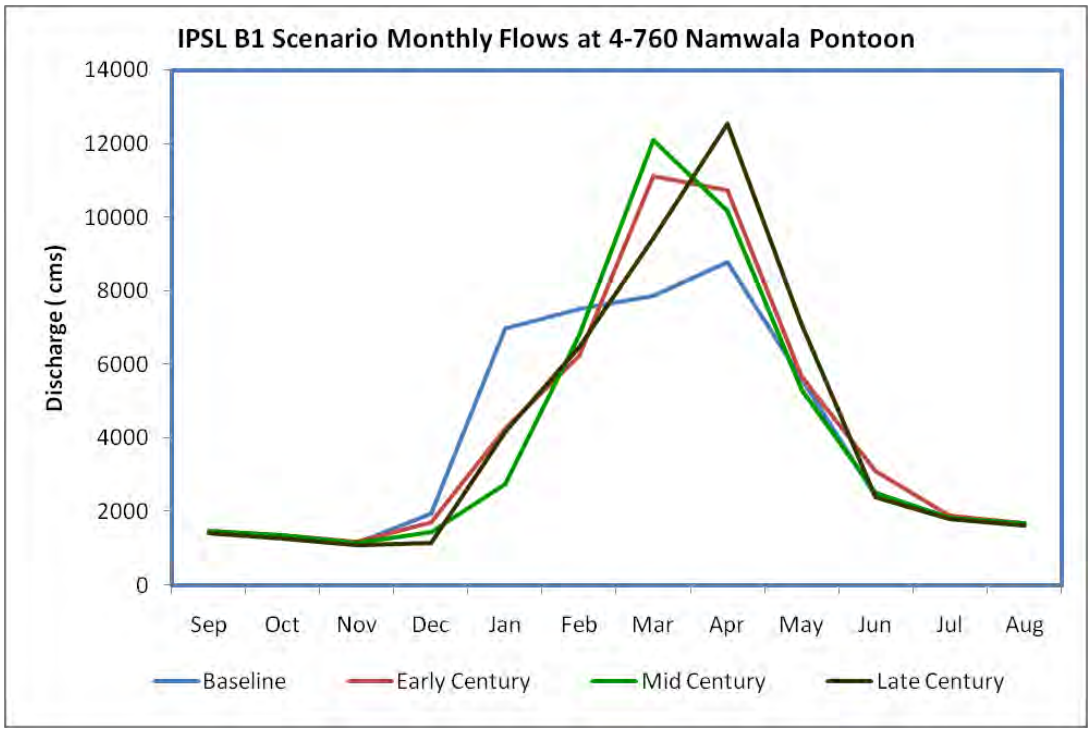

Notes: Discharge in cubic meters/second-months.

For the IPSL A2 scenario (Figure A2-24), early and late century maximum average monthly flows are greater than for the baseline period. In the mid century period, the maximum average monthly flows are nearly equal to the baseline period flows. During the late century, the maximum average monthly flow occurs earlier than for the baseline period.

For the IPSL B1 scenario (Figure A2-25), an increase in the maximum average monthly flows is observed across all three time horizons of projected climate compared to the baseline period. The maximum average monthly flows occur earlier during all of the time horizons of projected climate change, compared to the baseline period.

Figure A2-26: Flow comparison for MRI A2 Scenario at the 4-760 Namwala Pontoon

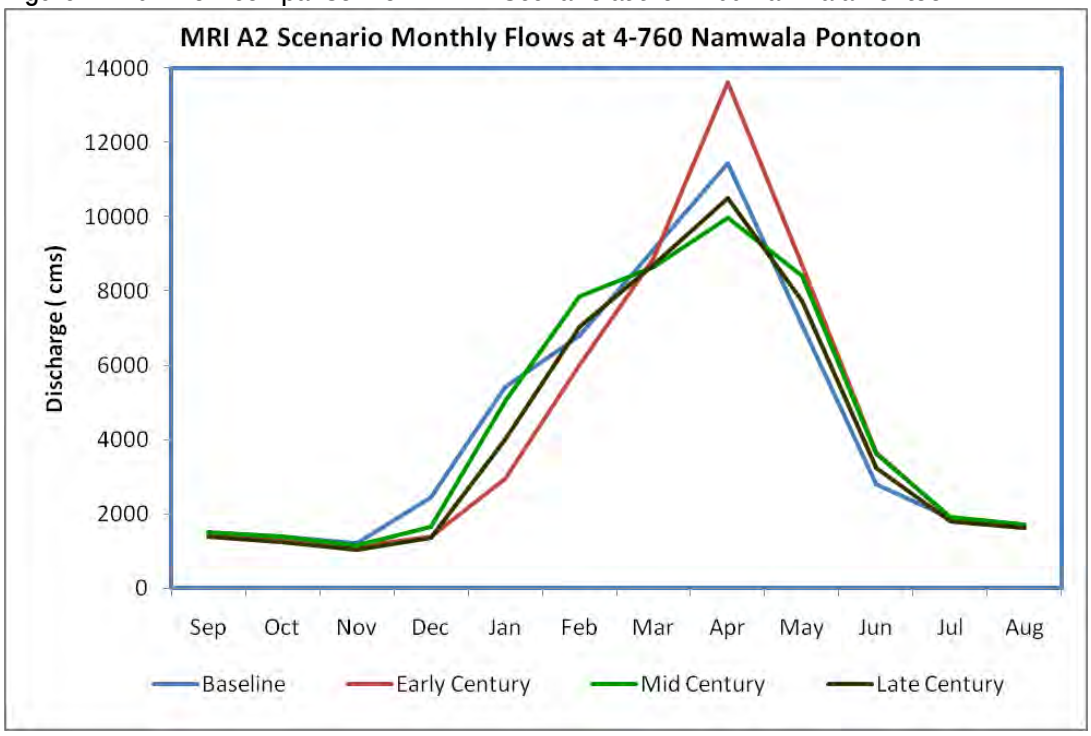

Notes: Discharge in cubic meters/second-months.

Figure A2-27: Flow comparison for MRI B1 Scenario at the 4-760 Namwala Pontoon

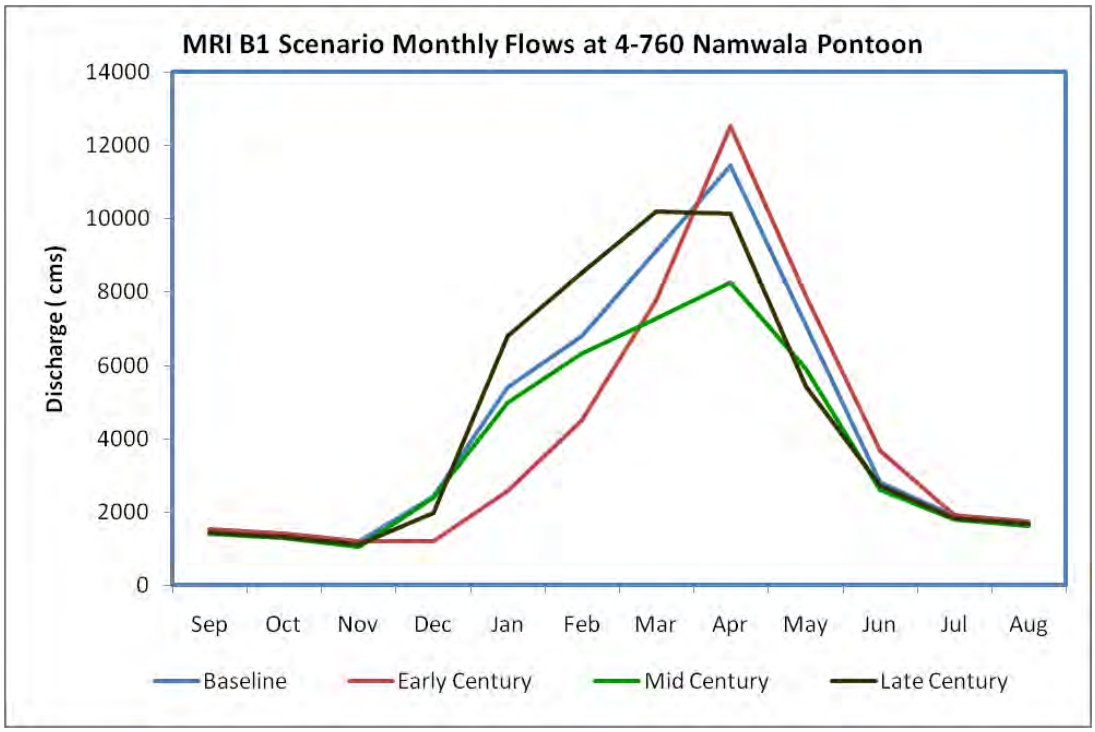

Notes: Discharge in cubic meters/second-months.

For the MRI A2 scenario (Figure A2-26), early century maximum average monthly flows are greater than for the baseline period. In the mid and late century, maximum average monthly flows are lower than the baseline period. The maximum average monthly flows for all time horizons occur in a similar time frame.

For the MRI B1 scenario (Figure A2-27), an increase in the maximum average monthly flow is observed in the early century period compared to the baseline period. In the mid and late century, there is a reduction in the maximum average monthly flows compared to the baseline period. The maximum average monthly flows during the late century time horizon occur earlier than for the baseline period.

To screen the highest positive and negative changes in flows compared to their respective baseline periods, average annual flows at 4-760 Namwala Pontoon flow gauge station were estimated for three GCMs, two emissions scenarios, and three projected time horizons. Average annual flows for the A2 and B1 emissions scenarios are shown in Table A2-11 and Table A2-12, respectively.

Table A2-11: Average Annual Flows at 4-760 Namwala Pontoon for Emissions Scenario A2 (cms)

GCM	Baseline (1961-1990)	Early 21st Century 2010-2039)	Mid 21st Century (2040-2069)	Late 21st Century 2070-2099)
ECHAM5	51,963	44,053	51,361	57,751
MRI	52,780	52,714	52,868	49,649
IPSL	48,575	48,186	50,982	51,724

Notes: Results are in cubic meters per second (cms)-days.

Table A2-12: Average Annual Flows at 4-760 Namwala Pontoon for Emissions Scenario B1 (cms)

GCM	Baseline (1961-1990)	Early 21st Century (2010-2039)	Mid 21st Century (2040-2069)	Late 21st Century (2070-2099)
ECHAM5	51,461	51,048	39,766	46,758
MRI	52,780	47,935	44,909	53,048
IPSL	48,548	50,378	48,587	50,444

Notes: Results are in cubic meters per second (cms)-days.

The percent change in the average annual flows with respect to the baseline flows for each GCM/emissions scenario were computed. These percent changes are provided in Table A2-13 and Table A2-14 for the A2 and B1 emissions scenarios, respectively.

Table A2-13: Percent Change in Average Annual Flows at 4-760 Namwala Pontoon for Emissions Scenario A2

GCM	Baseline (1961-1990)	Early 21st Century (2010-2039)	Mid 21st Century (2040-2069)	Late 21st Century (2070-2099)
ECHAM5	-	-15%	-1%	11%
MRI	-	0%	0%	-6%
IPSL	-	-1%	5%	6%

Notes: Changes are from the baseline period; - indicates no change from the baseline period.

Table A2-14: Percent Change in Average Annual Flows at 4-760 Namwala Pontoon for Emissions Scenario B1

GCM	Baseline (1961-1990)	Early 21st Century (2010-2039)	Mid 21st Century (2040-2069)	Late 21st Century (2070-2099)
ECHAM5	-	-1%	-23%	-9%
MRI	-	-9%	-15%	1%
IPSL	-	4%	0%	4%

Notes: Changes are from the baseline period; - indicates no change from the baseline period.

For the A2 emissions scenario (Table A2-13), flow changes are -15% in the early century, -1% in the mid century, and +11% in the late century period for ECHAM5. For MRI, there is no change in early and mid century flows, but flows increase by 6% in the late century period compared to the baseline period. For IPSL, flows decrease by 1% in the early century period compared to the baseline period, with increased flows during the mid (5%) and late century (6%).

For the B1 emissions scenario (Table A2-14), flow changes are -1% in the early century, -23% in the mid century, and -9% in the late century for ECHAM5 (compared to the baseline period). For MRI, flow changes are -9% in the early century, -15% in the mid century, and +1 % in the late century (compared to the baseline period). For IPSL, there is minimal change in the mid century period flows, but flows increase by 4% in the early and late century periods (compared to the baseline period).

Based on the above analysis, the ECHAM5 A2 late century period has the highest positive change in flows (+11%) compared to its respective baseline period and the ECHAM5 B1 mid century period shows the highest negative change, -23%, in the flows compared to its respective baseline period. Therefore, these two GCM/emissions scenarios and time horizons were selected to study variability over a long term simulation (200 years) using a weather generator (WXGEN) simulation and additional HEC-HMS runs.

The ability of WXGEN to simulate variability of events compared to the input data is shown in Table A2-15. The table provides a statistical comparison of annual maximum 1-day precipitation (one of the precipitation indices) for ECHAM 5 –A2 late century GCM derived data and the WXGEN simulation data generated based on the ECHAM 5 –A2 late century GCM data. The comparison shows that the WXGEN simulated data has higher values for maximum, minimum, and average of annual maximum 1-day precipitation, while the standard deviations are almost equal. The plot (Figure A2-28) between daily rainfall data with and without WXGEN simulation also shows that the WXGEN derived data includes a greater numbers of minimum and maximum events. Figure A2-29 shows that the flows also are higher using WXGEN outputs than that the flows based on the GCM data.

Table A2-15: Comparison of Annual Maximum 1-day Precipitation with and without WXGEN Simulation

Statistical Parameters	Comparison Parameter	WXGN Input: (ECHAM5 A2 Late Century 30 Years)	WXGN Outputs: ECHAM5_A2_Late Century_200 Years
Annual maximum 1-day precipitation, mm	Maximum	119	144
	Average	60	65
	Minimum	24	28
	Standard Deviation	23	22

Notes: mm = millimeter.

Figure A2-28: Comparison of Daily Rainfall for the ECHAM5 A2 Late Century (GCM Data) and WXGEN Simulation of the ECHAM5 A2 Late Century Data

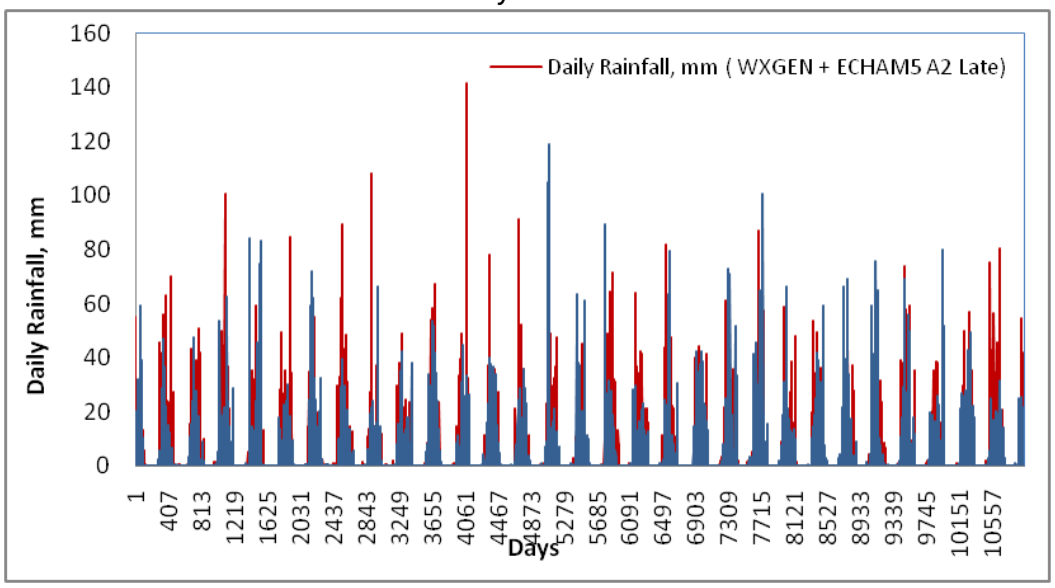

Figure A2-29: Comparison of Daily Flows for the ECHAM5 A2 Late Century GCMD and WXGEN Simulation of the ECHAM5 A2 Late Century GCM Data

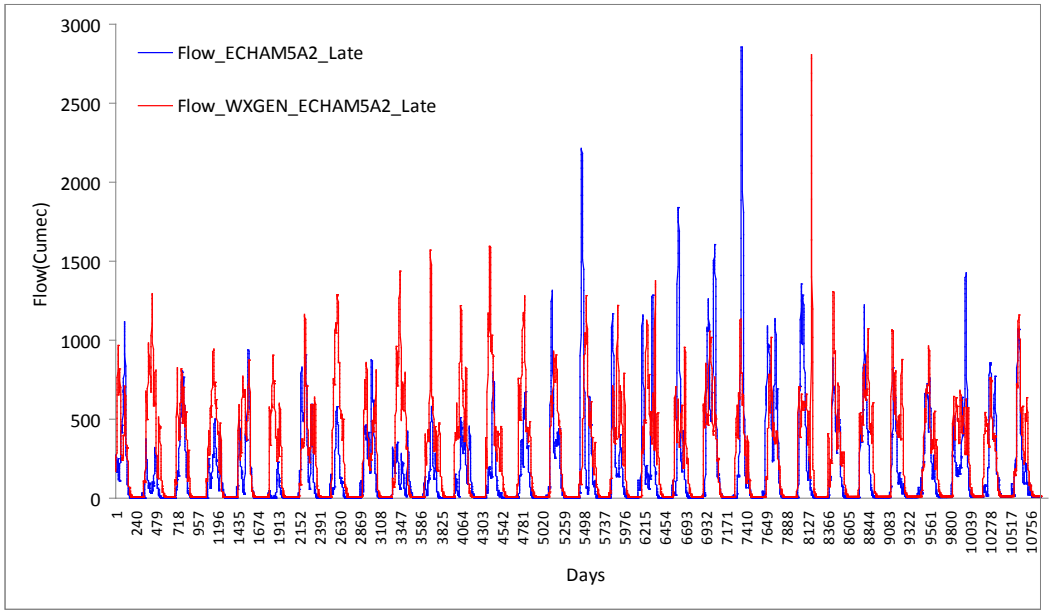

2.7.2 Analysis of Precipitation Variability and Flow Impacts

Estimating the impact of climate change on the hydrology of the watershed was a major challenge due to complex hydrological processes and the combined, interrelated impacts of various physical and meteorological parameters. These parameters include spatial and temporal distributions of rainfall, evapotranspiration, temperature, solar radiation, sunshine hours, relative humidity, and wind speed. Various researchers and studies have noted the interrelationships between some of these parameters and subsequent impacts on flows. Some of the significant studies are discussed in the following paragraphs.

A rainfall pattern where high rainfall tends to occur in continuous sequences is likely to result in higher runoff than similar rainfall values which are distributed more randomly or evenly. This increased runoff occurs because of catchment wetness (Mansell, 1997). Studies of the response of runoff to climate change suggest that the annual runoff volume is more sensitive to changes in precipitation than to changes in potential evapotranspiration. In addition, studies have shown that a given percentage change in precipitation results in a greater percentage change in runoff (Najjar, 1999), with arid catchments showing a greater sensitivity than humid ones (Gordon and Famiglietti, 2004). For example, an increase in annual precipitation of 10% can be enough to offset the higher evaporation associated with a 2°C temperature rise (http://www.libraryindex.com/pages/3394/Rivers-Impacts-Climate-Change.html). Also warmer average global temperatures mean greater evaporation, with a warmer atmosphere able to hold more moisture aloft that can fall as precipitation, increasing the potential for flooding (Water Aid, undated).

Riverine stream flow is a function of hydrologic inputs in the form of rainfall, the rainfall distribution, and physical and climatic characteristics (Mutreja, 1986). Since the amount of rainfall and the spatial and temporal distribution of rainfall have the most governing roles as input in the flow generation, these variables were studied in detail to evaluate the changes in the flows across three GCMs and future time horizons.

In order to study the long term impact of precipitation changes associated with climate change to the water availability in the Kafue River Basin study area, spatial and temporal changes in the annual average rainfall were analyzed using RClimDex.

RClimDex is widely used in response to the general consensus within the climate community that any change in the frequency or severity of extreme climate events would have profound impacts on nature and society. It is thus very important to analyze extreme events. The monitoring, detection and attribution of changes in climate extremes usually require daily resolution data. However, the compilation, provision, and update of a globally complete and readily available full resolution daily dataset is a very difficult task. This comes about, in part, because not all National Meteorological and Hydrometeorological Services (NMHS) have the capacity or mandate to freely distribute the daily data that they collect. Consequently, the ET and its predecessor, the CCl/CLIVAR Working Group (WG) on Climate Change Detection have been coordinating an international effort to develop, calculate, and analysis a suite of indices so that individuals, countries, and regions can calculate the indices in exactly the same way such that their analyses will fit seamlessly into the global picture (Karl et al. 1999, Peterson and Co-authors 2001).

To quantify the impact of precipitation changes more precisely in terms of rainfall intensity, the daily average rainfall over the Kafue River Basin (for the three GCMs and two emissions scenarios) was analyzed. Various extreme precipitation indices such as consecutive wet days, consecutive dry days, maximum 1-day precipitation (Rx1Day), maximum 5-day precipitation (Rx5Day), total annual precipitation (PRECPTOT), and simple daily intensity index (SDII is the annual total precipitation divided by the number of wet days in the year) were estimated using RClimDex (Zhang and Yang, 2004). The findings of these analyses are provided for each of the three GCMs in the following sub-sections.

2.7.2.1 Analysis of Precipitation Variability and Flow Impacts for ECHAM5

This section analyzes rainfall projections for the ECHAM5 GCM, including temporal and spatial projections for rainfall and impacts on flow.

Temporal Variation in Rainfall - Figure A2-30 (a-c) shows the temporal variation in the average annual rainfall for the baseline, A2 emissions scenario, and B1 emissions scenario for the ECHAM5 GCM. Average annual rainfall shows a more or less constant trend for the A2 emissions scenario, with significant increases in the last decade of the late 21st century period and a decreasing trend in the B1 emissions scenario (compared to the baseline period). The long term average annual rainfall changes are about -5% (early 21st century) and -2 % (mid and late 21st century) for the A2 emissions scenario and are -3% (early), -10% (mid), and -7% (late) respectively, for the B1 emissions scenario (compared to the baseline period).

Figure A2-30: Temporal Variation of Annual Rainfall to Baseline - ECHAM5 A2

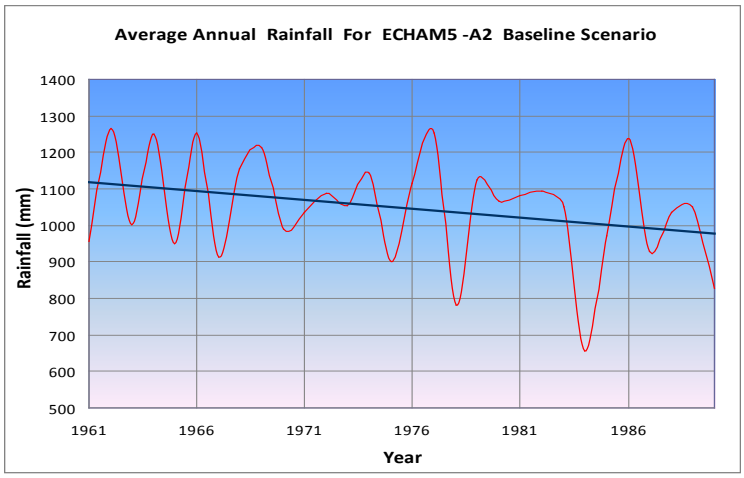

A2-30(a): ECHAM5 - Baseline Average Annual Rainfall

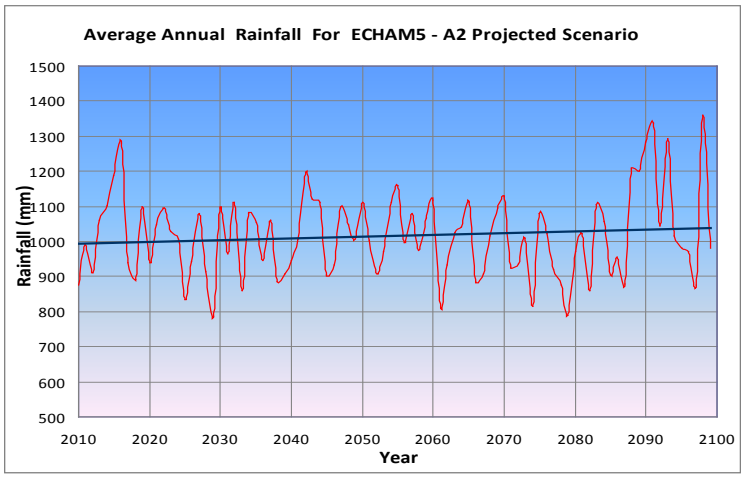

A2-30 (b): ECHAM5 A2 - Average Annual Rainfall

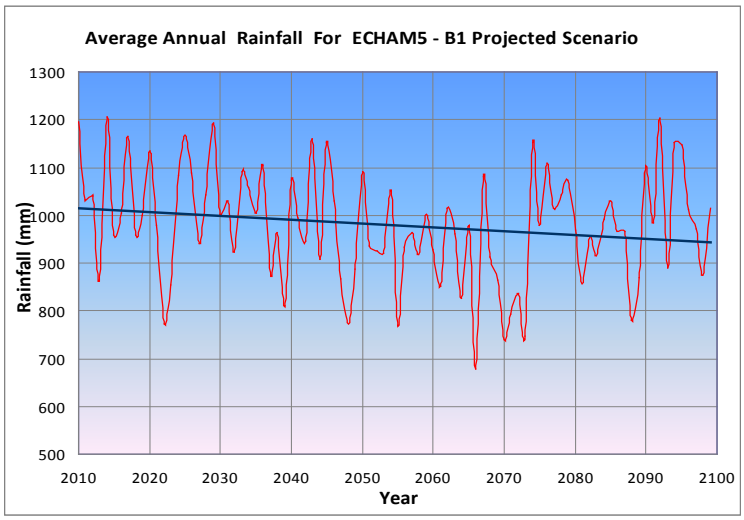

A2-30 (c): ECHAM5 B1 - Average Annual Rainfall

Spatial Variation in Rainfall - The spatial variation in average annual rainfall for ECHAM5 A2 baseline scenario is shown in Figure A2-31(a). Figure A2-31(b-d) shows the percentage change in the average annual rainfall with respect to baseline for the early, mid, and late 21st century periods, respectively.

The spatial pattern of average annual rainfall in the baseline period is well captured when compared with the historical annual average rainfall maps (Zambezi River Basin Atlas, 1998) and shows a continuous decrease in rainfall from north to south across the Kafue River Basin.

For the ECHAM5 GCM and A2 emissions scenario, decreasing trends are observed in long-term average annual rainfall across the study area during the early and mid century periods compared to the baseline period. Spatial variation shows a change in average annual rainfall in the range of -5 to -11%, -2.5 to -10%, and +1 to -13% during the early, mid, and late 21st century periods, respectively. Most of the study area experiences decreases in average annual rainfall. During the late century period, areas in the north of the Kafue River Basin show a slight increase in average annual rainfall compared to the baseline period.

Figure A2-32 (a) shows the spatial variation in the average annual rainfall for the for ECHAM5 B1 baseline period and FigureA2-32 (b-d) shows the percentage change in the average annual rainfall with respect to the baseline period for the early, mid, and late 21st century periods, respectively. For the B1 emissions scenario, decreasing trends are observed in long-term annual average rainfall over the study area during entire 21st century. The spatial variation shows a change in average annual rainfall in the range of -2.5 to -10%, -9 to -16%, and -6.5 to -14% in the early, mid, and late 21st century periods, respectively.

Overall, long-term changes in the average annual rainfall show that the mid century period may experience the most severe decrease in rainfall, compared to the early and late century periods. In the mid century period, most of the study area experiences a decrease, with the Kafue Flats showing a higher magnitude of change.

Figure A2-31: ECHAM5 A2 Baseline Average Annual Rainfall and Percent Change with Respect to the Baseline Period

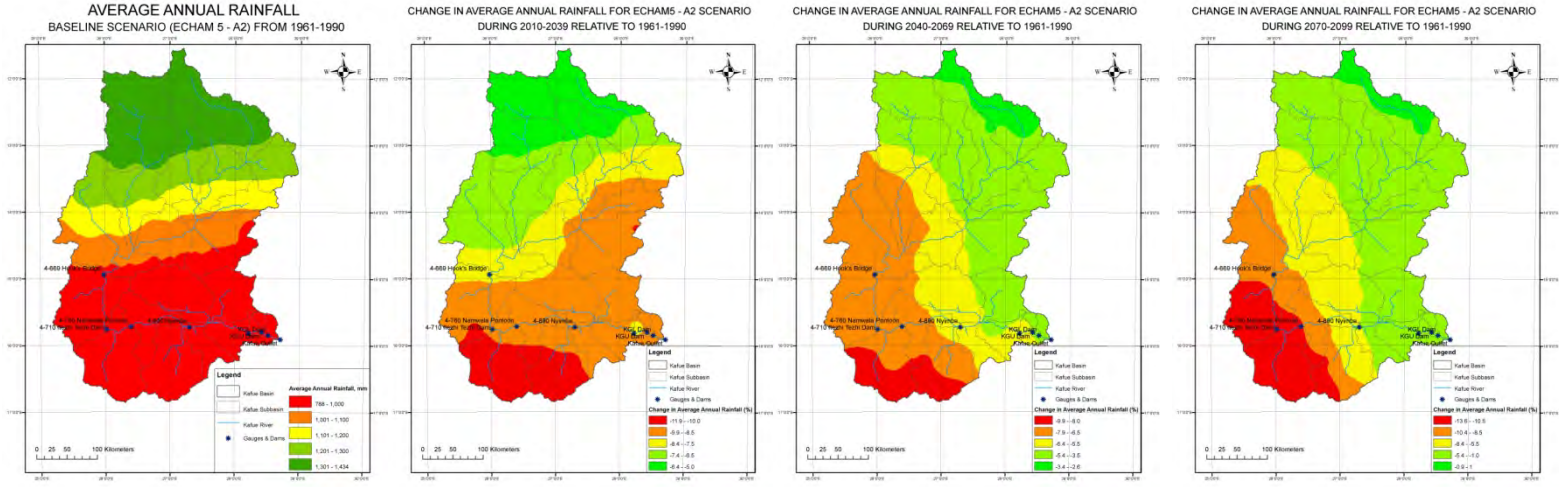

(A, Baseline) (B, Early Century) (C, Mid Century) (D, Late Century)

Figure A2-32: ECHAM5 B1 Baseline Average Annual Rainfall and Percent Change with Respect to the Baseline Period

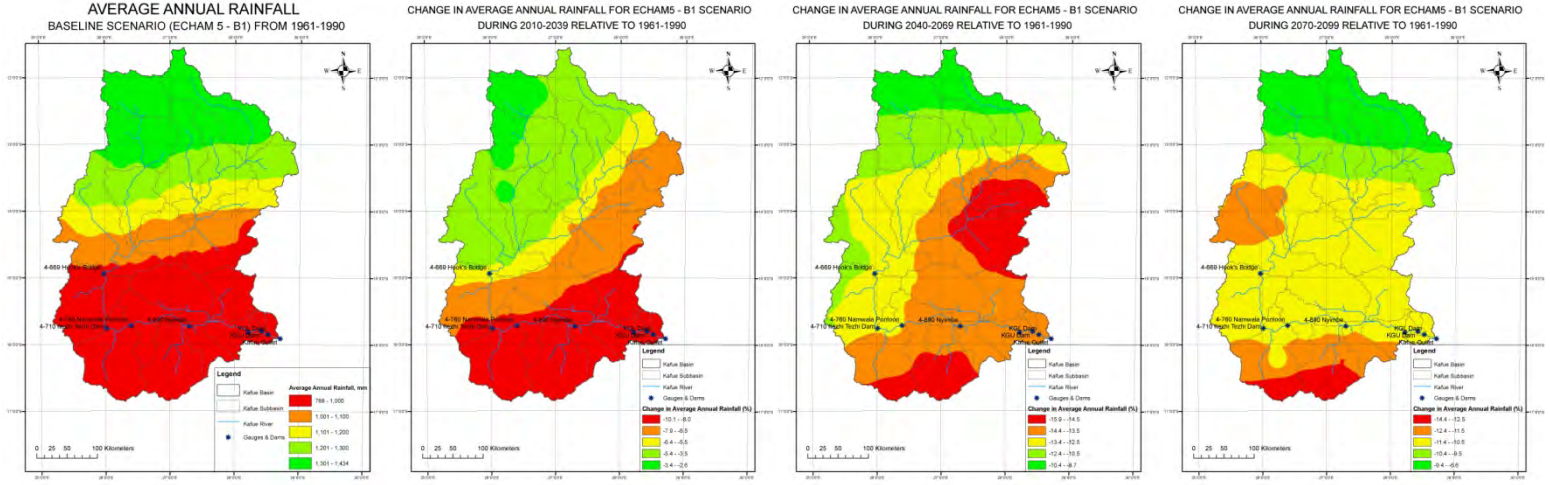

(A, Baseline) (B, Early Century) (C, Mid Century) (D, Late Century)

Impacts of Rainfall Pattern on Flows For the ECHAM5 A2 emissions scenario, the spatial and temporal changes in the long term average annual rainfall correspond to the mixed changes in the long term average annual projected flows.

The decrease in flows is much more significant than the decrease in rainfall during the early century period: an approximate -15% change in flows compared to an estimated -5% change in rainfall for the temporal variation and -5 to -11% changes for the spatial variation. Based on a review of the data and various indices, this greater decrease in flow appears to be attributable to the significant decrease in the 1-day maximum rainfall during the early century period (see Figure A2-33(a)).

During the mid century period, there is no significant change in the rainfall (an estimated -2% change from the baseline period) and similar results are observed for flows (an estimated -1% change).

During the late century, the -2% change in rainfall temporally and the +1 to -13% change in rainfall spatially results in a positive change of +11% in the flows. In this period, the maximum 1-day rainfall (Figure A2-33(a)) and annual rainfall (Figure A2-33(b)) (particularly for the last 8-10 years) are increasing compared to baseline period. The average maximum 1-day rainfall during late century period is 31mm (minimum – 13mm, maximum – 56mm and standard deviation – 9.3) as compared to 27mm (minimum – 19mm, maximum – 46mm and standard deviation – 7.1) during the baseline period. The average annual rainfall during the last 8-10 years of this period is about 1,065 mm (minimum – 848 mm, maximum – 1,341 mm and standard deviation – 164) as compared to 1,020 mm (minimum – 619 mm, maximum – 1,233 mm and standard deviation – 149) during the baseline period. As a result, the rainfall intensity (Figure A2-33(c)) is greater than in the baseline period (also showing a considerable increase in the last 8-10 years of the period). These combined factors, including the greater rainfall intensity, result in increased flows (a positive 11% change), compared to the baseline period.

Figure A2-33: Variations in Extreme Rainfall Indices (ECHAM5 A2 Emissions Scenario)

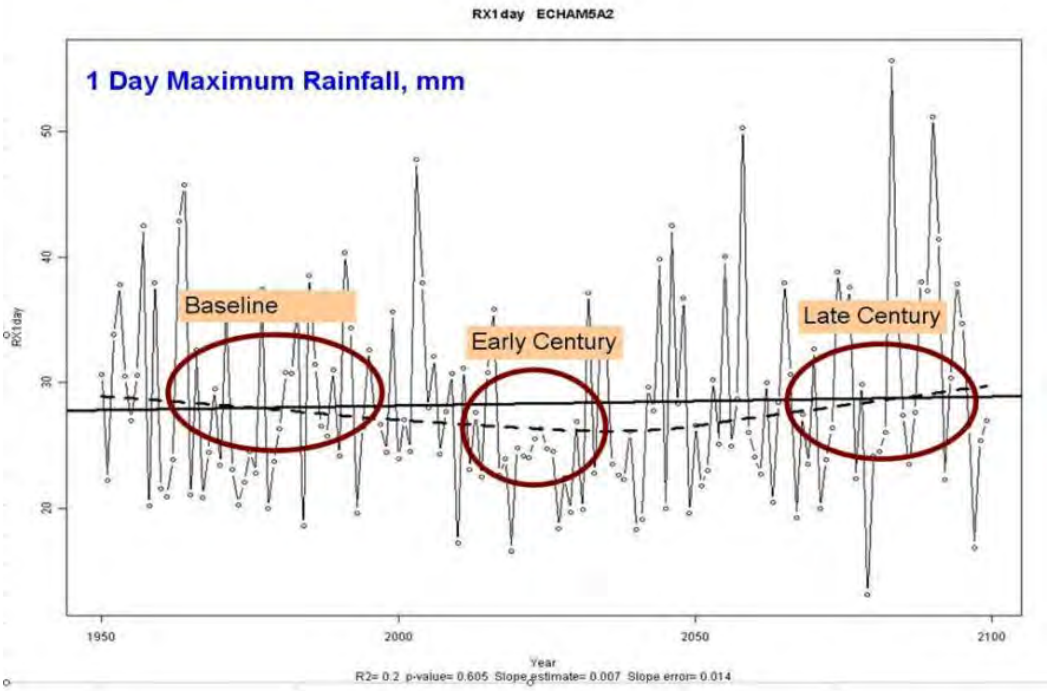

A2-33(a): ECHAM5 A2 - 1-Day Maximum

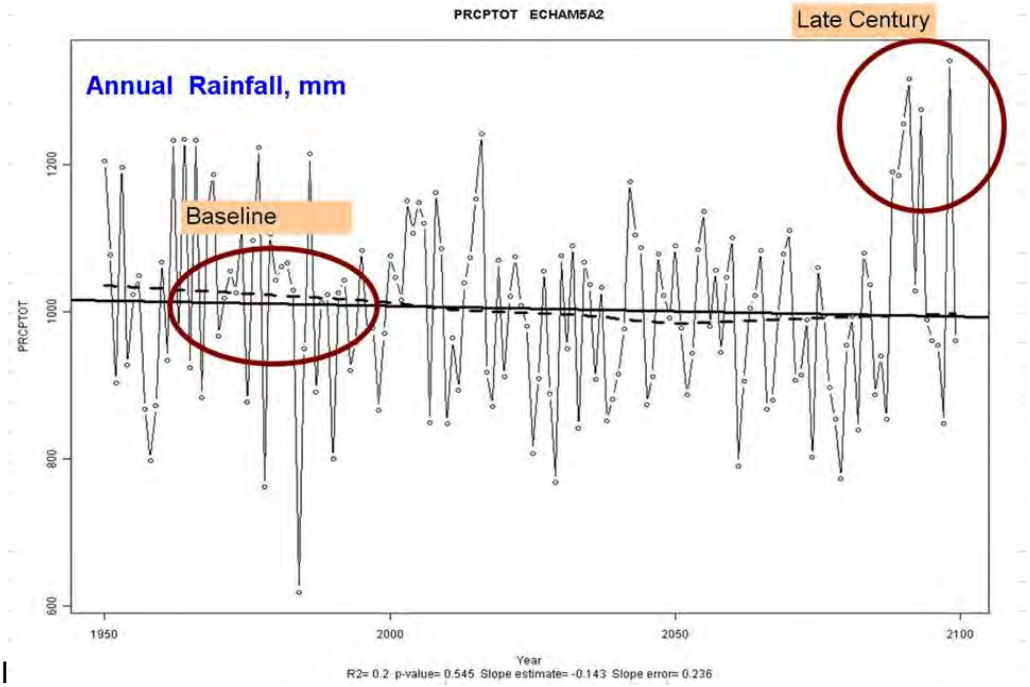

Rainfall

A2-33(b): ECHAM5 A2 - Annual Rainfall

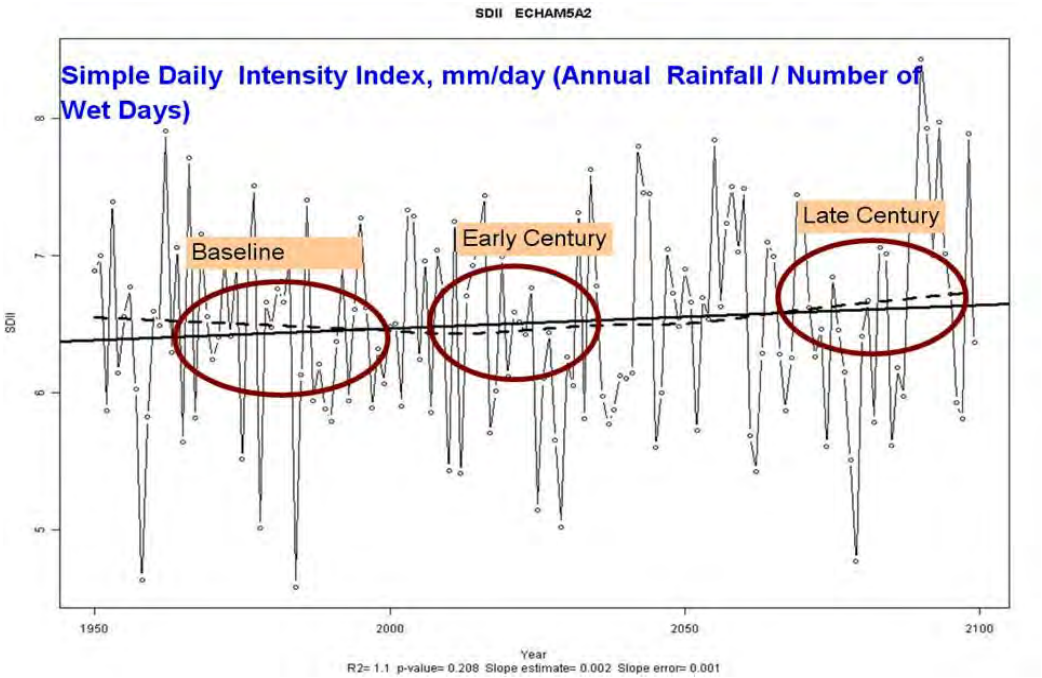

A2-33(c): ECHAM5 A2 - Rainfall Intensity

For the B1 emissions scenario, the spatial and temporal changes in long term average annual rainfall correspond to the change in the long term average annual flows. During the early century period, there is no significant change in the rainfall (an estimated -3% change) and similarly, there is no significant change in flows (an estimated -1% change). During the mid century period, however, the decrease in flows is much more significant than the decrease in rainfall. Flows change by an estimated -23% compared to a -10% change in rainfall (long term temporal variation) and a -9 to -16% change in rainfall (spatial variation). This result may be attributed to decreases in the maximum 1-day rainfall (Figure A2-34(a)), the annual total rainfall (Figure A2-34(b)), and the rainfall intensity (simple daily intensity index) (Figure A2-34(c)). During the late century, the -7 % change in rainfall (temporally) and -6.5 to -14 % change in rainfall (spatially) results in a change of -9% in Kafue River Basin flows. During this period, maximum 1-day rainfall and average annual rainfall are increasing compared to the mid century period, but decreasing compared to baseline period. The average maximum 1-day rainfall during the late century period is 29 mm; during the mid century period it is 24 mm (minimum – 17mm, maximum – 40mm and standard deviation – 5.3) as compared to 27 mm (minimum – 19mm, maximum – 46mm and standard deviation – 7.1) during the baseline period. The average annual rainfall during late century is about 970 mm and during the mid century period is 923 mm (minimum – 646mm, maximum – 1134mm and standard deviation – 111) as compared to 1020 mm (minimum – 619mm, maximum – 1233mm and standard deviation – 149) during the baseline period. As a result, the rainfall intensity is greater in the late century than in the mid century period, but still lower than during the baseline period; this results in a reduction in flows (-9% change) compared to the mid century period.

There are several factors including (but not limited to) the evapotranspiration, temperature, solar radiation, sunshine hours, relative humidity, and wind speed in addition to the spatial and temporal distribution of rainfall that govern the hydrological processes of the watershed. For

studying the combined and interrelated impact of all these parameters, a detailed distributed hydrological model such as SWAT (Soil and Water Assessment Tool) could be employed.

In the absence of a distributed hydrological model, the most influential inputs (Mutreja, 1986) were analyzed in detail to estimate the spatial and temporal variability of rainfall and its impacts on the flow regime of the Kafue River basin. The rainfall data used was the daily rainfall from all three GCMs across all four time horizons. Various extreme precipitation indices such as consecutive wet days, consecutive dry days, maximum 1-day precipitation (Rx1Day), maximum 5-day precipitation (Rx5Day), total annual precipitation (PRECPTOT), and simple daily intensity index (SDII, annual total precipitation divided by the number of wet days in the year) were estimated and compared with the trends in the flow changes. Based on this analysis, it is seen that rainfall intensity (Figure A2-33 (a), Figure A2-34 (a), and Figure A2-34(c)) and variability (Figure A2-33 (b) and Figure A2-34 (c)) have considerable impact on the changes (highest positive and highest negative) in the flow regime of the watershed across the climate change scenarios with respect to the baseline period.

Figure A2-34: Variations in Extreme Rainfall Indices (ECHAM5 B1 Emissions Scenario)

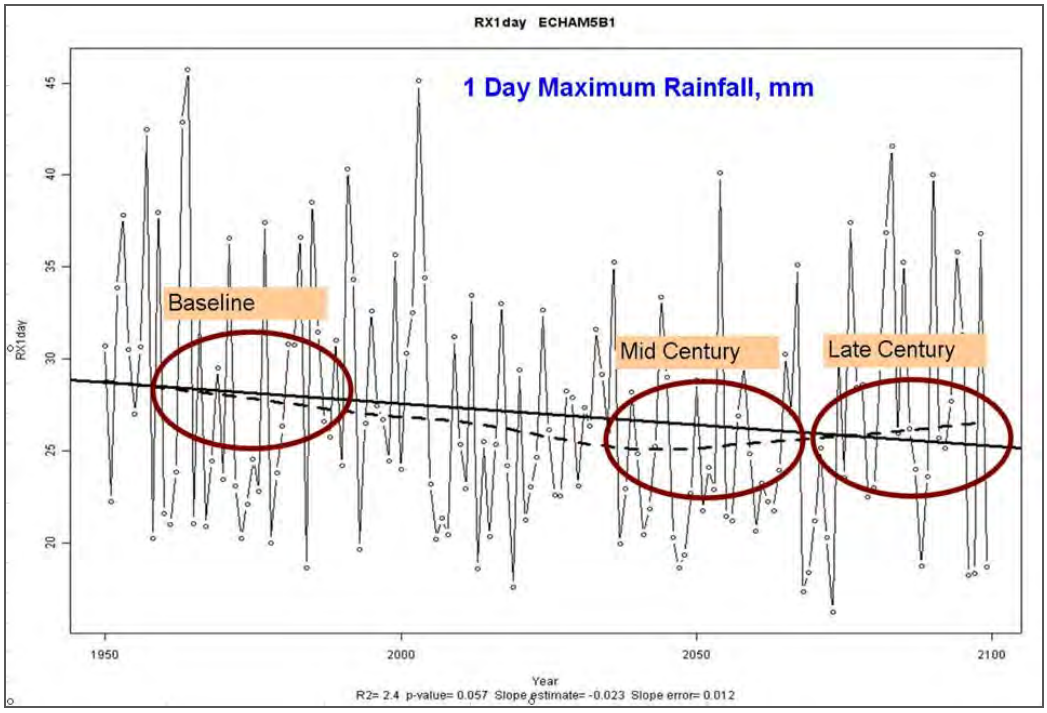

A2-34(a): ECHAM5 B1 - 1-Day Maximum Rainfall

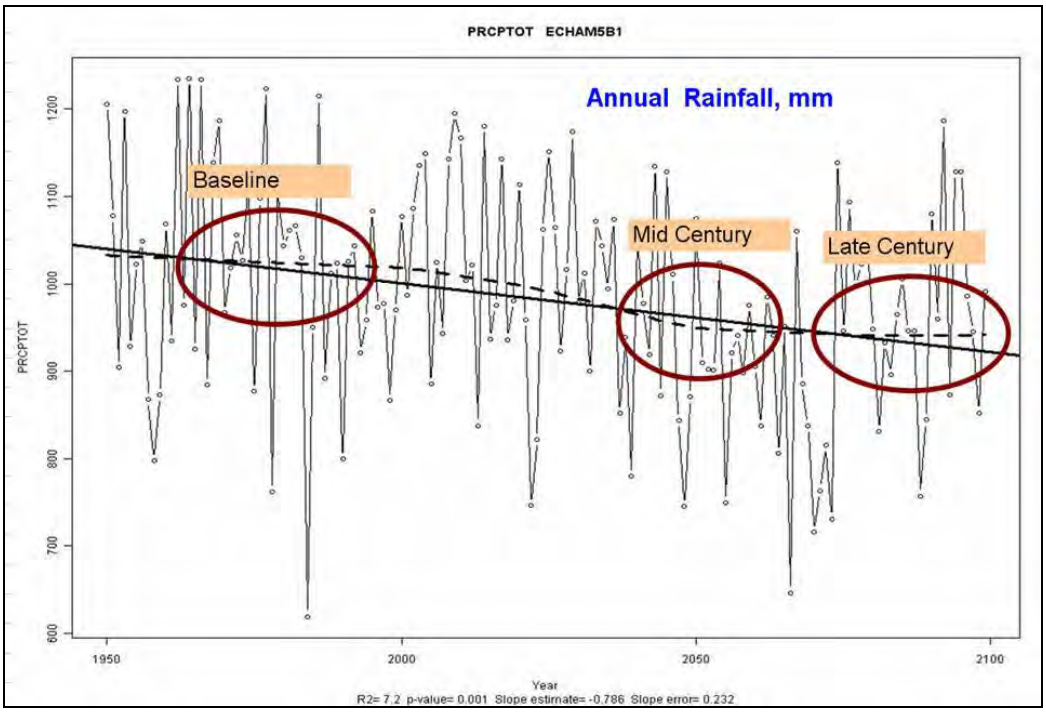

A2-34(b): ECHAM5 B1 - Annual Rainfall

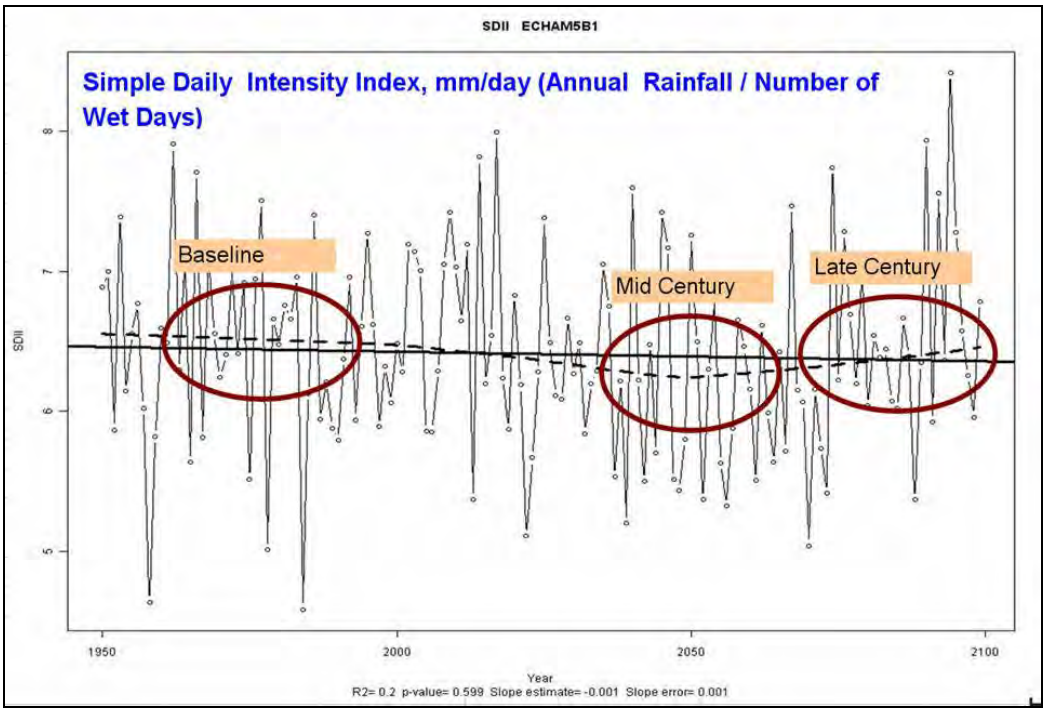

A2-34(c): ECHAM5 B1 - Rainfall Intensity

2.7.2.2 Analysis of Precipitation Variability and Flow Impacts for IPSL

This sub-section analyzes rainfall for the IPSL GCM including temporal and spatial projections for rainfall and flow impacts.

Temporal Variation in Rainfall (IPSL GCM) - Figure A2-35 (a-c) shows the temporal variation in the annual rainfall for the baseline, A2 emissions scenario, and B1 emissions scenario for the IPSL GCM. Annual rainfall shows a decreasing trend for the A2 emissions scenario and a more or less constant trend with a slight decrease in the mid and late 21st century for the B1 emissions scenario. The long term average annual rainfall changes are about -5% (early 21st century), -1% (mid 21st century) and -5% (late 21st century) for the A2 emissions scenario; changes for the B1 emissions scenario are +3 %, -2%, and -1%, across the future periods, respectively.

Figure A2-35: Temporal Variation of Annual Rainfall to Baseline (IPSL, A2 and B1 Scenario)

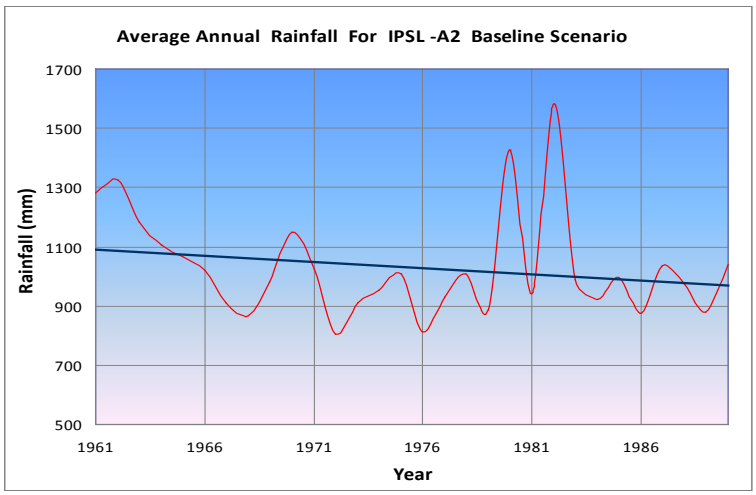

A2-35(a): IPSL - Baseline Average Annual Rainfall

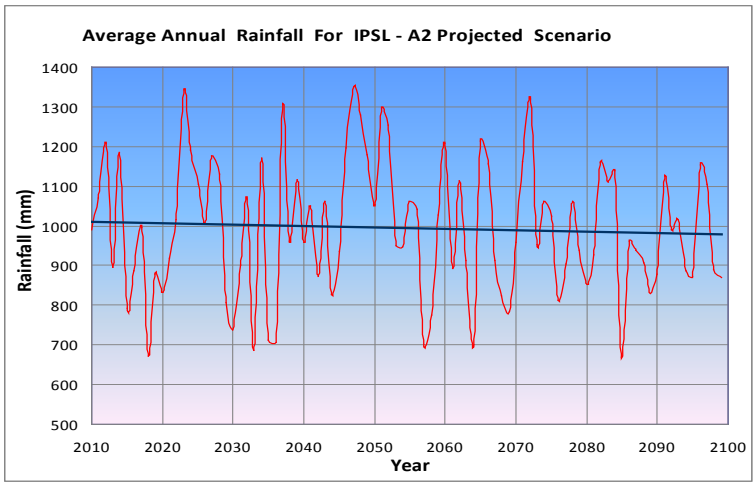

A2-35 (b): IPSL A2 - Average Annual Rainfall

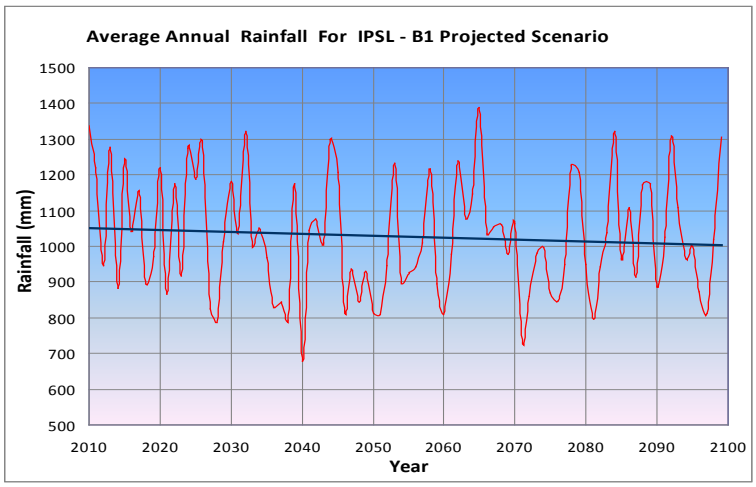

A2-35: IPSL B1 - Average Annual Rainfall

Source: RMSI.).

Spatial Variation in Rainfall (IPSL) - The spatial variation in average annual rainfall for IPSL, A2 baseline scenario is shown in Figure A2-36(a). Figure A2-36(b-d) shows the percentage change in average annual rainfall with respect to the baseline in the early, mid, and late 21st century periods, respectively.

For the A2 scenario, decreasing trends are observed in long-term annual average rainfall over the study area across the entire 21st century. Spatial variation shows a change in average annual rainfall in the range of -6 to -11%, -1.7 to -8.5%, and -1.6 to -18 % across the early, mid, and late 21st century periods, respectively. Most of the study area experiences a decrease in long term annual average rainfall. During the early century period, an area in the south (particularly in and around the Kafue Flats) shows a higher decrease in long-term average annual rainfall, compared to other parts of the basin. Areas in the south-western part of the basin near the IT dam show greater decreases in the long-term average annual rainfall, but lesser decreases in magnitude during the mid century period when compared to the early century period. During the late century period, areas near the IT dam in the southwestern part of the basin show a higher decrease in the long-term average annual rainfall, compared to other parts of the basin.

The long term trend shows that rainfall decreases are more severe in the late century period than in the early and mid century periods.

For the IPSL, B1 baseline scenario, Figure A2-37(a) shows the spatial variation in the average annual rainfall over the basin and Figure A2-37(b-d) shows the percentage change in the average annual rainfall, with respect to the baseline period for the early, mid and late 21st century periods, respectively.

For the B1 scenario, mixed trends are observed spatially in long-term annual average rainfall across the study area for the entire 21st century. In the early 21st century, mixed patterns are observed in the annual average rainfall. The spatial variation shows a change in average annual rainfall in the range of +1 to -4%, -3 to -8%, and -3 to -9% during the, mid and late 21st century periods, respectively. During the early century period, slight decreases in long-term average annual rainfall are observed in the western part of the basin, while areas in the southern and eastern parts of the basin shows slight increases in the long-term average annual rainfall. Areas in the southern part of the basin (from the IT dam to the Kafue Gorge [including the Kafue Flats]) show a greater decrease in long-term average annual rainfall, compared to other parts of the basin. During the late century period, the area from near the IT dam to the Nyamba flow gauge station and areas near the Kafue Gorge projects in the south show higher decreases in long-term average annual rainfall compared other parts of the basin.

Figure A2-36: IPSL A2 Baseline Average Annual Rainfall and Percent Change with Respect to the Baseline Period

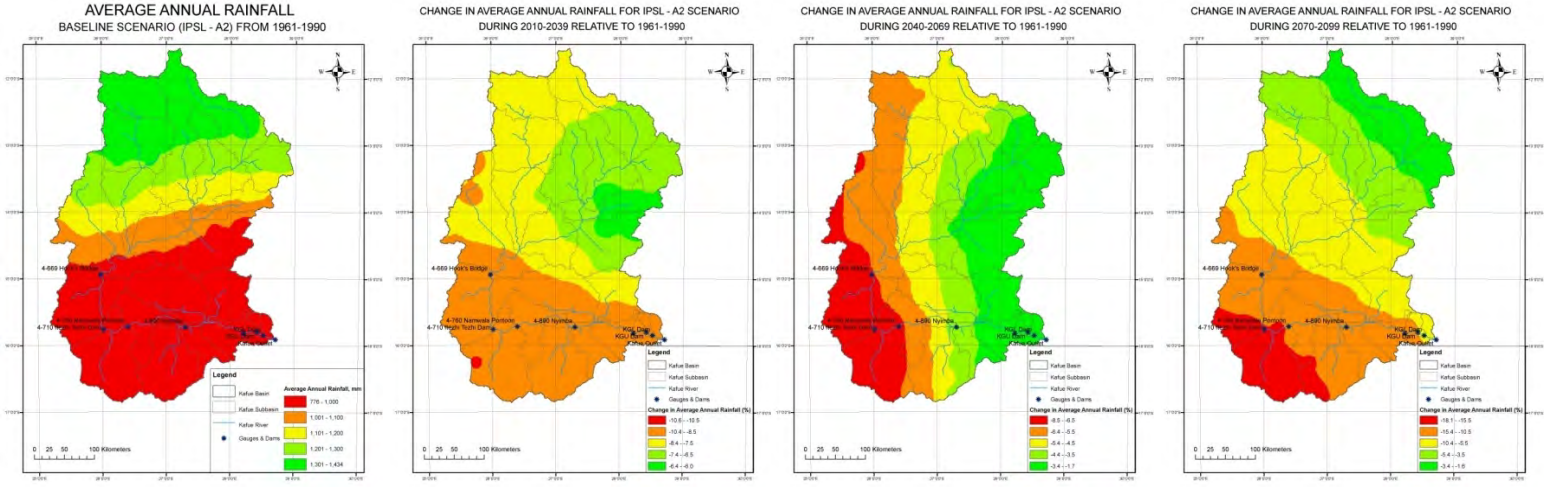

(A, Baseline) (B, Early Century) (C, Mid Century) (D, Late Century)

Figure A2-37: IPSL B1 Baseline Average Annual Rainfall and Percent Change with Respect to the Baseline Period

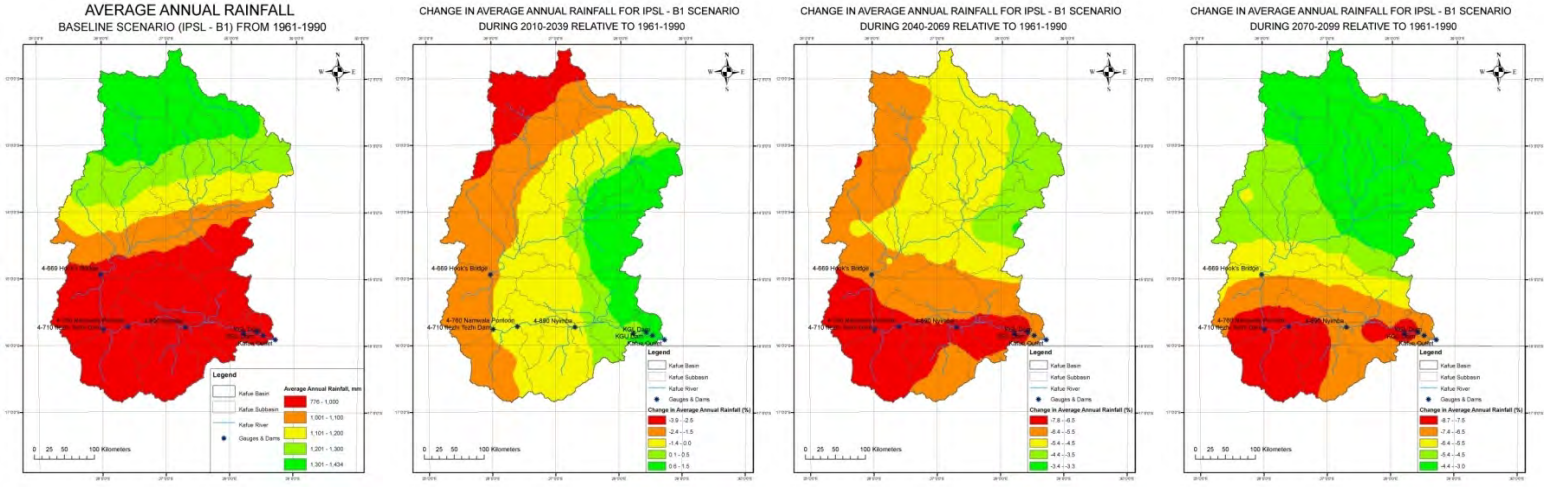

(A, Baseline) (B, Early Century) (C, Mid Century) (D, Late Century)

Impacts of Rainfall Pattern on Flows (IPSL GCM) - For the IPSL GCM, A2 emissions scenario, the spatial and temporal changes in long term annual average rainfall correspond to the resulting mixed changes observed in long term average annual flows in the Kafue River Basin.

The decreases in flows are in line with the decrease in rainfall during the early century period: an estimated -5% change in flows compared to an estimated -1% change in rainfall (temporal variation) and a -6 to -11% change in rainfall (spatial variation).

During the mid century, the rainfall changes of -1% temporally and -1.7 to -8.5% spatially, result in an estimated +5% change in the Kafue Basin flows.

In the late century period, the change of -5% in rainfall temporally and -1.6 to -18% in rainfall spatially result in a +6% changes in Kafue Basin flows. These increases in flow during the mid (5%) and late century (6%) may result from the higher maximum 1-day rainfall (Figure A2-38 (a)), higher maximum 5 day rainfall (Figure A2-38 (b)), and higher consecutive wet days (Figure A2-38(c)), compared to the baseline period. These changes in the extreme indices parameters result in more runoff producing events in the mid and late century periods.

Figure A2-38: Variations in Extreme Rainfall Indices (IPSL A2 Emissions Scenario)

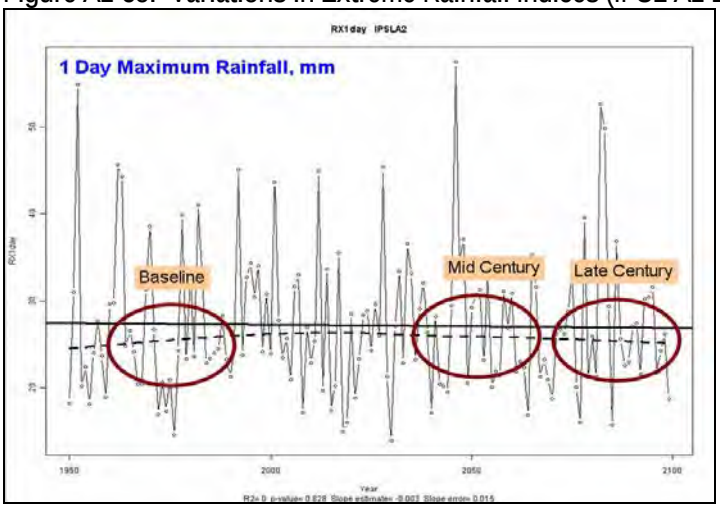

A2-38(a): IPSL A2 - 1-Day Maximum Rainfall

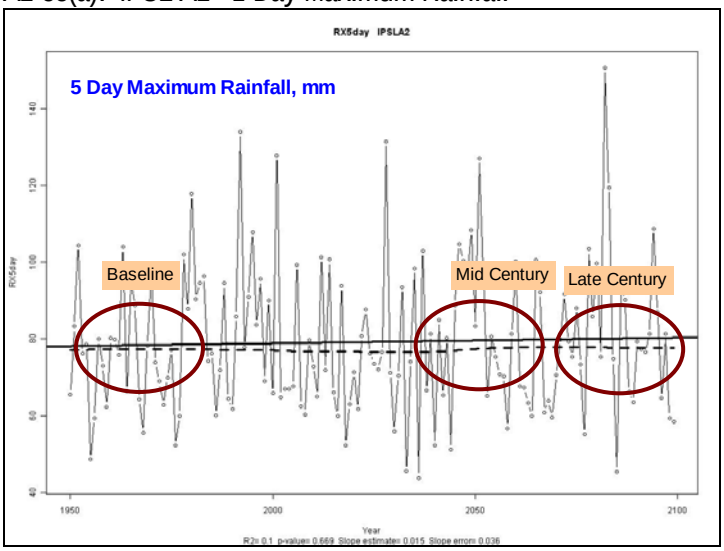

A2-38(b): IPSL A2 - 5-Day Maximum Rainfall

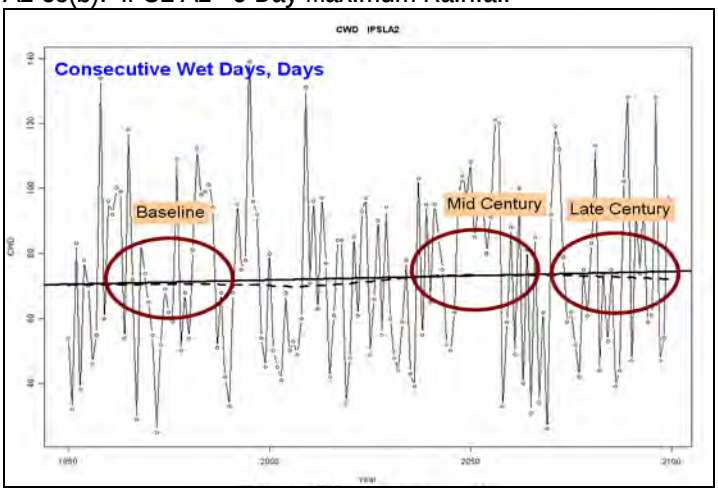

A2-38(c): IPSL A2 - Consecutive Wet Days

For the B1 emissions scenario, the spatial and temporal changes in the long term annual average rainfall correspond to the mixed changes in long term average annual flows in the study area.

During the early century period, there is a one to one change in rainfall and runoff. The estimated 3% increase in rainfall temporally and estimated +1.5 to -3.9% changes in rainfall spatially correspond to a flow increase of about 4% during this period.

During the mid century period, the -2% change in rainfall temporally and the -3 to -8% changes in rainfall spatially result in zero to minimal flow changes compared to the baseline period flows.

During late century, the estimated 1% decrease in rainfall temporally and -3 to -9% changes in rainfall spatially correspond to increased flows of about 4%. This increase in flows is driven by the changes in the extreme indices. For example, during this period, there is an increased maximum 1-day rainfall (Figure A2-38(a)), increased annual total rainfall (Figure A2-38(b)), and increased rainfall intensity (simple daily intensity index) (Figure A2-38(c)) compared to the baseline and mid century periods. Similar trends in rainfall patterns are observed during the early century period, which also results in increased average annual flows (about 4%).

2.7.2.3 Analysis of Precipitation Variability and Flow Impacts for MRI

This sub-section analyzes rainfall for the MRI GCM including temporal and spatial projections for rainfall and flow impacts.

Temporal Variation in Rainfall (MRI GCM) - Figure A2-39(a-c) shows the temporal variation in the annual rainfall for the baseline, A2 emissions scenario, and B1 emissions scenario for the MRI GCM. Annual rainfall shows a decreasing trend for the A2 and B1 emissions scenarios compared to baseline. The long term average annual rainfall changes are about -7% (early 21st century), -6% (mid 21st century) and -10% (late 21st century) under the A2 emissions scenario; changes for the B1 emissions scenario are -7 %, -11%, and -6%, respectively for the early, mid, and late century periods compared to baseline.

Figure A2-39: Temporal Variation of Annual Rainfall to Baseline (MRI, A2 and B1 Scenarios)

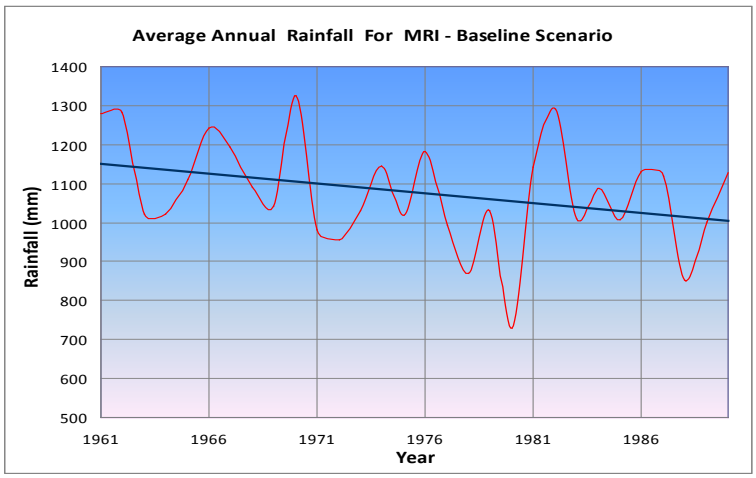

A2-39(a): MRI - Baseline Average Annual Rainfall

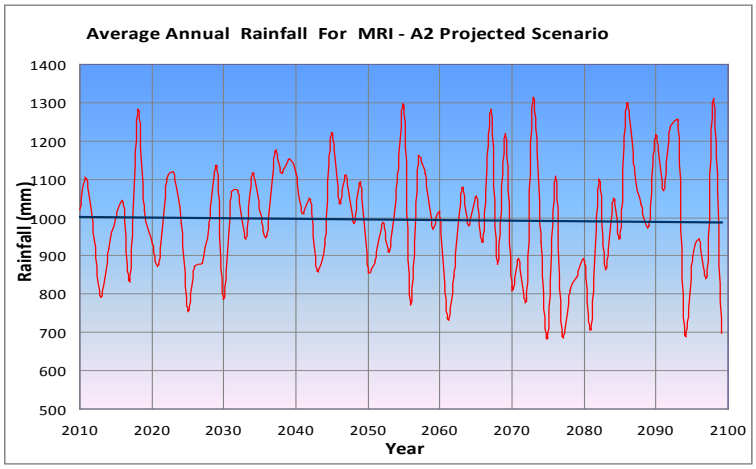

A2-39(b): MRI A2 - Average Annual Rainfall

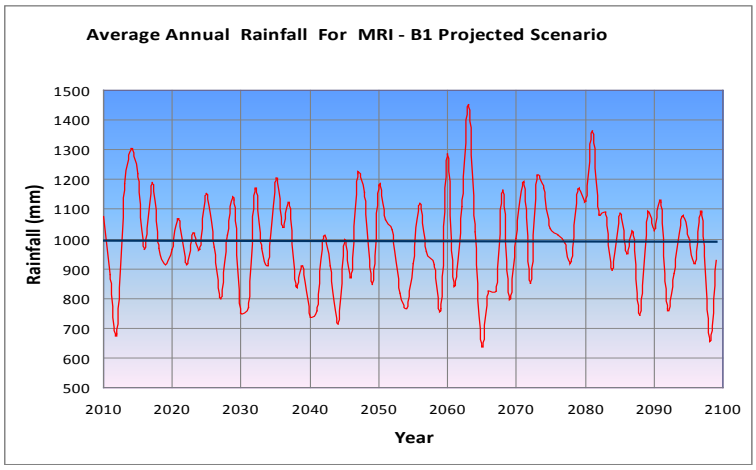

A2-39(c): MRI B1 - Average Annual Rainfall

Spatial Variation in Rainfall (MRI GCM) - The spatial variation in average annual rainfall for the MRI, A2 baseline scenario is shown in Figure A2-40(a). Figure A2-40(b-d) shows the

percentage change in average annual rainfall with respect to baseline across the early, mid and late 21st century periods, respectively.

For the A2 scenario, decreasing trends are observed in long-term average annual rainfall over the study area during entire 21st century. The spatial variation shows a change in average annual rainfall in the range of -6 to -13%, -4 to -10 % and -6 to -16 % for the early, mid and late 21st century periods, respectively. During the early century period, greater decreases in long-term average annual rainfall are observed in south-western part of the basin (from Hook's bridge to the KGL dam comprising the Kafue Flats). During the mid century period, the small area in the central west part of the basin near Hook's bridge shows a greater decrease in long-term average annual rainfall, compared to the other parts of the basin. During the late century period, areas in the west (near the IT Dam to the Namwala Pontoon flow gauge station) and in the southwest below the Kafue Flats shows a higher decrease in the long-term average annual rainfall, compared to other parts of the basin.

The long term trend in average annual rainfall shows that rainfall decreases are more severe in the late century period than for the early and mid century periods, with most of the study area experiencing a decrease during this time period.

For the MRI, B1 baseline scenario, Figure A2-41(a) shows the spatial variation in the average annual rainfall and Figure A2-41(b-d) shows the percentage change in the average annual rainfall with respect to the baseline for the early, mid and late 21st century periods, respectively.

For the B1 scenario, decreasing trends are observed in long-term annual average rainfall over the study area across the entire 21st century study period. Spatial variation shows a change in average annual rainfall in the range of -6 to -12%, -7 to -17 % and -4 to -11 % during the early, mid and late 21st century periods, respectively. During the early century period, higher decreases in long-term average annual rainfall are observed in south eastern part of the basin (near the Kafue Gorge hydropower projects), compared to other parts of the basin. Areas in the southern part of the basin (from Hook's Bridge to the Kafue Gorge [including the Kafue Flats]) show a greater decrease in long-term average annual rainfall, compared to other parts of the Kafue Basin. During the late century period, areas in the west (near Hook's Bridge to the IT Dam) and in the southwest (below the Kafue Flats) show a higher decrease in long-term average annual rainfall, when compared to other parts of the basin.

The long term trend in the average annual rainfall shows that rainfall decreases are more severe in mid century period than for the early and late century periods.

Figure A2-40: MRI A2 Baseline Average Annual Rainfall and Percent Change with Respect to the Baseline Period

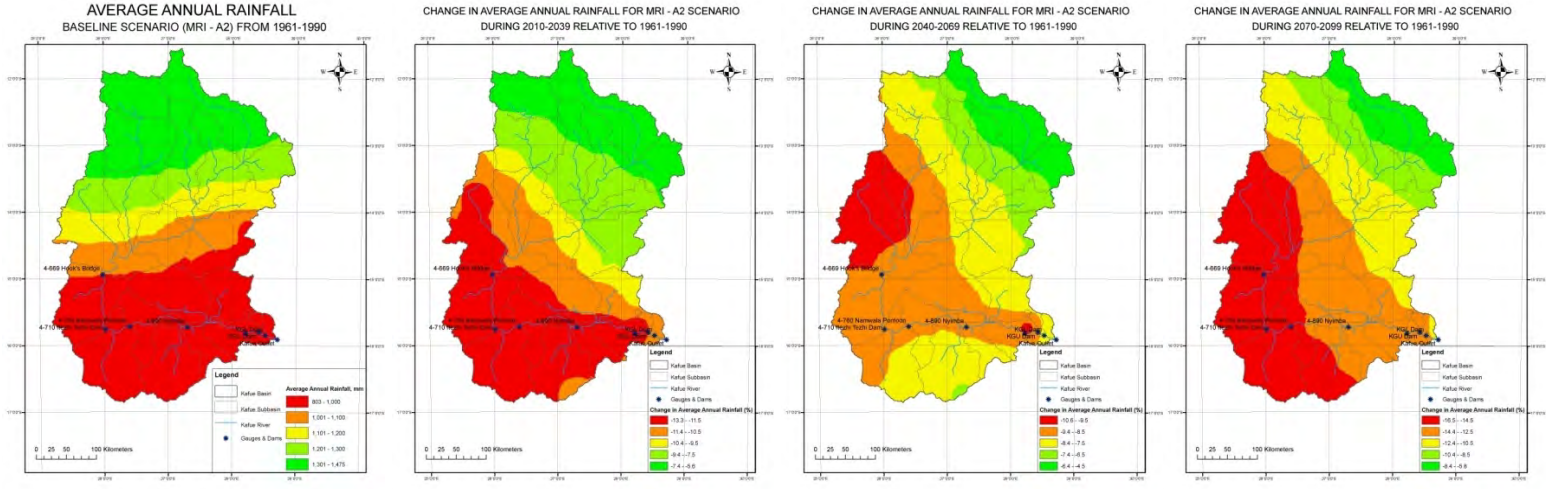

(A, Baseline) (B, Early Century) (C, Mid Century) (D, Late Century)

Figure A2-41: MRI B1 Baseline Average Annual Rainfall and Percent Change with Respect to the Baseline Period

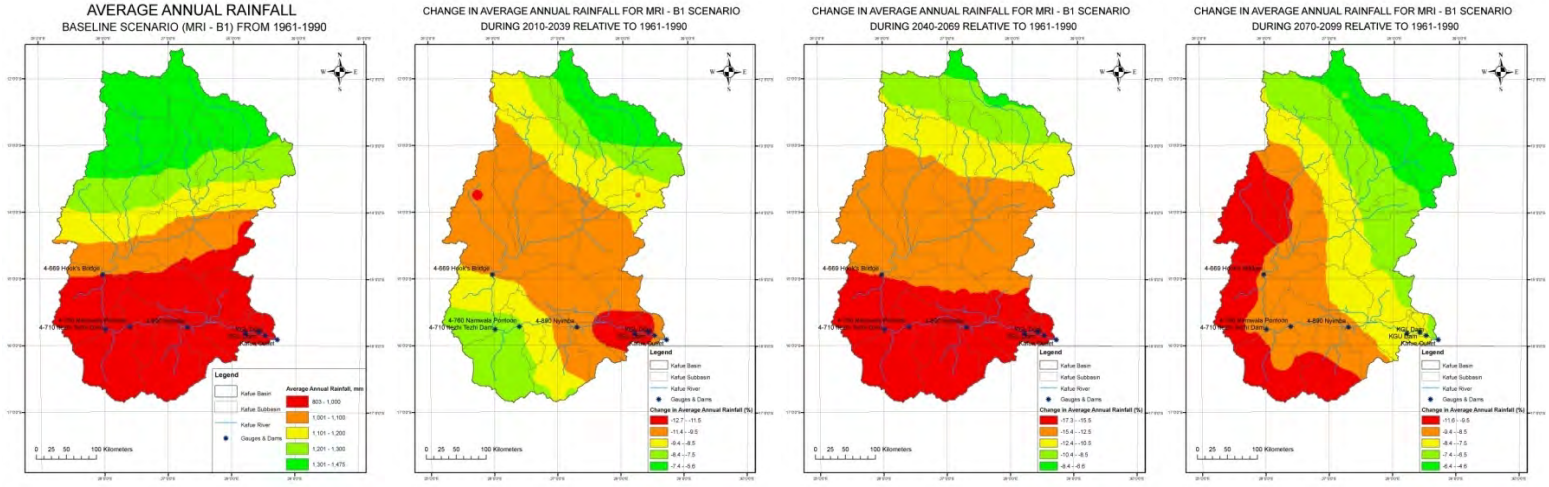

(A, Baseline) (B, Early Century) (C, Mid Century) (D, Late Century)

Source: RMSI (additional detail is provided in Appendix A2).

Impacts of Rainfall Pattern on Flows (MRI GCM) - For the MRI GCM, with the A2 emissions scenario, the spatial and temporal changes in the long term annual average rainfall correspond to the mixed changes in long term average annual flows.

For the early and mid century periods, there is no change in the flows despite decreases in rainfall temporally (-7% and -6% during the early and mid century periods, respectively) and decreases in the rainfall spatially (-4 to -10% and -6 to -16 % during the early and mid century periods, respectively). The generally constant maximum 1 day rainfall (Figure A2-42(a)) and decreasing annual total rainfall (Figure A2-42(b)) during the early and mid century periods, show that the rainfall intensity (simple daily intensity index) is nearly equal to the intensity in the baseline period (Figure A2-42(c)). This constant rainfall intensity during the early and mid century period can be attributed to the relatively constant flows observed in the model.

The decrease in flows is much more significant than the decrease in rainfall during the late century period. An estimated -10% change in flows is observed compared to the approximate -6% change in rainfall over the long term (temporal variation) and the estimated -6 to -16% changes in rainfall for spatial variation. This decrease in the flows may result because of the decrease in maximum 1-day rainfall (particularly, in the last 10-20 years), combined with an overall decrease in average annual rainfall during this period, compared to baseline period.

Figure A2-42: Variations in Extreme Rainfall Indices (MRI, A2 Scenario)

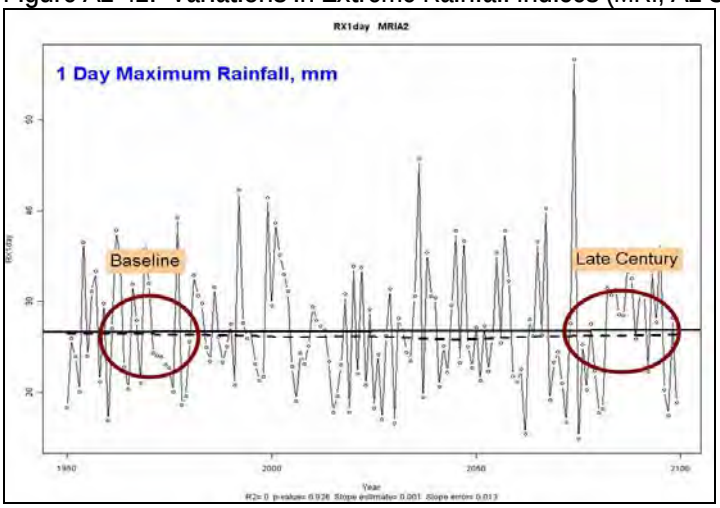

A2-42(a): MRI A2 - 1-Day Maximum Rainfall

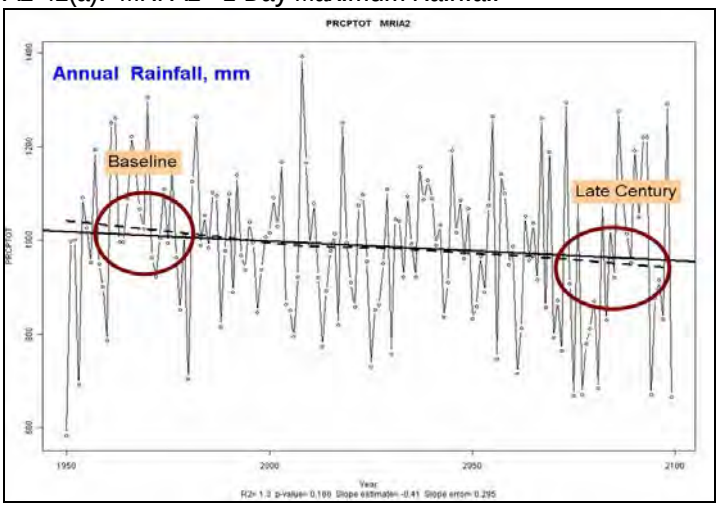

A2-42(b): MRI A2 - Annual Rainfall

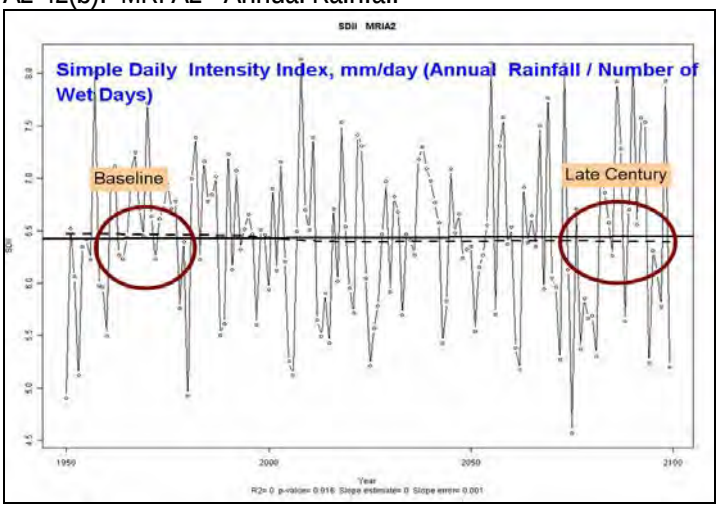

A2-42(c): MRI A2 - Rainfall Intensity

For the MRI B1 emissions scenario, the spatial and temporal changes in the long term annual average rainfall correspond to the mixed changes in the long term average annual flows.

During the early and mid century period, there is one to one change in rainfall and runoff. During the early century, the 7% decrease in rainfall temporally and -6 to -12% changes in rainfall spatially correspond to a decrease in average annual flows of about 9%. An 11% decrease in the rainfall temporally and -7 to -17% changes in rainfall spatially correspond to flow decreases of about 15%. This may be due to a decrease in the maximum 1 day rainfall (Figure A2-43(a)), decrease in annual total rainfall (Figure A2-43(b)), and a lower rainfall intensity (Figure A2-43(c)), compared to the baseline period.

During late century, about 6% decrease in the rainfall temporally and -4 to -11% changes in rainfall spatially correspond to flow increases of about 1%. This slight increase in flows is due to increases in the annual rainfall and rainfall intensity, compared to baseline period.

Figure A2-43: Variations in Extreme Rainfall Indices (MRI, B1 Scenario)

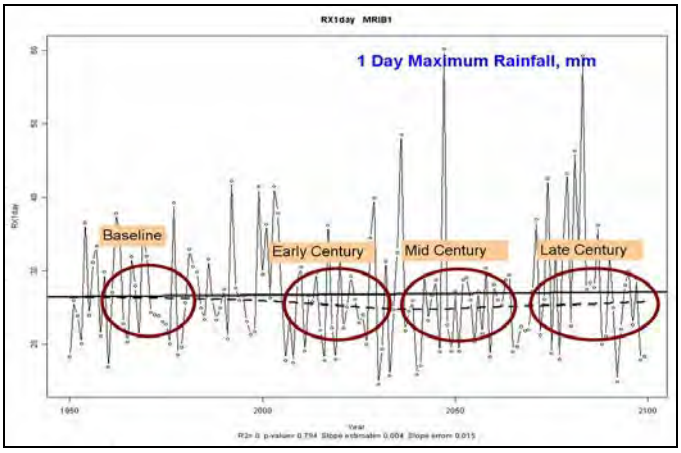

A2-43(a): MRI B1 - 1-Day Maximum Rainfall

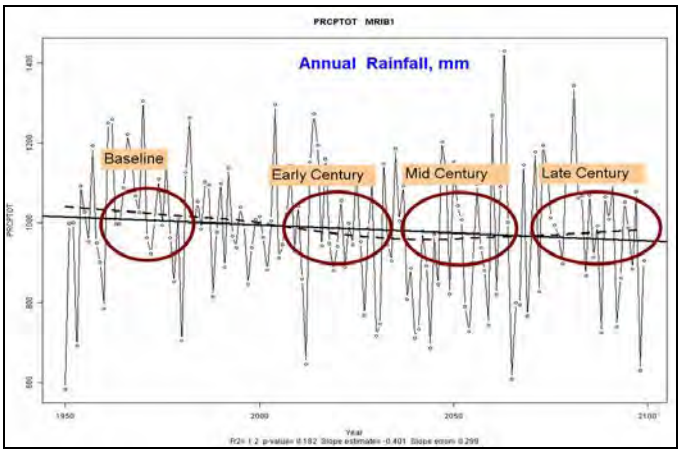

A2-43(b): MRI B1 - Annual Rainfall

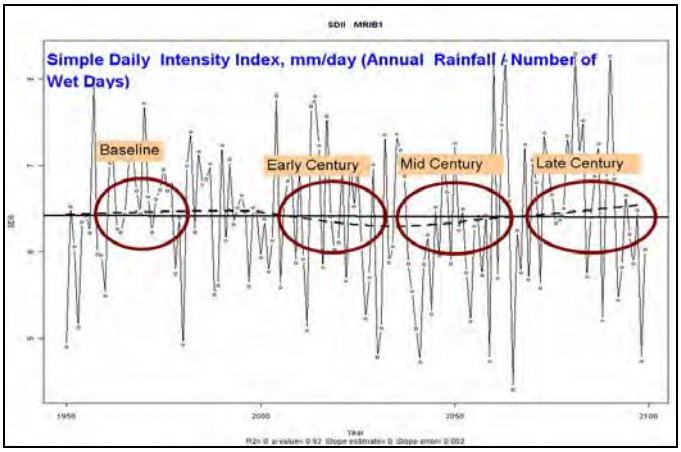

A2-43(c): MRI B1 - Rainfall Intensity

2.7.3 Discussion and Outputs for HEC-ResSim

Sections 2.7.1 and 2.7.2 show that the ECHAM5 GCM is generating the highest positive and negative flow changes compared to its respective baseline. The maximum average monthly flows occur earlier for this GCM as compared to the baseline flows in both emissions scenarios. The daily flows from all 24 combinations of scenarios from HEC-HMS runs were provided as inputs to the HEC-ResSim model for the energy modeling. The inflows to the IT reservoir and flows from the sub basins joining the Kafue River downstream of the IT reservoir were provided as separate DSS files. An example screen shot of a DSS file for input to the HEC-ResSim model is shown in Figure A2-44 for the ECHAM5 A2 scenario for the late century time period.

Figure A2-44: Screen Shot of DSS File for Input to HEC-ResSim Model

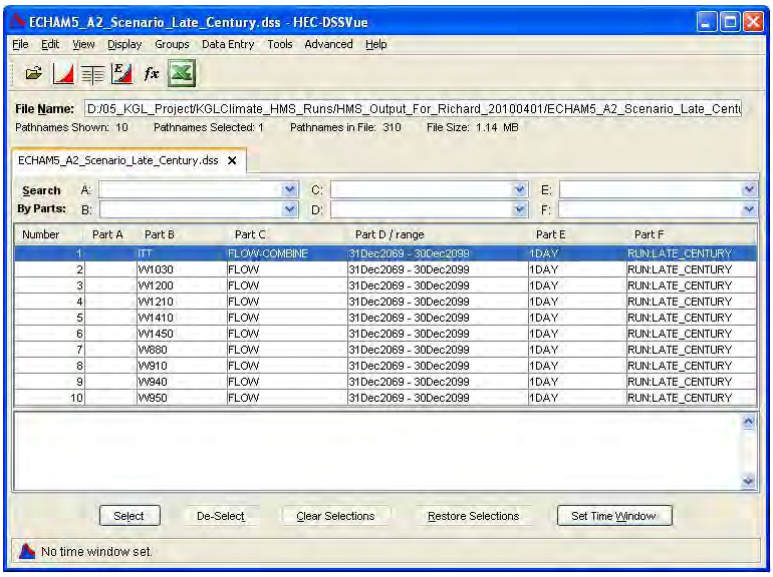

2.8 Probabilistic Variability (WXGEN) Analysis

This section discusses the analysis performed using WXGEN and HEC-HMS for the two selected scenarios of highest positive and negative change in flow compared to their respective baseline periods. This subsection includes (1) an introduction to WXGEN models, (2) a description of WXGEN set up and validation, and (3) a presentation of the analysis findings for the two scenarios selected.

2.8.1 Introduction to WXGEN

A stochastic WG produces a synthetic time series of weather data of infinite length for a location based on the statistical characteristics of observed weather at that location. A WG is not a predictive tool that can be used in weather forecasting; it is simply a means of generating time-series of synthetic weather statistically "identical" to the observed data. Applications of WG approaches can support areas where meteorological data is scarce and can support climate change studies (as discussed below).

Primarily, there are two types of WGs, Richardson (Richardson, 1981; Richardson and Wright, 1984) and Serial (Racsko et al., 1991; Semenov et al., 1998).

In the Richardson type WG (e.g., WXGEN), precipitation is modeled using a first-order, two-state Markov procedure, which describes two precipitation classes (i.e., wet or dry), and takes into account precipitation on the previous day only. More complex models may involve more than one precipitation class (e.g., low, medium and high precipitation amounts) as well as considering the occurrence of precipitation on a number of days prior to the current day, rather than just considering the previous day. The Markov process provides information on transition probabilities (e.g., the probability of a wet day following a dry day or the probability of a wet day following a wet day), calculated from the observed station data. If precipitation occurs, then the amount of precipitation falling on wet days is determined. The determination is usually made by using a predefined frequency distribution, most commonly the gamma distribution (although mixed-exponential distributions may provide a better representation of the precipitation amount at some locations). The remaining climate variables are then calculated based on their correlations with each other and on the wet or dry status of each day.

In the Serial type of WG, the first step in the process is to model the sequential series of dry and wet days. The amount of precipitation and the remaining climate variables are then generated and are dependent on the wet or dry series. The Serial Type WG (e.g., LARS-WG), first developed by Racsko et al. (1991), has been substantially updated (Semenov et al., 1998), and the software is now freely available.

Both WGs have a similar structure as both use observed data to fit the parameters for the daily distributions of the variables for minimum and maximum temperature, precipitation, and solar radiation. Both generators analyze dry and wet days separately and include a mechanism for selecting the precipitation status of each day in the generated weather data.

Both types of WGs require initial calibration based on observed station data. The calibration process results in a parameter file containing information about the statistical characteristics of the observed data, which is then used to generate a series of synthetic data. Data for any length of time may be used to calibrate a WG, although at least 10 years of data should be available and longer lengths are recommended in highly variable climates. Model verification is generally undertaken by comparing the statistics of the synthetic data with those of the observed data set used to calibrate the model.

In addition to generating a time series of daily weather data of almost infinite length based on the statistics of an observed station record, stochastic WGs are also useful for generating synthetic time series in regions of data scarcity. A WG can be run at a number of stations within a particular region, with a parameter file produced for each station. These parameters can then be spatially interpolated and interrogated for a particular location at which observational data is unavailable. This allows the generation of synthetic data at this location. The larger the number of stations available for use in a WG in a particular region, the more confidence there will be in the parameters derived from the interpolation procedure and consequently in the statistical characteristics of the synthetic data at the location lacking historical observations. The generation of synthetic data in regions of data scarcity is generally only recommended for areas where the regional climate is relatively homogeneous.

The main use of stochastic WGs, however, is in the generation of synthetic daily weather data for climate change scenarios. Most climate change scenarios consist of monthly changes with respect to a particular baseline period (currently 1961-1990), while many impact applications require daily weather data. At present there is little confidence in the daily data output by GCMs, particularly for use in impact applications. However, it is possible to derive daily weather data from monthly GCM-derived scenario information by perturbing the WG parameter files by the monthly scenario changes. For example, a particular scenario may indicate an increase in mean temperature of 2.4°C in January. This value would be added to the monthly mean temperature value for January contained in the model's parameter file.

WG applications are used for a number of study goals, including:

- The first is to provide weather data time series long enough to assess risk in hydrological or agricultural applications. Observed daily weather data (maximum temperature, minimum temperature, precipitation, solar radiation, and relative humidity) is one of the major inputs into mathematical models in hydrology, agriculture, and land use, but the length of the time series is often insufficient to allow a good estimation of the probability of extreme events. Moreover, the observed time series represents only one 'realization' of the climate, whereas a WG can simulate many 'realizations,' providing synthetic data for a wider range of feasible situations.

- The second reason is to provide a means for extending the simulation of weather to locations where observed weather data is not available. This can be achieved by interpolating the parameters of a WG between sites using an interpolation technique such as Kriging or thin-plate smoothing splines (Hutchinson, 1995).

- A third application has recently arisen from climate change studies. The output GCMs, which are the main tools for predicting the evolution of climate on Earth, cannot be used directly at a site because of their very coarse spatial resolution. A WG can serve as a tool to produce site-specific climate change scenarios at the daily time-step. The changes in both climatic means and climate variability predicted by the GCM experiments can be applied to the parameters derived by the WG for the current climate at the site in question. Daily scenario data can then be obtained by running the WG using this revised set of parameters (Wilks, 1992, Semenov & Barrow, 1997).

- The fourth application of a stochastic WG is to simulate synthetic weather series that resemble the observed ones in selected statistical characteristics. This application is particularly advantageous if one is concerned with rarely occurring (extreme) events, such as drought and flood, the probabilities of which may be estimated from these long runs with a smaller uncertainty than from short runs and/or observed weather series.

For the purposes of the KGL study, the fourth application of the WG tool is used.

2.8.2 WXGEN Model Set up and Validation

The WG selected for this study is the Richardson model, WXGEN. This model has been developed at USDA/ARS Grassland Soil & Water Research Laboratory, based on the techniques described in the literature (Richardson, 1981). It was applied for this pilot study in order to obtain long term synthetic weather series (200 years) and to estimate the magnitude and frequency of events from the 200 years of simulated weather data. The WXGEN was used to simulate observed weather data for 10 stations and 3 GCMs for 70 grid points. Observed weather data was provided for the area for the years 1975 to 2005 by the Lusaka Meteorological Department. Daily observed weather data is available for 11 stations for the period 1975 to 2005 and was used for this study. Gridded daily observation-based data is available for the period 1950 to 1999.

Table A2-16 summarizes the future time horizons established for the study.

Table A2-16: Future Time Horizons Used for Study

Time Horizons	
Early Period	2010-2039
Mid-Century Period	2040-2069
End of Century Period	2070-2099

After reviewing the available data and references, the following data inputs were selected for WXGEN modeling:

- *Data input one:* Historical weather data for 10 stations.
- *Data input two:* Three GCMs (ECHAM5, MRI and IPSL), 2 emissions scenarios (A2 and B1), and 3 time horizons (early, mid, and late century) for 70 grid points. Subsequently, a subset of these models was selected, ECHAM5 A2 late century and ECHAM5 B1 mid century, to analyze the minimum and maximum range of changes in flow compared to a baseline period.

The selected inputs were simulated for 200 years using WXGEN. A total of 1,270 simulation exercises were carried out. The robustness of WXGEN simulated data was then tested by comparing the average and standard deviation of maximum temperature (T_{max}), minimum temperature (T_{min}), and rainfall (R) for WXGEN simulated and observed data. Tables A2-17 and A2-18 show the comparative results for observed and simulated (WXGEN) weather data for the Kafiro station.

Table A2-17: Comparative Results of Monthly Means between Observed and Simulated Weather Data for Kafue Station

Month	Mean					
	T_{max} (°C)		T_{min} (°C)		Precipitation (mm)	
	Observed	Simulated	Observed	Simulated	Observed	Simulated
Jan	27.7	27.5	16.8	16.8	320.6	312.4
Feb	27.9	27.7	16.7	16.7	239.7	225.3
Mar	28.4	28.4	16.1	16.2	201.5	195.7
Apr	28.6	29.0	12.8	12.9	57.0	64.5
May	28.0	28.1	7.3	7.4	7.4	9.3
Jun	26.4	26.4	3.6	3.6	0.0	0.0
Jul	26.4	26.3	3.2	3.2	0.5	0.5
Aug	28.8	28.7	6.0	5.8	0.3	0.4
Sep	31.8	31.8	9.6	9.6	3.4	2.9
Oct	32.3	32.7	13.4	13.2	31.5	27.5
Nov	30.5	30.6	15.9	15.9	124.7	123.0
Dec	28.2	28.0	16.9	16.9	280.2	281.0

Notes: mm = millimeters.

Table A2-17 (above) presents the comparison of the mean historical and WXGEN simulated maximum and minimum temperatures for the Kafiro station. In the case of temperature, the differences between observed and simulated means are in the range of $\pm$ 0.4°C. For precipitation, the difference between observed and simulated means are $\pm$ 5%.

Table A2-18: Comparative Results of Monthly Standard Deviation between Observed and Simulated Weather Data for Kafue Station

Month	Mean					
	T_{max} (°C)		T_{min} (°C)		Precipitation (mm)	
	Observed	Simulated	Observed	Simulated	Observed	Simulated
Jan	1.81	1.54	1.01	0.82	14.52	14.3
Feb	1.76	1.65	1.04	0.88	12.32	11.7
Mar	1.52	1.68	1.40	1.16	12.19	11.3
Apr	1.66	1.49	2.77	2.03	5.26	6.0
May	1.74	1.44	2.71	2.07	0.85	1.2
Jun	1.62	1.40	2.29	1.50	0.00	0.0
Jul	1.71	1.29	2.22	1.35	0.09	0.1
Aug	1.96	1.48	2.45	1.76	0.05	0.1
Sep	1.52	1.15	2.76	1.95	0.47	0.5
Oct	2.04	1.71	2.67	1.89	3.35	3.1
Nov	2.39	2.31	1.63	1.24	8.41	8.2
Dec	1.84	1.72	1.00	0.81	12.47	12.3

Notes: mm = millimeters.

Table A2-18 (above) presents the comparison of standard deviation for historical and WXGEN simulated maximum and minimum temperatures for the Kafiro station. In case of temperature, the differences between observed and simulated means are in the range of ± 0.8 °C. For precipitation, the difference between observed and simulated means are ± 8%.

This statistical analysis shows that WXGEN is robust enough to be used for long term simulation of weather data using these two data sets since the ranges described above fall within an acceptable scale as indicated in previous studies (Thompson and Mullan, 1995). Figure A2-45 and A2-46 compare characteristics of the observed and WXGEN simulated precipitation series for the Kafiro station. Figure A2-45 shows the annual precipitation deviation from the long term average precipitation for the Kafiro station based on the observed data provided by the Zambia Meteorological Department.

Figure A2-45: Annual Precipitation Standard Deviation (Observed Data)

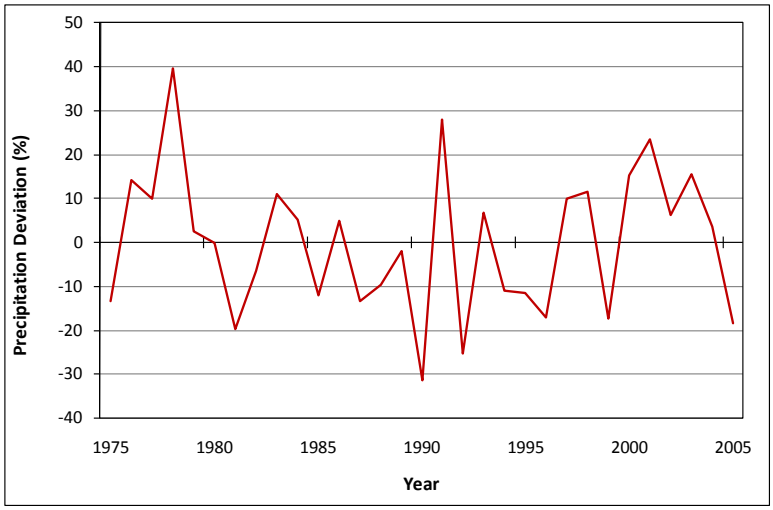

Figure A2-46 shows the annual precipitation standard deviation from the long term average precipitation for WXGEN data (200 years of simulated data).

Figure A2-46: Annual Precipitation Standard Deviation (WXGEN Simulated Data for 200 Years)

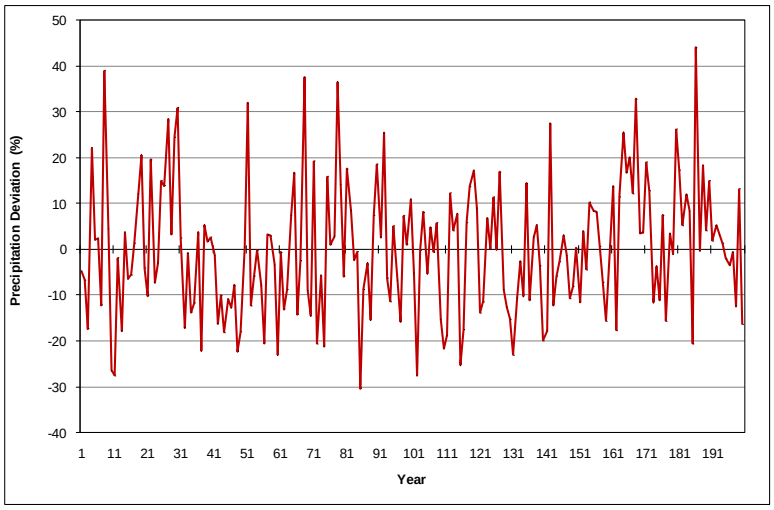

The standard deviation ranges are provided in Table A2-19:

Table A2-19: Comparison of Historical and WXGEN Simulated Annual Deviation (Precipitation)

Series	Annual Deviation (Precipitation)
Historical Series (Observed)	-31% to +40%
Simulated Series (WXGEN)	-31% to +44%

From Figures A2-45 and A2-46 and the annual deviation percentages in Table A2-19 show that the WXGEN simulated data results show a greater number of extreme events than the observed data. This indicates that the WXGEN is a very useful statistical model for generating realistic daily sequences of weather variables generally referred to as synthetic data. This long term data captures climate extremes and prolonged high and low rainfall periods which will support the risk assessment analysis later in this study. Table A2-20 summarizes the data inputs and outputs for WXGEN efforts.

Table A2-20: Summary of WXGEN Simulation Inputs and Outputs

Data Set	Source/Description
Inputs	
Observed 10 out of 11 station's meteorological data	Zambia Meteorological Department - Daily observed weather data is available for 11 stations for the period 1975 to 2005.
Gridded climatic projections for the 21st century data for 70 grid points	University of Santa Clara
WXGEN Outputs	
200 years of simulated data for 1,270 simulations (3*70*2*3 = 10), which includes 3 GCMs for 70 grid points, 2 emissions scenarios for each GCM, and three time horizons (early, mid and late century) for each scenario plus the observed data for 10 stations.	

2.8.3 HEC-HMS Model Runs for Two WXGEN Simulations

Figure A-47 shows the process used for WXGEN and HEC-HMS modeling. The two extreme flow change scenarios selected are the ECHAM5 A2 late century (highest positive flow change compared to the baseline period) and ECHAM5 B1 mid century (highest negative flow change compared to the baseline periods). These were further analyzed to study long term extreme variability. A daily time step for 30 years of precipitation and temperature data was used to simulate the daily data for 200 years using WXGEN. This simulated data was used for HEC-HMS runs as shown in Figure A2-50 in section 2.8.4.

A meteorological model from the HEC-HMS model using GCM runs was modified for WXGEN data simulated for 200 years. For the precipitation data, Thiessen Polygons generated for the GCM grid points were used. As with the other HEC-HMS runs, solar radiation was estimated using the Hargreaves-Samani method. The time series data for precipitation, temperature, and solar radiation for each grid point for 200 years was provided as an input through the time series manager in DSS file format. The various hydrological model parameters for sub basins and streams for the basin model were adopted from the validation runs. Model set up was implemented for each set of meteorological data for two selected scenarios. Each scenario model was run for a 200 year time period at a daily time step. The water flows at various flow gauge locations were then modeled and compared.

Figure A2-47: Process flow for WXGEN and HEC-HMS Simulation

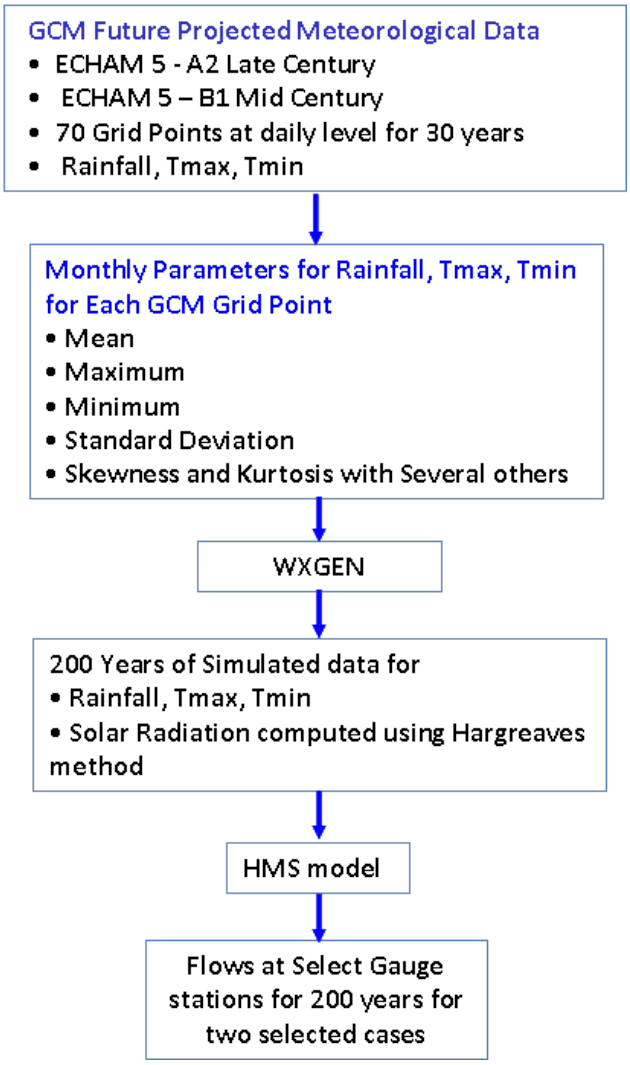

2.8.4 Discussion of Results and Output for Reservoir (Energy) Modeling

After setting up the HEC-HMS model of the Kafue River Basin for WXGEN runs, the model was run for the two extreme scenarios. As with the GCM runs, daily flows were generated for all the model elements (sub basins, streams, flows gauges, and reservoirs). For comparison of the flows, average monthly flows were generated from the daily flow data (from 200 years of simulated data). The average monthly flow variation for WXGEN ECHAM5 A2 late century compared to the baseline (ECHAM5 GCM) is shown in Figure A2-48. Figure A2-49 shows the average monthly flow variation for WXGEN ECHAM5 B1 mid century, compared to the baseline scenario.

For the WXGEN ECHAM5 A2 late century period, the flows are higher than the baseline flows. For the WXGEN ECHAM5 B1 mid century period, flows are nearly equal to the baseline flows.

When studied further, mean flows for the WXGEN ECHAM5 B1 mid century period are greater than that of the GCM run from the corresponding time horizon and emissions scenario. This

may be caused by the following limitations of WXGEN (theoretically WGs produce synthetic weather data that are statistically similar to the observed data):

- The WXGEN does not accurately reproduce the temporal auto-correlation of the annual precipitation.
- The WXGEN generator cannot generate multiple correlated precipitation inputs (i.e., implies zero spatial correlation of precipitation).

The above observations were cited by Matthew C. Carney and others in 2008 (Carney, et al., 2008). Since the HEC-HMS model has input data from various station locations, it significantly impacts the frequency distribution of flows.

Figure A2-48: Comparison of ECHAM5 A2 Baseline and WXGEN ECHAM5 A2 Late Century Monthly Flows at 4-760 Namwala Pontoon

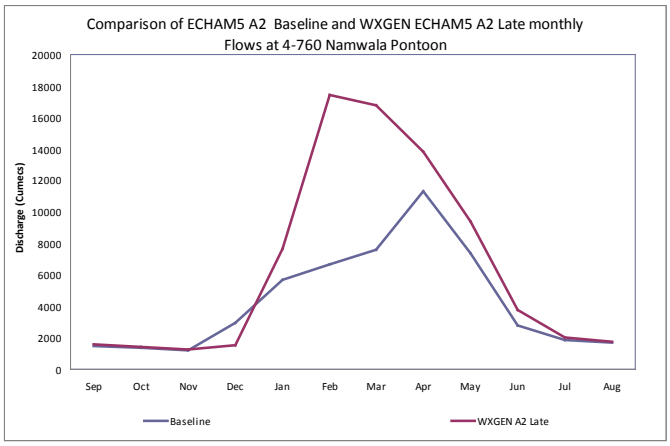

Notes: Discharge in cubic meters/second-months.

Figure A2-49: Comparison of ECHAM5 B1 Baseline and WXGEN ECHAM5 B1 Mid Century Monthly Flows at 4-760 Namwala Pontoon

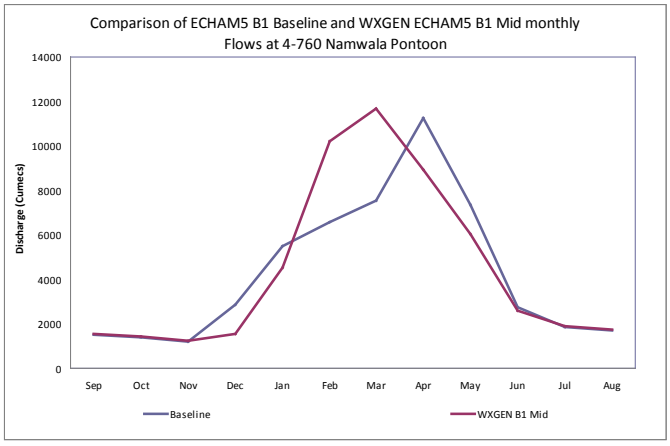

Notes: Discharge in cubic meters/second-months.

The daily flows from the two WXGEN HEC-HMS runs are output as DSS files, and are then used as inputs to the reservoir model for energy modeling. A screen shot DSS file is shown in

Figure A2-50; these files were inputs to the HEC-ResSim model (WXGEN ECHAM5 A2 late century is shown).

Figure A2-50: Screen Shot of DSS File for Input to HEC-ResSim Model

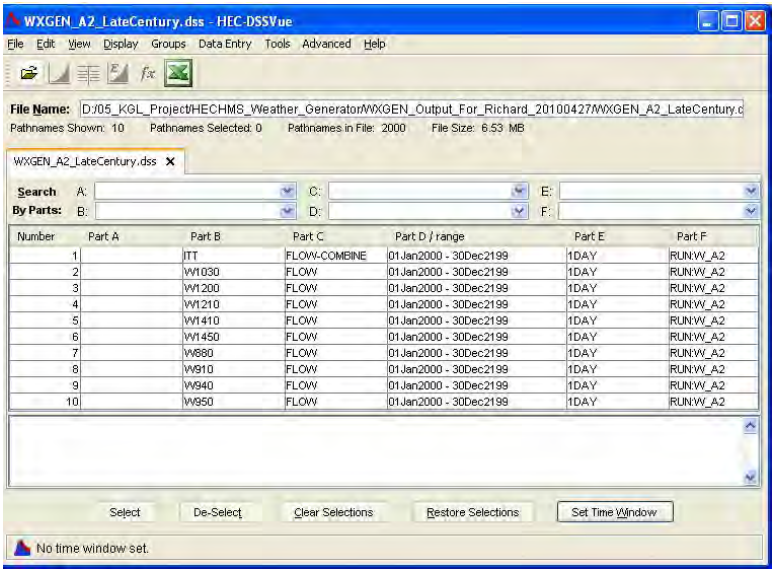

2.9 Modeling Strengths, Limitations, and Uncertainty

This section overviews strengths, limitations, and uncertainty associated with the pilot project hydrologic modeling effort. The time horizon that was selected for the project (through 2100) captures the planned lifetime of the KGL Hydropower Project. It is worth noting, however, that it is widely acknowledged in the climate change science community that the ability of models to forecast the future climate beyond 2050 with reasonable confidence is very low.

This section reviews strengths, limitations, and uncertainties associated with hydrologic modeling for three GCMs, two emissions scenarios, and the baseline and three future time horizons analyzed. It also addresses the WXGEN simulations included with this analysis to study extreme flow changes (highest positive and negative changes in flow compared to the base period for that respective GCM and emissions scenario combination).

- The hydrologic flow projections build on the temperature and precipitation outputs from the GCMs, emissions scenarios, and time horizon projections. Therefore, the uncertainties associated with those outputs (discussed above) are carried forward through the hydrologic flow modeling effort.

- Development of the basic model for the hydrologic system incorporated available background information, including land use, hydrology, precipitation, hydrologic flow, rivers, basin designations and other data. Background documents and other publically available data were used to develop the model. Data limitations introduce uncertainty associated with the model; for example, land use data are from the United Nations Food and

Agriculture Organization (FAO) and may not be current for the entire basin. Where assumptions or input data differ from actual conditions, limitations and uncertainty are introduced into the modeling effort.

- Seven meteorological stations with observed, daily historic precipitation and temperature data were selected for model establishment, calibration and validation. Daily, observed meteorological data was used as the basis for the daily time step flow modeling effort. These seven stations are generally located near the boundary of the study area, rather than within the interior of the basin. Generally, for a large area basin, with significant elevation differences and variable rainfall, such as the Kafue River Basin, a much higher number of meteorological stations would be used. Therefore, the spatial distribution of this limited data set includes significant averaging of precipitation across the basin that is likely not completely representative of the actual precipitation variability in the basin area. The historical data set included observed, daily data from 7 meteorological stations. This data set was selected for model establishment for the following reasons: (1) these data were made available by the national agency for project use, (2) these data are observed data, and (3) the temporal resolution is daily which is useful in a daily time-step modeling effort.

- The model calibration and validation were conducted using available data at three flow gauge locations. The observed and simulated flows do not closely match for all three gauge locations. As noted above, one of the major limitations in the calibration and validation runs is the number of meteorological stations and their dispersed location across the study area. The seven meteorological stations (most of them located near to the boundary) are severely limited for a basin of the study area's size (about 150,000 km^2). According to U.N. World Meteorological Organization criteria, ideally, there would be 50 to 150 stations in a basin of this size, with hilly areas benefitting from a higher density of stations. The findings and conclusions from this study note that similar to other studies in Africa, modeling and analysis of climate change would benefit from better local data – such as is available for many other parts of the world. "The climate observing system in Africa is in a far worse state than that of any other continent, and is deteriorating (Washington et al., 2004). There are eight time fewer weather stations on the continent than the minimum recommended level (Elasha et al., 2004) and vast part of central Africa remain unmonitored (IISD, 2009)."

- As agreed with IFC for the pilot project, the hydrologic model is run at a daily time step, with daily level input for rainfall, temperature, and solar radiation. Previous study efforts, have been run at a monthly time step (e.g., using the Pitman Model) and used additional meteorological stations (28 were used for a study using the Pittman Model), with data available as a monthly average. Generally, a monthly time step model gives better calibration results compared to a daily analysis, based on lesser uncertainties of temporal distribution; however, daily modeling was requested for this study and supports the analysis of energy modeling (including peak and base energy periods).

- A stochastic WG (WXGEN) produces synthetic time series of weather data of infinite length for a location based on the statistical characteristics of observed weather at that location. It is worth noting that a WXGEN is not a predictive tool that can be used in weather forecasting, but is simply a means of generating time-series of synthetic weather statistically "identical"

to the observations. This long term data captures climate extremes prolonged high and low rainfall periods which is very useful in risk assessment for hydrological or agricultural purposes. Some of the major limitations in the application of WXGEN as observed by Carney et al., 2008 are (1) the WXGEN does not accurately reproduce the temporal auto-correlation of the annual precipitation and (2) the WXGEN cannot generate multiple correlated precipitation inputs.

- The hydrologic model incorporates the impact of increased temperatures in calculating water losses due to evapotranspiration in the run-off generation process. However, because rainfall is the most crucial factor in the run-off generation process, it is used in the pilot study to evaluate the variability of flows across the GCMs (see Section 3.2.2, Projected Impacts of Rainfall Variability on Flow). In the future, additional analysis of temperature (spatial and temporal distribution of minimum and maximum temperature) and other parameters (such as relative humidity and vapor pressure) could be evaluated. However, such analysis was beyond the resources and scope of this hydrologic modeling effort. Gridded temperature and precipitation data for Zambia and the study area - for the six GCMs, two emissions scenarios, and future time horizons - are provided with the electronic study outputs for further evaluation, if desired.

- The hydrologic data sets generated by the project will be provided electronically with the final report and will support the use of the hydrologic framework through the HEC-HMS model for refinement or additional analysis efforts in the future. The HEC-HMS model is publically available and has been applied for related modeling efforts in this area in the past.

While uncertainty is associated with the modeling effort, it is clear that climate change impacts will increase temperatures and impact precipitation patterns over time. This will impact flows to the ZESCO operation; combined with development (increasing water abstractions) and indirect climate change impacts (on natural hazards and other sectors), the need for adaptation planning becomes clear. The climate change, hydrologic, and reservoir modeling undertaken for this pilot study, combined with the other risk considerations discussed later in this report point to reasonable priorities for adaptation that will prepare ZESCO for potential climate change impacts.

2.10 References

Adam, J. C. and Lettenmaier, D. P. 2003 (Adam, 2003). Adjustment of Global Gridded Precipitation for Systematic Bias. *J. Geophys. Res.* 108: 1–14.

Allen, R.G. 1997 (Allen, 1997). Self-calibrating Method for Estimating Solar Radiation from Air Temperature. *ASCE J. Hydrol. Eng*. 2:56–67.

Carney, et. al, 2008.

Elasha, et. al, 2004.

Gordon, W.S., and J. S. Famiglietti. 2004 (Gordon and Famiglietti, 2004). "Response of the Water Balance to Climate Change in the United States over the 20th and 21st Centuries: Results from the VEMAP Phase 2 Model Intercomparisons." Global Biogeochemical Cycles 18.

Goudie, A.S. 2006 (Goudie, 2006). Global Warming and Fluvial Geomorphology. *Geomorphology*. Volume 79. Pages 384–394.

Hargreaves, G.H., and Z.A. Samani. 1982 (Hargreaves, 1982). Estimating Potential Evapotranspiration. ASCE, *J. Irrigation and Drainage Division*, 108(3): 225-230.

Hargreaves, G.H., and Z.A. Samani. 1985 (Hargreaves, 1985). Reference Crop Evapotranspiration from Temperature. *Applied Engineering in Agriculture*. 1:96-99.

Hargreaves, G.H., 1994 (Hargreaves, 1994). Defining and Using Reference Evapotranspiration. *J. Irrig. Drain. Eng*. 120 (6), 1132-1139.

Hutchinson, M. 1995 (Hutchinson, 1995). Stochastic Sape-time Weatehr Models from Ground-based Data. *Agric for Meterolog*. Volume 73. Pages 237-265.

Imagen Consulting Ltd. 2008 (Imagen, 2008). Rapid Resource Assessment of Irrigation and Land over for the Kafue River Basin, World Bank – Country Water Resources Assistance Strategy. 3.

Kirpich Z.P. 1940 (Kirpich, 1940). The Time of Concentration in Small Agricultural Watersheds. *Civil Engineering*. 10 (6) 362.

Kunkel, K.E. 2003 (Kunkel, 2003). "North American Trends in Extreme Precipitation." *Natural Hazards*. 29.2 (2003), 291–305. DOI: 10.1023/A:1023694115864

Leavesley, G. H. 1994 (Leavesley, 1994). Modeling the Effects of Climate Change on Water Resources - A Review. *Climatic Change*. 28, 159–177.

Mansell, M.G. 1997 (Mansell, 1997). The Effect of Climate Change on Rainfall Trends and Flooding Risk in the West of Scotland. *Nordic Hydrology*. 28, 37-50.

McCarthy G.T. 1938 (McCarthy, 1938). The Unit Hydrograph and Flood Routing. U.S. Army Corps of Engineers.

Mutreja, K.N. 1986 (Mutreja, 1986). Applied Hydrology. McGraw Hill Publishing Company Limited, New Delhi, India.

Mwelwa, Elenestina Mutekenya, 2004 (Mwela, 2004). The Application of the Monthly Time Step Pitman Rainfall-Runoff Model to the Kafue River Basin of Zambia. Thesis Submitted in Fulfillment of the Requirements for the Degree of Master of Science. Rhodes University, Grahamstown, South Africa.

Najjar, R.G. 1999 (Najjar, 1999). The Water Balance of the Susquehanna River Basin and Its Response to Climate Change. *Journal of Hydrology*. 219(1), 7–19.

Nakicenovic, N., J. Alamo, G. Davis, B. De Vries, J. Fenhann, S. Gaffin, K. Gregory, A. Grübler, T. Yong Jung, T. Kram, E. Lebre La Rovere, L. Michaelis, S. Mori, T. Morita, W. Pepper, H. Pitcher, L. Price, K. Riahi, A. Roehrl, H.-H. Rogner, A. Sankovski, M. Schlesinger, P. Shukla, S. Smith, R. Swart, S. van Rooijen, N. Victor, and Z. Dadi. 2000 (Nakicenovic, et. al, 2000). Special Report on Emissions Scenarios. Cambridge University Press. 570 pp.

National Adaptation Program of Action. 2007 (NAPA, 2007). Formulation of the National Adaptation Program of Action on Climate Change (NAPA). Prepared by the Government of the Republic of Zambia.

Nijssen, B., R. Schnur, and D.P. Lettenmaier. 2000 (Nijjsen, et. al, 2001). Global Retrospective Estimation of Soil Moisture Using the VIC Land Surface Model, 1980-1993. *J. Climate*. 14: 1790-1808.

Racsko, P., Szeidl, L. and Semenov, M.A. 1991 (Racsko, et. al., 1991). A Serial Approach to Local Stochastic Weather Models. *Ecological Modeling*. 57: 27-41.

Richardson, C.W. 1981 (Richardson, 1981). Stochastic Simulation of Daily Precipitation, Temperature, and Solar Radiation. *Water Resources Research*. 17: 182-190.

Richardson, C.W. and Wright, D.A. 1984 (Richardson, et. al, 1984). WXGEN: A Model for Generating Daily Weather Variables. U.S. Department of Agriculture, Agricultural Research Service. ARS-8. 83 pp.

Schelle, P. and Pittock, J. 2005 (Schelle and Pittock, 2005). Restoring the Kafue Flats, *A Partnership Approach to Environmental Flows in Zambia.* Representatives of World Wildlife Federation International, Dams Initiative (Schelle) and Global Freshwater Programme (Pittock). Accessed in August 2010 at: http://assets.panda.org/downloads/restoringkafueflatsschellepittockriversymposium3sept05.pdf.

Semenov, M.A. and Barrow, E.M. 1997 (Semenov and Barrow, 1997). Use of a Stochastic Weather Generator in the Development of Climate Change Scenarios. *Climate Change*. 35, 397–414.

Semenov, M.A., Brooks, R.J., Barrow, E.M. and Richardson, C.W. 1998 (Semenov, et. al., 1988). Comparison of WXGEN and LARS-WG Stochastic Weather Generators for Diverse Climates. *Climate Research*. 10, 95-107.

Scott Wilson Piesold. 2003 (SWP). Integrated Kafue River Basin Environmental Impact Assessment Study: Power Rehabilitation Project. Strategic Environmental Impact Assessment. September.

SWP. Undated (SWP, Undated). Analysis of Options for Water Resources Development in the Central and Kafue Flats Sub-basins of the Kafue River Basin

Sheffield, J., G. Goteti, and E.F. Wood. 2006 (Sheffield, et. al., 2006). Development of a 50-yr High-resolution Global Dataset of Meteorological Forcings for Land Surface Modeling. *J. Climate*. 19: 3088-3111.

Shepard, D., 1968 (Shepard, 1968). A Two-dimensional Interpolation Function for Irregularly Spaced Data. In *Proceedings of the 1968 23rh ACM National Conference.* Pages 517-523.

Thompson, C.S., and Mullan, A.B. 1995 (Thomson and Mullan, 1995), CLIMPACTS 1995/96: Intercomparison of Stochastic Weather Generators, National Institute of Water and Atmospheric Research Ltd.

U.S. Army Corps of Engineers. 1994 (USACE, 1994). Engineering and Design, Flood-Runoff Analysis, Engineer Manual 1110-2-1417. Department of the Army. USACE.

USACE. 2000 (USACE, 2000). Hydrologic Engineering Center. Hydrologic Modeling System, HEC-HMS: Technical Reference Manual. USACE Hydrologic Engineering Center. Davis, CA, USA.

USACE. 2005 (USACE, 2005). Hydrologic Modeling System: User's Manual Version 3.0.0, USACE

USACE. 2009 (USACE, 2009). Hydrologic Modeling System, HEC-HMS: User's Manual. USACE Hydrologic Engineering Center. Davis, CA, USA.

USACE and South Florida Water Management District. 2002 (USACE and SFWMD, 2002). Central and Southern Florida Project, Comprehensive Everglades Restoration Plan, B.2 Hydraulics, Final Model Evaluation Report. Accessed in May 2010 at: http://www.mikebydhi.com/upload/dhisoftwarearchive/papersanddocs/waterresources/MSHE_Code_Evaluations/SFWMD_pdp_08_final_model_eval_report.pdf.

van Rheenen, N.T., A.W. Wood, R.N. Palmer, and D.P. Lettenmaier. 2004 (van Rheenen, 2004). Potential Implications of IPCM Climate Change Scenarios for Sacramento-San Joaquin River Basin Hydrology and Water Resources. *Climatic Change*. 62:257-281.

Wilks, D.S. 1992 (Wilks, 1992). Adapting Stochastic Weather Generation Algorithms for Climate Change Studies. Climatic Change 22. 67-84.

Williams, G.J., 1977 (Williams, 1997). The Kafue Hydro-Electric Scheme and its Environmental Setting, In Development and Ecology in the Lower Kafue Basin in the Nineteen Seventies. Eds. G.J. Williams and G. W. Howard, 13-27. Lusaka: Zambia: University of Zambia.

Willmott, C.J., C.M Rowe, and W.D. Philpot. 1985 (Willmott, et. al., 1985). Small-scale Climate Maps: A Sensitivity Analysis of Some Common Assumptions Associated with Grid-point Interpolation and Contouring. *American Cartographer.* 12: 5-16.

Willmott, C.J., and D.R. Legates. 1991 (Willmott and Legates, 1991). Rising Estimates of Terrestrial and Global Precipitation. *Climate Research.* 1: 179-186.

Willmott, C.J. and Matsuura, K. (Willmott and Matsuura, 2001). Terrestrial Air Temperature and Precipitation: Monthly and Annual Time Series (1950-1999). Center for Climate Research, University of Delaware, Newark, DE. Accessed in November 2010 at http://climate.geog.udel.edu/~climate/html_pages/archive.html.

World Bank. 2009 (World Bank, 2009). Report prepared for World Bank, Zambezi River Basin Multi-Sector Investment Opportunities Analysis. Prepared by NIRAS, BRL Ingenierie. 2009 (NIS, BRL, Ingenierie, Preliminary Report with Updated Water Tables Provided to Study Team in Spring 2010).

Zambezi River Basin Atlas. 1998 (Zambezi River Basin Atlas, 1998). Average Rainfall Map of Kafue Basin.

ZESCO. Undated (ZESCO, Undated): Average KGU Turbine and Spillage Tables for 1977-2008.

Zhang, Xuebin and Yang, Feng. 2004 (Zhang and Yang, 2004). RClimDex (1.0), User Manual, Climate Research Branch, Environment Canada, Downsview, Ontario, Canada.

Appendix A3
Reservoir (Energy) Modeling

This section describes hydrodynamic and energy modeling implemented for the Kafue Gorge Lower (KGL) pilot project. The section includes (1) an introduction to the HEC RES SIM model, (2) model development for the pilot project study area, (3) model calibration and validation, (4) energy modeling using inputs from hydrologic modeling (Appendix 2), and (5) findings and recommendations.

3.1 Introduction to HEC-ResSim

The software selected to model the hydrodynamic and energy impacts of possible climate change on the Kafue River hydropower projects is HEC-ResSim, Reservoir System Simulation program (HEC, 2007). HEC-ResSim has been developed by the U.S. Army Corps of Engineers (USACE) Hydrologic Engineering Center (HEC) to aid engineers and planners performing water resources studies in predicting the behavior of reservoirs and to help reservoir operators plan releases in real-time during day-to-day and emergency operations. Based on a review of background documents, HEC tools have been applied in the Kafue Basin and other basins in Zambia for previous studies.

For example, a May 2009 World Bank study (Zambezi River Basin Multi-Sector Investment Opportunities Analysis, Preliminary Report, May 2009) (NIRAS, BRL Ingenierie, 2009) indicates that the HEC-3, Reservoir System Analysis for Conservation computer program was implemented at a monthly time step during the South African Development Community (SADC) 3.0.4 project to investigate joint operation of Kariba, Kafue, and Cahora Bassa hydropower plants to generate combined system energy estimates (NIRAS, BRL Ingenierie, 2009). The Strategic Environmental Impact Assessment prepared for ZESCO used HEC-5/HEC-RAS to assess environmental impacts associated with three development scenarios related to the Kafue Basin (1) hydroelectric power, (2) irrigation, and (3) wetlands conservation (Scott Wilson Piesold, 2003). Another study appears to have used HEC-5 to model water availability for prescribed releases from the Cahora Bassa Dam (another basin and hydropower dam in Zambia) (Beilfuss, 2001). Based on its applicability to pilot study goals, integration with HEC Hydrologic Modeling System (HMS) tools (used for hydrologic modeling), widespread use, previous applications in Zambia, and public availability, HEC-ResSim was used to support the KGL pilot study's hydrodynamic and energy modeling.

HEC-ResSim replaces the HEC's previous reservoir system simulation program, HEC-5 (HEC, 1998). HEC-ResSim is a Windows-based program that includes significant improvements over the DOS-based HEC-5, which is no longer supported by USACE HEC. HEC ResSim is a public domain program and is available for download, without charge, at http://www.hec.usace.army.mil. The following text describes some of the primary features of HEC-ResSim.

Generalized Reservoir System Program - HEC-ResSim is a reservoir system simulation program capable of modeling the sequential operation of reservoirs for at-site, system, and downstream constraints and demands. Reservoir releases are routed through the stream system using familiar hydrologic routing techniques such as coefficient, modified Puls, Muskingum, or others. Simulation intervals can range from minutes to one day. Time series data inputs and program outputs are managed using the HEC Data Storage System (HEC DSS) (HEC, 2009).

Modern Interface - HEC-ResSim's user interface follows Windows® software development standards. Familiar data entry features support model development and localized "mini plots" graph the data entered in most tables so that any errors can be identified and corrected. HEC-ResSim provides a realistic view of the physical river/reservoir system using a map-based schematic with a set of element drawing tools. Also, using the hierarchical outlet structure, the modeler can represent each outlet of the reservoir rather the being limited to a single composite outlet (as was the case with HEC-5).

Map Schematic - The program's user interface allows the modeler to draw the network schematic either as a stick figure or as an overlay on one or more geo-referenced maps of the watershed. Program inputs and outputs may be selected from the schematic. The schematic format allows easy review of the simulation results.

Level Pool Routing - HEC-ResSim assumes that the reservoir storage pool is level (i.e., it has no routing behavior) and that its hydraulic behavior is completely defined by an elevation-storage-area table. This assumption could present a problem in long, narrow, riverine reservoirs simulated with short time intervals. However, this assumption is not problematic for the Kafue River system and level pool routing is assumed for this project.

Hydrologic vs. Hydraulic Routing - The hydrologic routing methods used in HEC-ResSim allow the program to simulate long time sequences with relatively short compute times. However, the hydrologic routing methods do not account for backwater conditions and resulting downstream conditions as accurately as hydraulic computations. For example, tributary flood flows may raise stages at a confluence and slow routed main stem releases.

For real-time forecast and operations with HEC-ResSim, the USACE would run HEC-ResSim with hydrologic routing methods (to determine reservoir releases) and then route the computed reservoir releases with the 1-D unsteady flow simulation program, HEC-RAS, River Analysis System (HEC, 2008).

Rule-Based Operations - Typically, reservoirs are constructed for one or more of the following purposes: flood control, power generation, navigation, water supply, recreation, or environmental quality. These purposes typically define the goals and constraints that describe the reservoir's release objectives. Other factors that may influence these objectives include: time of year, hydrologic conditions, water temperature, current pool elevation (or zone), and simultaneous operations by other reservoirs in a system. HEC-ResSim is unique among reservoir simulation models because it attempts to reproduce the decision making process that human reservoir operators must use to set releases. It uses an original rule-based description of the operational goals and constraints that reservoir operators must consider when making release decisions. As

HEC-ResSim has developed, advanced features such as outlet prioritization, scripted state variables, and conditional logic have made it possible to model more complex systems and operational requirements.

Hierarchical Outlet Structure - The dam is the root of an outlet hierarchy or "tree," which allows the user to describe the different outlets of the reservoir in as much detail as necessary for a given purpose. There are two basic and two advanced outlet types. The basic outlet types are controlled and uncontrolled. An uncontrolled outlet can be used to represent an outlet of the reservoir, such as an overflow spillway, that has no control structure to regulate flow. Controlled outlets are used to represent any outlet capable of regulating flow, such as a gate or valve. The advanced outlet types are power plant and pump, both of which are controlled outlets with additional features to represent their special purposes. The power plant outlet can compute energy production. The pump outlet type is even more specialized because its flow direction is opposite that of the other outlet types, and it can draw water up into the reservoir from the pool of another reservoir. The pump outlet type was added to allow the user to model pump-back operation in hydropower systems, although hydropower is not required for its operation.

3.2 Model Development for Kafue River Basin

This section discusses (1) background information, (2) watershed development, stream alignment, and routing, (2) identification of physical parameters, and (4) operational considerations and rules.

Background Information - Background information indicates that the Kafue Basin dam and reservoir system were built to accommodate the natural rainy and dry seasons in this area of the country. The Itezhi Tezhi dam (constructed in the 1970s) creates the primary reservoir for storage because the topography around the Kafue Gorge Upper (KGU) dam location did not allow for sufficient reservoir storage for the power generation needed.

Therefore, the IT reservoir was designed to provide primary storage for water collected during the rainy season, with a capacity sufficient to allow steady flow releases to the KGU power generation unit (located over 260 kilometers (km) downstream) across the entire year.

The dam and release system to support hydropower disrupts the natural seasonal flooding that previously occurred in the Kafue Flats, which lie downstream of IT dam and upstream of KGU dam. In developing the hydropower system, the designers attempted to address natural ecological flood needs and added capacity to the IT reservoir sufficient to allow flood releases that mimic the natural flood regime. The capacity was designed to allow sufficient storage to open the IT discharge gates for all of March to release a flow or 300 cubic meters per second (cms/s) to flood (refresh, also called a freshet release) the Kafue Flats and mimic the natural flood cycle. At the time, ecological needs and impacts of the dams was not a common consideration in the design of dam systems. Adding the additional storage capacity to IT, increased initial capital costs for the reservoir and dam by 15%; the additional cost was funded based on the recognized natural value of the flats and the determination to maintain this ecological area to the degree possible (Beilfus, 2001).

In practice, freshet releases have not been regularly implemented because water collected in the IT reservoir was not sufficient or the release scheme was not enforced. However, recent ZESCO information and World Wildlife Federation (WWF) data appear to indicate the freshet releases or natural overflow of the basin occurred for some years around 2004. For example, U.S. National Aeronautic and Space Administration (NASA) images and data indicate that the 2003 and 2004 rainy season was particularly wet in Zambia and the IT dam did allow the flats to flood (NASA, 2007). During times of high rainfall, such releases may also result from flood release controls at the IT dam or operator decisions regarding release needs for operational and structural reasons at the IT dam.

Ecological impacts from development of the IT dam have been studied for years and continue to be a priority as further development and use of the hydropower regime are implemented. For example, the WWF has worked with government partners and ZESCO to develop an Integrated Water Management approach (Nsongela, 2004). Water withdrawals for ecological needs (Kafue Flats) and for urban water supply and irrigation are addressed as Competing Uses in the HEC-ResSim modeling effort for the KGL pilot study (as discussed in Section 3.4 of this appendix).

Data sources requested at project start up included past studies, as well as electronic data inputs and outputs from previous modeling efforts. Various written studies were provided in a report format and were used to support model establishment. However, electronic files (e.g., previous modeling files) were not available from team stakeholders in a timely manner. After a period of inquiry, IFC directed the Tetra Tech team to move forward using the background documents and other information obtained to initiate modeling efforts. The team then worked with available data (from project partners and other sources) to establish and implement HEC-ResSim model for this study.

Based on background documents provided by IFC and ZESCO, operating data provided by ZESCO, and information on-line (for example, Google Earth) and available from recent news stories, combined with professional experience (Richard Hayes, PE, of Tetra Tech (retired from the USACE HEC center)), the team established HEC-ResSim model for the KGL project. Table A3-1 provides a summary of data categories, purposes, sources, and file names/types used as input to the model.

Using these data sources, the KGL pilot study HEC-ResSim model was developed. The following text describes steps taken to establish the model.

Watershed Development, Stream Alignment, and Routing – A variety of data sources were reviewed and applied to establish the watershed (basin), stream alignment, and routing for the Kafue Basin and hydropower flow system. Geographic Information System (GIS) data for basins, streams, gauge and dam locations, and land elevation were provided and used as presented in Appendix 2 to develop the HMS model. In addition, specific dam and reservoir locations, as well as inflow and outflows (through river, irrigation assumptions, and tributary flows) were established using this primary information. Data was confirmed through other background documents and on-line resources.

Table A3-1: Summary of Data Inputs Used to Establish HEC-ResSim Model

Data Category	Purpose(s)	Source(s)	Notes/Filenames
Basins, Rivers, Tributaries	Delineate the Kafue Basin, including sub-basins and major and minor flows	RMSI	• Projected Coordinate System: GS_1984_UTM_Zone_35S • Geographic Coordinate System: GCS_WGS_1984 • Datum: D_WGS_1984 • Shapefiles_for_RES SIM.zip
Dams and Reservoirs	Establish length, height, Capacity, location or each dam/reservoir system	RMSI, Google Earth, Background Documents, ZESCO e-mails, RMSI	• Shapefiles_for_RES SIM.zip • ZESCO SEIA • World Bank 2009 (Draft MSIOA) • Google Earth
Flows and Routing	Model volume of inflow, outflow, and routing through system	RMSI, ZESCO, Background documents	• DSS files for (1) each GCM, emissions scenario, and time period) – 24 files; and (2)each WXGEN scenario – 2 files • ZESCO means for addressing Kafue Flats as a natural/pseudo reservoir • Shape Files and Reports
Power Capacity	Support estimates of energy production based on flows and operating rules	ZESCO, background documents, e-mails, Internet data	• Background documents • E-mails from ZESCO • News articles regarding planned units at Itezhi-Tezhi
Operating Rules	Establish operating rules for baseline and peaking power during normal and high/low water	ZESCO, background documents	• Storage area elevation curves provided (e.g., Volume-Area-Elevation.xls) • Historic flow and operational data (20 years)
Competing Uses	Estimated freshet releases (C) and potential irrigation abstractions (I)	ZESCO input, background documents, on-line information (WWF documents)	• 2003 SEIA Report • Input from ZESCO /other available data • Later compared to data provided by World Bank from MSIOA work (received April 2010)

Notes: DSS = Data Storage System

The routing of flows through the Kafue Flats reach required special consideration. The challenge was primarily one of flow translation and not one of decision making for the upstream IT Reservoir. Upstream reservoir decision making was simulated using operational rules developed based on information provided by ZESCO regarding current and historic operations and other background documents (as discussed under operating considerations and rules below).

To route IT releases to the KGU Reservoir, two approaches were possible. The available digital terrain data could be coupled with calibration results to account for channel characteristics (width, depth and roughness) as the basis for HEC-RAS routing. Secondly, a combination of HEC-ResSim hydrologic routing coupled with routing the Kafue Flats as pseudo storage reservoir could be applied and then calibrated to produce the routing effect. Given the limited channel data available to the project team, HEC-RAS was not used. Instead, hydrologic routing was coupled with available operational data provided by ZESCO and discussions of the Kafue Flats provided in background documents, to translate and attenuate releases from the IT Reservoir through the Kafue Flats and into the KGU Reservoir. The Kafue Flats were modeled following the approach ZESCO uses, as a natural (or pseudo) reservoir. Flow time through the flats was estimated at 6 weeks for modeling purposes.

Figure A3-1 shows the Kafue Basin, highlighting the hydropower system elements for HEC-ResSim modeling. To the left, one can see the IT dam; the long reservoir between Namwala and CP-4 represents the Kafue Flats. KGU dam lies near the right of the figure, followed further to the right by the KGL power generating unit and dam.

Figure A3-1: Kafue Basin Flow Assumptions

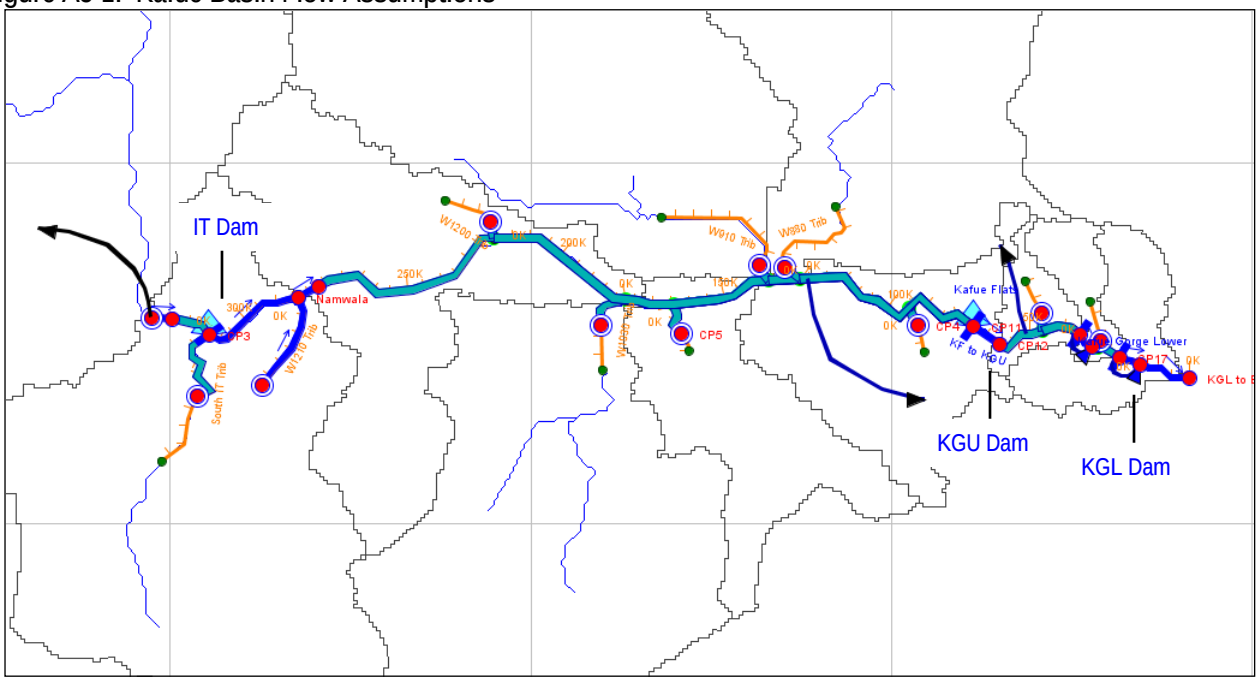

Notes: Red dots indicate flow junctions (inflow or outflow); halo circles around red dots indicate inflows (incoming water); light blue areas indicate reservoirs and pseudo reservoirs (IT, Kafue Flats, KGU, and KGL); black arrows indicate outflow locations (discussed under conservation/development uses); blue arrows indicate inflows based on HMS modeling.

Physical Parameters – Physical parameters were entered for the three dams and reservoirs (IT, KGU, and KGL). The reservoirs were established as pools with controlled outlets. Linear interpolation, rather than conic interpolation was used. Table A3-2 overviews some of the physical parameters included for dams, reservoirs, and existing or planned power generating units. All of the existing and planned power generating stations are modeled as operating for the analysis.

Table A3-2: Physical Parameters for Dams, Reservoirs, and Power Stations

Dam	Dam Parameters			Generating Capacity	Combined Efficiency (turbine and generator)	Structural Features/Notes
	Top of dam elev. (m)	Length (m)	Storage (mcm)			
IT	1035	1800	6,008 @1030.5m	120 MW	88%	3 spillway gates (4,425 cms @1030.5m), low level outlet for powe releases
KGU	980	300	1,178 @977m	990 MW	91%	4 spillway gates (3,660 cms @ 978m) 11 Km tailrace tunnel, 400 m head
KGL	586	300	80@580m	750 MW	88%	3 spillway gates (3,959 cms @ 582 m), 7 km tailrace tunnel, 200 m head

Notes: Physical parameters were developed using background information, research, input from ZESCO, and professional experience. Though the IT and KGL power generating units are not yet in place, they are modeled as operating units for this study. Acronyms: elev. = elevation; m = meters; mcm = million cubic meters; MW = Mega Watt; km = kilometer; and cms = cubic meters per second.

Operational Parameters - The operational rules established for they hydropower system in the HEC-ResSim model integrated background documents, operational data for 20 years provided by ZESCO, and professional experience. In reviewing the data, it was noted that it appeared that freshet releases had occurred in recent years. This flow was modeled as a block flow during the indicated period of the year. Based on observation of the data, rules and alternative rules were developed to address normal and low reservoir volume conditions.

Based on ZESCO data, operational rules were established to guide the release and flow of water from reservoirs to support power generation at each of the power plants. These rules were then applied across all of the time horizons and scenarios modeled. Table A3-3 presents the units, overflow mechanisms, power operation, and minimum release assumptions applied for modeling.

Table A3-3: Operating Assumptions for Power Stations

Unit	Overflow Mechanisms	Power Operation	Minimum Releases
IT	Guide Curve Operation, Spillway with radial gates	Peak (9 hours) Base (15 hours) 7 days/week	Minimum Flow for Uses Above IT (40 cms)
KGU	Guide Curve Operation, Spillway with radial gates	Peak (6 hours) 7 days/week	Minimum Flow to River (7.2 cms)
KGL	Power Pool (582 to 578 m), Spillway with radial gates	Peak (4 hours) 7 days/week	Minimum Flow to River (7.2 cms)

Notes: Acronyms: m = meters; cms = cubic meters per second.

3.3 Model Calibration and Validation

After establishing the model, various runs were implemented to check the model outputs compared to observed flow and elevation data for the IT Reservoir. The primary focus of these checks was to refine the IT hydropower rules to provide sufficient releases to support power production at KGU and KGL, without exhausting the IT Reservoir during the P-1 scenario

(current water demand). The hydropower rules for IT Reservoir were refined with test runs using a variety of time horizon and global circulation model (GCM)/emissions scenario combinations. The model was then adjusted before proceeding to enter the remainder of flow inputs from the GCM projections and GCM weather generator (WXGEN) hydrologic modeling runs. All three power generating units (IT, KGU, and KGL) were assumed to be operating for the energy modeling scenarios.

3.4 Project Inputs for Energy Modeling: Climate Change Scenarios and Competing Uses

The flow inputs provided from HEC-HMS modeling of GCM outputs and WXGEN simulations were integrated as DSS files to support the hydrodynamic and energy output modeling. These included 24 GCM flow scenarios and two WXGEN flow scenarios. In addition to varying flows over time associated with climate change, the analysis included a range of abstraction scenarios, presented in Table A3-4, based on data available in the background documents for the project (primarily, relying on information included in the 2003 Strategic Environmental Impact Assessment (SEIA) and 2009 Multisector Investment Opportunities Analysis (MSIOA)). In addition to varying flows over time based on the climate change scenarios, a range of conservation and development scenarios were developed based on data available in the background documents for the project (primarily, relying on information included in the 2003 SEIA (SWP, 2003). In addition, a new development scenario was included to present a higher level of abstraction for irrigation.

The P-1 (maximum power) scenario was modeled to establish baseline energy for the climate change scenarios. The baseline flow for P-1 includes assumptions regarding present baseline flows and withdrawals, including 15 cms (for other users between IT and KGU) and 25 cms (for base flow maintenance) for a total of 40 cms of minimum required flow from above IT (SWP, 2003). In addition, mid- and upper-basin withdrawal for domestic, mining, and industry (DMI) use--for a combined 6.6 cms is included above IT. A withdrawal of 11.1 cms for DMI is included above the Kafue Flats and above the KGU Dam. In addition, a 5.7 cms withdrawal is included below the Kafue Flats and above KGU (for domestic use). Below IT, a baseline abstraction of 7.2 cms for minimum flow requirements in the stream around the tailraces is maintained; this amount is withdrawn from both the KGU and KGL reservoirs, but represents a non-consumptive use. Any withdrawals or uses below KGL were not modeled as they would not be material to power in the system.

Table A3-4: Water Withdrawals for Baseline and Development and Conservation Scenarios

Scenario	Above IT Dam		Below IT Dam to KGU Dam (Kafue Flats Area)		Total Abstractions			Total Conservation Releases (cms/yr)
	New Ag (ha/cms)	Total Req (cms)	New Ag (ha/cms)	Total Req (cms)	Total Ag (cms)	Total DMI (cms)	Total Req (cms)*	
P-1	0	6.6	0	16.8	14.3	9.1	23.4	0
C-1	0	6.6	0	16.8	14.3	9.1	23.4	300
C-2	0	6.6	0	16.8	14.3	9.1	23.4	1,200
C-3	0	6.6	0	16.8	14.3	9.1	23.4	1,600
I-3	20,000/5.3	11.9	0	16.8	19.6	9.1	28.7	0
I-6	0	6.6	20,000/ 11.4	28.2	11.1	9.1	34.8	0
I-9	20,000/5.3	11.9	10,000/ 5.7	22.5	11.0	9.1	34.4	0
I-10	60,000/17.2	23.8	40,000/ 26.9	43.7	58.4	9.1	67.5	0

Notes: Based on information in the 2003 SEIA (SWP, 2003), with I-10 developed as a "new" total abstraction based on the project proposal submitted to IFC. Acronyms: cms = cubic meters per second; Ag = agriculture; DMI = domestic, mining, industry; ha = hectare; Req = required.

In addition to the P-1 and the consumptive use scenarios, three conservation scenarios were modeled to consider freshet releases above the baseline flow of 40 cms as follows: (1) C-1 provides 300 cms during March; (2) C-2 provides 300 cms during March and April; and (3) C-3 provides 400 cms during February and 600 cms during March and April (SWP, 2003). These are non-consumptive in that they impact timing of water releases, but the water stays in the river system.

Additionally, four development scenarios were modeled to evaluate the impact of future expansion of irrigation and DMI demand above the IT and from the Kafue Flats areas. These consumptive uses were compared to the P-1 scenario and modeled separately from the conservation scenarios for this study. The starting point for these scenarios is the assumed potential additional irrigation discussed in the 2003 SEIA with additional increases for anticipated irrigation and DMI assumed for a new scenario, I-10. These development-driven scenarios are as follows: (1) I-3, an irrigation withdrawal equivalent to an additional 20,000 hectare (ha) of irrigated land in the Upper Kafue Basin (above IT); (2) I-6, equivalent to an additional 20,000 ha in the Middle Kafue Basin (in the flats); (3) I-9 equivalent to an additional 20,000 ha in the Upper Kafue Basin and 10,000 ha in the Kafue Flats; and (4) I-10 equivalent to additional 60,000 ha in the Middle Basin (above IT) and 40,000 ha in the Kafue Flats.

To evaluate the combined impacts of conservation and other demands, the team modeled a combination C-3 and I-9 for the base and early century time horizons and C-3 and I-10 for the mid and late century time horizons. These combined scenarios were run for the ECHAM5 GCM, for both emissions scenarios (A2 and B1). I-10 is a higher abstractions and is considered more realistic for the later time horizons. Conservation and development scenarios and associated water abstractions are summarized in Table 2-4.

3.5 ResSim Outputs

This section presents the reservoir simulation outputs for power production for the scenarios modeled. Base case power scenario outputs are discussed first, followed by development/conservation scenario power outputs.

3.5.1 Base Case Scenario Power Outputs

This section begins with the power output results for each of the GCMs/emissions scenarios modeled at the KGL plant. Tables A3-5 to A3-8 provide summaries of power generation at the KGL power plant for the three GCMs (ECHAM5, IPSL, and MRI), two emissions scenarios (A2 and B1), across four time horizons (base, early, mid, and late century). In addition, two additional simulations using a weather generator (WXGEN) are presented. Table A3-5 presents results for the ECHAM5 GCM.

Table A3-5: KGL Energy Production for ECHAM5 Scenarios

KGL 750MW Capacity Unit – Annual Energy Production (GWh/Yr)									
GCM	SRES	Development Scenario	Base	Early	% Change from Base	Mid	% Change from Base	Late	% Change from Base
ECHAM5	A2	P-1	2,227	1,847	-17.1%	2,182	-2.0%	2,487	11.7%
ECHAM5	B1	P-1	2,160	2,099	-2.8%	1,682	-22.1%	1,970	-8.8%

Notes: GWh/Yr = Gigawatt hour per year; MW = Megawatt.

As shown in Table A3-5, energy production decreases in the early period for both the A2 and B1 scenarios, but rebounds for A2 in the mid and late century periods, based on higher water flows during these time horizons. For ECHAM5, B1, energy production at KGL decreases in the mid and late century, compared to the base period. Table A3-6 shows results for the IPSL GCM.

Table A3-6: KGL Energy Production for IPSL Scenarios

KGL 750MW Capacity Unit – Annual Energy Production (GWh/Yr)									
GCM	SRES	Development Scenario	Base	Early	% Change from Base	Mid	% Change from Base	Late	% Change from Base
IPSL	A2	P-1	2,081	1,905	-8.5%	2,165	4.0%	2,120	1.9%
IPSL	B1	P-1	2,081	2,107	1.2%	2,021	-2.9%	2,090	0.4%

Notes: GWh/Yr = Gigawatt hour per year; MW = Megawatt.

As shown in Table A3-6, energy production decreases in the early period for A2 and increases in the early period for B1 (compared to their respective base period rates). In the mid-century period, IPSL A2 shows an energy increase from the base period, but a decrease occurs for IPSL B1. In the late century, both IPSL A2 and B1 show modest increases from the base period energy (0.4% and 1.9%). Table A3-7 provides results for the MRI GCM.

Table A3-7: KGL Energy Production for MRI Scenarios

KGL 750MW Capacity Unit – Annual Energy Production (GWh/Yr)									
Model	SRES	Development	Base	Early	% Change	Mid	%	Late	%

		Scenario			from Base		Change from Base		Change from Base
MRI	A2	P-1	2,239	2,087	-6.8%	2,211	-1.3%	2,125	-5.1%
MRI	B1	P-1	2,246	1,953	-13.0%	1,836	-18.3%	2,326	3.6%

Notes: GWh/Yr = Gigawatt hour per year; MW = Megawatt.

As shown in Table A3-7, energy production decreases in the early period for both the A2 and B1 emissions scenarios compared to the respective base periods. Power generation remains lower than the base period for both A2 and B1 in the mid-century. In the late century, MRI A2 shows a decrease in energy production compared to the base period, while B1 shows an increase.

Increased and decreased flow scenarios were studied further using the WXGEN tool. The WXGEN scenarios simulated 200 years for the ECHAM5, A2, late century results (highest increase in flow compared to its respective base period) and the ECHAM5, B1, mid century results (highest decrease in flow compared to its respective base period). Table A3-8 presents these results for the KGL power plant.

Table A3-8: KGL Energy Production for WXGEN Scenarios (GWh/yr)

GCM	SRES and Period	Use Scenario	Base	WXGEN	% Change from Base
ECHAM5	A2-Late	P-1	2,227	3,328	49.4
ECHAM5	B1-Mid	P-1	2,160	2,189	1.3

Notes: GWh/Yr = Gigawatt hour per year; MW = Megawatt.

As shown in Table A3-8, KGL energy production under the WXGEN simulation is greater than the base period for both scenarios. The increase from the base period is greatest for the ECHAM5 A2 scenario.

A combined system review for all three power plants was also performed. Tables A3-9 to A3-11 provide these results. Table A3-9 provides the combined power analysis for the ECHAM5 A2 and B1 scenarios for the IT, KGU, and KGL power stations.

Table A3-9: Combined Energy Production for ECHAM5 Scenarios

Combined Power Analysis IT, KGU, KGL - Annual Energy Production (GWh/Yr)

Model	SRES	Use Scenario	Station – MW	Base	Early	% Change from Base	Mid	% Change from Base	Late	% Change from Base
ECHAM5	A2	P-1	IT-120	414	347	-16.2%	402	-2.9%	403	-2.7%
ECHAM5	A2	P-1	KGU-1050	4,096	3,463	-15.5%	3,989	-2.6%	4,446	8.5%
ECHAM5	A2	P-1	KGL-750	2,227	1,847	-17.1%	2,182	-2.0%	2,487	11.7%
ECHAM5	A2	P-1	System	6,737	5,657	-16.0%	6,573	-2.4%	7,336	8.9%
Model	SRES	Use Scenario	Station – MW	Base	Early	% Change from Base	Mid	% Change from Base	Late	% Change from Base
ECHAM5	B1	P-1	IT-120	404	394	-2.5%	329	-18.6%	361	-10.6%

ECHAM5	B1	P-1	KGU-1050	3,985	3,853	-3.3%	3,178	-20.3%	3,640	-8.7%
ECHAM5	B1	P-1	KGL-750	2,160	2,099	-2.8%	1,682	-22.1%	1,970	-8.8%
ECHAM5	B1	P-1	System	6,549	6,346	-3.1%	5,189	-20.8%	5,971	-8.8%

Notes: GWh/Yr = Gigawatt hour per year; MW = Megawatt.

As shown in Table A3-9, the combined power analysis using ECHAM5 for the IT, KGU, and KGL power stations and system shows decreases in power generation for the early- and mid-century for individual power stations and for the system, across both emissions scenarios (A2 and B1) compared to the base period; the percentage decrease in power is greater for the A2 scenario during this period. In the mid-century, the B1 scenario shows a greater negative change in power from the base period (compared to the A2 decrease). In the late period, the overall system change in power for the A2 scenario is positive (8.9%) compared to the base period, while the overall system change in power for the B1 scenario is negative (-8.8%).

Table A3-10 provides the individual and combined power analysis for the IPSL A2 and B1 scenarios for the IT, KGU, and KGL stations. The combined power analysis using the IPSL GCM results for the IT, KGU, and KGL power generating systems shows a decrease in power for the early century for the A2 scenario only (compared to the base period). For the other periods of A2 and for the B1 scenario, power generation changes are positive compared to the base period (with the exception of a -3.6% change from the base period for KGL in the mid century, B1 scenario). However, even for that period for B2, a slight overall positive change occurs compared to the baseline for the total system (0.6% increase over the base period).

Table A3-10: Combined Energy Production for IPSL Scenarios

Combined Power Analysis IT, KGU, KGL - Annual Energy Production (GWh/Yr)										
GCM	SRES	Use Scenario	Station - MW	Base	Early	% Change from Base	Mid	% Change from Base	Late	% Change from Base
IPSL	A2	P-1	IT-120	378	357	-5.6%	388	2.6%	393	4.0%
IPSL	A2	P-1	KGU-1050	3,832	3,463	-9.6%	3,878	1.2%	3,919	2.3%
IPSL	A2	P-1	KGL-750	2,081	1,905	-8.5%	2,163	3.9%	2,120	1.9%
IPSL	A2	P-1	System	6,291	5,725	-9.0%	6,429	2.2%	6,432	2.2%
Model	SRES	Use Scenario	Station - MW	Base	Early	% Change from Base	Mid	% Change from Base	Late	% Change from Base
IPSL	B1	P-1	IT-120	377	393	4.2%	381	1.1%	393	4.2%
IPSL	B1	P-1	KGU-1050	3,581	3,884	8.5%	3,688	3.0%	3,848	7.5%
IPSL	B1	P-1	KGL-750	2,081	2,107	1.2%	2,007	-3.6%	2,090	0.4%
IPSL	B1	P-1	System	6,039	6,384	5.7%	6,076	0.6%	6,331	4.8%

Notes: GWh/Yr = Gigawatt hour per year; MW = Megawatt.

Table A3-11 provides the combined power analysis for the MRI A2 and B1 scenarios for the IT, KGU, and KGL stations and for the system as a whole.

Table A3-11: Combined Energy Production for MRI Scenarios

Combined Power Analysis IT, KGU, KGL - Annual Energy Production (GWh/Yr)

GCM	SRES	Use Scenario	Station - MW	Base	Early	% Change from Base	Mid	% Change from Base	Late	% Change from Base
MRI	A2	P-1	IT-120	417	397	-4.8%	409	-1.9%	386	-7.4%
MRI	A2	P-1	KGU-1050	4,149	3,830	-7.7%	4,040	-2.6%	3,981	-4.0%
MRI	A2	P-1	KGL-750	2,239	2,087	-6.8%	2,211	-1.3%	2,125	-5.1%
MRI	A2	P-1	System	6,805	6,314	-7.2%	6,660	-2.1%	6,492	-4.6%
GCM	SRES	Use Scenario	Station – MW	Base	Early	% Change from Base	Mid	% Change from Base	Late	% Change from Base
MRI	B1	P-1	IT-120	417	379	-9.1%	360	-13.7%	399	-4.3%
MRI	B1	P-1	KGU-1050	4,260	3,617	-15.1%	3,410	-20.0%	4,232	-0.7%
MRI	B1	P-1	KGL-750	2,246	1,953	-13.0%	1,836	-18.3%	2,326	3.6%
MRI	B1	P-1	System	6,923	5,949	-14.1%	5,606	-19.0%	6,957	0.5%

Notes: GWh/Yr = Gigawatt hour per year; MW = Megawatt.

As shown in Table A3-11, the MRI combined power analysis shows a consistent decrease in power for the early and mid century periods across stations and across emissions scenarios (A2 and B1) compared to the base period, with a greater decrease in flow and associated power for the B1 scenario. In the late period, the overall change in power for the A2 scenario is negative compared to the base period (-4.6%), while the overall change in power for the B1 scenario is slightly positive but about equal to the base period (+0.5%).

The combined power analysis results for the ECHAM5 A2 late century and ECHAM5 B1 mid century WXGEN simulations for 200 years are provided in Tables A3-12 and A3-13.

Table A3-12: Combined Energy Production for WXGEN High Flow Change Simulation

Combined Power Analysis IT, KGU, KGL - Annual Energy Production (GWh/Yr)

Simulation	GCM, SRES, Time Period	Use Scenario	Station – MW	Base Period	WXGEN Simulation	% Change from Base
WXGEN	ECHAM5, A2, Late-Century	P-1	IT-120	414	559	35.0%
WXGEN	ECHAM5, A2, Late-Century	P-1	KGU-1050	4,096	5,846	42.7%
WXGEN	ECHAM5, A2, Late-Century	P-1	KGL-750	2,227	3,328	49.4%
WXGEN	ECHAM5, A2, Late-Century	P-1	System	6,805	9,733	44.5%

Notes: GWh/Yr = Gigawatt hour per year; MW = Megawatt.

Table A3-12 shows significant power increases using the WXGEN simulation; this is expected because the period modeled represents the period with the highest positive change in flow compared to its respective base period. Table A3-13 shows the combined energy production for the low flow change simulation for the ECHAM5 B1, mid-century scenario for each of the power generating units and for the system as a whole.

Table A3-13: Combined Energy Production for WXGEN Low Flow Change Simulation

Combined Power Analysis IT, KGU, KGL - Annual Energy Production (GWh/Yr)						
Simulation	GCM, SRES, Time Period	Use Scenario	Station – MW	Base Period	WXGEN Simulation	% Change from Base
WXGEN	ECHAM5, B1, Mid-Century	P-1	IT-120	404	455	12.6%
WXGEN	ECHAM5, B1, Mid-Century	P-1	KGU-1050	3,985	4,106	3.0%
WXGEN	ECHAM5, B1, Mid-Century	P-1	KGL-750	2,160	3,328	1.0%
WXGEN	ECHAM5, B1, Mid-Century	P-1	System	6,549	6,743	3.0%

Notes: GWh/Yr = Gigawatt hour per year; MW = Megawatt.

The individual changes in power generations compared to the base period range from 1.0% at KGL to 12.6% at IT. The combined system power change compared to the base period for the WXGEN simulation of ECHAM5, B1 in the mid-century period is 3.0%.

3.5.2 Development/Conservation Scenarios and Power Outputs

As discussed previously, in addition to considering the impact of climate change alone, the team modeled a number of development and conservation scenarios. These included potential increases in irrigated agriculture and DMI needs, as well as the impacts of different approaches to freshet releases.

The 2003 SEIA includes a discussion of potential agriculture needs in the Kafue River Basin. It includes assumptions for present uses as well as new irrigation uses over time. This pilot project builds on those assumptions to model three irrigation scenarios I-3, I-6 and I-9, similar to the SEIA. In addition, the team proposed to increase the irrigation assumptions, along similar lines as the SEIA. To achieve this higher water use assumption, the team developed scenario I-10, which increases irrigation for agriculture above I-9 and adds new DMI water use above and below the IT. The impacts of the development scenarios on power are shown for KGL and for total system generation (combined IT, KGU, and KGL).

The SEIA found that power generation would be reduced by up to 7% in the highest withdrawal scenario (impacted most by withdrawals above the IT). However, food deficits and hunger likely warranted additional agriculture in the basin (SWP, 2003). Through analysis of the I-3, I-6, I-9, and I-10 scenarios, one also sees impacts on total power generation. Tables 3-18 and 3-19 show KGL power generation for development scenarios and the ECHAM5 A2 and B1 emissions scenario for the early, mid, and late century time horizons.

Table A3-14 shows energy production at KGL for the development scenarios for the ECHAM5 A2 scenario.

Table A3-14: KGL Energy Production for Development Scenarios: ECHAM5 A2

Combined Power Analysis KGL - Annual Energy Production (GWh/Yr)

Use Scenario	Base Period Power	Change from Base P-1	Early Century Power	Change from Base P-1	Mid Century Power	Change from Base P-1	Late Century Power	Change from Base P-1
P-1	2,227	0.0%	1,847	-17.0%	2,182	-2.0%	2,487	11.9%
I-3	2,183	-2.0%	1,806	-18.9%	2,142	-3.8%	2,447	9.9%
I-6	2,057	-7.6%	1,678	-24.7%	2,102	-5.6%	2,319	4.1%
I-9	2,098	-5.8%	1,721	-22.7%	2,057	-7.6%	2,363	6.5%
I-10	1865	-16.3%	1,478	-33.6%	1,815	-18.5%	2,126	-4.5%

Notes: GWh/Yr = Gigawatt hour per year.

Table A3-15 shows energy production at KGL for the development scenarios for the ECHAM5 B1 scenario.

Table A3-15: KGL Energy Production for Development Scenarios: ECHAM5 B1

Combined Power Analysis KGL - Annual Energy Production (GWh/Yr)								
Use Scenario	Base Period Power	Change from Base P-1	Early Century Power	Change from Base P-1	Mid Century Power	Change from Base P-1	Late Century Power	Change from Base P-1
P-1	2,160	0.0%	2,099	-2.8%	1,682	-22.1%	1,970	-8.8%
I-3	2,172	0.6%	2,058	-4.7%	1,643	-23.9%	1,933	-10.5%
I-6	2,044	-5.4%	1,928	-10.7%	1,512	-30.0%	1,801	-16.6%
I-9	2,087	-3.4%	1,974	-8.6%	1,558	-27.9%	1,847	-14.5%
I-10	1,850	-14.4%	1,735	-19.7%	1,142	-47.2%	1,608	-25.6%

Notes: GWh/Yr = Gigawatt hour per year.

Tables A3-16 and A3-17 show the combined energy production for the development scenarios for the ECHAM5 A2 and ECHAM5 B1 scenarios, respectively.

Table A3-16: Combined Energy Production for Development Scenarios: ECHAM5 A2

Combined Power Analysis KGL - Annual Energy Production (GWh/Yr)								
Use Scenario	Base Period Power	Change from Base P-1	Early Century Power	Change from Base P-1	Mid Century Power	Change from Base P-1	Late Century Power	Change from Base P-1
P-1	6,737	0%	5,657	-16.0%	6,573	-2.4%	7,336	8.9%
I-3	6,615	-1.8%	5,537	-17.8%	6,433	-4.5%	7,221	7.2%
I-6	6,269	-6.9%	5,187	-23.0%	6,106	-9.4%	6,876	2.1%
I-9	6,382	-5.3%	5,296	-21.4%	6,228	-7.5%	6,990	3.8%
I-10	5,740	-14.8%	4,618	-31.4%	5,560	-17.5%	6,346	-5.8%

Notes: GWh/Yr = Gigawatt hour per year.

Table A3-16 shows that additional withdrawals above the current use, P-1, impact power generation compared to the P-1 in the base period scenario, particularly in the early and mid century periods (negative changes in power production compared to the P-1 base period power) for I-3 through I-10. Given the increase in flows and energy generation associated with ECHAM5 A2 climate change scenario over time, power generation in the late century increases compared to the base period for development scenarios (I-3 to I-9), until the I-10 scenario is considered. For the I-10 withdrawal scenario, the power generation in the late century is negative compared to the base period P-1 scenario, even with the increased flows through the Kafue River system. Given that the higher flow to the basin will come at the expense of infiltration of water into the land, irrigation withdrawal water needs will be important in the future time horizons. As shown in Table A3-17, an analysis of total power was also implemented for the ECHAM5 B1 scenario.

Table A3-17: Combined Energy Production for Development Scenarios: ECHAM5 B1

Combined Power Analysis IT, KGU, KGL - Annual Energy Production (GWh/Yr)

Use Scenario	Base Period Power	Change from Base P-1	Early Century Power	Change from Base P-1	Mid Century Power	Change from Base P-1	Late Century Power	Change from Base P-1
P-1	6,550	0%	6,346	-3.1%	5,189	-20.8%	5,972	-8.8%
I-3	6,558	0.2%	6,229	-4.9%	5,070	-22.6%	5,864	-10.5%
I-6	6,210	-5.2%	5,870	-10.4%	4,705	-28.2%	5,501	-16.0%
I-9	6,324	3.4%	5,994	-8.5%	4,827	-26.3%	5,626	-14.1%
I-10	5,676	-13.3%	5,332	-18.6%	3,645	-44.4%	4,966	-24.4%

Notes: GWh/Yr = Gigawatt hour per year.

Table A3-17 shows that additional withdrawals above the current use, impact power generation compared to the P-1 scenario in the base period and across all of the time horizons (negative power production changes in the future time horizons compared to the P-1 base period power for I-3 through I-10). Changes are most significant the mid-century time period.

Tables A3-18 through A3-24 show KGL power projected for each of the GCMs comparing the base and each of the conservation scenarios over time. Table A3-18 provides a summary of KGL energy production for the conservation scenarios with the ECHAM5 GCM.

Table A3-18: KGL Energy Production Conservation Scenarios: ECHAM5 A2 and B1

Annual Energy Production (GWh/Yr)

GCM	SRES	Conser. Scenario	Base	% Change	Early	% Change from Base P-1	Mid	% Change from Base P1	Late	% Change from Base P1
ECHAM5	A2	P-1	2246	0.0	1847	-17.8	2182	-2.8	2487	10.7
ECHAM5	A2	C-1	2216	-1.3	1866	-16.9	2192	-2.4	2496	11.1
ECHAM5	A2	C-2	2224	-1.0	1823	-18.8	2202	-2.0	2502	11.4
ECHAM5	A2	C-3	2241	-0.2	1892	-15.8	2217	-1.3	2501	11.4
ECHAM5	B1	P-1	2160	0.0	2099	-2.8	1682	-22.1	1970	-8.8
ECHAM5	B1	C-1	2164	0.2	2113	-2.2	1687	-21.9	1986	-8.1
ECHAM5	B1	C-2	2170	0.5	2125	-1.6	1705	-21.1	1998	-7.5
ECHAM5	B1	C-3	2187	1.3	2140	-0.9	1721	-20.3	2010	-6.9

Notes: "Conser." indicates conservation. GWh/Yr = Gigawatt hour per year.

Table A3-18 shows a negative change from the base period for A2 and B1 for each of the conservation release scenarios, with the percent changes greatest for the A2 scenario. For the mid-century period, negative changes are observed for all of the conservation scenarios, with the percent changes greatest for the B1 scenario. In the late century, positive changes in power relative to the base period are observed for the A2 scenarios, and negative changes are observed for the B1 scenarios. Table A3-19 provides a summary of KGL energy production for the conservation scenarios with the IPSL GCM.

Table A3-19: KGL Energy Production for Conservation Scenarios: IPSL A2 and B1

Annual Energy Production (GWh/Yr)

GCM	SRES	Conser. Scenario	Base Period	% Change from Base P-1	Early	% Change from Base P-1	Mid	% Change from Base P1	Late	% Change from Base P1
IPSL	A2	P-1	2081	0.0	1905	-8.5	2163	3.9	2120	1.9
IPSL	A2	C-1	2097	0.8	1918	-7.8	2181	4.8	2131	2.4
IPSL	A2	C-2	2122	2.0	1938	-6.9	2198	5.6	2140	2.8
IPSL	A2	C-3	2132	2.5	1975	-5.1	2211	6.2	2153	3.5
IPSL	B1	P-1	2081	0.0	2107	1.2	2007	-3.6	2090	0.4
IPSL	B1	C-1	2095	0.7	2218	6.6	2019	-3.0	2098	0.8
IPSL	B1	C-2	2120	1.9	2131	2.4	2054	-1.3	2103	1.1
IPSL	B1	C-3	2129	2.3	2140	2.8	2068	-0.6	2115	1.6

Notes: "Conser." indicates conservation. GWh/Yr = Gigawatt hour per year.

For the IPSL GCM, negative changes are observed for the A2 and conservation scenarios in the early century period, while positive changes are observed for the B1 and conservation scenarios. Positive change is observed in the mid and late century compared to the base period for the conservation scenarios and the A2 emissions scenario. For the B1 emissions scenario, power changes are negative in the mid century and slightly positive in the late century (0.4 to 1.6%) compared to the base period. Table A3-20 provides a summary of KGL energy production for the MRI GCM for the conservation scenarios compared to the P-1 base period production.

Table A3-20: KGL Energy Production for Conservation Scenarios: MRI A2 and B1

Annual Energy Production (GWh/Yr)

GCM	SRES	Conser. Scenario	Base Period	% Change from Base P-1	Early	% Change from Base P-1	Mid	% Change from Base P1	Late	% Change from Base P1
MRI	A2	P-1	2239	0.0	2087	-6.8	2210	-1.3	2125	-5.1
MRI	A2	C-1	2252	0.6	2089	-6.7	2220	-0.8	2137	-4.6
MRI	A2	C-2	2260	0.9	2106	-5.9	2233	-0.3	2149	-4.0
MRI	A2	C-3	2276	9.4	2131	-4.8	2250	0.5	2144	-4.2
MRI	B1	P-1	2246	0.0	1953	-13.0	1836	-18.3	2326	3.6
MRI	B1	C-1	2216	-1.3	1959	-12.8	1847	-17.8	2340	4.2
MRI	B1	C-2	2224	-1.0	1977	-12.0	1875	-16.5	2350	4.6
MRI	B1	C-3	2241	-0.2	2007	-10.6	1885	-16.1	2343	4.3

Notes: "Conser." indicates conservation. GWh/Yr = Gigawatt hour per year.

For the MRI scenario, early century and mid century changes are negative across the conservation uses for both the A2 and B1 scenarios (compared to the base period). In the late century power changes are negative for the MRI A2 scenario and positive for the MRI B1 scenario with conservation considered. Tables A3-21 through A3-23 present the combined energy production for all three power plants in the Kafue system (IT, KGU and KGL) for the base scenario and the three conservation scenarios. Table A3-21 provides a summary of combined (IT, KGU, and KGL) energy production for the ECHAM5 GCM for the conservation scenarios compared to the P-1 base period.

Table A3-21: Combined Energy Production Conservation Scenarios: ECHAM5 A2 and B1

Annual Energy Production (GWh/Yr)

GCM	SRES	Conser. Scenario	Base Period	% Change from Base P-1	Early	% Change from Base P-1	Mid	% Change from Base P1	Late	% Change from Base P1
ECHAM5	A2	P-1	6737	0.0	5657	-16.0	6573	-2.4	7336	8.9
ECHAM5	A2	C-1	6752	0.2	5692	-15.5	6593	-2.1	7336	8.9
ECHAM5	A2	C-2	6717	-0.3	5612	-16.7	6573	-2.4	7310	8.5
ECHAM5	A2	C-3	6601	-2.0	5552	-17.6	6441	-4.4	7098	5.4
ECHAM5	B1	P-1	6550	0.0	6346	-3.1	5189	-20.8	5972	-8.8
ECHAM5	B1	C-1	6560	0.2	6368	-2.8	5168	-21.1	6004	-8.3
ECHAM5	B1	C-2	6533	-0.3	6355	-3.0	5149	-21.4	6010	-8.2
ECHAM5	B1	C-3	6421	-2.0	6263	-4.4	5090	-22.3	5881	-10.2

Notes: "Conser." indicates conservation. GWh/Yr = Gigawatt hour per year.

Table A3-22 provides a summary of combined (IT, KGU, and KGL) energy production for the IPSL GCM for the conservation scenarios compared to the P-1 base period production.

Table A3-22: Combined Energy Production Conservation Scenarios: IPSL A2 and B1

Annual Energy Production (GWh/Yr)

GCM	SRES	Conser. Scenario	Base Period	% Change from Base P-1	Early	% Change from Base P-1	Mid	% Change from Base P1	Late	% Change from Base P1
IPSL	A2	P-1	6291	0.0	6263	-0.4	6430	2.2	6431	2.2
IPSL	A2	C-1	6342	0.8	5774	-8.2	6519	3.6	6454	2.6
IPSL	A2	C-2	6366	1.2	5799	-7.8	6529	3.8	6438	2.3
IPSL	A2	C-3	6263	-0.4	5786	-8.0	6472	2.9	6335	0.7
IPSL	B1	P-1	6308	0.0	6382	1.2	6076	-3.7	6330	0.3
IPSL	B1	C-1	6339	0.5	6405	1.5	6106	-3.2	6388	1.3
IPSL	B1	C-2	6365	0.9	6395	1.4	6170	-2.2	6367	0.9
IPSL	B1	C-3	6257	-0.8	6302	-0.1	6082	-3.6	6248	-1.0

Notes: "Conser." indicates conservation. GWh/Yr = Gigawatt hour per year.

Table A3-23 provides a summary of combined (IT, KGU, and KGL) energy production for the MRI GCM for the conservation scenarios compared to the P-1 base period production.

Table A3-23: Combined Energy Production for Conservation Scenarios: MRI A2 and B1

Annual Energy Production (GWh/Yr)

GCM	SRES	Conser. Scenario	Base Period	% Change from Base P-1	Early	% Change from Base P-1	Mid	% Change from Base P1	Late	% Change from Base P1
MRI	A2	P-1	6805	0.0	6314	-7.2	6660	-2.1	6403	-5.9
MRI	A2	C-1	6847	0.6	6314	-7.2	6688	-1.7	6430	-5.5
MRI	A2	C-2	6822	0.2	6330	-7.0	6694	-1.6	6425	-5.6
MRI	A2	C-3	6706	-1.5	6269	-7.9	6667	-2.0	6190	-9.0
MRI	B1	P-1	6823	0.0	5949	-12.8	5605	-17.9	6957	2.0
MRI	B1	C-1	6739	-1.2	5932	-13.1	5611	-17.8	7011	2.8
MRI	B1	C-2	6712	-1.6	5935	-13.0	5654	-17.1	7028	3.0
MRI	B1	C-3	6608	-3.2	5936	-13.0	5561	-18.5	6856	0.5

Notes: "Conser." indicates conservation. GWh/Yr = Gigawatt hour per year.

A range of positive and negative changes respective to the base period are seen for the system across the ECHAM5, MRI, IPSL GCMs for the A2 and B1 emissions scenarios and the three conservation scenarios. Negative power changes as great as 22.3% compared to the base period are seen for the C-3 conservation scenario for the ECHAM5, B1 scenario in the mid century.

3.6 Discussion of Results

The Kafue River System hydropower system is able to produce positive annual average power across the scenarios and time horizons analyzed. However, both decreases and increases in average annual power generation are observed over time across various GCM/emission and development/conservation scenarios (compared to each respective base period). It should be noted that the same set of operational rules were applied across all scenarios and time horizons; in reality, the operators of ZESCO would regularly revisit operational rules to adjust to changing conditions, which provides additional adaptive capacity for the system (see adaptation strategies in Section 5.0).

The extra capacity which was added at IT Reservoir during development of the KGU power station (World Bank, 2009 and Beilfus, 2001), provides storage that supports productive management of the power system in the face of rainfall variability, potential precipitation decreases, and changing water withdrawals associated with some climate change scenarios and conservation/development scenarios. However, for some scenarios and time periods, decreases in KGL or system average annual power generation are observed compared to the P-1 scenario.

For the highest positive flow change from the base period scenario (WXGEN Simulation for the A2, late-century period), individual power increased compared to the base period in all three locations, with a total positive system change of 44.5%. For the greatest negative flow change from the base period scenario (WXGEN simulation for B1, mid-century period), individual power station energy generation in the mid-century compared to the base period also has a positive change, but less total energy is produced (6,743 GWh/Yr for ECHAM5 B1 mid-century system power for the WXGEN simulation compared to 9,733 GWh/Yr system power for ECHAM5 A2 late-century WXGEN simulation) and the positive change compared to the baseline period is 3%.

Negative changes in average annual energy production compared to the P-1 baseline period are observed for some future periods for the low to moderate development scenarios (I-3, I-6, and I-9). In addition, negative energy production impacts are observed for all time horizons for the ECHAM5 GCM for both the A2 and B1 emission scenarios (compared to the P-1 and baseline periods) for the highest development scenario (I-10). These decreases in power compared to the base period for the higher demand assumption highlight the need to view hydropower operations in a systemic manner (that is, considering future power needs in combination with climate change impacts and conservation/development needs) within the Kafue River Basin.

Development scenarios include abstractions for domestic, mining, and industry (DMI), and irrigation uses. Scenarios I-3, I-6, and I-9 are based on information in a Strategic Environmental Impact Assessment (SEIA) prepared in 2003. These withdrawals have clear negative impacts on specific power station generation, but generally the power generation capacity of the system remains positive. The I-10 scenario assumes abstractions greater than the SEIA to accommodate additional irrigation and DMI use; for this scenario, negative power generation impacts are observed across more scenarios and time periods. These abstractions are discussed further in light of potential temperature and run-off impacts on agriculture and in regards to agricultural development projections in Sections 4.2 of this report.

Background information indicates that the IT Reservoir constructed with a storage volume to accommodate planned conservation releases, as well as planned storage requirements for power generation. This extra storage capacity (compared to storage for power needs alone) at the IT Reservoir has supported operators in managing water storage and release to accommodate power needs across high and low flow periods. The IT Reservoir, combined with operational practices indicated by ZESCO, should allow power to be generated at the three stations (IT, KGU, and KGL) in the present and future. However, during times of lower flows, this may result in water for power generation rather than conservation releases (see paragraph below).

Conservation releases (C-1, C-2, and C-3) can be accommodated by the system but cause some power impacts and draw down the IT Reservoir in dry years. Some spillage or loss of power occurs at the IT Power Station for these releases (particularly, for C-2 and C-3 releases), but because these releases are non-consumptive, flow in the lower portions of the power system appears sufficient for positive system power generation (through power generation at the lower two stations KGU and KGL). The C-1 scenario causes the least impacts overall and appears to

have been implemented occasionally in recent years. The combined impacts of conservation, development, and climate change scenarios are discussed in Sections 4.0 and 5.0 of the report.

The impacts associated with conservation needs and development scenarios show that while the hydropower plants may remain viable in light of climate change predictions if operating in isolation, hydropower must be considered within the systemic framework of the study area. A systemic view indicates that adaptation planning is warranted. Climate change impacts on the hydropower and river system, combined with increasing development and indirect climate change impacts on natural hazards and other sectors merit integrated water planning to help ensure that power, ecological, agriculture, and DMI water needs are managed sustainably.

In addition to the uncertainty described previously for precipitation and temperature projections, and hydrologic (flow) modeling, there is considerable uncertainty associated with the reservoir (energy) modeling. This uncertainty is driven by limited stream channel information in the flats, inputs regarding planned power stations, assumptions regarding operating rules, and related factors.

3.7 References

Beilfuss, Richard. 2001 (Beilfuss, 2001). International Crane Foundation, USA. Prescribed Flooding and Restoration Potential in the Zambezi Delta, Mozambique. Working Paper #3. Program for the sustainable Management of Cahora Bassa Dam and the Lower Zambezi Valley.

U.S. Army Corps of Engineers, Hydrologic Engineering Center (HEC). 2007 (HEC, 2007). "*HEC-ResSim, Reservoir System Simulation, User's Manual, Version 3.0, Ap*ril 2007,CPD-82", U S Army Corps of Engineers, Davis, CA, USA.

HEC. 1998 (HEC, 1998). "HEC-5, Simulation of Flood Control and Conservation Systems, User's Manual, Version 8.0,October 1998,CPD-5", U S Army Corps of Engineers, Davis, CA, USA.

HEC. 2008 (HEC, 2008). "*HEC-RAS River Analysis System, User's Manual, Version 4.0, March 2008,CPD-68*", U S Army Corps of Engineers, Davis, CA, USA.

HEC. 2009 (HEC, 2009). "*HEC-DSSVue, HEC Data Storage System, Visual Utility Engine, User's Manual, Version 3.0, July 2009,CPD-79*", U S Army Corps of Engineers, Davis, CA, USA.

World Bank. 2009 (World BankNIS, BRL, Ingenierie, 2009). Report prepared for World Bank, Zambezi River Basin: A Multi-Sector Investment Opportunities Analysis. Prepared by NIRAS, BRL, Ingenierie. Preliminary Report. May.

Nsongela, Shadreck (editor). Kafue River Basin Dialogue on Water, Food and the Environment: The Role f the Kafue Flats Fishery in Sustaining the Socia-economic Livelihoods of the Local Communities. Study Report by Shirley Ndalama, Student Researcher, University of Zambia.

Scott Wilson Piesold. 2003 (SWP, 2003). Integrated Kafue River Basin Environmental Impact Assessment Study: Power Rehabilitation Project. Strategic Environmental Impact Assessment. September.

Appendix A4
Financial Modeling

The assessment of the potential financial impacts of climate change on the Kafue Gorge Lower (KGL) hydropower project provides additional perspective on past evaluations. This financial assessment is not intended to establish or re-evaluate the financial viability of the KGL project. IFC has conducted previous financial analysis to evaluate the financial impacts of a variety of factors on the ability of the KGL project to meet investor requirements. This project's financial assessment evaluates the potential changes in power and revenue that may occur as the result of specific climate change scenarios. The financial analysis uses the climate change results from the ECHAM5 model as an example, and examines two operational levels, P-1 (maximum power) and I-9 (maximum development), for each of the two emission scenarios, A2 and B1. This Because the conservation scenarios (particularly C-2 and C-3) introduce the tendency to violate KGL operating rules, they are excluded from this financial analysis. This evaluation focuses on the early-century period because it is consistent with the period that is most relevant to investors.

4.1 Introduction to the RETScreen Model

A priority for this project has been to complete each stage of analysis using modeling resources that are in the public domain, in order to facilitate further evaluation of the project outputs by project stakeholders and to identify tools that could be used to apply similar approaches to other climate change risk assessment studies. The financial assessment has been completed using the RETScreen International Model (RETScreen). RETScreen is a tool developed to "screen" the financial viability of new renewable energy technology projects around the world.

Developed with multilateral funding and data from the Global Environment Fund (GEF), U.S. National Aeronautics and Space Administration, and others, this spreadsheet-based tool is available in 35 languages and includes modules that capture major macroeconomic factors, project-specific costs, financing and energy production inputs. These are used to project cash flow from operations and from a potential carbon market. For each RETScreen module, at least two "methods" are available; one uses more limited information for a preliminary analysis and the other uses more detailed information for a more advanced analysis. RETScreen can be downloaded from the Natural Resources Canada web site (www.retscreen.net), as can extensive support and training documentation.

RETScreen is intended to reduce the cost associated with evaluating clean energy projects throughout the world by providing a high quality, easy to use, and flexible assessment tool. Because large entities are expected to have their own analytic tools, the primary beneficiaries of this resource are expected to be smaller developers who have fewer resources for feasibility assessments. In the interest of reducing the barriers for the development of clean energy projects, the support documentation for RETScreen anticipates small projects, including hydropower projects, but the formulas are scalable and are appropriate for use in assessing a project the size of KGL (Ziegler, 2010). The RETScreen analysis includes seven modules, each of which is introduced below.

4.1.1 Climate Module

With support from NASA, RETScreen provides climate-relevant information specific to the location of the project under evaluation. Using a series of drop-down lists, the project country, province/state (if appropriate) and nearest location can be selected. The resulting information presents the nearest latitude/longitude point for which satellite data are available. For KGL, that location corresponds to the Itezhi-Tezhi (IT) site, which is included in the drop down list of locations. The following corresponding meteorological information is provided for the site's elevation: monthly average temperature, relative humidity, air pressure, solar radiation, heating degree days, and cooling degree days.

4.1.2 Energy Module

RETScreen models energy production from several types of renewable energy technologies. This module has two "method" categories calculating energy; "Method 1" is limited to capacity and capacity factor inputs, whereas "Method 2" allows for more detailed inputs. For this stud's financial assessment, grid-connected hydropower with storage is specified and Method 2 is used. Method 2 includes sections for resource assessment (gross head, residual flow, and maximum tailwater effect), hydroturbine parameters (turbine type, number, design flow, and efficiency), and flow duration curve inputs. Hydropower results kilowatt hours (kWh) per year, total and firm capacity in kilowatt (kW), and the resulting capacity factor. RETScreen provides a graph of the resulting power and flow duration curves. The use also enters the price of electricity in this module.

4.1.3 Cost Module

The major cost categories included for both Methods 1 and 2 include: initial costs, annual costs, and periodic costs. This module can accept up to two currencies (for cases where costs may be expressed in a currency that differs from the local currency). For this analysis, Method 1 is used based on the availability of construction cost information for KGL. For initial costs, inputs can be provided for the feasibility assessment, development costs, civil works, engineering, the power system, "balance of system," and miscellaneous elements including contingencies and interest during the construction period. The operation and maintenance (O&M) section addressed costs for parts and labor, contingency costs, and other user defined costs. Finally, additional periodic or one-time costs can also be included for the year in which they would occur.

4.1.4 Emission Analysis Module

RETScreen's project evaluation includes the potential revenue stream from the sale of greenhouse gas (GHG) credits. Therefore, this module allows for the calculation of carbon emission reductions that could result from the reduced use of fossil fuel energy sources when the new project becomes operational. This module has three calculation "methods," providing the opportunity to quantify net electricity available after transmission and distribution losses, up to four types of fossil fuel, and their relative presence in the country's energy mix, whose use is avoided due to the new project and the resulting avoided GHG emissions. This module was not included in the analysis for this project.

4.1.5 Financial Analysis Module

This module captures other financial information relevant to the total costs and revenues that will occur over the life of the project. Inputs are categorized as "general" (discount rate, inflation rate, fuel cost escalation rate, and project life), "finance" (debt ratio, debt interest, and debt term), and "income tax analysis" (income tax rate and depreciation method). Calculations generated in this module incorporate information from prior modules to yield annual costs and revenues in a variety of subcategories. The module produces a table of yearly cash flow (pre-tax, after-tax, and cumulative) for the life of the project and a cumulative cash flow graph.

4.1.6 Sensitivity and Risk Analysis Module

The final RETScreen module provides for the evaluation of four financial parameters: internal rate of return (IRR) on equity (after tax), IRR on investment (after tax), net present value, and the equity payback period. The sensitivity of these parameters can be evaluated based on the price of electricity, the price of GHG credits, and debt interest rate. Results are presented in a table format with columns for the assumed value for the parameter and two sensitivity increments above and two increments below the assumed value. This increment is selected by the user. The threshold rate for the result can also be entered; the table automatically highlights those cells whose results exceed the threshold, providing an effective visual cue for the combination of inputs and outputs that meet the user's criteria.

4.2 RETScreen Model: Calibration

RETScreen's evaluation of the KGL hydropower project began with a two-stage calibration process. RETScreen was first calibrated against the HEC-ResSim (reservoir energy) model by using the flow-exceedence curves generated by ResSim for each of the target scenarios and comparing the resulting ResSim and RETScreen electricity generation results. Once calibrated with ResSim for energy production, the RETScreen model was then calibrated against the IFC financial analysis for the major financial impacts of the KGL plant under several operational scenarios. Each of these calibration processes is explained in the following sub-sections.

4.2.1 Energy Calibration: RETScreen and HEC-ResSim

HEC-ResSim modeling (presented in Section 3.3 and Appendix A3) uses HEC-HMS modeled flow estimates (presented in Section 3.2 and Appendix A2) and the structural and operational characteristics of the KGL power plant to project energy generation from KGL across a range of scenarios. Similarly, RETScreen uses water supply information and power plant structural and operational characteristics to estimate generation from KGL. Because ResSim is a more detailed model, the RETScreen model's electricity projections were calibrated against the HEC-ResSim modeling results.

The period of interest for the financial assessment is the early-century time period, capturing five years of construction costs and the first 25 years of operation. The calibration process was completed for both the P-1 and I-9 operational scenario for the ECHAM5 A2 and B1 emission scenarios.

4.2.1.1 Model Set-up and Calibration

RETScreen can evaluate a project based on varying levels of available information. For the KGL assessment, "Method 2" was used in Energy Module. The relevant KGL power plant features were entered, as shown in Table A4-1.

Table A4-1: RETScreen Energy Module KGL Power Plant Inputs

Resource Assessment	Project Information
Proposed project type	Reservoir
Gross head	200.0 m
Maximum tailwater effect	384.70 m
Residual flow	7.20 cms
Percent time firm flow available	90.0%
Hydro Turbine Features	Project Information
Design flow	464.0 cms
Turbine type	Francis
Turbine efficiency	Standard
Number of turbines	4

Notes: m = meters; cms = cubic meters per second.

Because four turbines are specified, the Energy Module divides the design flow value by four to yield flow per turbine. From these inputs, the RETScreen Energy Module calculates additional parameters as shown in Table A4-2.

Table A4-2: Plant Operational Features Calculated by RETScreen

Calculated Parameters	Units	Value
Firm flow	cms	124.80
Turbine peak efficiency	%	92.6
Flow at peak efficiency	cms	365.3
Turbine efficiency at design flow	%	89.5

Notes: cms = cubic meters per second.

Other operational features of the plant are also captured, including: maximum hydraulic losses for the plant (1.2%), miscellaneous losses (2.0%), generator efficiency (95%), availability (99%), and available flow adjustment factor (1.0). With these inputs, the Energy Module calculates the power capacity of the plant to be 749.5 megawatts (MW).

4.2.1.2 Model Calibration: Electricity Generation

The next section of the Energy Module allows entry of flow-exceedence information, which is defines a curve showing the percentages of time that a range of flow rates occurs. This curve is unique for each scenario analyzed with HEC-HMS stage; it is entered into the Energy Module of

RETScreen as the basis for the calibration of RETScreen's energy outputs. Because the financial analysis for the project focuses on the early-century time period, the RETScreen model's electricity output will be calibrated with ResSim for the early-century period for two key operating scenarios: P-1 (maximum power) and I-9 (maximum development). These flow-exceedence inputs for both the A2 and B1 emission scenarios are shown in Table A4-3.

Table A4-3: Flow Exceedence Inputs (cms), for P-1 and I-9, ECHAM5 A2 and B1, Early-Century Period

Exceedance Level	P-1		I-9	
	A2	B1	A2	B1
0	537	681	524	671
5%	298	346	297	333
10%	297	297	297	297
15%	297	297	297	297
20%	248	280	238	266
25%	226	241	226	229
30%	226	226	217	226
35%	189	226	175	211
40%	154	186	137	168
45%	128	152	112	136
50%	101	129	79	118
55%	74	99	26	81
60%	26	77	16	38
65%	16	27	16	16
70%	16	16	16	16
75%	16	16	14	16
80%	11	16	7.2	11
85%	7.2	7.2	7.2	7.2
90%	7.2	7.2	7.2	7.2
95%	7.2	7.2	7.2	7.2
100%	7.2	7.2	7.2	7.2

Notes: cms = cubic meters per second.

A comparison of ResSim and RETScreen energy output results for each scenario is provided in Table A4-4.

Table A4-4: Power Output Comparison (GWh/year; ResSim and RETScreen), Early-Century Period, ECAHM5

Scenario		ResSim	RETScreen	Difference
A2	P-1	1,847	1,345	(0.27)
B1	P-1	2,099	1,465	(0.30)

Notes: GWh/yr = gigawatt hour per year.

When compared to the HEC-ResSim projections, the RETScreen results consistently underestimated the annual electricity generation. In order to achieve energy results that align more closely with HEC-ResSim, the low flows at the upper exceedance levels were then adjusted upward. The adjusted flow exceedance inputs are shown in Table A4-5.

Table A4-5: Adjusted Flow Exceedence Inputs (cms), for P-1 and I-9, ECHAM5 A2 and B1, Early-Century Period

Exceedance Level	P-1		I-9	
	A2	B1	A2	B1
0	537	524	681	671
5%	298	297	346	333
10%	297	297	297	297
15%	297	297	297	297
20%	248	238	280	266
25%	226	226	241	229
30%	226	217	226	226
35%	189	175	226	211
40%	154	161	219	198
45%	128	115	175	168
50%	124	115	175	168
55%	124	85	175	167
60%	124	85	144	100
65%	124	85	125	100
70%	124	82	100	85
75%	124	75	90	85
80%	90	75	85	85
85%	85	60	85	85
90%	26	60	85	80
95%	26	60	85	80
100%	26	60	85	80

Notes: cms = cubic meters per second.

The resulting energy estimates are shown in Table A4-6 and show a much better alignment.

Table A4-6: Power Output Comparison (GWh/year; ResSim and RETScreen), Early-Century Period

Scenario		ResSim	RETScreen	Difference
A2	P-1	1,847	1,847	0
B1	P-1	1,721	1,721	0

Notes: GWh/yr = gigawatt hour per year.

4.2.2 Financial Calibration: RETScreen and IFC Financial Analysis

As a potential lender to support the development of the KGL project, the IFC has supported numerous engineering, economic and environmental studies to evaluate project costs and revenues, including assessing the project's financial viability. This IFC financial analysis was used as the baseline projection of financial performance for the project without consideration of climate change. RETScreen was calibrated against the IFC financial analysis to establish a baseline financial scenario ("without climate change"), for comparison to results that reflect the impact of climate change. For the purpose of this analysis, "Method 1" was used in the Cost Module of RETScreen.

The IFC's financial analysis evaluates several potential combinations of KGL plant capacity and operating parameters using electricity generation and project cost information from previous

technical and economic analysis (Montgomery Watson Harza, 2009). For a KGL plant capacity of 750 MW, operating as a peaking unit for four hours per day, the IFC financial analysis assumes annual electricity generation of 2,491 GWh/yr.

The project construction costs used for the IFC financial analysis are shown in Table A4-7. These values were entered into the Cost Module of the RETScreen tool.

Table A4-7: IFC KGL Project Costs Inputs

Project Cost (US$ Millions)	
Civil works	$422.5
E&M works	$463.5
	$886.0
Civil works	
Unmeasured	$84.5
Contingency	$63.4
	$147.9
E&M works	
Unmeasured	$69.5
Contingency	$46.4
	$115.9
Other costs	
Engineering/Admin.	$138.0
Development cost	$92.0
	$1,379.8
Re-reg dam	**$150.0**
Total Project Cost	**$1,529.8**

Development and construction costs occur over the first five years, followed by annual operation and maintenance costs of 7% of the total investment for the 40-year operational life assumed for the project.

Consistent with the IFC financial analysis, additional inputs used in the RETScreen analysis include a discount rate of 10%, annual inflation rate of 2.5%, and financing of 75% debt to 25% equity. The debt interest rate is 9% with a term of 16 years with repayment beginning after a six-year grace period. A corporate tax rate of 35% is included after the first five years of operation and a straight-line depreciation method is used. RETScreen allows for the inclusion of other costs used in the IFC financial analysis, including interest accrued during construction, front-end and other financing fees, and a debt service reserve account, for total of about $528 million USD. It also captures the IFC's financial analysis assumption of an annual $10 million USD insurance premium.

The IFC financial analysis includes an average electricity price of $0.153/kWh, which is escalated over time at a rate equal to inflation.

4.2.2.2 Financial Calibration Results

Using the assumptions and inputs described above, annual cash flow results for the two financial analyses are shown in Figure A4-1.

Figure A4-1: Comparison of Annual Cash Flow Projections

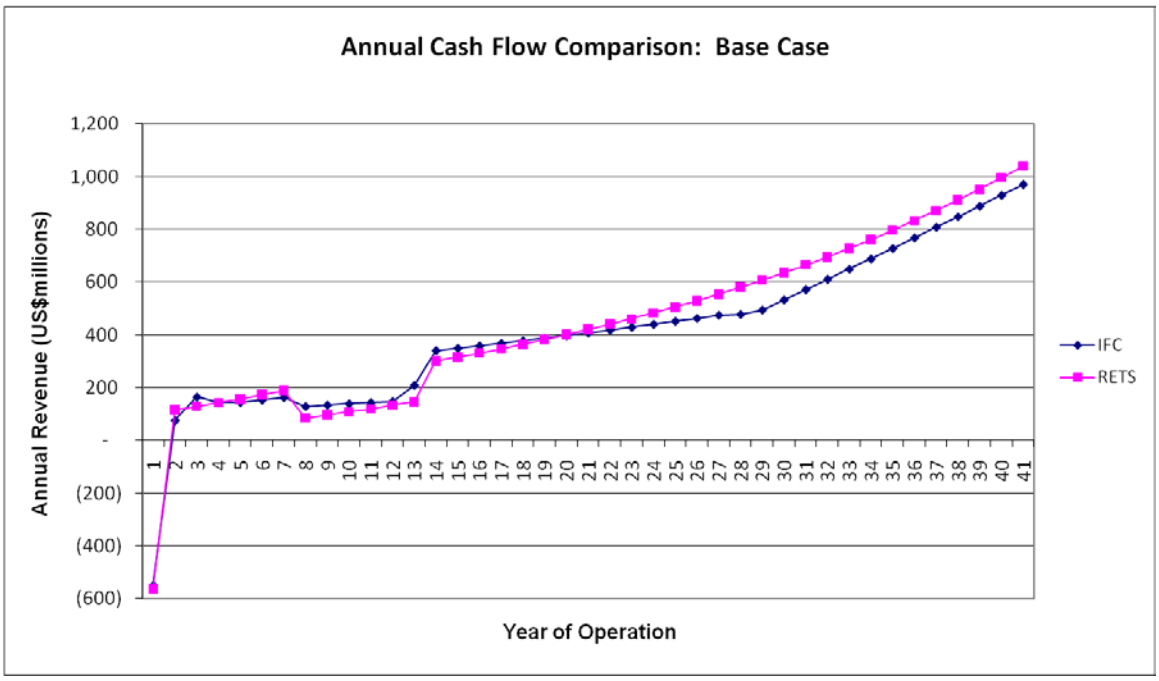

In this case, the IFC value used for comparison is “cash available for dividend payment”; the RETScreen value is “after tax yearly cash flow”. Using $150.33/MWh as the electricity price, the RETScreen analysis yields an after-tax internal rate of return (IRR) of 22.7% compared to the IFC value of 22.3%. The resulting cumulative cash flow from the RETScreen analysis is shown in Figure A4-2 below, which illustrates that cumulative cash flow becomes positive after 4.9 years of operation.

Figure A4-2: RETScreen Output: KGL Base Case Cumulative Cash Flow

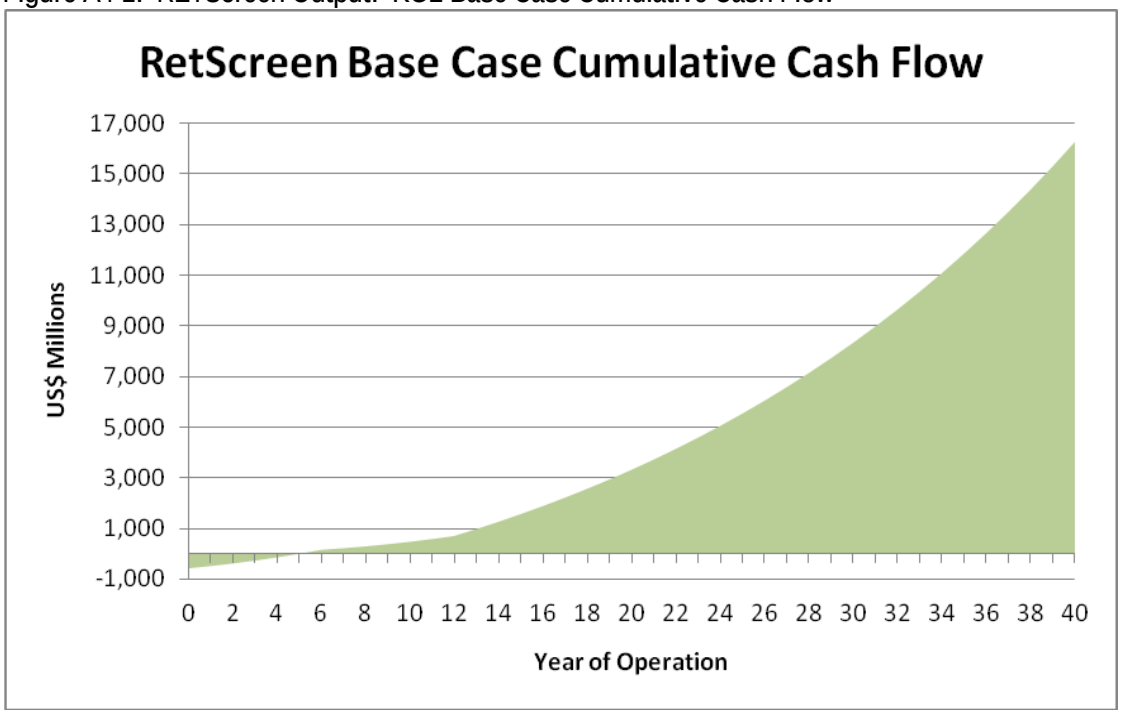

The corresponding cash flow from the IFC analysis yields a four-year breakeven period as shown in Figure A4-3 below.

Figure A4-3: IFC Cumulative Cash Flow for Base Case

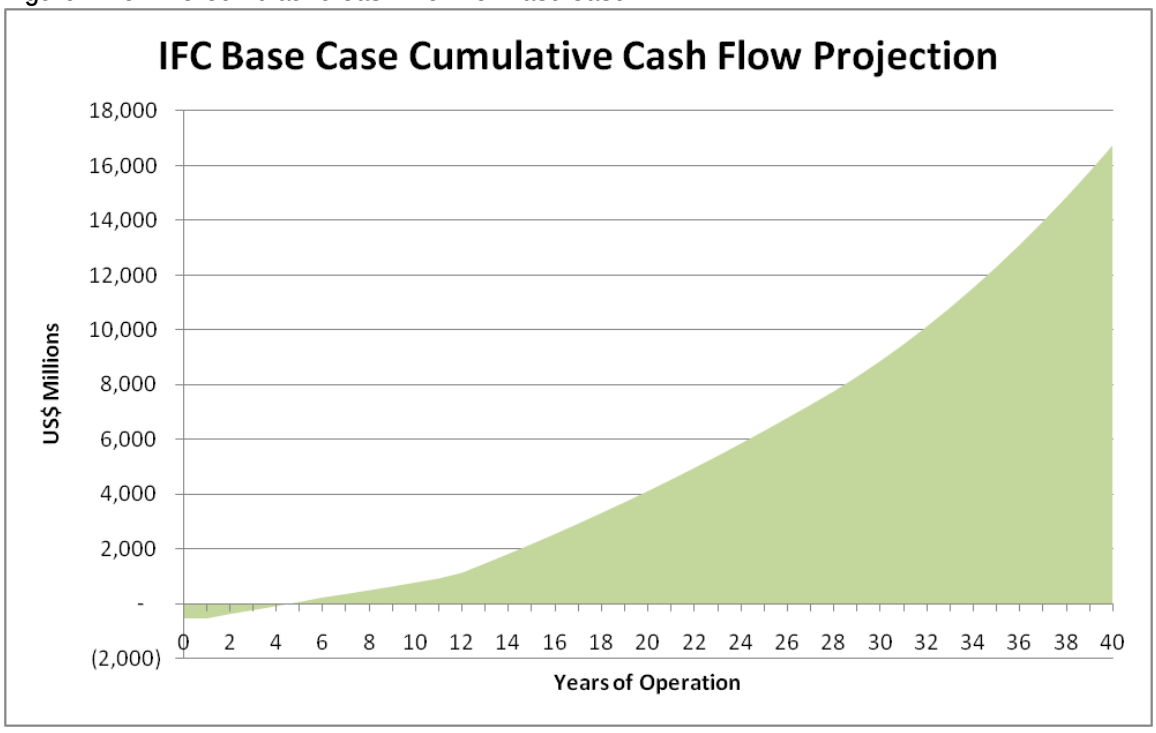

These results were considered acceptable for the calibration stage and this calibrated version of RETScreen was used for the financial analysis of climate scenarios and competing uses.

4.3 Financial Analysis of Climate Scenarios and Competing Uses

This study focused on potential water supply available to KGL in the face of climate change impacts on flow in conjunction with additional demands on the water supply from economic development. While the IFC financial analysis included a range of possible plant capacity and operating combinations, it did not consider the potential financial impact of these potential changes in water supply to KGL. The potential impacts on the financial viability of KGL were evaluated using RETScreen, as described in the following sub-sections.

4.3.1 Analysis

Assessment of the climate change scenarios in RetScreen for future periods involves holding the KGL financial and power plant operational variables constant while changing the flow inputs in RetScreen to reflect the effect of climate change on available flow.

The financial viability of KGL will be determined within the early-century period, the period within which the major investments will require key returns or repayment. The first row of Table A4-8 shows the projected level of energy production in the early century period for both the A2 and B1 climate change scenarios, and reflects the additional effects of the expected irrigation scenario (I-9). The remaining rows in Table A4-8 provide the corresponding impacts on key financial parameters from the RetScreen financial assessment.

Table A4-8 Financial Performance for A2 Scenario Comparing Base ad Early Time Horizons

Performance Category	IFC	ECHAM5 A2, Early Scenarios		ECHAM5 B1, Early Scenarios	
		P-1	I-9	P-1	I-9
Average Annual Generation (GWh/yr)	2,491	2,025	1,920	2,269	2,129
Internal Rate of Return (%) (after tax)	22.3	15.4	14.1	18.6	16.7
Net Present Value (USD Millions)	1,261	646	507	967	782
Payback Period (on Equity, in years)	5.4	9.4	11.3	6.8	8.1

Notes: GWh/yr – Gigawatt hour per year; IRR = internal rate of return; NPV = net present value.

Based on the assumptions in each of the scenarios, for the "climate change only" P-1 operating scenario, primary financial debts would be paid back between 6 and 10 years compared to about 5.5 years in the "without climate change" scenario as represented by the IFC analysis. Figure 4-4 shows the relationship between projected annual generation and after-tax IRR in each of these scenarios. The red line indicates the threshold return requirement of 20%, making it clear that the effect of climate change interferes with the ability of the project to meet investment requirements.

Figure A4-4: Comparison of Early Century Annual Generation and After-Tax Internal Rate of Return

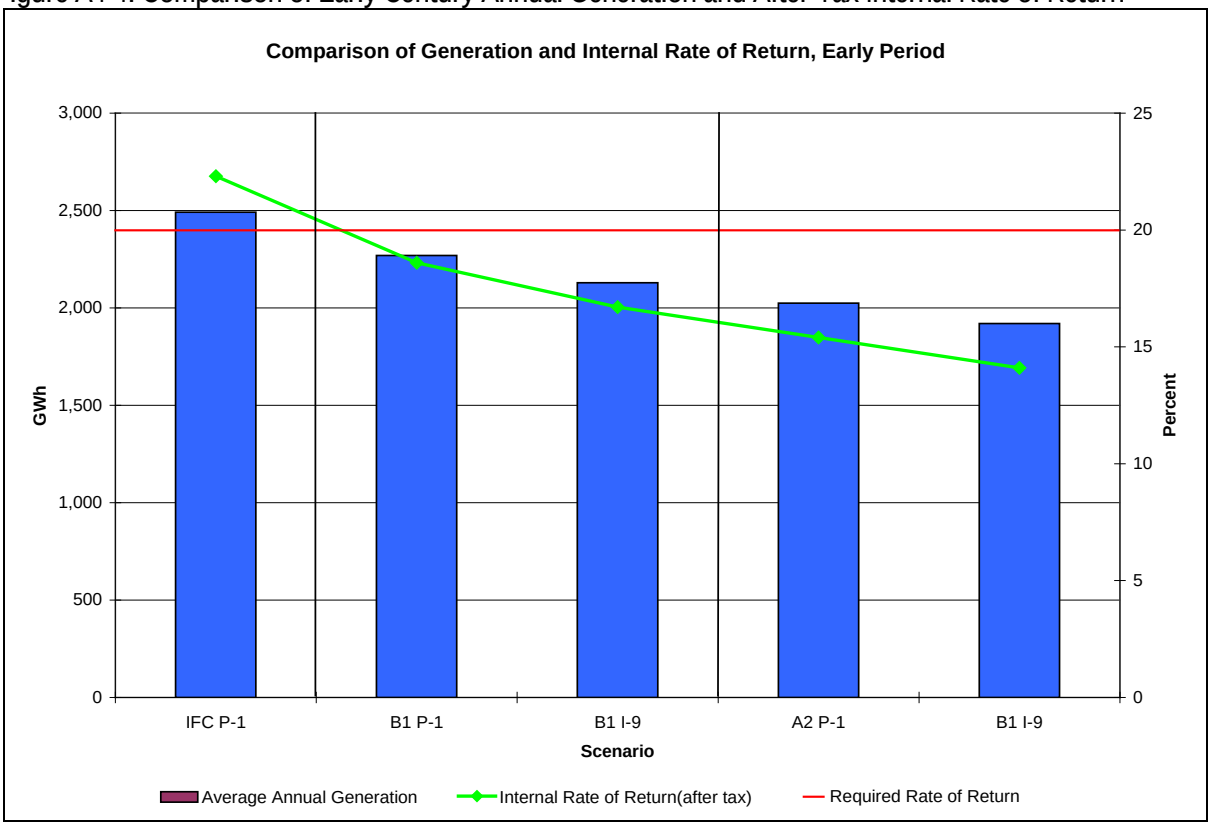

4.3.2 Discussion

Assuming that financing were to be considered in light of both projected climate change and additional water use for development, the primary financial debts would be repaid between eight and 12 years; subsequent operation would allow the project to yield substantial subsequent annual cash flows.

On-going performance of KGL through the rest of the century can be characterized by the projected flows and corresponding electricity production during the mid and late century periods. For each set of results, A2 and B1, includes two time periods, mid and late century. For A2, the additional set of results reflects the WXGEN alternative analysis of the late century period (simulation of the highest positive change in flow for a future time horizon compared to its respective baseline period); for B1, the additional set is for the WXGEN alternative for the mid-century period simulation of the highest negative change in flow for a future time horizon compared to its respective baseline period).

The variability among these sets of results reflects the projected combined effects of climate change and the competing uses of irrigation or conservation. Uncertainty exists with regard to the true future impact of all three influences. Irrigation demand levels will be driven by the growth of the agriculture sector and authorized by the Department of Water Affairs. The International Panel on Climate Change (IPCC), which established the range of future emission scenarios that include A2 and B1, clearly states that no one scenario is a more likely outcome than any other. Given the significance of water flow on the financial viability of hydropower

projects, the study shows that considering influences that introduce variability into the project's available water flow schemes as well as those that introduce economic variability to a project will help to better assess a hydropower project's future financial performance.

For each of these emission scenarios, these results effectively consider one possible outcome for the future time periods. A probability assessment provides a better characterization of the likelihood of a range of outcomes for the same period, varying the results of key inputs according to their distribution around their respective averages. In this case, a limited probability assessment was performed for the "maximum power" option in the A2 emission scenario. The results for power generation and for the corresponding IRRs are shown in Figures 4-5 (a) and (b). In light of the variability of the actual annual generation over the 30 years of the early-century period, these figures show that the actual average generation of KGL may be closer to 2,221 GWh, with an IRR of nearly 18%. The change in these results provides an indication of the fact that a more robust probability analysis will deliver different results, which should better inform planning decisions.

Figure 4-5: Probability Assessment of KGL Performance, Early Century

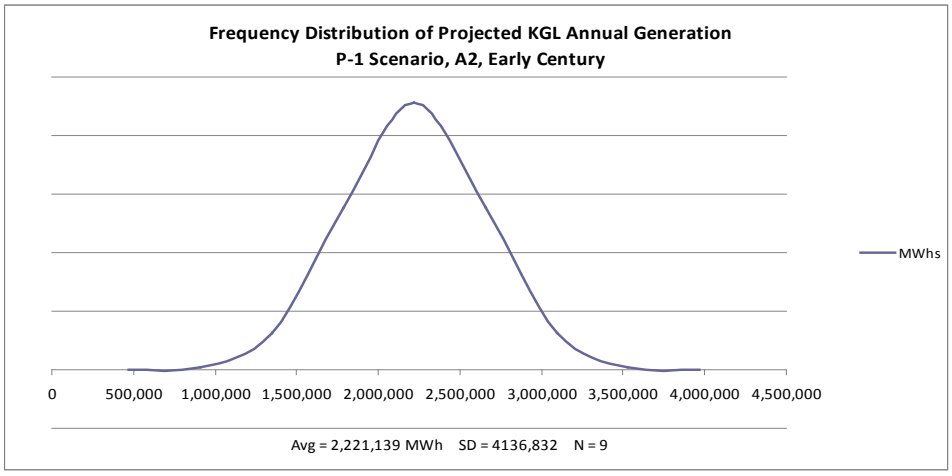

4-10(a): Projected Frequency Curve, KGL Annual Generation

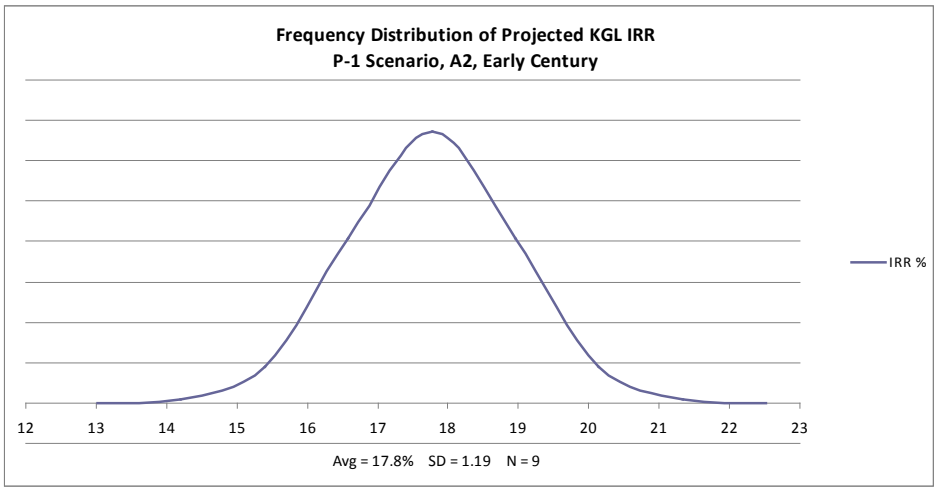

4-10(b): Projected Frequency Curve, KGL Internal Rate of Return

As discussed further in Section 4.5 below, there is uncertainty associated with a number of factors that tie to the above financial analysis; in addition, the financial analysis uses the outputs of the modeling efforts which also include uncertainty in regards to climate change projections, flow, and energy. For example, the IPCC, which established the range of future emissions scenarios that include A2 and B1, states that no one scenario is a more likely outcome than any other (Nakicenovic, N., et al., 2000). In addition to uncertainty discussed for the modeling steps, there is also uncertainty in regards to the future demands for conservation release and other uses of water in the basin. Irrigation and DMI water demand levels will be driven by the growth of the agriculture sector and authorized by the Department of Water Affairs; in addition, climate change may impact the need for increased irrigation (see Section 5.2). Other uses such as DMI are anticipated to increase – but the precise value is uncertain. These sectors are considered further in Section 5.

Given the significance of water flow on the financial viability of hydropower projects, adaptation planning should include considerations such as climate change, conservation, and development that introduce variability.

4.4 Findings

Financial analysis of multiple scenarios suggests that KGL's financial viability is acceptable (i.e., IRR greater than 20%) when annual power generation exceeds about 2,450 GWh per year, using IFC financial assumptions.

The RETScreen model suggests that the impact of climate change on available flow, and therefore on electricity production, compromises the financial viability of the plant during the early period, which is the timeframe that most investors will use to evaluate the viability of the project:

- The impact of climate change alone is projected to yield power production levels of about 10% to 20% below the 2,350 GWh per year threshold during the early period.
- When high levels of competing water demand from development is included, the maximum impact in the early period rises to nearly a 30% reduction in power below the threshold.

These results should be considered in light of the fact that several types of key inputs are held constant (or adjusted linearly) throughout the evaluation period. These include the average annual flow to KGL. Average flows to KGL reflect not only the potential impact of climate change, but also competing demands for water from the Kafue River, such as from the mining sector, other industrial sectors, agricultural irrigation and residential usage.

Investors can be better informed about the viability of future hydropower projects by including projected changes in available water flow to the project. Rather than assuming a constant level of power output throughout the investment period, evaluations should reflect potential changes in

flow due to climate change and due to competing uses, which themselves may be affected by climate change.

4.5 Uncertainty

There is uncertainty associated with a number of factors relevant to the above financial analysis; in addition, the financial analysis uses the outputs of the modeling efforts which also include uncertainty in regards to climate change projections, flow, and energy. For example, the IPCC, which established the range of future emissions scenarios that include A2 and B1, clearly states that no one scenario is a more likely outcome than any other (Nakicenovic, N., et al., 2000). In addition to uncertainty discussed for the modeling steps, there is also uncertainty in regards to future impact of conservation release needs and competing uses for water in the basin. Irrigation and DMI water demand levels will be driven by the growth of the agriculture sector and authorized by the Department of Water Affairs; in addition, climate change may impact the need for increased irrigation. Other competing uses such as DMI are anticipated to increase – but the precise value is uncertain. These sectors are considered further in Section 5.

4.6 References

International Finance Corp/World Bank. 2009. KGL Structuring Options Report.

Montgomery Watson Harza/IFC. 2009 (MWH/IFC, 2009). KGL Hydroelectric Power Project: Interim Summary Report and Appendices.

Natural Resources Canada. RETScreen Website and Technical Information. Accessed at: http://www.retscreen.net

World Bank. 2009b (World Bank, 2009b). Zambezi River Basin Multi-Sector Investment Opportunities Analysis. Prepared by NIRAS, BRL Ingenierie. 2009 (NIS, BRL, Ingenierie, Preliminary Report with Updated Water Tables Provided to Study Team in Spring 2010.

Ziegler, Urban. May, 2009. Personal Communication between Tetra Tech, Donna Boysen and Urban Zieglar, RETScreen Development Engineer.

Appendix A5

Flood Risk

Several million people in Africa suffer impacts from droughts and floods on a regular basis (IPCC 2007). Floods are critical because they endanger lives and impact development and the economy in African countries. Recurrent floods in some countries are linked, in some cases, with El-Nino Southern Oscillation (ENSO) events. ENSO is a quasi-periodic climate pattern that occurs across the tropical Pacific Ocean on average every five years, but over a period which varies from three to seven years. It is characterized by variations in the temperature of the surface of the tropical eastern Pacific Ocean and causes extreme weather events.

When major flood events occur, important economic and human losses result (Mirza, 2003; Obasi, 2005). For urban planners in Africa, the biggest threats to local populations and economies posed by climate variability and change are often expected to result from little-characterized and unpredictable, rapid-onset disasters such as storm surges, flash floods, and tropical cyclones (Freeman, 2003). In general, Zambia faces a flood event at a current frequency of 0.42 events per year (about once every 2.3 years) (Prevention Web, 2010).

As discussed in Section 3.2, climate change may lead to an increase in intense rainfall events. More intense rainfall may cause more frequent or larger floods. This could result in direct economic losses from damage to ZESCO facilities and utility lines or potential suspension of hydropower operations. Such flood events also may cause substantial impacts to ZESCO customers and area stakeholders, which indirectly can impact ZESCO.

This appendix presents the flood hazard assessment and flood vulnerability assessment; findings are summarized in Section 4.1 of the report.

5.1 Flood Hazard Assessment

This section reviews current and future hazard conditions for the flood hazard.

5.1.1 Flood Hazard Current Conditions

A University of Zambia report released in 2008 states Southern Zambia will continue to experience more rainfall than ever because of changing weather patterns and that the region is likely to face a growing number of deaths from more floods (Kabange, 2008). The current flood frequency and magnitude was reviewed for the entire country of Zambia to assess the impact to ZESCO customers. Figure A5-1 provides a flood frequency map based on three sources: (1) a geographic information system (GIS) model using a statistical estimation of peak-flow magnitude and a hydrological model using the HydroSHEDS dataset and the Manning equation to estimate river stage for the calculated discharge value; (2) observed flood data for 1999 to

2007, obtained from the Dartmouth Flood Observatory (DFO); and (3) frequency data from the UNEP/GRID-Europe PREVIEW flood dataset.

Figure A5-1 shows areas of more frequent flooding as dark blue and areas of more infrequent flooding in light blue. The Kafue Gorge Upper (KGU) Dam and the potential Kafue Gorge Lower (KGL) dam location are shown. There is a low flooding frequency around the dams, which serve to regulate water flow. The units for the figure are the expected average number of events per 100 years.

Figure A5-1: Flood Frequency Map

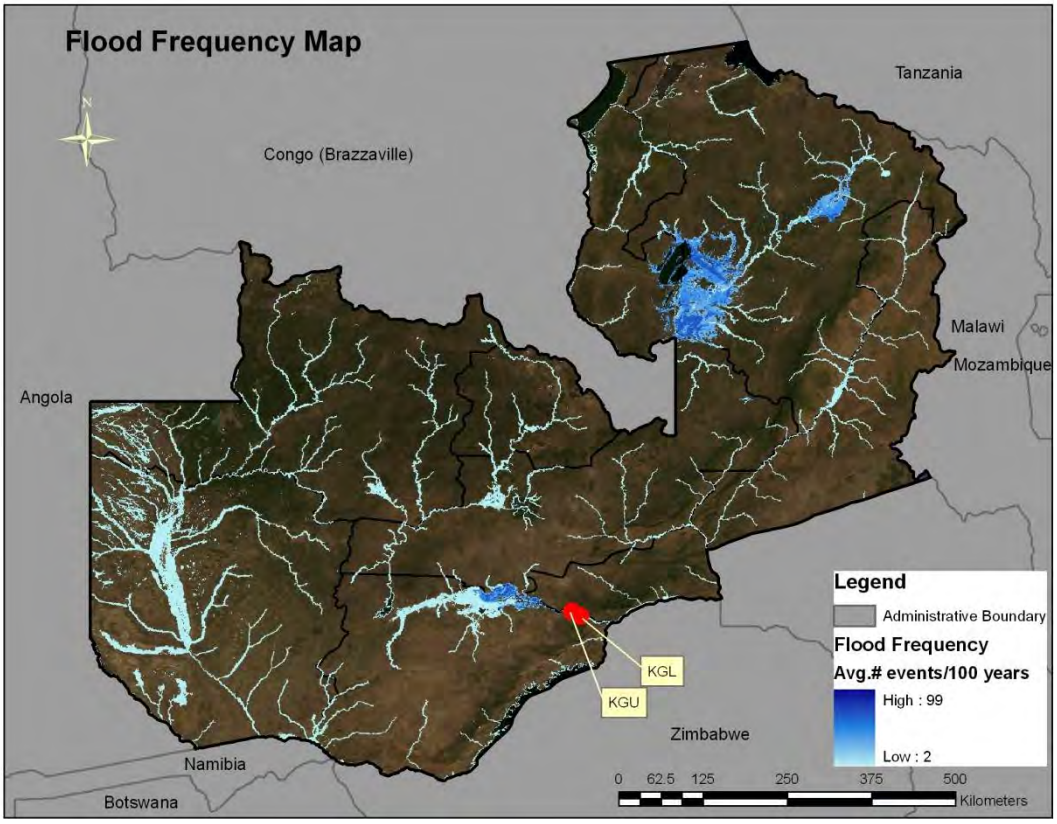

Source: Developed from UNEP/GRID-Europe, Global Assessment Report on Risk Reduction.

Figure A5-1 shows that there are floodplains throughout the country including the Kafue Flats regions which frequently are flooded. KGU and KGL experience more infrequent flooding, since ZESCO has some control over the water flow along the river.

Historical losses were evaluated using data collected by the United States Agency for International Development (USAID) Office of Foreign Disaster Assistance (OFDA) from 1982 to the 2007. To help understand the conditions which caused each flood event, precipitation data were analyzed for each flood time period. This data was used to identify a rainfall deviation from normal seasonal rainfall (October to March) that constitutes a flood event; this "flood threshold" was identified as 15% in Lusaka. That is, a 15% deviation from the normal rainfall for the rainy season results in a flood. Table A5-1 shows national losses associated with flood events based on data from the OFDA/CRED International Disaster Database. It also shows the

rainfall deviation from the observed seasonal average. This historical deviation is used as a threshold in the next sub-section. Floods have been a great cause of concern for Zambia, with historical flood events being ranked as two of the top five disasters recorded from 1982 to 2007 (OFDA/CRED 2007).

Table A5-1: Historical Flood Events for Zambia

Start[1]	End[1]	Humans Killed[1]	Tot. Pop. Affected[1]	Est. Damage (US$ Million)[1]	Rainfall Deviation (% Above Avg.)[2]
27/02/2009	27/03/2009	31	614,814	NA	NA
09/02/2008	01/05/2008	4	15,000	NA	NA
30/12/2007	27/02/2008	10	34,766	NA	NA
20/01/2007	10/03/2007	NA	118,755	NA	NA
10/01/2007	10/05/2007	4	1,400,000	NA	NA
00/11/2005	00/11/2005	NA	4,000	NA	NA
01/02/2004	02/06/2004	2	196398	NA	51
25/12/2003	25/12/2003	4	1,000	NA	NA
11/03/2003	15/03/2003	NA	10,000	NA	15
00/02/2001	00/02/2001	5	617,900	NA	26
03/03/2000	04/03/2000	NA	12,000	NA	55
06/02/1998	06/02/1998	NA	1,300,000	20.7	15
23/01/1989	23/01/1989	NA	800,000	NA	60
00/02/1978	00/02/1978	11	30,900	0.2	48

[1] Source of Data: OFDA/CRED International Disaster Database, Version vv11.08.
[2] Source of Data: Historical precipitation data from the Zambia Meteorological Dept.
NA=Not Available. Tot. Pop. = total population. Est. = estimated. Avg. = average.

The weather generator (WXGEN) was used to model future conditions as well as historical conditions to calibrate and validate that the WXGEN tool accurately represented the historical rainfall amounts and frequency. Table A5-2 shows a comparison between the historical rainfall and WXGEN simulation including: number of events, probability, and frequency. The 14.9% in the fifth column of Table A5-2 is taken from the last column in Table A5-1 (14.9% has been rounded to 15% in the column). The WXGEN modeled rainfall was analyzed and found to provide a comparable threshold of 15.0%, and is shown in the historical data row in Table A5-2.

Table A5-2: Historical Rainfall and Historical Weather Generator Simulation

Historical (1975-2005) and WXGEN Historical Simulation Rainfall Comparisons								
Source	**Station**	**Normal Seasonal Rainfall (mm)**	**Seasonal Rainfall (mm)**	**Percent Change from Normal**	**Number of Events in History**	**Total Years**	**Probability of Event in Each Year**	**Event Occurs Every "X" Years**
Historical Data	Lusaka	760	873	14.9	9	31	0.29	3.4
WXGEN	Lusaka	735	845	15.0	46	200	0.23	4.3

Notes: mm = millimeter

5.1.2 Flood Hazard Future Conditions

To help predict future flood conditions, the probability of exceeding the flood threshold seasonal rainfall of 873 mm (15% deviation from normal precipitation) was identified for three GCMs and two emissions scenarios. These probabilities are shown in Table A5-3 and for a 200-year simulation period (from WXGEN).

Table A5-3: Probabilities of Exceeding Seasonal Rainfall Flood Threshold

GCM	**Emissions Scenario A2**			**Emissions Scenario B1**		
	Early Century (2010-2039)	**Mid Century (2040-2069)**	**Late Century (2070-2099)**	**Early Century (2010-2039)**	**Mid Century (2040-2069)**	**Late Century (2070-2099)**
ECHAM5	25%	35%	39%	29%	16%	23%
IPSL	21%	36%	16%	43%	26%	29%
MRI	22%	28%	18%	19%	14%	27%

Using the ECHAM5 A2 late century results, the analysis shows the probability of flood conditions are high at 39% (once in 2.5 years). These results align with hydrologic modeling findings (Section 3.2) showing the average annual flows increasing by 11% compared to the respective baseline period. Using the mid century ECHAM5 B1 results, the probability of floods is 16% (once in 6. 2 years). With reduced flows during this time horizon, it is expected that droughts could occur more frequently than floods in this time horizon for this climate change scenario. Using the MRI B1 mid century results, the analysis shows there is a lower probability of flooding (14%), or about once in 7 years. This result aligns with the 15% decrease in average annual flows for this scenario and time horizon compared to the baseline.

Another analysis conducted to help depict the magnitude of flooding involves plotting the monthly average rainfall with the lows and highs for each month. Figures A5-2(a), A5-2(b), and A5-2(c) show the ECHAM5 A2 early, mid, and late century results compared to the baseline results. The bar graph shows that the average monthly rainfall values do not change very much; however, precipitation variability does change considerably for some months. The high rainfall values are higher during the wettest months (December and January, in particular), sometimes as much as 15 to 20 percent higher. This indicates that the rainfall will be more intense when it

occurs, which would favor flood conditions. The black lines in the bar charts show the range of rainfall in the respective month and scenario. The figure A5-2(c) shows that the highest value of rainfall in the projected climate during the months of December and January show a 20% increase as compared to the baseline.

Figure A5-2(a): ECHAM5 A2 Early Century Precipitation Results with Baseline

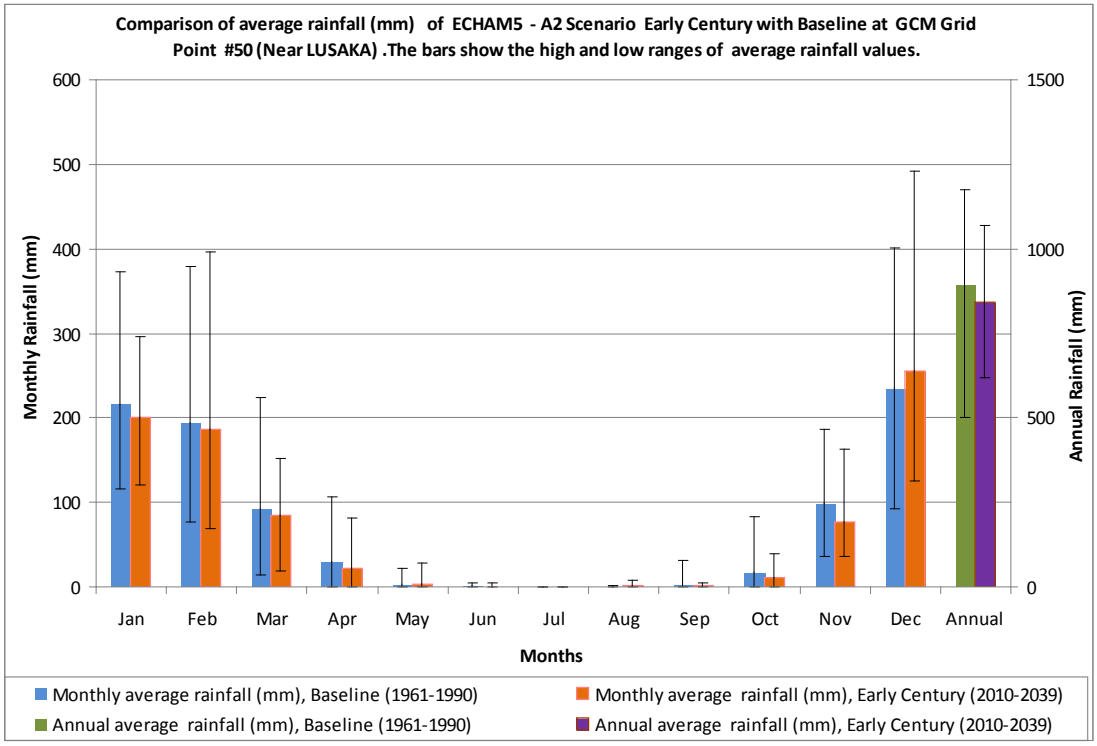

Figure A5-2(b): ECHAM5 A2 Mid Century Precipitation Results with Baseline

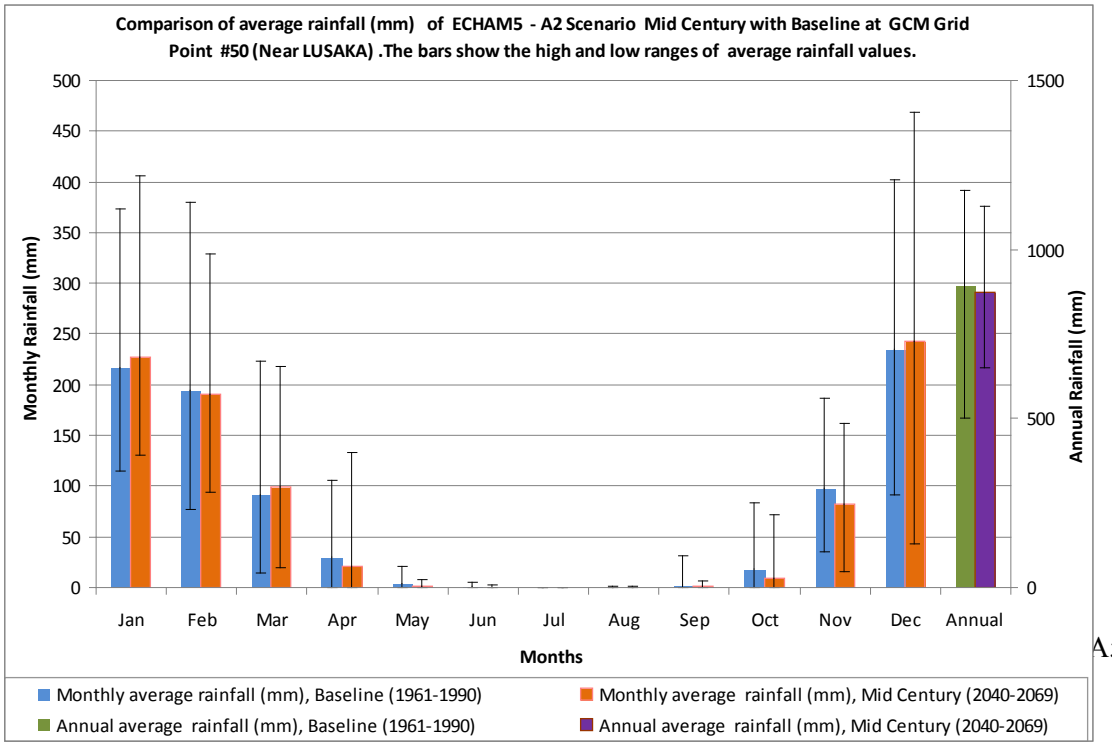

Figure A5-2(c): ECHAM5 A2 Late Century Precipitation Results with Baseline

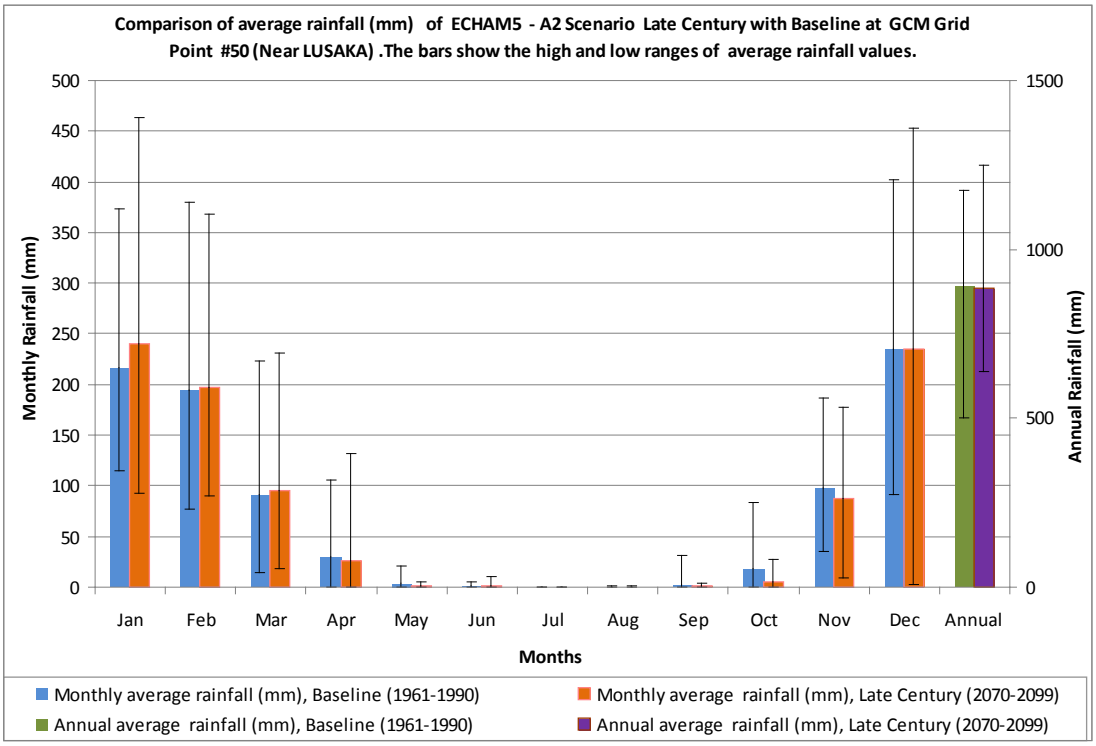

The results of this analysis show that flood conditions will continue into the future. Two GCM/emissions scenario combinations show an increase and four combinations show a decrease in the probability of achieving flood conditions for each of the three future time horizons. In addition, an important consideration for flood risk is the severity of the flood; the precipitation variability analysis (see Figures A5-2(a) through A5-2(c)) shows that when floods occur they may be more severe, even if they occur less often.

As shown in Figure A5-3, the Kafue River Basin flows modeled using the HEC-HMS software show extreme flow events in the early and mid century results. The figure shows average annual flows modeled using the IPSL GCM A2 scenario at the Itezhi-Tezhi (IT) Reservoir inflow. In this data set, there are modeled flows which are twice as large as any recorded historical flow, indicating the potential for high severity flows, driven by the precipitation patterns. These outputs support those shown in Figure A5-2(b) and indicate that there is a potential for larger magnitude flood events in the future.

Figure A5-3: IPSL A2 Inflow to IT Reservoir

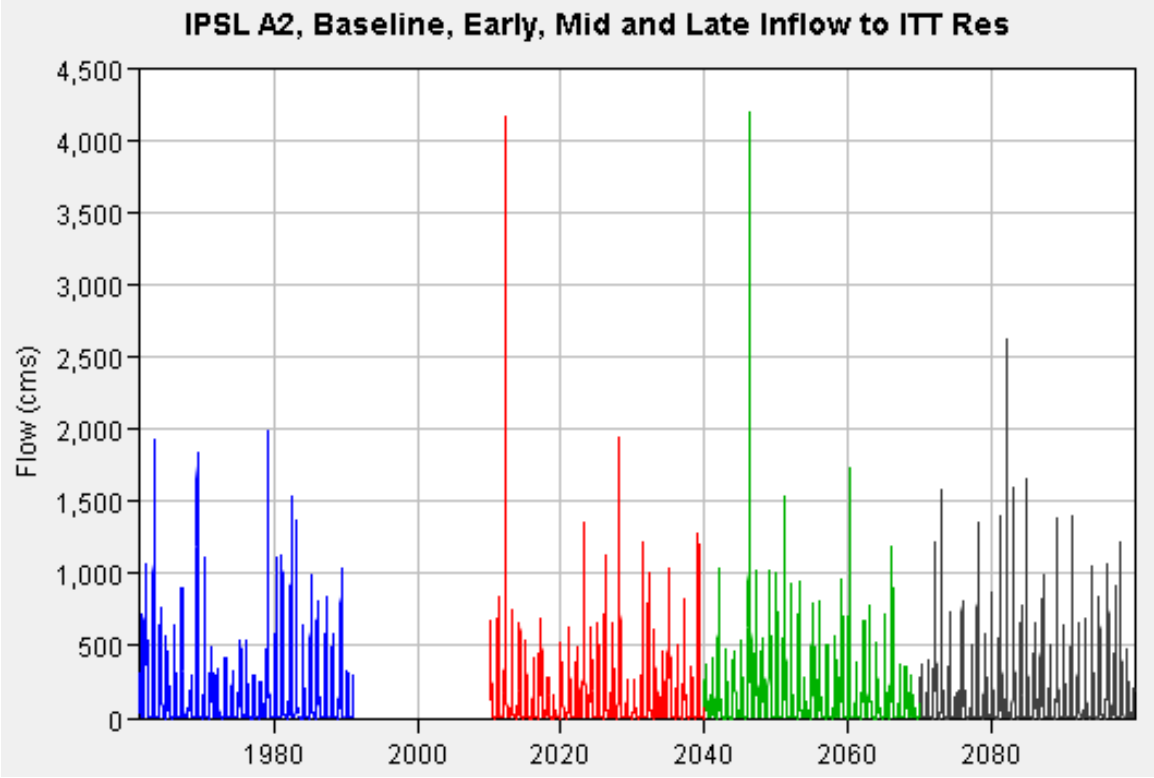

5.2 Flood Vulnerability Assessment

This section considers vulnerability to the flood hazard under both current and future conditions.

5.2.1 Flood Vulnerability Current Conditions

Vulnerability considers the people, assets, and areas exposed to a hazard. For the flood hazard, population exposure was reviewed for the entire country of Zambia to assess the impact to ZESCO customers. The flood population exposure map, Figure A5-4, was based on four sources: (1) a GIS model using a statistical estimation of peak-flow magnitude and a hydrological model using the HydroSHEDS dataset and the Manning equation to estimate river stage for the calculated discharge value; (2) observed floods from 1999 to 2007, obtained from the Dartmouth Flood Observatory (DFO); (3) the frequency from the UNEP/GRID-Europe PREVIEW flood dataset; and (4) a population grid for the year 2007, provided by LandScanTM Global Population Database (Oak Ridge, TN: Oak Ridge National Laboratory). The map unit is the average annual population exposed. This product was designed by UNEP/GRID-Europe for the Global Assessment Report on Risk Reduction (GAR).

Figure A5-4: Flood Population Exposure Map for Zambia

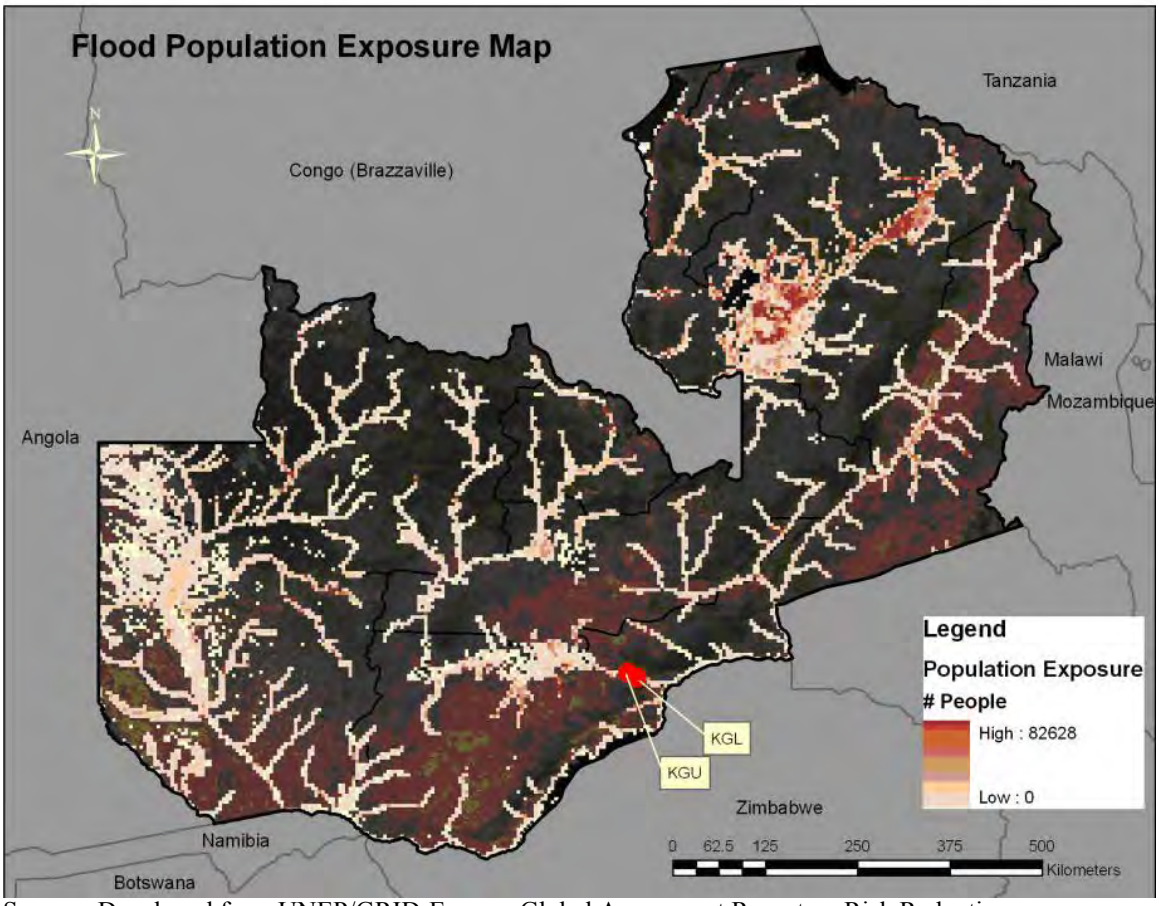

Source: Developed from UNEP/GRID-Europe, Global Assessment Report on Risk Reduction.

Figure A5-4 shows that there are a large number of people in the Kafue Flats and upstream towards the IT dam who would be impacted by a flood event. The floodplain and potentially impacted population shrink near the KGU and KGL.

Economic exposure to the flood hazard was reviewed for the entire country to assess the impact to ZESCO customers. Figure A5-5, the flood economic exposure map, was based on four sources: (1) a GIS model using a statistical estimation of peak-flow magnitude and a hydrological model using the HydroSHEDS dataset and the Manning equation to estimate river stage for the calculated discharge value; (2) observed floods from 1999 to 2007, obtained from the Dartmouth Flood Observatory (DFO); (3) the frequency from the UNEP/GRID-Europe PREVIEW flood dataset; and (4) A Global Domestic Product grid for the year 2007, available from the World Bank. The map unit is the expected average annual GDP (2007 as the year of reference) exposed in (USD, year 2000 equivalent).

Figure A5-5: Flood Economic Exposure Map for Zambia

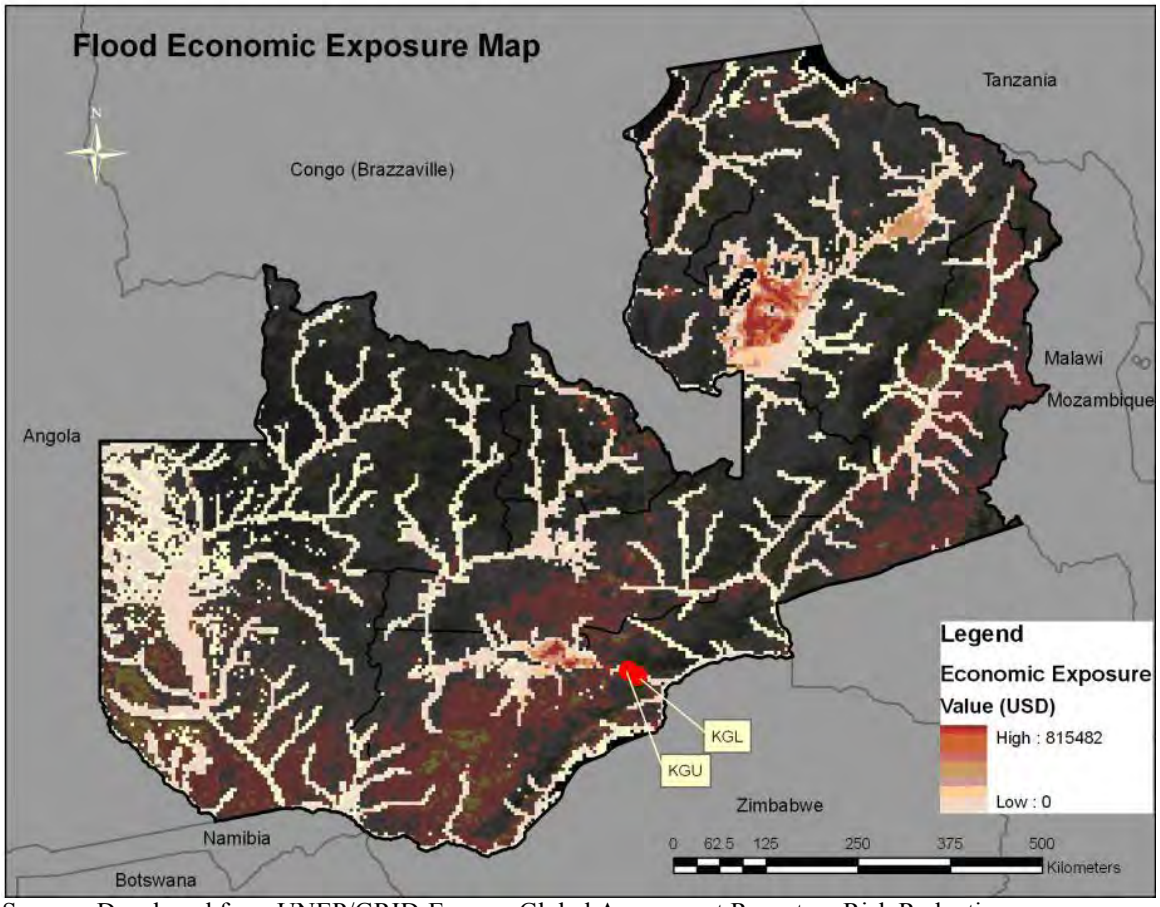

Source: Developed from UNEP/GRID-Europe, Global Assessment Report on Risk Reduction

Figure A5-5 shows that there are homes and infrastructure in the Kafue Flats and upstream towards the IT dam which would be impacted by a flood event. The floodplain and potentially impacted buildings shrink near the KGU and KGL.

In addition to considering strictly the number of persons exposed, vulnerability assessments should consider the sensitivity of the exposed population to a hazard. The population of Zambia is very susceptible to disasters due to a high degree of poverty (which means there are fewer resources to prepare for, respond to, and recover from a hazard event) and large numbers of children. Children and the elderly are always some of the most sensitive population groups to hazards needing special consideration for evacuation and protection from harsh climates or disease. From 2009 data, 51% of the population was considered extremely poor and 14% are considered moderately poor (United Nations Environment Programme / Global Resource Information Database). The percentage of the population aged 0 to 14 years is 46.2% while the percentage aged 60+ years is 9.6%.

In Zambia, many residential structures in floodplains are also particularly susceptible to flood damage. The people mostly affected are fishermen living along river banks and herdsmen who graze their cattle in the floodplain (APFM, 2007). Residential building materials may include

wood and mud among others. Homes, schools, and roads may be damaged during the rainy season. These may not be ZESCO facilities, but some are owned by customers who may need their electrical lines repaired after a flood event.

Figure A5-6 shows a photograph of citizens repairing a flood-damaged building in the Liyoyela Village along the Zambezi River in Zambia.

Figure A5-6: Repairing a Flood Damaged Structure in Zambia

Source: James Oatway/OXFAM.

ZESCO operations have been impacted by floods in the past. In 2005, hydropower activities were suspended because of flood-induced mudslides (see Appendix 7) which caused USD 1,665,131 in damage including power generation loss. Since ZESCO can control the flow of water by releasing the spillway gates, hydropower operations could continue even under flood conditions. However, it could become difficult to get power plant workers to the plants during a major flood. Causes of concern related to the flood hazard for KGL, could still be present and include: line and transformer structural impacts which would need to be repaired by KGL staff and damage to the transportation routes leading to KGL facilities.

5.2.2 Flood Vulnerability Future Conditions

Based on a review of population data, the population of Zambia has been increasing by about three percent per year. Table A5-4 shows population projections for the country. Given that many citizens reside along rivers and in river basins, the population within the floodplain areas will increase over time. This will increase the exposed population and structures, increasing vulnerability over time.

Table A5-4: 2000, 2025, and 2,050 Populations

Province		All Ages	0 to 4 Years Old	5 to 9 Years Old	10 to 14 Years Old	15 Years and Older
CENTRAL	2000	840883	151892	133523	119225	436243
CENTRAL	2025	1521500	274835	241598	215726	789341
CENTRAL	2050	2753016	497289	437150	390336	1428241
COPPERBELT	2000	1869085	337621	296791	265008	969665
COPPERBELT	2025	3381938	610894	537016	479508	1754520
COPPERBELT	2050	6119308	1105356	971682	867626	3174644
EASTERN	2000	1135608	205130	180323	161012	589143
EASTERN	2025	2054778	371163	326277	291337	1066001
EASTERN	2050	3717933	671586	590369	527147	1928831
LUAPULA	2000	565501	102149	89796	80180	293377
LUAPULA	2025	1023222	184829	162477	145077	530838
LUAPULA	2050	1851426	334431	293987	262504	960504
LUSAKA	2000	1424734	257356	226233	202006	739140
LUSAKA	2025	2577926	465662	409347	365511	1337405
LUSAKA	2050	4664521	842572	740677	661359	2419913
NORTH WESTERN	2000	425480	76856	67562	60327	220735
NORTH WESTERN	2025	769867	139064	122247	109156	399400
NORTH WESTERN	2050	1393004	251624	221194	197507	722678
NORTHERN	2000	1218730	220144	193522	172798	632267
NORTHERN	2025	2205181	398331	350159	312662	1144029
NORTHERN	2050	3990073	720744	633582	565733	2070015
SOUTHERN	2000	1091590	197178	173333	154771	566307
SOUTHERN	2025	1975132	356776	313630	280044	1024681
SOUTHERN	2050	3573821	645554	567485	506714	1854067
WESTERN	2000	712609	128722	113155	101037	369695
WESTERN	2025	1289401	232910	204743	182818	668930
WESTERN	2050	2333053	421429	370464	330792	1210368

(Source: Population distribution model from the United Nations Environment Programme / Global Resource Information Database).

Flood impacts in the southern parts of Zambia are causing impacts to a large amount of persons. Zambians in some areas of the study region are considering relocating to higher grounds, building their houses with cement, and planting their gardens further from river banks and valleys (Kabange, 2008). They also are turning to different farming techniques and different livelihoods. If efforts such as these are successful, the population would become less vulnerable to future flood events.

5.3 Flood Risk Assessment

Qualitative Assessment

The hazard assessment shows that floods are occurring frequently at approximately 0.42 times each year (OFDA/CRED, 2007). According to several of the GCMs/emissions scenarios, flood frequency will remain high in the country. Based on reviews of historic events and corresponding water depths, flood magnitudes should also be rated as high. This study shows that even if average annual precipitation may decrease, spatial and temporal variability may result in more extreme precipitation events, with high precipitation events becoming higher. The vulnerability assessment shows that there is an overall moderate degree of exposure to floods in Zambia, since the floodplains only cover areas around water bodies. Vulnerability was ranked as moderate because many people live in the floodplains and their livelihoods are often tied to the water and land. ZESCO's exposure is considered low because it controls water flow upstream and through its facilities. It is anticipated that ZESCO control over flows will be sustained in the future. Therefore, its facilities are not likely to be inundated except by the most extreme events. The country has a high sensitivity to floods which may be seen from the construction practices and social and economic losses from historical events. In particular those with subsistence livelihoods, or living in chronic poverty conditions, are a concern for hazard impacts because they are generally more vulnerable to hazard events and other economic shocks (World Bank, 2005), and have less resources to support recovery (World Bank, 2005). Since ZESCO can control the flow of water by releasing the spillway gates, hydropower operations could continue even under flood conditions. However, it still may be difficult to get power plant workers to the plant during a major flood. Causes of concern related to the flood hazard for KGL, could still be present and include: line and transformer structural impacts which would need to be repaired by KGL staff and damage to the transportation routes leading to KGL facilities.

The country has a low adaptive capacity to the flood hazard because there are few financial and social networks in place to support displaced people and rebuild homes. ZESCO has a moderate adaptive capacity through its ability to manage flow and cope with flooding events.

The risk assessment shows that the country is at high risk to floods and climate change may exacerbate the severity of flood events. ZESCO has a low flood risk due to its low vulnerability. This risk may increase in the future due to climate change.

Quantitative Assessment

In order to better compare the risk for all the climate exacerbated hazards which may impact ZESCO, the historic losses were annualized and, in the case that there are no historic losses, potential losses were modeled with an associated return period in order to calculate annualized loss.

KGU has been in operation since 1977 and there has only been one time when it has been damaged by flood waters and that occurred in 2005, an event recorded in Table A5-1 which shows there was a flood that year. Of the nine floods in 31 years, only one has resulted in a landslide causing damage. The annual loss for flood is USD 49,954. More historic losses would provide a more accurate value, but since the facility has only been in operation since 1977 there

is not a lot of data available. Table A5-3 was used to help calculate the modeled future annual loss. The modeled future annual loss is shown in Table A5-5 below.

Table A5-5: Flood Loss (Annualized USD)

GCM	Emissions Scenario A2			Emissions Scenario B1		
	Early Century (2010-2039)	Mid Century (2040-2069)	Late Century (2070-2099)	Early Century (2010-2039)	Mid Century (2040-2069)	Late Century (2070-2099)
ECHAM5	46254	64755	72156	53654	29602	42553
IPSL	38853	66605	29602	79556	48104	53654
MRI	40703	51804	33303	35153	25902	49954

5.4 Flood Hazard References

APFM. 2007 (AFPM, 2007). Strategy for Flood Management for Kafue River Basin, Zambia. Associated Programme for Flood Management (APFM). August.

Freeman, P.K., 2003. Natural hazard risk and privatization. Building Safer Cities: The Future of Disaster Risk, A. Kreimer, M. Arnold and A. Carlin, Eds., World Bank Disaster Management Facility, Washington, District of Columbia, 33-44.

HydroSHEDS 2007; (Hydrological data and maps based on SHuttle Elevation Derivatives at multiple Scales), World Wildlife Fund (WWF) Conservation Science Program.

Kabange. 2008 (Kabange, 2008). Technical Center for Agricultural and Rural Cooperation ACP-EU (CTA). Floods and droughts force Zambian farmers to change their livelihoods, October 26, 2008.

Landscan 2007, Oak Ridge National Laboratory, Computation Sciences and Engineering Division, population data (1 km resolution).

Mirza, M.M.Q., 2003. Climate change and extreme weather events: can developing countries adapt? Clim. Policy, 3, 233-248.

Oatway, James, OXFAM, Photo: Repairing flood damage in Liyoyela Village. April 29, 2009.
Obasi, G.O.P., 2005. The impacts of ENSO in Africa. Climate Change and Africa, P.S Low, Ed., Cambridge University Press, Cambridge, 218-230.

OFDA/CRED. 2007 (OFDA/CRED, 2007). EM-DAT: The OFDA/CRED International Disaster Database, Université Catholique de Louvain, Brussels, Belgium.

Prevention Web, 2010; UN International Strategy for Disaster Reduction, Information Management Unit, Geneva, Switzerland, http://www.preventionweb.net.

Appendix A6

Drought Risk

One-third of the people in Africa live in drought-prone areas and are vulnerable to the impacts of droughts (World Water Forum, 2000). During the mid-1980s the economic losses from droughts totaled several hundred million U.S. dollars (Tarhule and Lamb, 2003). Based on data for the years 1982 to 2007, Zambia faces drought events at a frequency of 0.19 events per year (PreventionWeb, 2010); this is equal to once in five years. Climate variability, including extreme events such as storms, floods and sustained droughts, already has marked impacts on settlements and infrastructure (Freeman and Warner, 2001; Mirza, 2003; Niasse et al., 2004; Reason and Keibel, 2004). Climate change may cause increased or prolonged periods of drought, which could impact water supply for power generation, other areas of economy (agriculture, power demand, etc.), as well as ZESCO customers.

6.1 Hazard Assessment

This section presents the current and future hazard assessment of the drought hazard.

6.1.1 Drought Hazard Current Conditions

Drought events were reviewed for the entire country to assess the impact to ZESCO customers and stakeholders. Figure A6-1 is based on two sources: (1) a global monthly gridded precipitation dataset obtained from the Climatic Research Unit (University of East Anglia); and (2) a geographic information system (GIS) model of global SPI data based on a Brad Lyon methodology (IRI, Columbia University).

Figure A6-1: Drought Events

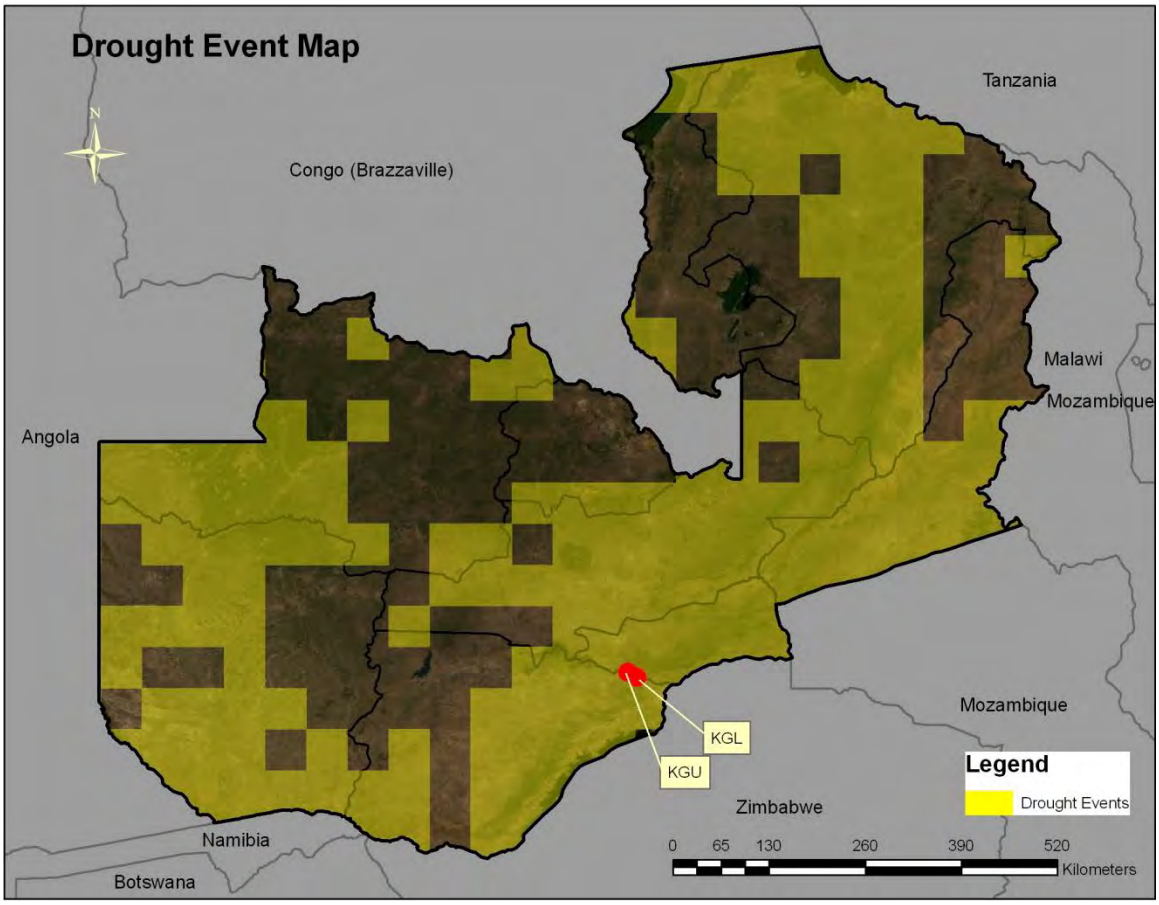

Source: Developed from UNEP/GRID-Europe, Global Assessment Report on Risk Reduction

Historical losses were identified in data collected by the United Nations from 1982 to 2007. To help understand the conditions which caused the drought events, precipitation data were analyzed for each drought time period. After analyzing the data, a rainfall deviation from normal seasonal rainfall was established that tied to the documented drought events. A drought threshold was set at -12% (that is, a negative 12 percent change from normal rainfall during a year indicates a drought event). Table A6-1 shows the five time periods which met this threshold.

Table A6-1: Historical Drought Events for Zambia

Start[1]	End[1]	Humans Killed[1]	Tot. Pop. Affected[1]	Est. Damage (US$ Million)[1]	Rainfall Deviation (% Below Avg.)[2]
06/2005	11/2005	NA	1,200,000	NA	-35
08/1995	1995	NA	1,273,204	NA	-58
1991	1992	NA	1,700,000	NA	-21
01/1983	1983	NA	1,200,000	NA	-12
01/1982	1982	NA	1,273,204	NA	-4

[1] Source of Data: OFDA/CRED International Disaster Database, Version vv11.08.
[2] Source of Data: Historical precipitation data from the Zambia Meteorological Dept.
NA=Not Available. Tot. Pop. = total population. Est. = estimated. Avg. = average.

The weather generator (WXGEN) was used to model future conditions as well as historical conditions to show that it accurately represented the rainfall amounts and frequency. Table A6-2 shows a comparison between the modeled and historical rainfall, number of events, probability, and frequency. The -12.1% in the fifth column of Table A5-2 came from the last column in Table A6-1. The WXGEN modeled rainfall was analyzed and found to be -12.7% and is shown in the historical data row in Table A6-2. The daily level station rainfall (historical) was used in the WXGEN to simulate long term series for 200 years, which was validated before simulation.

Table A6-2: Historical Rainfall and Historical Weather Generator Simulation

Historical (1975-2005) and WXGEN Historical Rainfall Simulation Comparisons								
Source	**Station**	**Normal Seasonal Rainfall (mm)**	**Seasonal Rainfall (mm)**	**Percent Change from Normal**	**Number of Events in History**	**Total Years**	**Probability of Event in Each Year**	**Event Occurs Every "X" Years**
Historical Data	Lusaka	760	668	-12.1	11	31	0.35	2.8
WXGEN	Lusaka	735	642	-12.7	59	200	0.30	3.4

Notes: mm = millimeter

6.1.2 Drought Hazard Future Conditions

To estimate future drought conditions associated with potential climate change impacts, the probability of exceeding the drought threshold for seasonal rainfall (668 millimeter [mm]), or a -12% deviation from normal average yearly precipitation was evaluated. The evaluation considered data generated by the climate change projections for precipitation of the three GCMs and two emissions scenarios (discussed in Sections 2.0 and 3.0 of the report). These probabilities are shown in Table A6-3 for a 200-year period simulated using WXGEN for each time horizon, GCM, and emissions scenario combination.

Table A6-3: Probabilities of Seasonal Rainfall at or Below Drought Threshold

GCM	Emissions Scenario A2			Emissions Scenario B1		
	Early Century (2010-2039)	Mid Century (2040-2069)	Late Century (2070-2099)	Early Century (2010-2039)	Mid Century (2040-2069)	Late Century (2070-2099)
ECHAM5	13%	9%	10%	14%	19%	17%
IPSL	15%	14%	22%	5%	9%	10%
MRI	19%	13%	22%	21%	26%	13%

For the ECHAM5 A2 late century results, the analysis shows the probability of drought conditions would be lower at 10% (once in 10 years), than for the threshold of 12%. These results align with average annual rainfall trends and precipitation variability analysis discussed in Section 3.2 for this GCM/emissions scenario in the late century period (compared to its respective baseline). For the mid century ECHAM5 B1 results, the probability of droughts is 19% (about once in 5 years). With reduced average annual precipitation projected during this time horizon for the same GCM/emissions scenario (compared to its respective baseline period) and the precipitation variability discussed in Appendix 5, it is expected that droughts will occur more frequently. For the MRI B1 mid century results, the analysis shows there is a higher probability of droughts, 26% or once in 3.8 years. This result aligns with the decrease in average annual precipitation and increase in precipitation variability for this GCM/emissions scenario/time horizon.

Another analysis was conducted to evaluate the potential severity of droughts. This analysis involved plotting the monthly average rainfall projected by a GCM/emissions scenario for a specified time horizon with the low and high modeled precipitation values for each month. Figure A5-2(c) in Appendix 5 shows the ECHAM5 A2 late century results for this analysis. The bar graph shows that the average monthly rainfall values do not change very much, but variability changes considerably for some months. The low rainfall values are lower in some cases, sometimes as much as 20 to 30 percent lower.

The last analysis completed involved calculating the Keetch-Byram Drought Index (KBDI) for the area. The KBDI is an indicator of soil moisture deficit and is based on a number of physical assumptions (Chu et al., 2002) and is a function of temperature and precipitation. The complete analysis is discussed in Appendix 8 and supports the conclusion that drought conditions will become more probable in the future.

6.2 Drought Vulnerability Assessment

This section considers vulnerability to the drought hazard under both current and future conditions.

6.2.1 Drought Vulnerability Current Conditions

Vulnerability considers the people and assets exposed to a hazard and their sensitivity to impact should the hazard occur. The population exposed to the drought hazard was reviewed for the entire country to assess the impact to ZESCO customers. Over the last 20 years, vulnerable groups such as subsistence farmers have been hit hard by droughts which are occurring more often and more intensely (CEEPA, 2006). Droughts have been a great cause of concern for the country of Zambia, with drought events being identified as three of the top five disasters recorded from 1982 to 2007 (OFDA/CRED, 2007). A literature review resulted in no findings of any direct losses to KGL due to drought, and the IT reservoir capacity is high which could potentially mitigate some of the effects of a drought.

Figure A6-2, the drought population exposure map, is based on three sources: (1) a global monthly gridded precipitation dataset obtained from the Climatic Research Unit (University of East Anglia); (2) a GIS modeling of global Standardized Precipitation Index based on the Brad Lyon methodology (IRI, Columbia University); and (3) a population grid for the year 2007, provided by LandScanTM Global Population Database (Oak Ridge, TN: Oak Ridge National Laboratory). The map units are expected average annual population exposed.

Figure A6-2: Drought Population Exposure Map

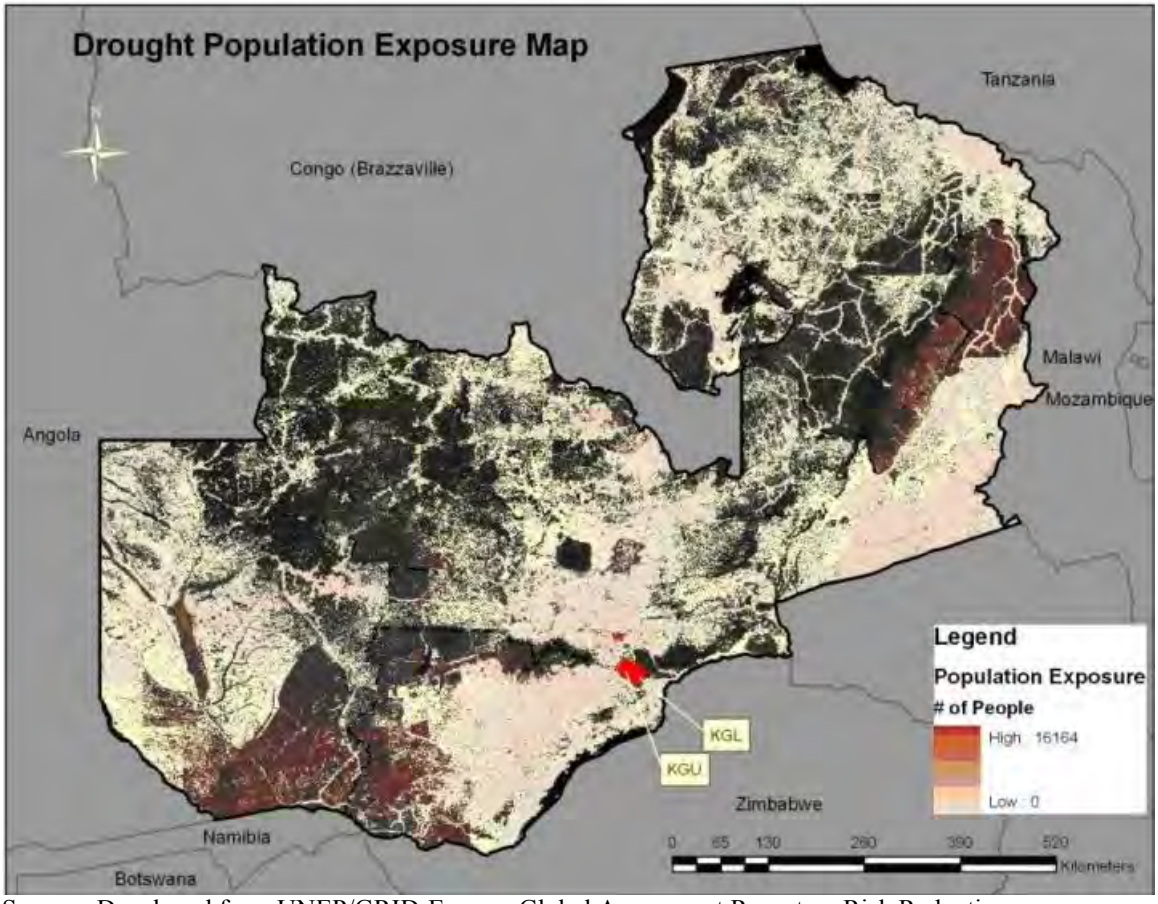

Source: Developed from UNEP/GRID-Europe, Global Assessment Report on Risk Reduction

Figure A6-2 shows that there are a large number of people throughout Zambia who could be impacted by a drought event. This area extends around the Kafue Flats, and near KGU and KGL.

Economic exposure to the drought hazard was reviewed for the entire country to assess the impact to ZESCO customers and stakeholder. Figure A6-3, the drought economic exposure map, is based on three sources: (1) a global monthly gridded precipitation dataset obtained from the Climatic Research Unit (University of East Anglia); (2) A GIS modeling of global Standardized Precipitation Index based on Brad Lyon (IRI, Columbia University) methodology; and (3) a Global Domestic Product grid for the year 2007, available from the World Bank. The map units are expected average annual GDP exposed.

Figure A6-3: Drought Economic Exposure Map

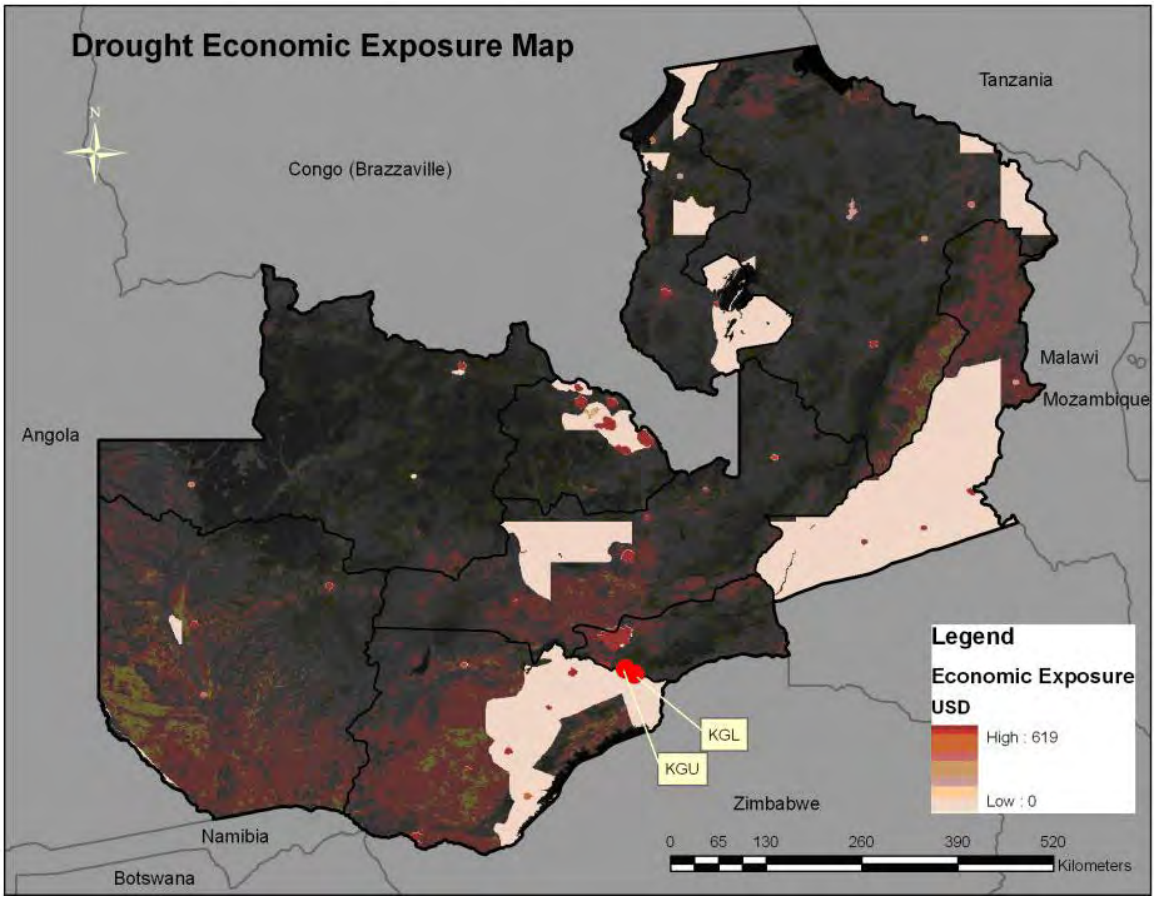

Source: Developed from UNEP/GRID-Europe, Global Assessment Report on Risk Reduction

6.2.2 Drought Vulnerability Future Conditions

The population of Zambia has been increasing by about three percent per year. The population table in Appendix 5 (Table A5-4) shows population projections for the future. The projections show that the population potentially impacted by drought in the country and study area will increase; this will increase the number of people exposed and vulnerable to the drought hazard with time.

The majority of the Zambia's poor reside in the rural areas and approximately 60 percent are dependent on agriculture for their livelihood. Agriculture also remains by far the main opportunity for income and employment for women who comprise 65 per cent of the rural population. There are approximately 800,000 small scale farmers who depend on agriculture for their livelihood (SCC, 2010). These farmers would be very vulnerable to a drought.

In some parts of the study area, small-holder farmers are now beginning to rearrange their livelihoods and are turning to different farming techniques like planting drought resistant food crops and water harvesting. Water harvesting is a technique used to collect extra water in excavations and furrows or behind small dams. The extra water is used in gardens and farms

when droughts occur. If more farmers move in this direction and increase their ability to adapt, their vulnerability will be reduced (Kabange, 2008).
The hydrologic and hydraulic modeling described in Chapter 3 along with other water demands described in Chapter 4 show the potential for decreased flow in number of the modeled scenarios. The IT Reservoir provides a great deal of capacity to collect water, but long term drought effects and multiple water demands could cause a strain on the water supply.

6.3 Drought Risk Assessment

Qualitative Assessment

The drought hazard assessment shows that the frequency of droughts should be considered moderate since they occur 0.19 times a year in the present (OFDA/CRED, 2007). The conditions exist for an increase in frequency of future drought events. According to several of the climate projection scenarios evaluated, the future frequency of droughts will increase to high in the country. After reviewing previous events and their durations, the drought magnitude is rated as high. For example, droughts constituted three of the top five disasters identified between 1982 and 2007. All of the GCMs and emissions scenarios considered for this study show that the temperature in Zambia, as well as within the Kafue River Basin, will increase significantly through 2100. This may exacerbate drought conditions (e.g., by increasing water needs for crop maintenance). A number of the GCM/emissions scenarios generally predict slight average annual precipitation decreases, but with increased temporal and spatial variability. This indicates there may be more intense periods of rainfall and some periods where there is little or no precipitation as a result of climate change impacts in the future.

The vulnerability assessment shows that there is high exposure to drought since the hazard has impacted most of the country at some point in time. ZESCO's exposure is high because there have been multiple drought events since 1982 and these have impacted the Kafue River Basin, as shown in Figure A6-1. The future conditions are estimated to remain similar, with a potential increase in drought frequency or severity, based on reviewing climate change projections of temperature and precipitation changes spatially and temporally across the 21st century.

The country has a high sensitivity to droughts, as evidenced by the social and economic losses and impacts from historical events. ZESCO has a lower sensitivity to drought since its operations include the IT Dam and Reservoir, which provide significant capacity to capture water when there is precipitation and store it through periods of drought. However, while power operations may not be impacted, it appears this is at the expense of conservation releases that are necessary to protect the Kafue Flats. However, ZESCO may be much more susceptible in the future due to more extreme drought events, ongoing development, and climate change impacts that are likely to increase the demands of competing water uses.

The country has a low adaptive capacity since there are few financial and social networks in place to support displaced people, impacted environmental areas, and failing agriculture. ZESCO has a moderate adaptive capacity to cope with drought events using operational procedures.

The risk assessment shows that the country is at high risk to drought and that climate change, combined with development pressures, population growth, and conservation needs may increase the risk of this hazard in the future. ZESCO has a low drought risk due to its low vulnerability. This risk may increase in the future due to climate change exacerbating the drought hazard and the additional pressure of non-climate stressors like competing water uses and needs.

Quantitative Assessment

In order to better compare the risk for all the climate exacerbated hazards which may impact ZESCO, the historic losses have been annualized and, in the case that there are no historic losses, potential losses were modeled with an associated return period in order to calculate annualized loss.

Daily power generation data was collected from ZESCO for the time period of October 2003 to August 2009. Table A6-1 shows that only one major drought, in 2005, occurred during that time period. The daily power generation data shows that during the period of the drought until several months after the drought, the daily power generation dipped to 81% of average. So, although ZESCO continued to produce power during this time period, the amount of power and corresponding revenue was reduced by 19%. If the average revenue/day is USD 769,503 then the reduced revenue would be USD 623,297. Over the six month drought period in 2005, this would amount to a USD 26,317,003 loss.

Looking at the events which impacted this system for ZESCO, two major droughts caused a reduction in power over twenty five years. There is only detailed loss information for the 2005 drought and not the 1995 drought. The average annual loss for drought is calculated to be USD 2,105,360. Table A6-3 was used to help calculate the modeled future annual loss. The modeled future annual loss is shown in Table A6-4 below.

Table A6-5: Flood Loss (Annualized USD)

GCM	Emissions Scenario A2			Emissions Scenario B1		
	Early Century (2010-2039)	Mid Century (2040-2069)	Late Century (2070-2099)	Early Century (2010-2039)	Mid Century (2040-2069)	Late Century (2070-2099)
ECHAM5	3,421,210	2,368,530	2,631,700	3,684,380	5,000,231	4,473,891
IPSL	3,947,550	3,684,380	5,789,741	1,315,850	2,368,530	2,631,700
MRI	5,000,231	3,421,210	5,789,741	5,526,571	6,842,421	3,421,210

6.4 Drought Hazard References

CEEPA 2006, *The Economic Impacts of Climate Change on Agriculture in Zambia*, Climate Change and African Agriculture Policy Note No. 27, August 2006, Centre for Environmental Economics and Policy in Africa (CEEPA).

Freeman, P. and K. Warner, 2001: Vulnerability of infrastructure to climate variability: how does this affect infrastructure lending policies? Report commissioned by the Disaster Management Facility of the World Bank and the ProVention Consortium, Washington, District of Columbia, 42 pp.

Kabange. 2008 (Kabange, 2008). Technical Center for Agricultural and Rural Cooperation ACP-EU (CTA). Floods and droughts force Zambian farmers to change their livelihoods, October 26, 2008.

Landscan 2007, Oak Ridge National Laboratory, Computation Sciences and Engineering Division, population data (1 km resolution).

Mirza, M.M.Q., 2003. Climate change and extreme weather events: can developing countries adapt? Clim. Policy, 3, 233-248.

Niasse, M., A. Afouda and A. Amani, Eds., 2004: Reducing West Africa's Vulnerability to Climate Impacts on Water Resources, Wetlands and Desertification: Elements for a Regional Strategy for Preparedness and Adaptation. International Union for Conservation of Nature and Resources (IUCN), Cambridge, 84 pp.

OFDA/CRED. 2007 (OFDA/CRED, 2007). EM-DAT: The OFDA/CRED International Disaster Database, Université Catholique de Louvain, Brussels, Belgium.

Prevention Web, 2010; UN International Strategy for Disaster Reduction, Information Management Unit, Geneva, Switzerland, http://www.preventionweb.net.

Reason, C.J.C. and A. Keibel, 2004: Tropical Cyclone Eline and its Unusual Penetration and Impacts over the Southern African Mainland. Weather Forecast., 19, 789-805.

Swedish Cooperative Centre (SCC), 2010, SCC Eastern and Southern Africa and Vi Agroforestry Programme, http://www.sccportal.org/countries/Zambia.aspx

Tarhule, A. and P.J. Lamb, 2003: Climate research and seasonal forecasting for West Africans: perceptions, dissemination, and use? B. Am. Meteorol. Soc., 84, 1741-1759.

World Water Forum, 2000: The Africa Water Vision for 2025: Equitable and Sustainable Use of Water for Socioeconomic Development. UN Water/Africa, 34 pp.

Appendix 7
Landslide Risk

Landslides are geological phenomena which include a range of ground movement, such as rock falls, deep failure of slopes, and shallow debris flows. Currently in Zambia, landslides can occur in areas with steep slopes (through natural terrain or development), particular soil types and ground cover, and erosion conditions. They are often caused by precipitation or earth moving events including earthquakes, volcanoes, or human-caused shaking. Climate change may cause large storm events, flooding, and expansion of rocky terrain due to temperature increases which would increase landslide frequency. This section considers the landslide hazard, including current and future conditions of the hazard (frequency, severity) and current and future vulnerability to the hazard (exposed population and structures). It also considers the potential exacerbating impacts of climate change.

7.1 Landslide Hazard Assessment

This section presents the current and future hazard assessment for the landslide hazard.

7.1.1 Landslide Hazard Current Conditions

Landslide frequency was reviewed for the entire country to assess the impact to ZESCO customers and stakeholders. Figure A7-1, the landslide frequency map, is an estimate of the annual frequency of landslides triggered by precipitation events. The map was developed using a landslide index based on six trigger and susceptibility parameters: (1) slope, (2) lithological (or geological) conditions, (3) soil moisture, (4) vegetation cover, and (5) precipitation conditions. Map units are expected annual probability and percentage of pixel of occurrence of a potentially destructive landslide event multiplied by 1,000,000.

Figure A7-1: Landslide Frequency

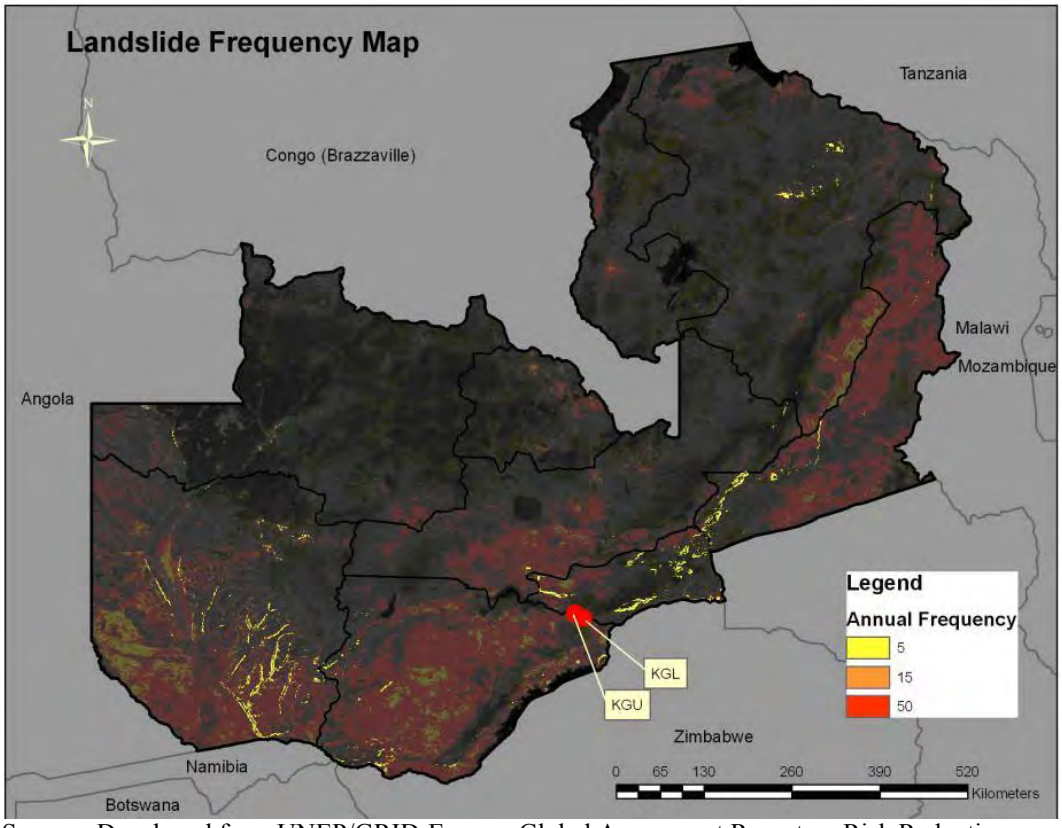

Source: Developed from UNEP/GRID-Europe, Global Assessment Report on Risk Reduction

The figure indicates that landslides are localized events in limited areas with "landslide appropriate" conditions. There are areas in the south and east shaded in red which show a higher annual frequency of landslide events where ZESCO facilities are located. Areas near KGU and KGL also have a higher frequency due to conditions including the elevation differences of gorges.

7.1.2 Landslide Hazard Future Conditions

To help predict future landslide conditions caused by floods, the probability of exceeding the flood threshold for seasonal rainfall of 873 mm (as identified and established in Appendix 5, Flood Hazard) was selected. A flood analysis building on Appendix 5 was then conducted and considered in light of climate change projections for flood impacts on the landslide hazard in the future.

Using the ECHAM5 A2 late century results, the analysis shows the probability of flood conditions are high at 39% (once in 2.5 years). These results align with hydrologic modeling findings (Section 3.2) showing the average annual flows increasing by 11% compared to the respective baseline period. Using the mid century ECHAM5 B1 results, the probability of floods is 16% (once in 6. 2 years). With reduced flows during this time horizon, it is expected that droughts could occur more frequently than floods in this time horizon for this climate change scenario. Using the MRI B1 mid century results, the analysis shows there is a lower probability of flooding (14%), or about once in 7 years. This result aligns with the 15% decrease in average

annual flows for this scenario and time horizon compared to the baseline. Because flood events and severe rainfall events are a parameter that drives landslide events, the results of the analysis show that landslides will continue to be a problem for the region and ZESCO, and likely may be in exacerbated by climate change impacts on precipitation, as well as through development along landslide-susceptible areas.

Another analysis conducted to help depict the magnitude of flooding involves plotting the monthly average rainfall with the lows and highs for each month. Figures A5-2(a), A5-2(b), and A5-2(c) show the ECHAM5 A2 early, mid, and late century results compared to the baseline results. The bar graph shows that the average monthly rainfall values do not change very much; however, precipitation variability does change considerably for some months. The high rainfall values are higher during the wettest months (December and January, in particular), sometimes as much as 15 to 20 percent higher. This indicates that the rainfall will be more intense when it occurs, which would favor flood conditions.

Some GCM/emissions scenario projections show an increase in flood frequency and some show a decrease, but the flood threat will remain and floods may become of greater magnitude in the future (based on greater rainfall variability and intense rainfall events).

7.2 Landslide Vulnerability Assessment

This section presents the current and future vulnerability assessment for the landslide hazard.

7.2.1 Landslide Vulnerability Current Conditions

Vulnerability considers exposure and sensitivity to a hazard. This assessment considers both population and structures exposed to the landslide hazard. The landslide population exposure was reviewed for the entire country to assess the impact to ZESCO customers and stakeholders. Figure A7-2, the landslide population exposure map, is based on seven factors: (1) slope, (2) lithological (or geological) conditions, (3) soil moisture condition, (4) vegetation cover, (5) precipitation conditions; and (6) a population grid for the year 2007, provided by LandScanTM Global Population Database (Oak Ridge, TN: Oak Ridge National Laboratory). Map units are the expected average annual population exposed.

Figure A7-2: Landslide Population Exposure Map

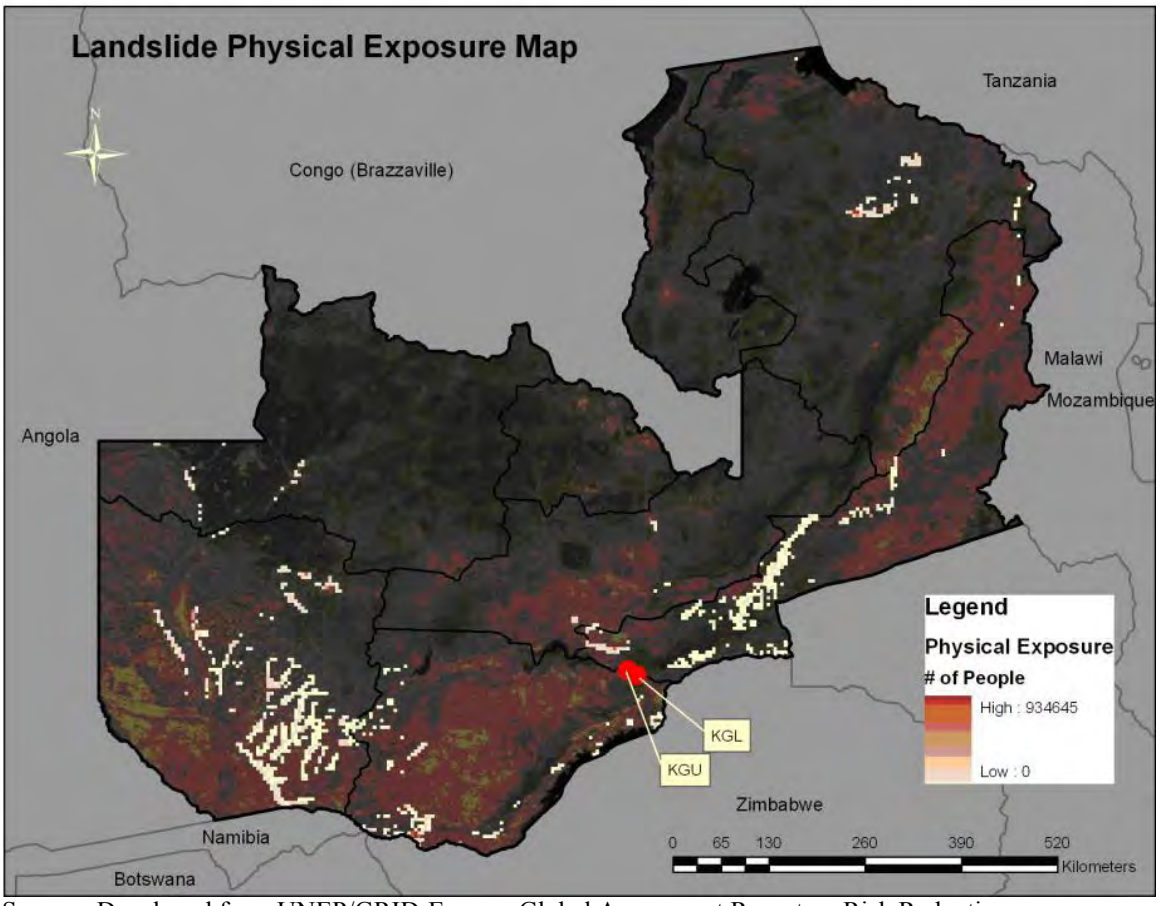

Source: Developed from UNEP/GRID-Europe, Global Assessment Report on Risk Reduction

The map indicates that in landslide prone areas, there is a high level of human exposure including in the study area.

Economic exposure to the landslide hazard was reviewed for the entire country to assess the impact to ZESCO customers and stakeholders. Figure A7-3, the landslide economic exposure map, is based on six factors: (1) slope, (2) lithological (or geological) conditions, (3) soil moisture condition, (4) vegetation cover, (5) precipitation conditions, and (6) a Global Domestic Product grid for the year 2007, provided by the World Bank. The map units are expected average annual GDP exposed.

Figure A7-3: Landslide Economic Exposure Map

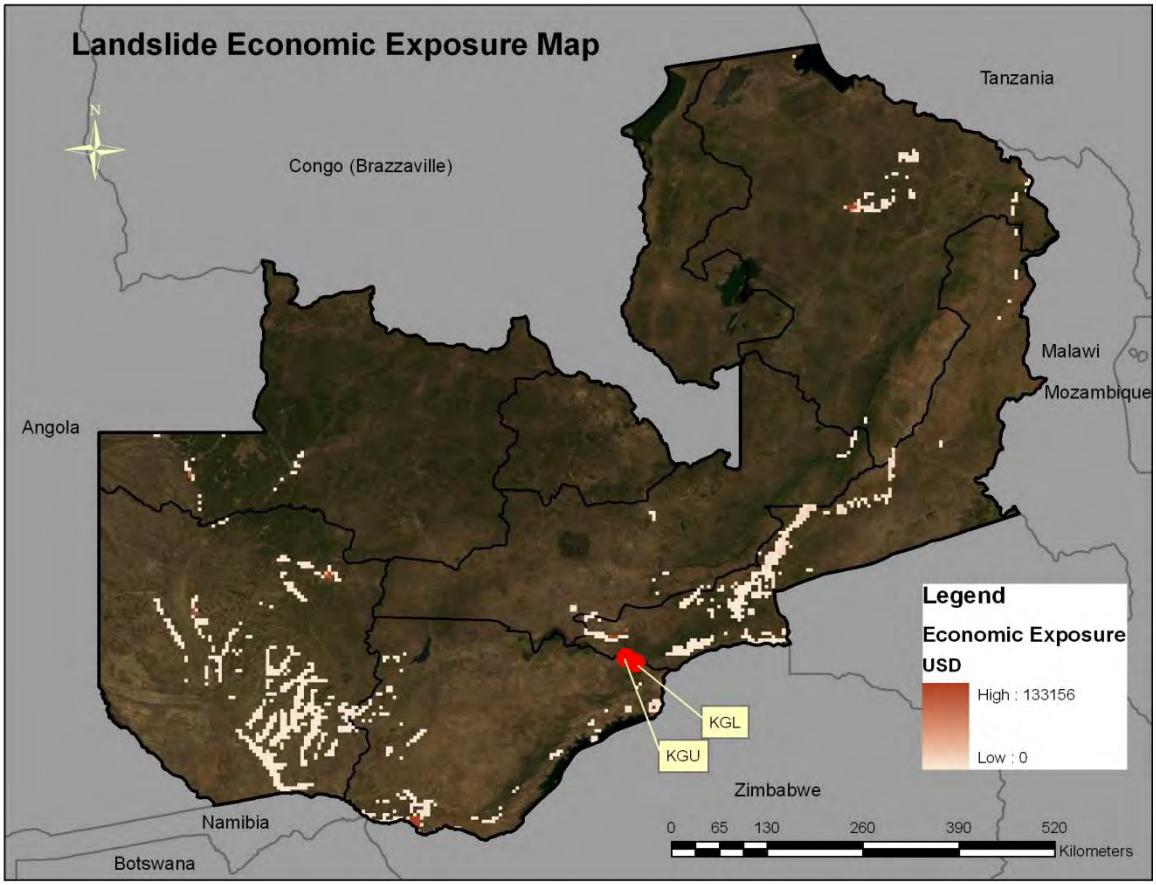

Source: Developed from UNEP/GRID-Europe, Global Assessment Report on Risk Reduction

Historical losses were identified in data collected by the United Nations from 1982 to 2007 (OFDA/CRED 2007). There have been no large scale landslides identified in Zambia over this time period. Large scale means one of four criteria must be fulfilled: (1) 10 or more people reported killed, (2) 100 people reported affected, (3) a call for international assistance, and (4) declaration of a state of emergency. However, landslide events have impacted ZESCO facilities directly. The conditions around KGU and KGL provide conditions that are vulnerable to the landslide hazard. That is, KGU and KGL (potentially) have steep slopes around the power generating and support facilities and are located in susceptible areas (APFM, 2007).

Information collected for this study indicates the following landslide event that impacted ZESCO. On December 24, 2005, the KGU power station was shutdown at approximately 9:00 p.m. due to massive landslides that were caused by heavy rains in the Namalundu area, where the power station is located. Water, mud, trees, stones, and other debris from the landslide gushed into the power station through the emergency access tunnel. Of the four, 150 megawatt (MW) generators in service at the time, two units were most affected by the deluge. The other two were restored to service at about 7:30 a.m. on December 25. ZESCO contracted energy imports of up to 300 MW from Eskom of South Africa and ZESA of Zimbabwe and also instituted load-shedding measures (ZESCO, 2005) to address the power shortfall caused by the outage. Table A7-1 provides a summary of the losses incurred during this event, as reported in the *Strategy for Flood Management for Kafue River Basin, Zambia* (APFM, 2007).

Table A7-1: ZESCO Losses Documented for Landslide in 2005

Category of Loss	Amount (USD)
Power generation loss	$1,000,000
Materials and labor for response	$75,821
Remedial civil works	$234,101
Mechanical and electrical materials	$354,209
Total	**$1,665,131**

Source: APFM, 2007.

7.2.1 Landslide Vulnerability Future Conditions

The population of Zambia has been increasing by about three percent per year. The population tables in Appendix 5 (Table A5-4) show population projections for the future. The population potentially impacted by landslides will increase with time. However, the vulnerability of the country's population to the landslide natural hazard is generally considered low, compared to the vulnerability of the population to other natural hazards (e.g., flood, drought, disease) due to limited exposure. The Kafue Flats are not susceptible to landslides due to topography. ZESCO facilities, however, are more vulnerable due to their locations in gorges.

7.3 Landslide Risk Assessment

Qualitative Assessment

The hazard assessment shows that landslides should be considered low since they occur very infrequently. The conditions exist for a rise in frequency and magnitude. After reviewing previous events and the amount of land moved, the landslide magnitude should be rated as moderate. KGU and potentially KGL have steep slopes around their facilities and are located in susceptible areas.

The vulnerability assessment shows that the country has a low exposure to landslides since they occur mostly in areas with large elevation changes, and certain soil types and land cover. ZESCO's exposure is high because its power generation facilities are located in gorges where there are large elevation changes where landslides have occurred in the past. The future conditions look similar since development will probably occur as it has in the past. The country has a high sensitivity to landslides which may be seen from the social and economic losses from historical events. The infrastructure and people in the impact area suffer severe losses although these areas are typically smaller when compared to drought, flood, or other hazard events. ZESCO also has a demonstrated high sensitivity to landslides since it operations have been interrupted by a landslide event in 2005. ZESCO may be more susceptible in the future due to non climate stressors like deforestation and land use changes around the facilities. The country has a low adaptive capacity since there are few financial resources and social networks in place to support displaced people and destroyed structures. ZESCO has a moderate adaptive capacity with the ability to cope with landslide events. This was seen during the last landslide when they were able to mobilize two hundred people to respond immediately.

The risk assessment shows that the country is at low risk to landslides due to a lack of exposure. The risk may increase in future conditions. ZESCO has a moderate risk due to its higher vulnerability. This risk may increase in the future due to climate change exacerbating the landslide hazard and the addition of several non-climate stressors like deforestation and land use changes.

Quantitative Assessment

In order to better compare the risk for all the climate exacerbated hazards which may impact ZESCO, the historic losses were annualized and, in the case that there are no historic losses, potential losses were modeled with an associated return period in order to calculate annualized loss.

KGU has been in operation since 1977 and there has only been one time when it has been damaged by a landslide and that occurred in 2005, an event recorded in Table A5-1 which shows there was a flood that year. Of the nine floods in 31 years, only one has resulted in a landslide causing damage. The annual loss for landslide is USD 49,954. More historic losses would provide a more accurate value, but since the facility has only been in operation since 1977 there is not a lot of data available. Table A5-3 was used to help calculate the modeled future annual loss. The modeled future annual loss is shown in Table A7-5 below.

Table A7-5: Landslide Loss (Annualized USD)

GCM	Emissions Scenario A2			Emissions Scenario B1		
	Early Century (2010-2039)	Mid Century (2040-2069)	Late Century (2070-2099)	Early Century (2010-2039)	Mid Century (2040-2069)	Late Century (2070-2099)
ECHAM5	46254	64755	72156	53654	29602	42553
IPSL	38853	66605	29602	79556	48104	53654
MRI	40703	51804	33303	35153	25902	49954

7.4 Landslide Hazard References

APFM 2007 - Strategy for Flood Management for Kafue River Basin, Zambia, August 2007, Associated Programme Flood Management (APFM)

Landscan 2007, Oak Ridge National Laboratory, Computation Sciences and Engineering Division, population data (1 km resolution).

OFDA/CRED. 2007 (OFDA/CRED, 2007). EM-DAT: The OFDA/CRED International Disaster Database, Université Catholique de Louvain, Brussels, Belgium.

Prevention Web, 2010; UN International Strategy for Disaster Reduction, Information Management Unit, Geneva, Switzerland, http://www.preventionweb.net.

Appendix 8
Wildfire Risk

Wildfire is a natural hazard event that constitutes the ignition of fuel sources such as grasses, trees, and shrubs. Climate change may decrease precipitation overall, or may impact its variability. Climate change in Zambia and the Kafue River Basin will increase temperatures, increasing evapo-transpiration (drying of land and plants) and providing greater conditions for ignition of fuel. These conditions increase the probability of wildfire in the future, in the face of climate change. Ongoing development also may increase the urban/wildfire fuel interface resulting in a higher risk of wildfire fuel ignition (caused by human activities) and a more immediate impact to economic assets and populations exposed (near the hazard). Wildfire also has the potential to impact power supply, infrastructure, population, and the environment.

8.1 Wildfire Hazard Assessment

This section presents the current and future hazard assessment for the wildfire hazard.

8.1.1 Wildfire Hazard Current Conditions

Data on the occurrence of fires shows that the frequency and magnitude of the fires have increased over the last five years (DMMU, 2008). Figure A8-1 provides wildfire frequency data for the period from 1997 to 2008. This figure is based on the modified algorithm 1 product of World Fire Atlas dataset (WFA, ESA-ESRIN). UNEP/GRID-Europe compiled the monthly data and processed the global fire density. The map unit is expected average number of events per year.

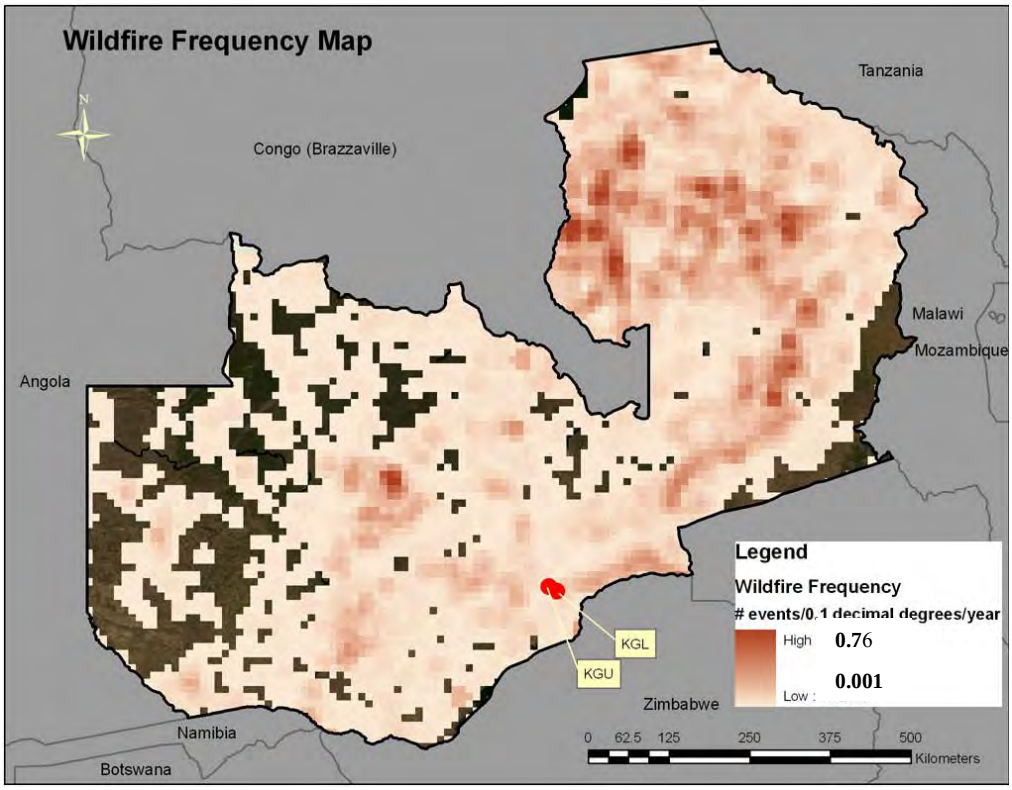

Figure A8-1: Wildfire Frequency Map
Source: Developed from UNEP/GRID-Europe, Global Assessment Report on Risk Reduction

Figure A8-1 shows that most of the country has at least some probability of encountering a wildfire. This potential wildfire area extends around the Kafue Flats, and near KGU and KGL too.

Wildfire Hazard Future Conditions

In order to assess future wildfire conditions, a methodology outlined in *"Trends in Global Wildfire Potential in a Changing Climate"* by Yongqiang Liu, John Stanturf, and Scott Goodrick in Forest Ecology and Management, 2010, pgs. 685-697, was applied (Lui, et al, 2010). This methodology measures fire potential using the Keetch-Byram Drought Index (KBDI), which is calculated using the observed maximum temperature and precipitation for a given time increment. This methodology was also used to consider the drought hazard presented in Appendix 6.

The KBDI is an indicator of soil moisture deficit and is based on a number of physical assumptions (Chu et al., 2002). The formula for calculating KBDI is:

$$Q = Q_0 + dQ - dP, \qquad \textbf{(1)}$$

$$dQ = \frac{10^{-3}(800 - Q)(0.968\, e^{0.0486T} - 8.3)\, d\tau}{1 + 10.88\, e^{-0.0441R}}, \qquad \textbf{(2)}$$

Where Q and Q_0 are the moisture deficiency (KBDI) of the current and previous time increment, respectively, dQ is the KBDI incremental rate, T is the maximum temperature for the time increment, dP is precipitation for the time increment, R is mean annual rainfall, and dτ is a time

increment. The precipitation and temperature variables were set for the ECHAM5 GCM baseline period (1961-1990) and the KBDI was calculated. The precipitation and temperature variables for the GCM time horizons were then used to calculate the future KBDI value. The time increment was set to one day. Table A8-1 and A8-2 show the temperature variables which were used for the analysis.

Table A8-1: ECHAM A2 Temperature Results

Statistical Parameter	Comparison Parameter	Time Horizon			
		Baseline (1961-1990)	Early Century (2010-2039)	Mid Century (2040-2069)	Late Century (2070-2099)
Annual Maximum Value of Daily Maximum Temperature (°C)	Maximum	47	48	49	52
	Average	39	41	43	45
	Minimum	36	38	38	41
	Standard Dev.	2	2	3	3
Annual Minimum Value of Daily Maximum Temperature (°C)	Maximum	21	22	24	26
	Average	19	21	22	24
	Minimum	12	14	19	21
	Standard Dev.	2	1	1	1
Annual Maximum Value of Daily Minimum Temperature (°C)	Maximum	27	31	35	39
	Average	24	26	27	31
	Minimum	21	23	24	27
	Standard Dev.	14	1	3	3
Annual Minimum Value of Daily Minimum Temperature (°C)	Maximum	4	6	7	9
	Average	3	4	5	7
	Minimum	1	3	2	4
	Standard Dev.	2	1	1	1
Mean Diurnal Temperature Range (°C) (difference between daily maximum temperature and minimum temperature)	Maximum	14	15	14	14
	Average	14	14	14	14
	Minimum	13	13	13	13
	Standard Dev.	0	0	0	0

Table A8-2: ECHAM B1 Temperature Results

Statistical Parameter	Comparison Parameter	Time Horizon			
		Baseline (1961-1990)	Early Century (2010-2039)	Mid Century (2040-2069)	Late Century (2070-2099)
Annual Maximum Value of Daily Maximum Temperature (°C)	Maximum	47	48	49	50
	Average	39	41	42	43
	Minimum	36	37	39	40
	Standard Dev.	2	3	3	2
Annual Minimum Value of Daily Maximum Temperature (°C)	Maximum	21	23	24	24
	Average	19	20	22	22
	Minimum	12	13	17	18
	Standard Dev.	2	2	1	1
Annual Maximum Value of Daily Minimum Temperature (°C)	Maximum	27	31	35	36
	Average	24	25	27	29
	Minimum	21	23	24	26
	Standard Dev.	1	2	3	3
Annual Minimum Value of Daily Minimum Temperature (°C)	Maximum	4	6	7	8
	Average	3	4	5	6
	Minimum	1	2	3	4
	Standard Dev.	1	1	1	1
Mean Diurnal Temperature Range (°C) (difference between daily maximum temperature and minimum temperature)	Maximum	14	15	14	14
	Average	14	14	14	14
	Minimum	13	13	13	13
	Standard Dev.	0	0	0	0

Using the temperature data above and previously projected precipitation data, the KBDI was calculated for the baseline and future time horizons. The future time horizon values were then compared to the baseline period and the change was expressed as a percentage. The results are shown in Table A8-3.

Table A8-3: Percent Change in KBDI for ECHAM5 A2 and B1 Scenario

	Early Century	Mid Century	Late Century
ECHAM5 A2	+25%	+50%	+80%
ECHAM5 B1	+25%	+37%	+50%

The table above shows a significant increase in the KBDI across the early, mid, and late century time horizons. This indicates that the climatic conditions for wildfire will increase in the future compared to the baseline conditions. This analysis does not include analyzing potential fuel sources or triggering events. These findings are also relevant for drought conditions, as discussed in Appendix 6

In addition to considering the combined impacts of temperature and precipitation changes on KBDI, temperature variability results are shown in Figures A8-2, A8-3, and A8-4. These figures display early century, mid century, and late century results for the ECHAM5 A2 scenario next to the baseline time horizon. The figures show that in some cases in the mid and late century, the

baseline highs become the new average temperature and the highs become more extreme (e.g., see December for each of the time horizons).

Figure A8-2: ECHAM5 A2 Early Century with Baseline Results

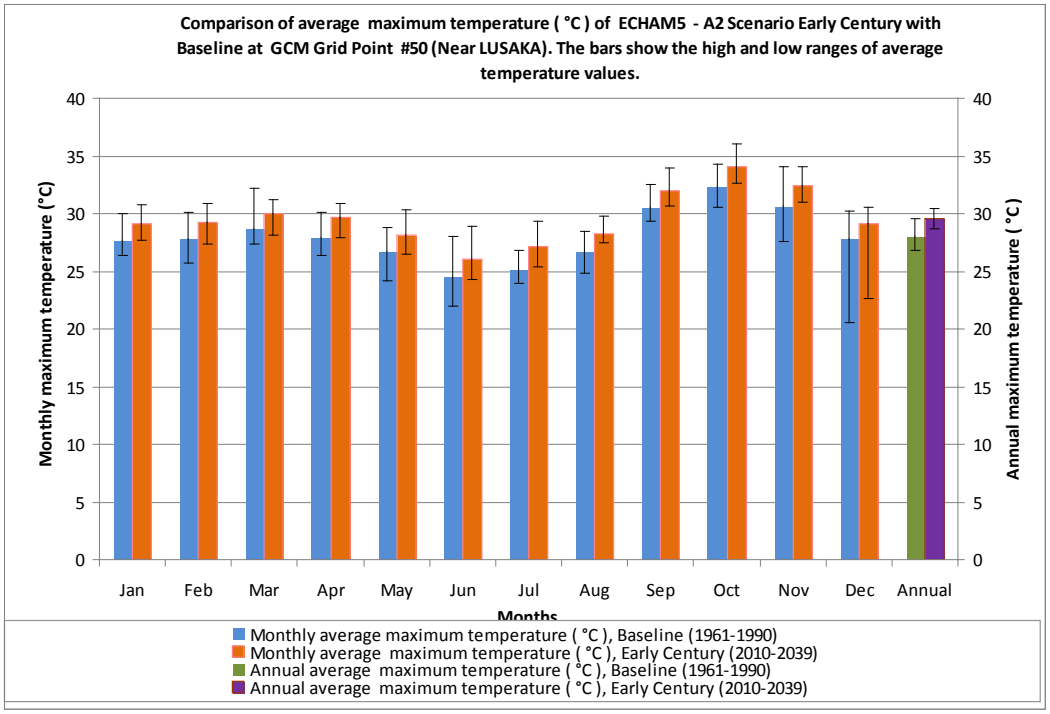

Figure A8-3: ECHAM5 A2 Mid Century with Baseline Results

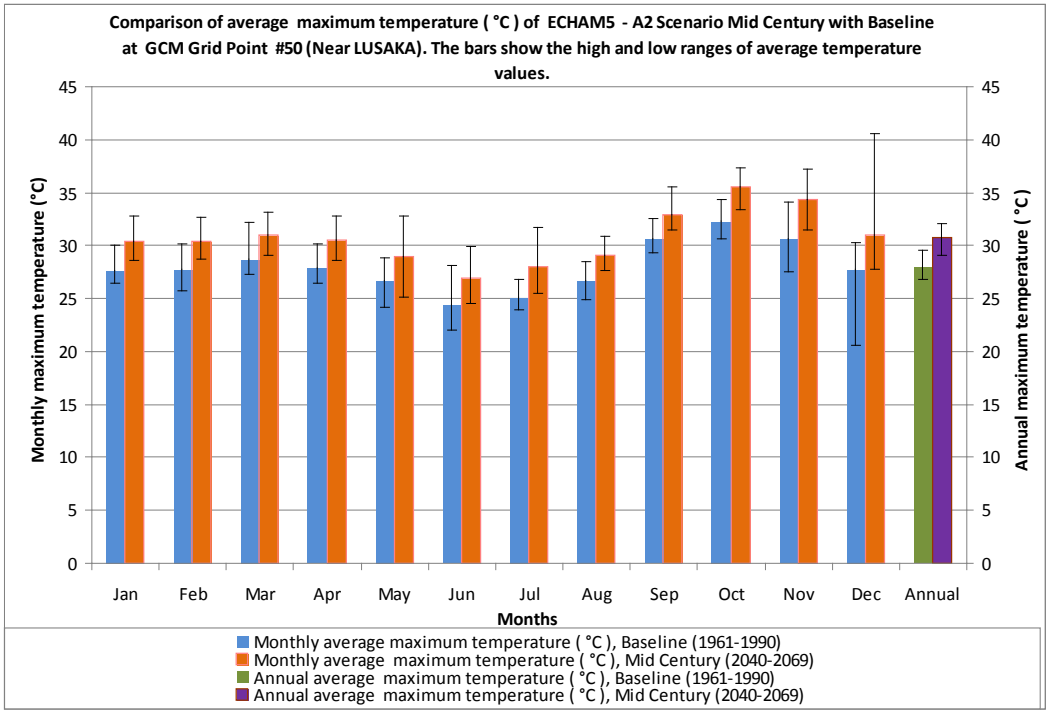

Figure A8-4: ECHAM5 A2 Late Century with Baseline Results

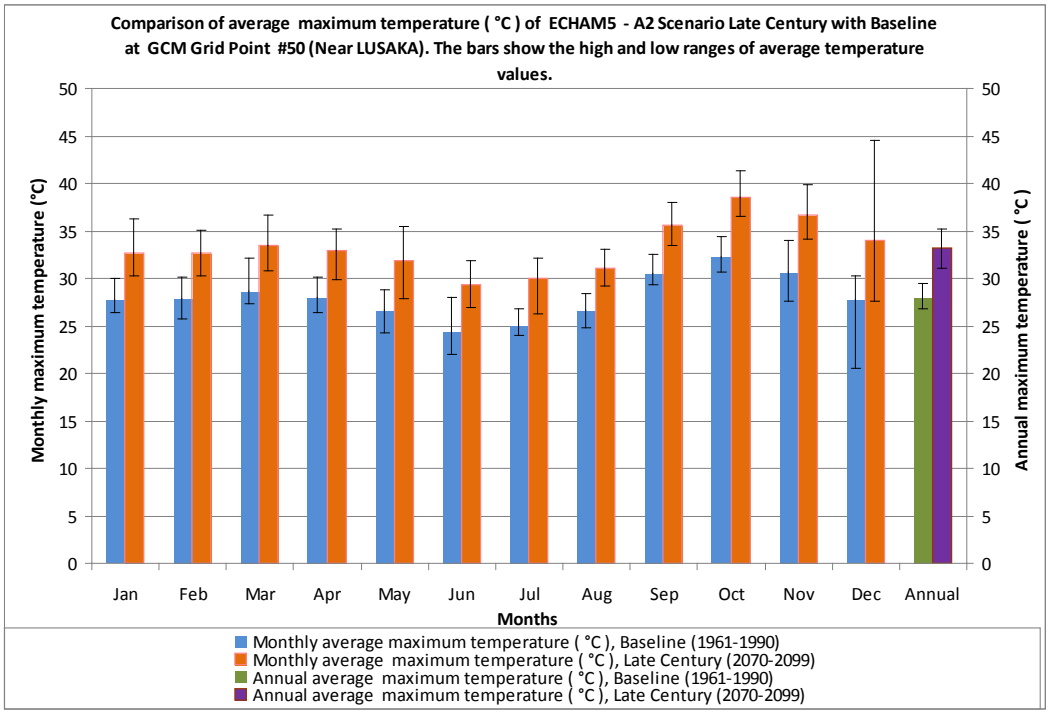

8.2 Wildfire Vulnerability Assessment

This section presents the current and future vulnerability assessment of the wildfire hazard.

8.2.1 Wildfire Vulnerability Current Conditions

Data on the occurrence of fires have shown that the frequency and magnitude of the fires has increased over the last five years, rendering the communities more vulnerable (DMMU 2008). Fires have occurred in all the provinces of the country and in most of the key sectors of the economy. Fire disasters have affected not only markets and private households but also strategic installations such as bridges and hydroelectric stations. The fires have been experienced in major sectors of the economy such as mining, manufacturing, construction and commerce. Examples of major fires that have occurred in Zambia include the Society House in 1997 and the Cabinet Office in the same year; Chisokone Market in Kitwe in 1998; Indeni Oil Refinery in 2000; and the KGU hydropower plant in 2008. The fires have resulted in the loss of lives and property damage worth billions of Kwacha (DMMU, 2008). On September 18, 2009, power generation was suspended after a fire at the KGU hydropower plant (Dow Jones Newswire, 2009). Three power generating units were damaged in the fire. While records do not generally distinguish between urban fires and wildfires, the potential impacts are clear.

8.2.2 Wildfire Vulnerability Future Conditions

The population of Zambia has been increasing by about three percent per year. The population table in Appendix 5 (Table A5-4) shows the population projections for the future. The

population potentially impacted by wildfire and thus the vulnerability will only increase with time.

Fuel sources in the study region may change as different farming techniques are used, different crops are grown, and land use changes. More people moving to high wildfire hazard areas would mean an increase in exposure and vulnerability as well. Sound fire management practices such as creating fire breaks and controlled burns would help reduce the vulnerability.

8.3 Wildfire Risk Assessment

Qualitative Assessment

The hazard assessment shows that wildfires should be considered a low risk since they occur very infrequently. The shows that the conditions exist for a rise in future frequency and magnitude. After reviewing previous events and the amount of land damaged, magnitude should be rated as low when compared to the other hazards.

The vulnerability assessment shows that there is moderate exposure to wildfires since they occur in areas with appropriate fuel sources which does not cover the entire country. ZESCO's exposure is moderate because its facilities are located in more remote areas (in areas with substantial wildfire fuel) and have been impacted by fires before. The only planned change in exposure would be the addition of the KGL hydropower plant. The country has a high sensitivity to wildfires which may be seen from the social and economic losses from historical events. ZESCO also has a high sensitivity to wildfires since their operations have come to a halt in the past due to this hazard. Zambia and ZESCO may be more susceptible in the future due to non climate stressors like land use changes and encroachment into forested areas. The country has a low adaptive capacity since there are no financial and few social networks in place to support displaced people and destroyed structures. ZESCO has a moderate adaptive capacity with the ability to cope with wildfire events as seen with their previous fire response.

The risk assessment shows that the country is at low risk to wildfires due to a lack of exposure and infrequency of the hazard. The risk may increase in future conditions due to the modeled increase in wildfire conditions and more urban/wildfire interface. ZESCO has a moderate risk due to its higher vulnerability. This risk may increase in the future due to climate change exacerbating the wildfire hazard and the addition of non-climate stressors like land use changes.

Quantitative Assessment

In order to better compare the risk for all the climate exacerbated hazards which may impact ZESCO, the historic losses were annualized and, in the case that there are no historic losses, potential losses were modeled with an associated return period in order to calculate annualized loss.

KGU has been in operation since 1977 and there has only been two times when operations have been suspended due to fire with damage to the power generating units. Unfortunately, the losses were not documented publicly and estimates were made to determine the loss for both events. The annual loss for wildfire is estimated at USD 93,750. More historic losses would provide a

more accurate value, but since the facility has only been in operation since 1977 there is not a lot of data available. Table A8-3 was used to help calculate the modeled future annual loss assuming the change in KBDI was directly related to the change in wildfire probability. The modeled future annual loss is shown in Table A7-5 below.

Table A8-4: Wildfire Loss (Annualized USD)

	Early Century	Mid Century	Late Century
ECHAM5 A2	117187.5	140625	168750
ECHAM5 B1	117187.5	128437.5	140625

8.4 Wildfire Hazard References

Chu, P.–S., Yan, W.P., Fujioka, F., 2002. Fire-climate relationships and long-lead seasonal wildfire prediction for Hawaii. International Journal of Wildland Fire 11, 25–31.

DMMU, 2008 – The Severity and Extend of Fire Disasters – Zambia's Technical Capabilities, Office of the Vice President, Disaster Management and Mitigation Unit, November 2008

Landscan 2007, Oak Ridge National Laboratory, Computation Sciences and Engineering Division, population data (1 km resolution).

Liu, Yongqiang; John Stanturf, Scott Goodrick, *Trends in Global Wildfire Potential in a Changing Climate*, Forest Ecology and Management, September 2009, pgs. 685-697

OFDA/CRED. 2007 (OFDA/CRED, 2007). EM-DAT: The OFDA/CRED International Disaster Database, Université catholique de Louvain, Brussels, Belgium.

Prevention Web, 2010; UN International Strategy for Disaster Reduction, Information Management Unit, Geneva, Switzerland, http://www.preventionweb.net.

Appendix 9
Disease Risk

Diseases such as malaria that are transmitted by biting insects and other vectors are among the most important causes of ill-health in tropical regions. Climate affects the reproduction and survival rates of both the infectious agents and their vectors, and hence their ability to infect humans. This is reflected in the temporal correlations between vector-borne disease rates and weather fluctuations over weeks, months, or years and also the close geographical correlations between climatic factors and the distribution of diseases. Climate does not act on the transmission of vector-borne infections in isolation: socio-economic conditions, control programs, human immunity, and other environmental conditions also influence disease rates.

The IPCC has concluded that climate change is likely to expand the geographical distribution of several vector-borne diseases, including malaria, dengue, and leishmaniasis to higher altitudes (high confidence) and higher latitudes with limited public health defenses (medium/low confidence), and to extend the transmission seasons in some locations (medium/high confidence) (IPCC, 2001). For some vector-borne diseases in some locations, climate change may decrease transmission by reducing rainfall or temperatures creating conditions that are not conducive to vector transmission (medium/low confidence) (IPCC, 2001). One out of ten of the world's annual one million malaria-caused deaths occur in sub-Saharan Africa (Lomborg, 2009).

9.1 Disease Hazard Assessment

This section reviews current and future disease hazard conditions, focusing on malaria.

9.1.1 Disease Hazard Current Conditions

The Zambian Ministry of Health estimates that the number of malaria cases has tripled in the past three decades to more than 4 million clinical cases and 50,000 deaths per year in a population of less than 11 million people (Ministry of Health, 2000). Malaria remains the leading cause of morbidity and mortality in Zambia.

In order to further evaluate current malaria conditions in Zambia, a malaria modeling program called Mapping Malaria Risk in Africa (MARA) was used. MARA is a biological model of *Falciparum* malaria transmission that includes decision rules which govern how minimum and mean temperature constrain the development of the parasite and the vector and how precipitation affects survival and breeding. MARA's decision rules were developed by reviewing laboratory and field studies throughout Sub-Saharan Africa and using current malaria distribution maps. The model uses three variables to determine climatic suitability: (1) mean monthly temperature, (2) winter minimum temperature, and (3) total cumulative monthly precipitation for each month to be analyzed. The MARA decision rules stipulate that both temperature and precipitation have to be favorable at the same time of the year to allow transmission, and suitable conditions must continue long enough for the transmission cycle to be completed. Based on the expert opinions

of scientists within the South African Medical Research Council, Malaria Research Programme, five months are used as a sufficient length of time for suitable conditions to be maintained and result in stable transmission.

Figure A9-1 shows the climate suitability for malaria based on its distribution in Zambia in 2002. Most of the country is very suitable for endemic malaria including several major cities. The unsuitable areas are in higher elevations where temperatures get lower (below 15 ^{o}C) and the mosquitoes can not survive. Figure A9-2 shows the duration of the malaria season in Zambia; it shows that some areas in Zambia do not have a malaria season, while some areas have a 1- to 4-month season, and most have a 5- to 6-month season based on data from 2001.

Figure A9-1: Distribution of Endemic Malaria in Zambia (2002)
Source: Developed using MARA Model, 2002.

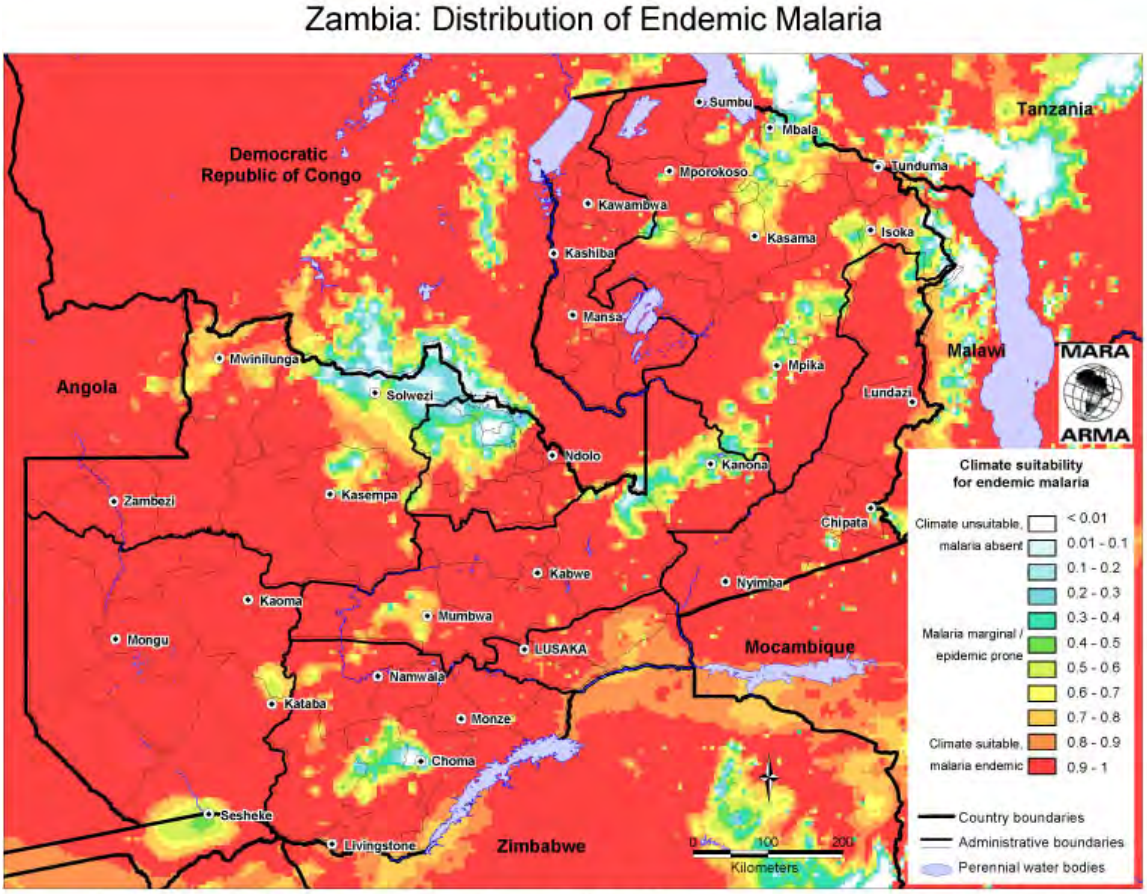

This map is a product of the MARA/ARMA collaboration (http://www.mara.org.za). July 2002, Medical Research Council, PO Box 70380, Overport, 4067, Durban, South Africa
CORE FUNDERS of MARA/ARMA: International Development Research Centre, Canada (IDRC); The Wellcome Trust UK; South African Medical Research Council (MRC); Swiss Tropical Institute, Multilateral Initiative on Malaria (MIM) / Special Programme for Research & Training in Tropical Diseases (TDR), Roll Back Malaria (RBM).
Malaria distribution model: Craig, M.H. et al. 1999. Parasitology Today 15: 105-111.
Topographical data: African Data Sampler, WRI, http://www.igc.org/wri/sdis/maps/ads/ads_idx.htm

Figure A9-2: Malaria Transmission Season (2001)

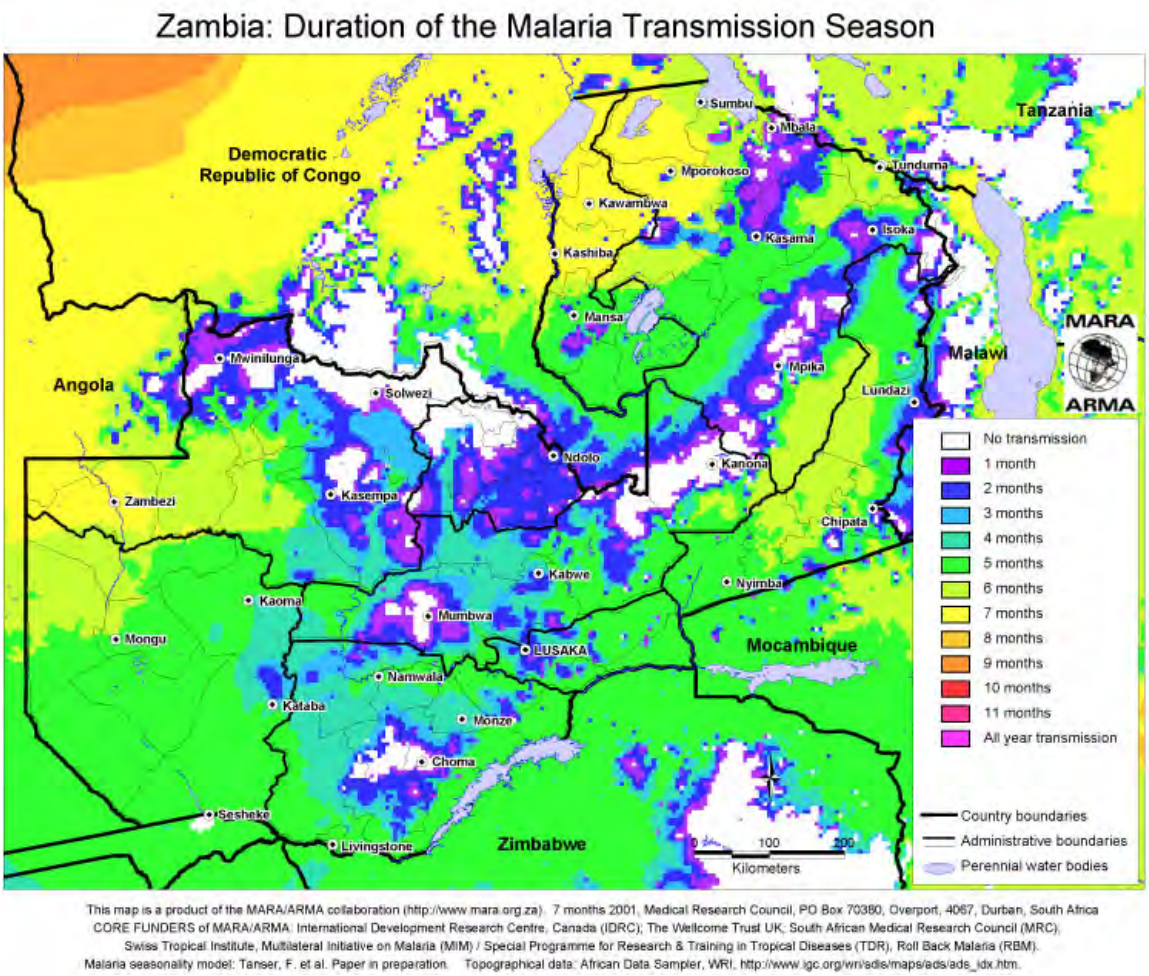

Source: Developed by MARA Model, 2001.

9.1.2 Disease Hazard Future Conditions

To analyze how malaria suitability areas and the transmission season in these areas will change with climate change, the climate projections of temperature and precipitation in the study area were compared to factors that restrict mosquitoes (the threshold temperature is set at 15°C with some moisture in the area). Figure A9-3 shows the Kafue River Basin study area and the GCM grid points across it. Areas that have traditionally had few or no malaria problems are identified with a red box. The GCM grid points analyzed for the malaria hazard are numbered in the figure.

Figure A9-3: GCM Grid Points with Map of Climate Suitability for Endemic Malaria

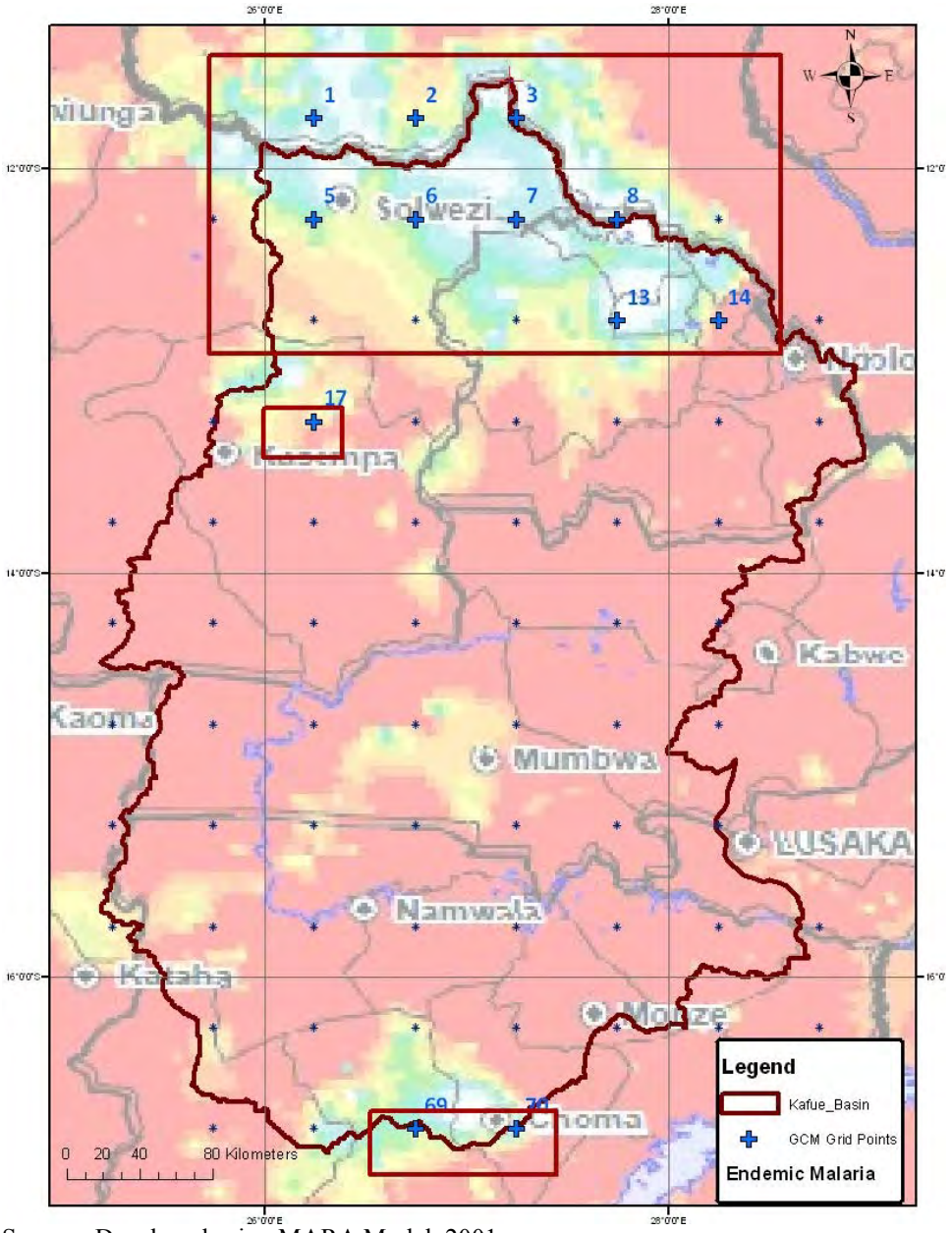

Source: Developed using MARA Model, 2001.
Notes: Enclosed boxes show GCM Grid Point Locations in High Elevation Areas

Figure A9-3 shows three areas with elevations that currently are not suitable, but merit further evaluation due to change in future temperatures. Climate change projections (Section 2.1 and 3.1) completed for this study indicate that average annual precipitation values do not change substantially (+/- 3%) for the study area, but they indicate that temperature values significantly increase over time. Therefore the focus of the malaria future analysis was on the temperature change since the precipitation change of +/-3% was not considered significant. The A2 and B1 emissions scenarios were analyzed for each of the time horizons to provide a range of possible temperature outcomes. Table A9-1 shows the percent number of days having a minimum

temperature greater than 15°C for the ECHAM5 A2 Scenario. This table has been summarized by averaging the GCM results for grid points that fall within each of the three regions for the baseline period and three time horizons as shown in Table A9-2.

Table A9-1: Percent Number of Days Having Minimum Temperatures Greater than 15°Celsius for the ECHAM5 A2 Scenario

Location	North of Kafue Basin near Solwezi									Near Kasempa	South of Kafue Basin near Choma	
GCM Grid No.	1	2	3	5	6	7	8	13	14	17	69	70
Baseline (1961-1990)	37%	41%	41%	39%	38%	39%	40%	40%	40%	43%	42%	46%
Early 21st Century (2010-2039)	51%	54%	54%	51%	49%	50%	50%	50%	50%	54%	55%	57%
Mid 21st Century (2040-2069)	60%	60%	60%	59%	57%	56%	56%	56%	58%	61%	60%	63%
Late 21st Century (2070-2099)	72%	72%	72%	70%	69%	67%	67%	66%	68%	72%	72%	73%

Table A9-2: Percent Number of Days Having Minimum Temperature Greater than 15°Celsius in ECHAM5 A2 Scenario

Location	North of Kafue Basin near Solwezi	Near Kasempa	South of Kafue Basin near Choma
Baseline (1961-1990)	39%	43%	44%
Early 21st Century (2010-2039)	51%	54%	56%
Mid 21st Century (2040-2069)	58%	61%	61%
Late 21st Century (2070-2099)	69%	72%	73%

Notes: This table uses the averaged temperature results for grid points within each of the three areas evaluated.

The analysis shows that the projected temperatures under climate change will provide a more suitable environment for malaria in all three high elevation areas and for all three time horizons. Some areas of higher elevation which have historically been mosquito free will no longer be unsuitable and the malaria transmission season also will be extended. The tables show that the number of days for suitable mosquito temperatures increases from four to six months in the baseline period to as much as eight to nine months in the late time horizon. This ECHAM5 A2 emissions scenario provides the upper end of the modeled results across the ECHAM5 B1 and A2 emissions scenarios.

Table A9-3 shows the percent number of days having a minimum temperature greater than 15ºC for the ECHAM5 B1 scenario.

Table A9-3: Percent Number of Days Having Minimum Temperature Greater than 15°Celsius for ECHAM5 B1 Scenario

Location	North of Kafue Basin near Solwezi									Near Kasempa	South of Kafue Basin near Choma	
GCM Grid No.	1	2	3	5	6	7	8	13	14	17	69	70
Baseline (1961-1990)	37%	41%	41%	39%	38%	39%	40%	40%	40%	43%	42%	46%
Early 21st Century (2010-2039)	48%	51%	51%	49%	47%	47%	48%	48%	48%	52%	51%	54%
Mid 21st Century (2040-2069)	60%	60%	60%	59%	58%	57%	57%	57%	58%	61%	60%	62%
Late 21st Century (2070-2099)	65%	65%	66%	63%	62%	61%	61%	60%	63%	65%	63%	66%

Table A9-4: Percent Number of Days Having Minimum Temperature Greater than 15°Celsius in ECHAM5 B1 scenario

Location	North of Kafue Basin near Solwezi	Near Kasempa	South of Kafue Basin near Choma
Baseline (1961-1990)	39%	43%	44%
Early 21st Century (2010-2039)	49%	52%	53%
Mid 21st Century (2040-2069)	58%	61%	61%
Late 21st Century (2070-2099)	63%	65%	64%

Notes: This table uses the averaged temperature results for grid points within each of the three areas evaluated.

The tables show that the number of days for suitable mosquito temperatures increases from four to six months in the baseline to seven to eight months in the late time horizon. This ECHAM5 B1 emissions scenario provides the lower end of the modeled results (across the ECHAM5 A2 and B1 results).

9.2 Disease Vulnerability Assessment

This section reviews current and future disease vulnerability conditions, focusing on malaria.

9.2.1 Disease Vulnerability Current Conditions

Disease kills more people each year than any of the other hazards described in this report. Nine of the top ten deadliest events in Zambia from 1982 to 2007 were caused by epidemics (OFDA/CRED 2007). Cholera, Plague, Acute Diarrheal Syndrome, Yellow Fever, and Malaria have all impacted the population in the past. Yellow Fever and Malaria are spread by contaminated mosquitoes. Table A9-5 lists the nine deadliest epidemic events since 1982.

Table A9-5: Deaths in Zambia Resulting from Epidemics

Disaster Type[1]	Year[1]	Killed[1]
Epidemic	1999	393
Epidemic	2003	179
Epidemic	2000	163
Epidemic	1990	85
Epidemic	1982	51
Epidemic	1999	44
Epidemic	1999	23
Epidemic	2005	21
Epidemic	2001	11

[1] Source of Data: OFDA/CRED International Disaster Database, Version vv11.08.

Malaria also is strongly related to poverty and the number of cases of malaria has risen in the past twenty years due to failing medical responses (Lomborg, 2009). Malaria also strikes children harder. In Africa, 1 in 20 children die from malaria, and in the worst affected areas, up to 1 in every 5 or 6 deaths are from malaria and its related diseases (e.g., anemia) (Kakkilaya, 2006).

9.2.2 Disease Vulnerability Future Conditions

Current models provide a measure of changing exposure to malaria, rather than a complete measure of infection incidence or disease burden. If the latter are required, it will be necessary to make an assumption about the relationship between changes in exposure and in disease burden. The simplest method, applied in the national analysis is to assume that proportional changes in disease exposure (e.g., the proportion of people livening in areas climatically suitable for malaria), are directly related to proportional changes in disease burden. For example, if climate change in a particular region is estimated to cause a 20% increase in the number of people living in areas that are defined as climatically suitable for malaria transmission, to the simple method would project a corresponding 20% increase in the malaria disease burden.. Estimates of current burden of malaria at the national level are usually available from national statistics, or from the World Health Organization.

Within Africa, little evidence exists of causal changes in disease transmission and climate. This lack of evidence does not mean that these changes do not exist; rather, it may reflect the lack of available epidemiological data as a result of poor or absent surveillance and health information systems. Within Africa, 71.3% of the burden of disease is attributed to infectious diseases; malaria is the single greatest contributor (10.8%). The effects of such climate change impacts on disease are likely to be most noticeable in areas that constitute the fringes of distribution of a particular disease. Changes in distribution often will cause susceptible populations (those with little or no immunity) to be exposed to diseases not previously encountered-and result in severe morbidity and mortality. Minimum temperatures are crucial parameters for vector survival and affect the latitude and elevation of distribution, as well as the length of season permissive to

transmission. Minimum temperature is known to play an important role in limiting the distribution of malaria vector populations at a given locality where summer conditions are suitable for transmission. Thus, meteorological variables can create conditions conducive to disease spread or even to clusters of outbreaks (in the case of flooding or drought). A drop in water level in dams and rivers also would affect the quality of household and industrial fresh water because reduced water volume would increase the concentration of sewage and other effluent in rivers-resulting in outbreaks of diseases such as diarrhea, dysentery, and cholera. It is important to distinguish between restrictions related to rainfall and those related to temperature. In cases where rainfall restricts distribution, increases in temperature may result in a decrease in disease incidence and distribution. Conversely, in areas where low temperature currently limits distribution, increased temperature may increase regional severity and cause distributional extension (IPCC, 2007).

For ZESCO, the increased suitability of disease will not directly affect flow potential but it could affect employees and customers which would affect operations.

9.3 Disease Risk Assessment

The hazard assessment shows that disease frequency should be considered high since there is an epidemic 0.58 times a year (OFDA/CRED 2007). The future hazard assessment shows that the number of days for suitable mosquito temperatures increases from four to six months in the baseline to seven to eight months in the late time horizon for ECHAM5 B1 scenario and to eight to ten months using the ECHAM5 A2 scenario. After reviewing previous events and the amount of individuals affected, magnitude should be rated as high when compared to the other hazards.

The vulnerability assessment shows that there is moderate exposure to diseases since they occur in most of the country but not all the time (seasonally). ZESCO's exposure is moderate because their facilities are located in areas which have been impacted by disease before. The climate models predict that in the future, areas never before impacted by disease due to mosquitoes will have more suitable conditions and the disease seasons will be extended. The country has a high sensitivity to disease which may be seen from the social losses from historical events and the average age of the population since 48 percent of the population is 14 years or younger. ZESCO also has a lower sensitivity to disease since their personnel are not children and they have health care. Zambia and ZESCO will probably have the same susceptibility in the future. The country has a low adaptive capacity since there are no financial and few social networks in place to support sick people. ZESCO has a moderate adaptive capacity with the ability to cope with disease.

The risk assessment shows that the country is at high risk to disease due to a severe hazard and vulnerability. The risk may increase in future conditions. ZESCO has a moderate risk due to its lower vulnerability. ZESCO's structures are not susceptible to the hazard, but its customers and workers are. This risk may increase in the future due to climate change exacerbating disease impacts.

9.4 Disease Hazard References

IPCC, 2001: Climate Change 2001: the scientific basis. Contribution of Working Group I to the third assessment report of the Intergovernmental Panel on Climate Change. In: Houghton JT, Ding Y, Griggs DJ, Noguer M., van der Linden P.J., Dai X., Maskell K., Johnson C.A. (eds) Cambridge University Press, 881 pp.

IPCC (2007): Working Group II: Impacts, Adaption and Vulnerability

Landscan 2007, Oak Ridge National Laboratory, Computation Sciences and Engineering Division, population data (1 km resolution).

Lomborg 2009, Climate Change and Malaria in Africa, The Wall Street Journal, November 1, 2009

Ministry of Health Sector-wide approach to health: a proposed health sector support investment programme (2001–2005) Joint identification and formulation mission for Zambia. Vol. 1. Ministry of Health, Lusaka; 2000.

OFDA/CRED. 2007 (OFDA/CRED, 2007). EM-DAT: The OFDA/CRED International Disaster Database, Université catholique de Louvain, Brussels, Belgium.

International Finance Corporation
2121 Pennsylvania Ave. NW
Washington, DC 20433
Tel. 1-202-473-1000
www.ifc.org/climatechange